Summer 8-17-2014

Poly(Arginine) Derived Cancer-Targeting Peptides for the Development of a Cancer-Targeted Gene Therapy Approach in HepG2 Liver Cancer Cells

Stesha C. Joseph
stesha.joseph@student.shu.edu

Poly(Arginine) Derived Cancer-Targeting Peptides for the Development of a Cancer-Targeted Gene Therapy Approach in HepG2 Liver Cancer Cells

A thesis submitted to Seton Hall University in partial fulfillment of the requirements for the degree of Doctor of Philosophy

By

Stesha C. Joseph

August 2014

Department of Chemistry and Biochemistry
Seton Hall University
South Orange, NJ, USA

DISSERTATION COMMITTEE APPROVALS

We certify that we have read this thesis and that in our opinion it is sufficient in scientific scope and quality as a dissertation for the degree of Doctor in Philosophy.
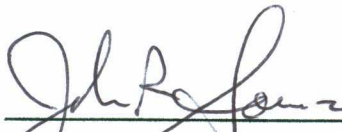
APPROVED BY:

David Sabatino, Ph.D.

Advisor, Seton Hall University

Allan D. Blake, Ph.D.

Reader, Member of Dissertation Committee, Seton Hall University

John R. Sowa, Jr., Ph.D.

Reader, Member of Dissertation Committee, Seton Hall University

Nicholas H. Snow, Ph.D.

Chair, Department of Chemistry and Biochemistry, Seton Hall University

Dedicated to my family, for all their support,
my fiancé Sean and beloved brother Kerlon – RIP

ABSTRACT

Cancer is a disease that has eluded medicinal approaches for many years and as a result new and improved therapeutic approaches are in constant demand. Although chemotherapy and radiation treatments have assisted in suppressing the growth of tumors, their poor selectivity and efficacy are major limitations for effective therapy en route towards the development of a cure for the cancer epidemic. With the mission of conquering cancer at heart, researchers have pursued a new form of cancer therapy, aptly named, *a cancer targeting approach*. This method revolves around the selection of a suitable biomarker, typically a cell surface receptor overexpressed or selectively localized on the surface of cancer cells but not on normal tissues. This biomarker forms the basis of a cancer targeting approach, in which high affinity and specific binding ligands (*e.g.* peptides) have been selected by phage display bio-panning methods or combinatorial chemistry to target cancer cells *in-vivo*.

Building on this approach, the identification of a cyclic peptide, Pep42, H_2N-CTVALPGGYVRVC-$CONH_2$, has been selected as a specific and high-affinity binding ligand of the cell surface receptor, Glucose Regulated Protein 78 (GRP78). GRP78 is a member of the heat shock family of chaperone proteins, assisting in protein folding events under physiological stress induced conditions that are mitigated by the unfolded protein response (UPR) mechanism. In cancer, GRP78 is overexpressed and cell surface localized where it functions as a hub for cell signaling pathways that lead to cancer cell initiation, proliferation and resistance towards chemotherapy. Thus, GRP78 has been classified as a valid biomarker for the development of targeted anti-cancer approaches.

Towards this goal, an Fmoc-based solid phase peptide synthesis (Fmoc-SPPS) method has been optimized on a polyethylene glycol (PEG) resin for the production of poly(arginine) derived

Pep42 sequences in good yields (14-46%) and purities (>95%) following RP-LCMS. The effect of the length (0-12) and stereochemistry (L/D) of the poly(arginine) sequences on Pep42 structure and stability were next evaluated by CD spectroscopy. Interestingly, peptides displayed varying folded conformations, transitioning between helical and turn structures, that were found to be contingent on the poly(arginine) sequence, solvent and disulfide bond formed within the Pep42 motif. Moreover, the peptide folds were found to be resilient towards thermal denaturation due to the covalent disulfide bond.

Structure-activity relationships were next assessed in HepG2 hepatoblastoma cells, in which the cancer-targeting peptides were found to bind to the GRP78 receptor and internalize within the HepG2 cells. This discovery has led to their applications in cancer-targeted gene therapy, from which a GRP78-silencing short-interfering RNA (siRNA) was effectively transfected within the HepG2 cells for potent oncogene knockdown effects (50-60%, 40 pmol siRNA) while triggering modest cell death effects (5-10%). This thesis will highlight my efforts and contribution in collaboration with Drs. Blake and Bitsaktsis research groups towards the development of an effective *cancer-targeted gene therapy approach.*

ACKNOWLEDGEMENTS

education. I will also like to thank for stepfather for always being there to help me along this journey. This accomplishment holds meaning only because I can share it with you. I would like to thank my father for helping me accomplish my goals. I would like to thank my extended family – aunts, uncles and cousins. You all have pushed me and believed in me. Special thanks to my aunt Juliet and uncle Sheldon for without you none of this would be possible.

I am extremely thankful and grateful to my fiancé Sean. Thank you for your patience, support, encouragement and love. I would like to apologize for the difficult times we have had to endure through this process, but we can rejoice in this moment together.

To everyone that has helped me grow as a person, supported and encouraged me, I thank and appreciate all that you have done.

TABLE OF CONTENTS

ABBREVIATIONS AND SYMBOLS

A2780	cell line human ovarian carcinoma
A549	adenocarcinoma cells
A_{274} or Abs	UV absorbance measured at 260 nm
A or Ala	Alanine
ε-Ahx	aminohexanoic acid
AchR	acetylcholine receptor
ADCC	antibody dependent cell cytotoxicity
ANOVA	analysis of variance
Arg	Arginine
BSA	bovine serum albumin
CTP	cancer targeting peptide
CD-21	cluster of differentiation 21 (glycoprotein)
CCD-11Lu	human lung fibroblast
C or Cys	Cysteine
CD	circular dichroism
D or Asp	Aspartate
DAPI	diamidino-2-phenylindole
DIC	*N,N′*-diisopropylcarbodiimide
DLS	dynamic light scattering
DOTA	1,4,7,10-tetraazacyclododecane-1,4,7,10-tetraacetic acid
DMF	*N,N′*-dimethyl formamide
DMEM	Dulbecco's Modified Eagle Medium

DMSO	dimethyl sulfoxide
DNA	2′-deoxyribonucleic acid
DTPA	diethylenetriaminepentaacetic acid
DTT	Dithioreitol
DU145	prostate cancer cell line
EDTA	ethylene-diamine tetraacetate dehydrate
Ex/Em	excitation/emission
ESI-MS	electrospray ionization mass spectrometry
EtOH	ethanol
ER	endoplasmic reticulum
^{18}F	Fluorine
FA	formic acid
FBOA	*p*-fluorobenzyloxime acetyl
FBS	fetal bovine serum
FDA	food and drug administration
FITC	fluorescein isothiocyanate
FGF-R	fibroblast growth factor receptor
Fmoc	Fluorenylmethyloxycarbonyl
G or Gly	glycine
g/mol	grams per mole
GRP78	glucose regulated protein 78 kDa
h	hours
HB	Hepatoblastoma

HCTU	O-(1H-6-Chlorobenzotriazole-1-yl)-1,1,3,3-tetramethyluronium hexafluorophosphate
HDFa	human dermal fibroblast
HepG2	human hepatoblastoma cell line
HER-2	human epidermal growth factor receptor 2
HIF-1	hypoxia-inducible factor 1
HOBt	1-hydroxybenzotriazole
hPTN	human pleiotrophin
HRP	horseradish peroxidase
HSP70	heat shock protein 70 kDa
HYD-1	hybrid peptide
^{123}I	iodine
Ile	Isoleucine
IC_{50}	concentration of inhibitor which causes 50% inhibition
K_D	dissociation constant
kDa	kilodalton
Λ	wavelength
LC/MS	liquid chromatography mass spectrometry
Leu	Leucine
m/z	mass to charge ratio
Θ	molar ellipticity
mAb	monoclonal antibody
MeCN	acetonitrile
MeOH	Methanol

Me6652/4	melanoma cells
$MgCl_2$	magnesium chloride
MHC	major histocompatibility complex
MW	Microwave
M.W.	molecular weight
μM	micromolar
μL	microliter
N:P	nitrogen to phosphate ratio
NK	natural killer
NMM	*N*-methylmorpholine
NMP	*N*-methylpyrrolidinone
NOTA	1,4,7-triazacyclononane-1,4,7-triacetic acid
OBOC	one-bead one compound
PAGE	polyacrylamide gel electrophoresis
PDA	photodiode array
Pbf	Ng-2,2,4,6,7-pentamethyldihydrobenzofuran-5-sulfonyl
PBS	phosphate buffered saline
Pep42-QD	Pep42- Quantum Dots
PET	positron emission tomography
PNA	peptide nucleic acid
Pro	proline
pIII	filamentous phage protein III
pVIII	filamentous phage protein VIII

PS-DVB	poly(styrene/divinyl benzene)
PSI	Peptide Scientific Inc.
PVDF	polyvinylidene difluoride
R	Arginine
RNA	ribonucleic acid
RNAi	RNA interference
RIPA	radioimmunoprecipitation assay
RP-HPLC	reverse-phase high performance liquid chromatography
RT	retention time
SEM	standard error of the mean
Sf-9	spodoptera frugiperda 9
siRNA	small interfering RNA
SJSA-1	osteosarcoma cells
SPPS	solid phase peptide synthesis
T or Thr	threonine
t-Bu	tertiary butyl
TAE	tris-acetate-EDTA
TBE	tris/boric acid/EDTA buffer
TE2A	Tetraazamacrocycles
TEM	transmission electron microscopy
TES	Triethylsilane
TETA	1,4,8,11-tetraazacyclotetradecane-1,4,8,11-tetraacetic acid
TFA	trifluroacetic acid

TFE	2,2,2-trifluoroethanol
TGF-β	transforming growth factor beta
TM	trademark
TMB	3,3′,5,5′tetramethylbenzidine
Tris-HCl	tris(hydroxymethyl)aminomethane hydrochloride
Tyr	Tyrosine
UPR	unfolded protein response
UV-Vis	ultraviolet-visible
Val	Valine
VEGF	vascular endothelial growth factor
v/v	volume per volume

LIST OF FIGURES

CHAPTER 1

LIST OF TABLES

CHAPTER 1: CANCER-TARGETING PEPTIDES AND THEIR APPLICATIONS IN ANTI-CANCER DRUG DESIGN AND DEVELOPMENT

1.1 CANCER-TARGETING APPROACHES

Anti-cancer drugs that are designed and fabricated to destroy cancer cells often do so non-selectively, rapidly dispersing in all tissue types rendering patients with severe side-effects that compromises the road to recovery.[1] Moreover, the bioavailability and tissue penetration properties of anti-cancer drugs based on biomacromolecules such as oligonucleotides,[2] peptides[3] and carbohydrates[4] results in limited passive diffusion through the phospholipid bilayer for cancer cell death activity. These major impediments have stimulated the search and application of alternative anti-cancer drug delivery methods that aim to a) target cancer cells exclusively, while b) facilitating the internalization of cytotoxic drugs that can trigger cancer cell death (**Figure 1.1**).
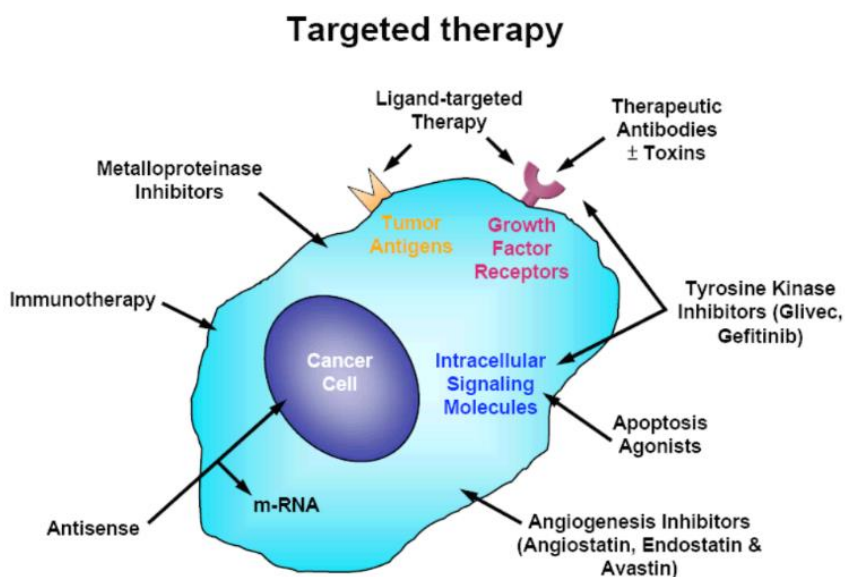
Figure 1.1. Cancer-targeting approaches. Figure adapted from Wu, H-C. et al *J. Cancer Mol.* **2006**, *2*, 57-66.[28]

Antisense oligonucleotides target oncogene expression compromising cancer cell activity. Immunotherapy uses antibodies to bind to cell surface tumor presenting antigens recruiting the immune response. Selective small molecule inhibitors can be designed to bind specifically and

with high affinity to tumor cell overexpressing metalloproteinases and kinases. Specific modulators of angiogenesis and apoptosis can also target cancer cell death.

Towards this effect, antibodies have served as Mother Nature's targeting biomolecules. They contain the ability to detect and bind to specific antigens on invading pathogens, allergens and cancers while recruiting the immune response for their eradication.[5,6] However, many types of resilient cancers have evolved to evade recognition of our natural immune system, and continue to proliferate without restriction forming the most resistant types of malignant tumors. In an attempt to rescue our immune response from cancer, monoclonal antibodies (mAb) targeting specific cancer cell surface markers that are vital to tumorigenesis and metastasis have been designed and validated in a clinical method referred to as cancer immunotherapy (**Figure 1.2**).[6] Using recombinant gene expression, mutagenesis and molecular evolution procedures, mAb retain the immunostimulatory effects of their naturally occurring counterparts, while recognizing cell surface antigens that were previously camouflaged on cancer cells.
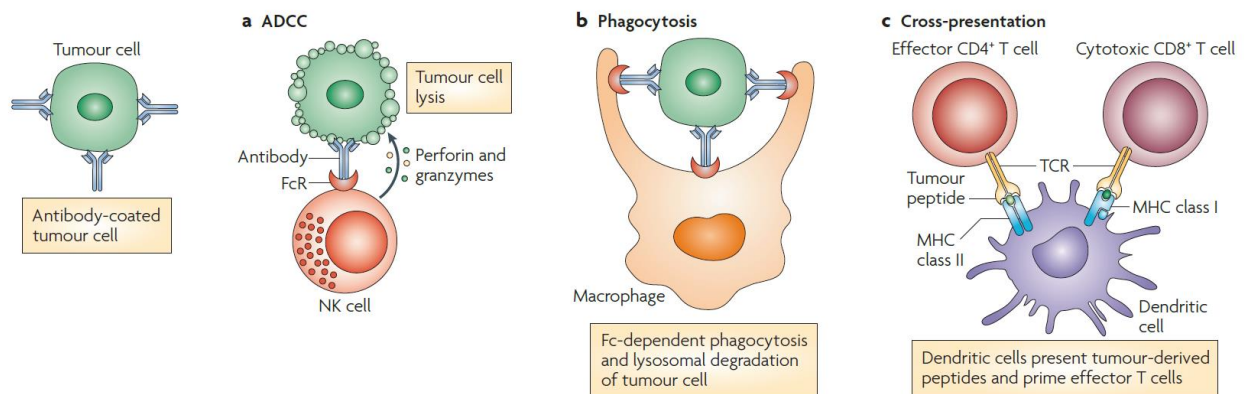
Figure 1.2. Cancer immunotherapy approach.[6] a) Antibody Dependent Cell Cytotoxicity (ADCC) mechanism activates NK cell secretion of perforin and granzyme tumor cell lysis enzymes, b) Phagocytosis leads to lysosomal degradation of tumor cells from the mAb-macrophage binding interaction and c) Cross-presentation leads to mAb-antigen (MHC class I and II) recognition on tumor derived dendritic cells for T cell activation and cytotoxicity. Figure adapted from Weiner, L.M. et al *Nature Rev. Immunol.* **2010**, *10*, 317-327.

Moreover, these methods have facilitated the bio-conjugation of anti-cancer drugs,[7] radionuclides,[8] toxins[9] and imaging agents[10] that have ushered a new wave of Food and Drug Administration (FDA) approved drugs for cancer diagnosis and treatment in the clinic.[6,11] In spite of their growing success, mAb and their bio-conjugates still retain severe limitations that prevent their widespread use as therapeutics.[11] mAb-based treatments are still affected by lengthy and expensive production costs associated with large-scale cell culture, bio-conjugation and purification methods. In addition to poor stability and pharmacokinetic properties which limits tumor tissue penetration for effective immunotherapy. Immunostimulatory-associated toxicities have also been found in patients that are immuno-compromised following exhaustive chemo- and radio-therapeutic treatments. Thus, the need to develop simpler, benign and effective modes of cancer therapy remains an elusive goal in the fight against cancer.

Inspired by their mAb counterparts, cancer-targeting peptides (CTPs) have emerged as fruitful types tumor-targeting ligands. They favor high affinity and selective binding to cancer cell surface receptors, while enabling membrane translocation for activity (**Figure 1.3**).[12] Moreover, CTPs and related analogs have led to the development of potent anti-cancer bioconjugates, endowed with favorable pharmacokinetic properties and armed with imaging agents, radionuclides, cytotoxic drugs or toxins that have improved detection and therapy.[13-17] For example, an RGD peptide, known to associate on cell surface integrin receptors overexpressed and membrane localized on solid tumor tissues have been conjugated with fluorescent probes to effect *in-vivo* tumor imaging in mice bearing tumor models.[13] Moreover, the RGD peptides have also been labeled with In-DOTA containing radionuclides for halting and shrinking tumor growth in human tumor xenograft models.[14,16] The conjugation of camptothecin as an apoptosis inducing agent with a leutinizing-hormone releasing hormone (LHRH, QHWSYkcLRPNHEt) resulted in

an accumulation in the tumor of mice bearing xenografts of A2780 human ovarian carcinoma with minimal dispersion to other tissues. This resulted in amplified induction of apoptosis in the tumor site as compared to treatment with camptothecin alone.[17] As a result, CTPs have provided a safe and effective alternative in cancer treatment methods. They effectively circumvent the limitations and cytotoxicities associated with the recombinant mAbs and the non-selective forms of cancer therapy.
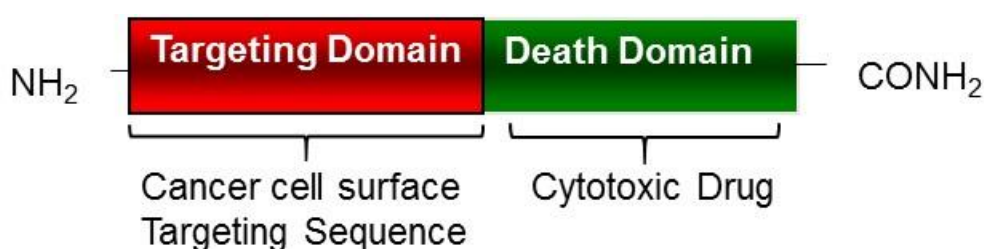
Figure 1.3. Design of cancer-targeting peptides.

1.2 PREPARATION OF CANCER-TARGETING PEPTIDES

Combinatorial chemistry involves the synthesis or biosynthesis of chemical libraries (a family of compounds having a base chemical structure) of molecules for the purpose of biological screening, leading to the discovery of a lead for further optimization and application.[18] The field of combinatorial chemistry has become a powerful tool in drug discovery especially applied to cancer-targeting peptides. There are six general methods for preparing and screening combinatorial libraries of peptides leading to the discovery of lead ligands for high affinity and selective oncoprotein binding.[19] These include:

    I.   The biological peptide library method (phage-display peptide library)

   II.   The one-bead-one-compound (OBOC) combinatorial library method

III.   The spatially addressable parallel library method

IV.   Combinatorial library methods requiring deconvolution

V.   The affinity selection method

VI.   Self-assembled peptide nucleic acid (PNA) encoded chemical microarrays

However, of these six methods, only the phage-display peptide library and the OBOC method have been applied to the discovery of cancer cell receptor-targeting peptides and will be highlighted in this chapter.

1.2.1 COMBINATORIAL PEPTIDE CHEMISTRY

Combinatorial chemistry was originally used to make peptide libraries from the multipin technology in 1984.[20] It has since then evolved into applications involving the generation of large arrays of molecules for molecular recognition against desired targets. The advantage of this method is related to the use of a solid support, which facilitates chemical reactivity by adding an excess of reagents, isolation of products bound to an insoluble support and separation of unwanted materials that may be simply washed away by solvent filtration. As such, solid-phase synthesis facilitates the rapid preparation of a library of molecules without having to perform step-wise work-up and purification steps. Thus, solid-phase synthesis is the method of choice for the preparation of lengthy and difficult peptide sequences for structure-activity relationship studies with receptor targets.[21]

Solid-phase peptide synthesis has facilitated the rapid production of biologically active sequences such as neurotransmitters, hormones, neuromodulators cell penetrating and targeting peptides.[22] At the cornerstone of its utility is an insoluble polymer support (typically polystyrene) that facilitates the prerequisite peptide coupling and deprotection steps for assembling the constituent amino acid building blocks into bio-active peptides (**Figure 1.4**). This iterative

procedure is now automated and optimized under microwave irradiation.[23] Following solid-phase synthesis, peptides are cleaved from the solid-support, deprotected and purified/analyzed using reverse-phase high performance liquid chromatography (RP-HPLC). As such, solid-phase peptide synthesis has facilitated combinatorial peptide synthesis for a wide range of applications, including those belonging to the cancer-targeting peptides as highlighted in Chapter 2 of this thesis.
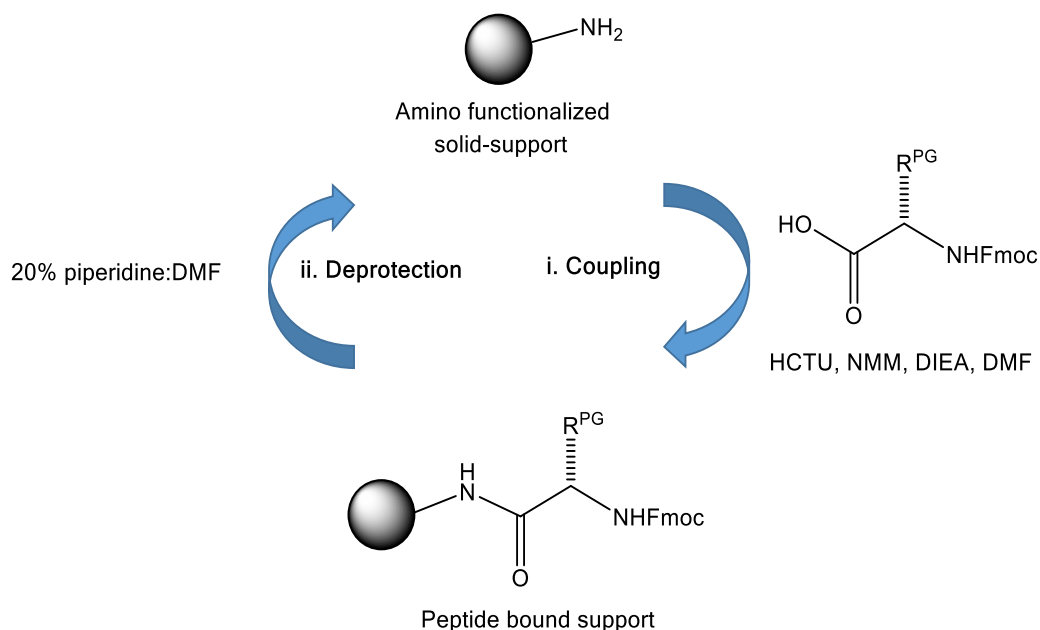
Figure 1.4. Solid-phase peptide synthesis based on the Fmoc-protecting group strategy. An amino-derived solid-support is coupled to an Fmoc-amino acid to generate the peptide bound support. Following peptide coupling, Fmoc deprotection liberates the free amino group for continued cycles of coupling and deprotection until the desired peptide has been synthesized on solid-phase.

1.2.2 PHAGE-DISPLAY PEPTIDE LIBRARY METHOD

Phage-display technology is an *in vitro* technique used for the expression of peptide ligands from bacteriophages.[24] Since this method enables the generation of 10^8-10^9 bacteriophages per iterative round of *in-vitro* amplification and selection, a library of peptides for screening specific interactions with proteins and other biomacromolecules (*i.e.* bio-panning) are rapidly generated. Moreover, the expressed peptides are not limited in size or sequence composition, which are both

challenges in solid-phase peptide synthesis. Since the peptides are expressed on the virion surface, naturally occurring peptide folds that are typically responsible for peptide-protein interactions are readily observed. However, these bio-panning methods are not amenable to the incorporation of modified amino acids that may be crucial in improving the pharmacokinetic properties of the lead peptide ligand.

In this method (**Figure 1.5**), genetically modified bacteriophages infect bacterial cells which allows for recombinant DNA replication and expression with the host cell machinery. Once replicated, the bacteriophages are programed to display the peptide library on their surface. This is referred to as a phage-display peptide library, a heterogeneous mixture of phage clones carrying different peptide sequences on its virion surface. The peptides in the phage-display library have two main characteristics required for chemical evolution – reproducibility and mutations. Introduction of mutations into the phage genome stimulates the expression of chemically diverse peptide populations that were not expressed during the first rounds of amplification and selection. The displayed peptides are then screened against receptor targets to determine the lead peptide ligands.

Screening and selection of the phage-display peptide libraries is next accomplished by standard affinity purification techniques. The target receptor is tethered to a solid support and the phage mixture is passed over the immobilized receptor. The phages whose displayed peptides bind to the receptor are captured on the surface allowing the unbound phages to be washed away. The bound phages are then eluted into a solution which loosens the receptor-peptide bonds that yields an eluant population of phages. These eluted phages are further amplified (10^6) by infecting fresh bacterial cell hosts to produce new clones. The amino acid sequences of the peptides that bind to the target receptors are then determined by sequencing the viral DNA and peptides. Peptides are

typically selected from libraries which express variants of 7 to 20 amino acids on the capsid protein

(pIII or pVIII) of the phages.
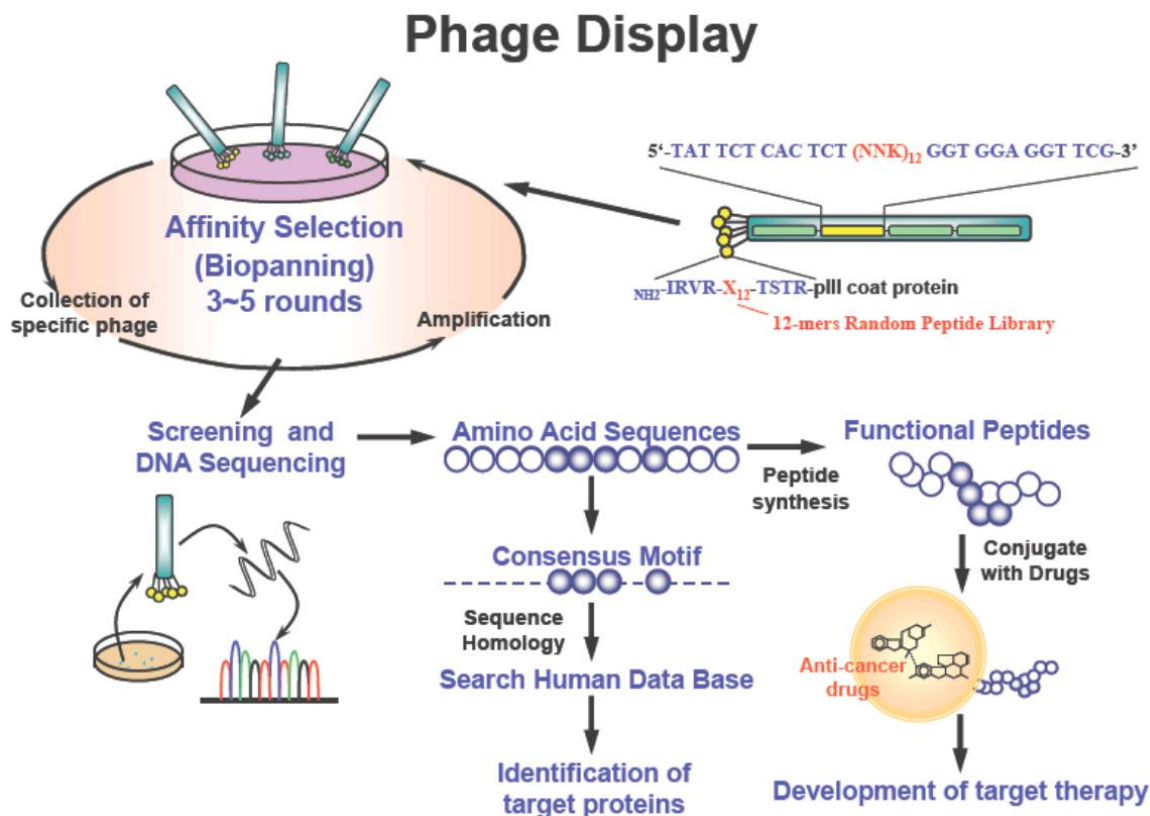
Figure 1.5. Phage-display bio-panning for the selection of cancer-targeting peptide ligands. Figure adapted from Wu, H-C. et al *J. Cancer Mol.* **2006**, *2*, 57-66.[28]

Fruitful applications of phage display peptide bio-panning experiments includes the selection of a

16-mer peptide targeting the VEGF receptor on endothelial tumor tissues,[25] peptides that bound to

the CD-21 B-cell Lymphoma cell surface marker[26] and a 26-mer peptide that bound to FGF-R on

the surface of Sf-9 cells,[27] among many others.[19]

1.2.3 OBOC COMBINATORIAL LIBRARY METHOD

OBOC combinatorial peptide library synthesis unleashes the power of synthetic chemistry

for the incorporation of chemical modification without restriction within bio-active sequences.[19]

Thus, peptide mimics (peptidomimetics) are crucial for improving the pharmacokinetic properties of the native sequences, while facilitating structure-activity relationship studies with receptor targets.[29] These are fundamental requirements for an effective cancer-targeting strategy.

The OBOC combinatorial library is developed using a "split-mix" synthesis approach in which each bead represents a unique chemical entity (peptide) for further diversification (**Figure 1.6**). This is the most common approach for synthetically making large peptide libraries (10^4-10^6) prior to high-throughput screening with receptor targets for evaluating their biological activity.[30]
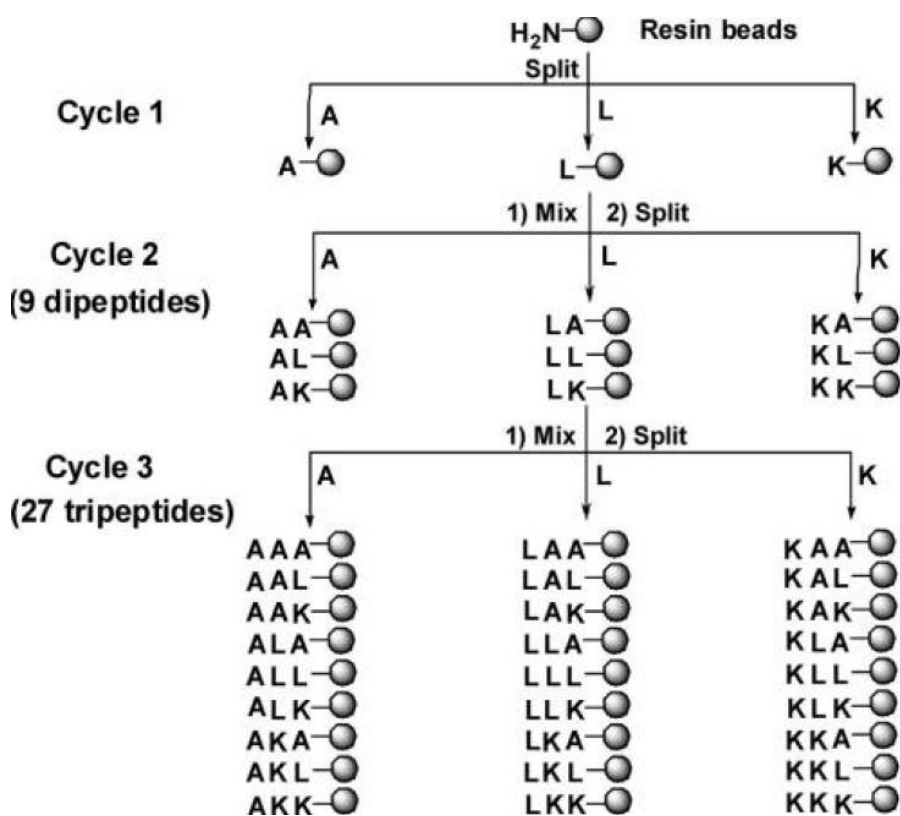
Figure 1.6. OBOC combinatorial library synthesis using the split-mix method. Figure adapted from Aina, O.H.; et al *Mol. Pharm.* **2007**, *4*, 631-651.[19]

With large libraries of peptides in hand, encoding methods (tags) are used to keep track of the individual peptide sequences on the beads.[31] At the end of the synthesis, a dye is attached to the target receptor which is washed across the polymer beads. A positive hit is identified when the

peptide bound bead adopts the color of the dye, and with growing color intensities validating tight ligand binding to the target receptor (*i.e.* identification of a lead). The colored beads are then selected and manually decoded to identify the chemical composition of the peptide sequence (**Figure 1.7**).
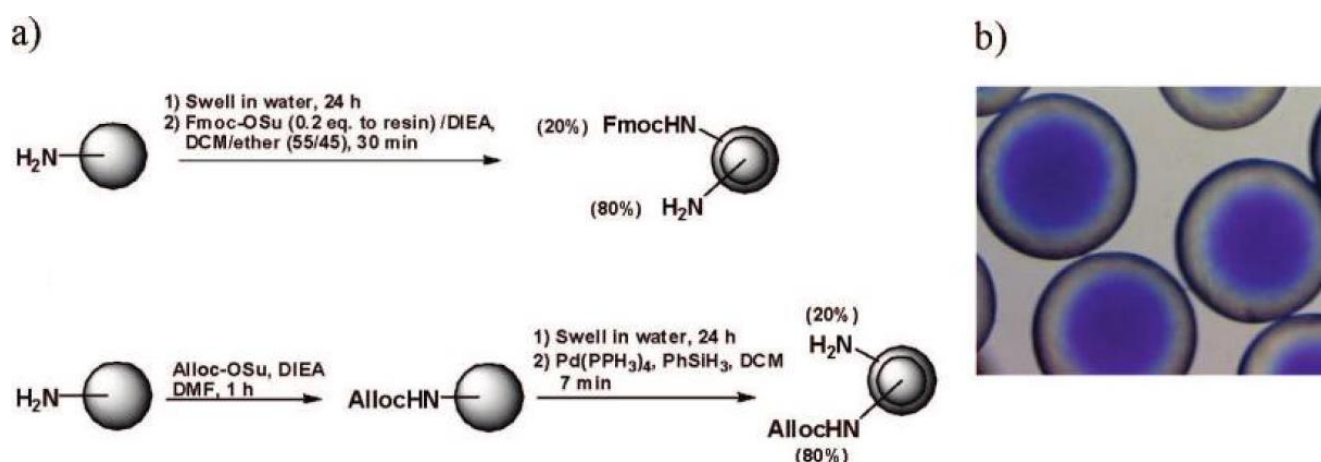
Figure 1.7. OBOC Combinatorial Peptide Library Method. a) Orthogonal solid-phase synthesis of one peptide per bead and b) Colorimetric detection of functionalized peptide bound to the solid support. Figure adapted from Aina, O.H.; et al *Mol. Pharm.* **2007**, *4*, 631-651.[19]

The peptide library screening method may also be developed on living cells, to identify ligands that bind to cell-surface receptors.[16,19] This method can be applied to both suspension and adherent cell cultures (specifically fresh cancer cells isolated from patient blood). This is performed by incubating the cells with the beads under favorable growth conditions. The beads with the appropriate ligands that bind to the cell surface receptors will be coated with a monolayer of cells. Since there are hundreds of different macromolecules on the cell surface, it is reasonably expected that some of the attachments are due to nonspecific binding and thus control experiments are necessary. These include: a) recycling the beads for replicate cell binding experiments (**Figure 1.8**) and b) a dual-color screening method that can allow colorimetric detection of the peptide ligands that have bound to the target cells (**Figure 1.9**).[19]
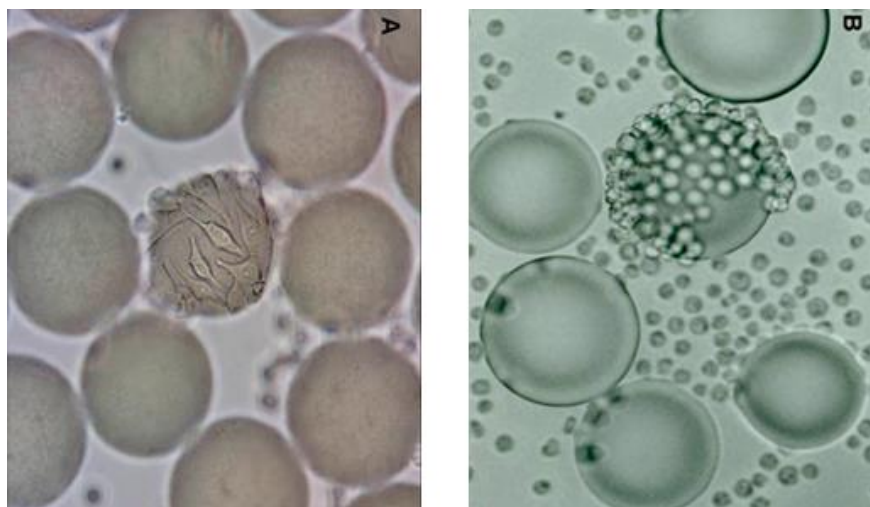
Figure 1.8. Recycling peptide-bound beads for replicate cell adhesion studies. a) The beads initially coated with the cancer cells are isolated and stripped by washing with 8 M guanidinium chloride and re-screened screened against non-cancer cell types. (b) If the beads bind to these non-cancer cells they considered false positives. Figure adapted from Aina, O.H.; et al *Mol. Pharm.* **2007**, *4*, 631-651.[19]
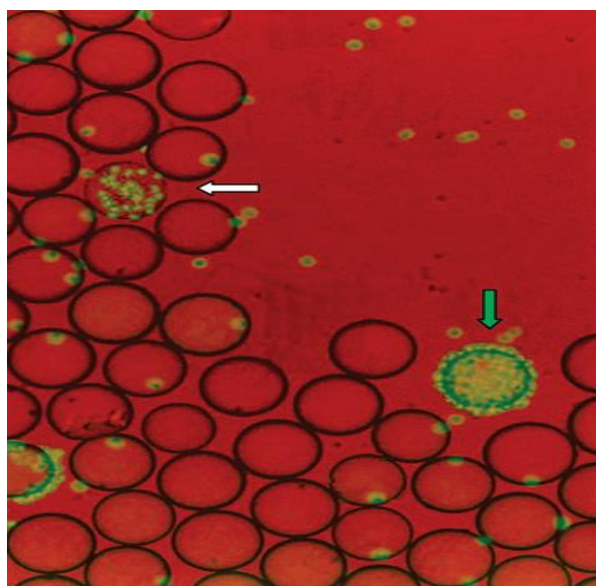
Figure 1.9. Dual-color screening methods involves tagging the cancer cells with a fluorophore (calcein AM) and mixing them with unlabeled non-cancer cells prior to screening with the OBOC library. The beads that only bind to the fluorescent cells are considered "true positive" beads and are isolated and retained. Figure adapted from Aina, O.H.; et al *Mol. Pharm.* **2007**, *4*, 631-651.[19]

In this manner, the selection of potent cancer-targeting peptides armed with anti-cancer or

imaging agents were tested in cancer cell lines and tumor bearing animal models for applications

in tumor-targeted detection and treatment. For example, the structure-function relationships of the hybrid D-peptide sequence (kikmviswkg, HYD-1) on DU145 prostate cancer cells demonstrated the ability to block the attachment of DU145 cells to anti-β1 antibody, fibronectin, laminin 1, laminin 5, collagen IV and dermal fibroblasts. Inhibition of tumor cell adhesion to extracellular matrix proteins and fibroblasts may halt human tumor cell progression and metastasis at distant locations.[32] Another example is associated with the selection of a high affinity peptidomimetic ligand OA02, that targets activated α3β1 integrin overexpressed on the cell surface of ovarian cancer. When conjugated with fluorescent dyes Cy5.5 or Alexa680, this peptide ligand-fluorophore conjugate facilitated imaging of the α3 integrin receptor expressed in ovarian adenocarcinoma xenografts in nude mice.[33]

There are several examples of OBOC combinatorial libraries used in the identification of high-affinity peptide ligands for applications in cancer research.[19] For the scope of our research, we have focused on the identification of peptides that target and bind to cancer cells – cancer targeting peptides.

1.3 MICROARRAY APPLICATIONS

The application of functionalized microarrays has facilitated the high-throughput peptide library screening for the rapid determination of substrate-receptor binding interactions.[34] This screening method has been used to elucidate the binding site domain and the active site residues responsible for high affinity and selective ligand-receptor interactions. Fluorogenic peptide ligands are particularly useful in this application, as measurements in substrate-receptor binding affinity (K_D values) can be determined by fluorescence signaling and quantitative analyses. For example, of the use of an oligonucleotide microarray was used to decode a library of peptide nucleic acid (PNA)-fluorogenic substrates for the protease enzymes (**Figure 1.10**).[35] In this assay an

oligonucleotide microarray is assembled on a glass slide and a combinatorial library of PNAs with 'caged' (inactive) fluorescent labels are added to the support-bound oligonucleotides. Complementary PNA:oligonucleotide sequences will hybridize on the microarray. The functionalized microarray is then incubated with protease enzymes (isolated or in cell lysates) and the PNA substrates are identified by the release of the fluorescent signal following proteolytic cleavage. Since the oligonucleotides are encoded within the microarray, sequence analyses of the fluorescent 'hits' identifies the sequence of the PNA substrates. Quantitative analyses measuring binding affinity (K_D values) and inhibitory activity (IC_{50} values) may also be determined by the intensity of the released fluorophore. These studies may be potentially useful in the identification of lead peptide inhibitors for the extracellular matrix metalloproteinases that have been found to contribute to the invasive behavior of malignant cancer cells.[36]
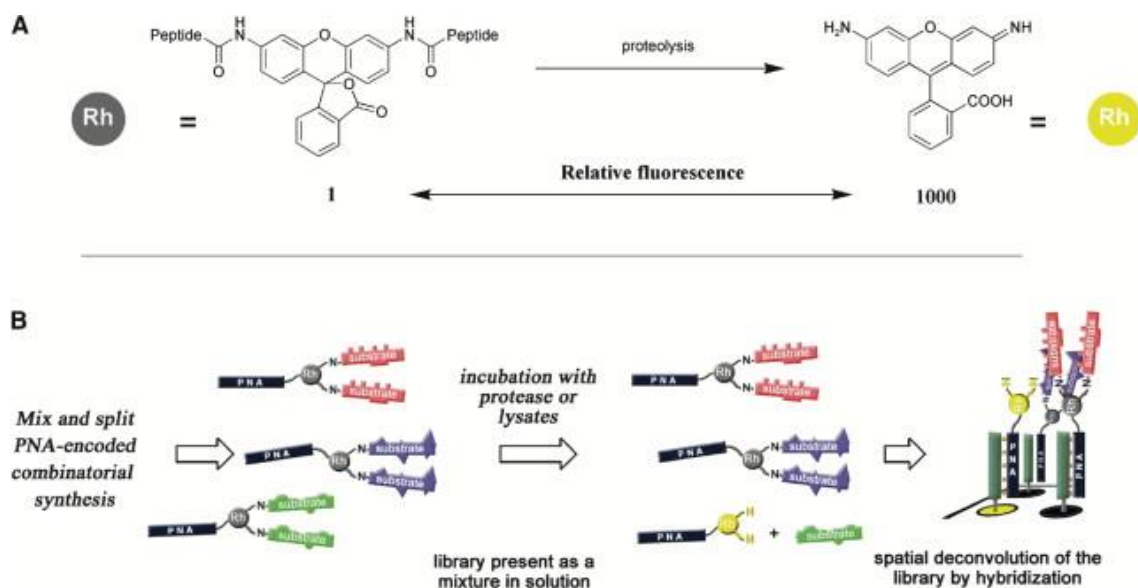
Figure 1.10. Oligonucleotide microarrays for profiling PNA:protease interactions. (a) Caged fluorescent PNAs exhibit fluorescence signaling during proteolysis, and (b) Caged PNA substrates are added and hybridized to an oligonucleotide microarray. Following administration of proteases, fluorescent signaling

on the microarray identifies the location of a PNA substrate for the protease enzyme. Figure adapted from Winssinger, N.; et al *Chem. Biol*. **2004**, *11*, 1351-1360.[35]

1.4 CHARACTERIZATION OF CTP ACTIVITY IN CANCER CELLS AND IN-VIVO

Following the identification of lead peptide ligands of cancer cell surface receptors, the incorporation of imaging and therapeutic agents have respectively facilitated, the characterization and anti-cancer activity of CTPs in cell lines and *in-vivo*. The ^{123}I-labeled RGD peptide and related analogs has been used for the development of integrin-$\alpha_v\beta_3$-targeted radiotracers in imaging rapidly growing metastatic tumors in nude mice.[37,38] Integrin-$\alpha_v\beta_3$ is overexpressed on the surface of activated endothelial cells and cancer cells, and thus serves as a valuable bio-marker in this tumor targeting approach. The radiotracers ^{123}I, ^{18}F, [86]Y, ^{68}Ga, and ^{64}Cu with bifunctional DTPA, DOTA, NOTA, FBOA, TETA, TE2A chelators have all been introduced within RGD peptidomimetics for monitoring tumor angiogenesis *in-vivo* by molecular PET scan imaging (**Figure 1.11**).[38]
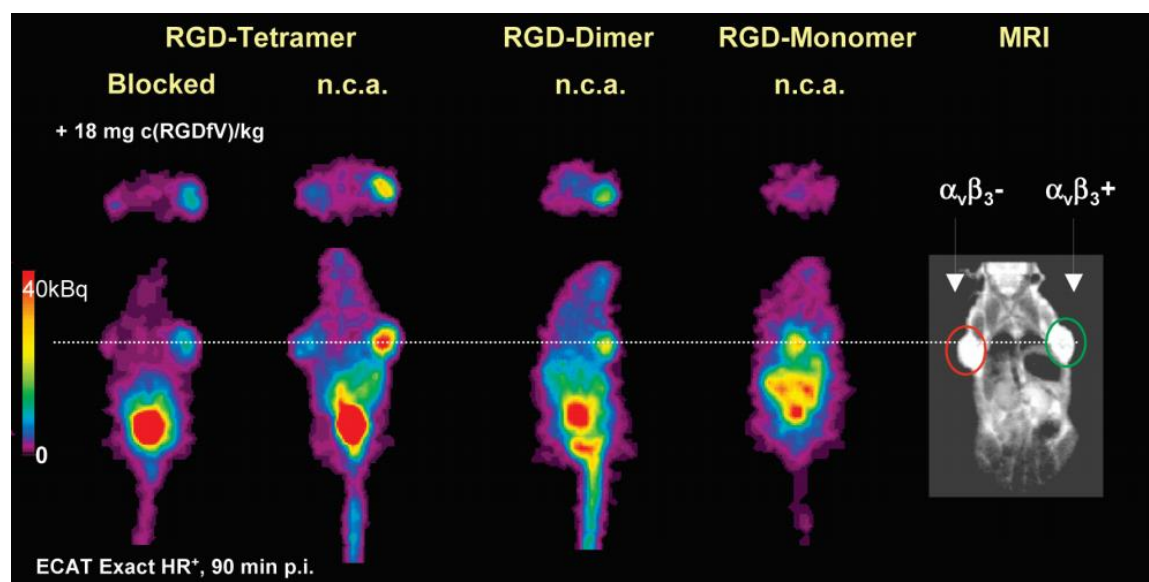
Figure 1.11. PET scan images of nude mice bearing M21 melanoma cancer cells. Mice treated with [cyclo(RGDfE)HEG]$_2$-K)$_2$-K-Dpr—[^{18}F]FBOA identifies the location of high integrin-$\alpha_v\beta_3$ expression at the localized tumor site. Figure adapted from Schottelisu, M.; et al *Acc. Chem. Res.* **2009**, *42*, 969-980.[38]

There are several other cell surface receptors that have been selected and exploited in tumor-targeting approaches.[19] These include: HIF-1, type II TGF-β, and ErbB1, but for the scope of our research we focused on the Glucose Regulated Protein 78 (GRP78). The GRP78 receptor, is a 78 kDa member of the heat shock family of proteins which functions as an intracellular chaperone in the lumen of the endoplasmic reticulum (ER). GRP78 activity is stimulated by the unfolded protein response (UPR) under stress-induced conditions that are typically associated with protein mis-folding events.[39] GRP78 regulates additional intracellular signaling events that are associated with embryonic development, aging, Ca^{2+} homeostasis and insulin/IGF-1 signal transduction applicable to glucose metabolism, cell proliferation and anti-apoptosis.[40] Moreover, GRP78 is expressed in all cell types, where it chaperones protein folding activity in the ER, it interacts with anti-apoptotic executors in the mitochondria and at the cell surface it directs cell signaling.[41]

In cancer, GRP78 is over-expressed and cell surface localized, where it exhibits a variety of signaling pathways which induce cancer initiation, proliferation and metastatic spread.[42] Significantly, GRP78 has been found on the surface of cancer cells but not in normal tissues, thereby making it a valuable biomarker for cancer-targeting therapy approaches.[40-43] Towards this goal, cell surface GRP78 ligands, such as antibodies[44] and short peptides derived from phage display bio-panning experiments[45] have been used to target tumors selectively for anti-cancer activity. For example, Janda and co-workers have reported the phage display peptide library selection of Pep42, a cyclic peptide, CTVALPGGYVRVC-CONH$_2$, that specifically binds to the GRP78 receptor, and internalizes into highly metastatic melanoma cells by receptor-mediated endocytosis.[46] Pep42 has been effectively conjugated with anti-cancer agents such as Taxol, and the pro-apoptotic D-(KLAKLAK)$_2$ sequence triggering programmed cell death specifically in

cancer cell lines and in xenograft mouse models (**Figure 1.12**).[46] Thus, the highly specific Pep42-GRP78 ligand-receptor interaction forms the basis of my thesis objectives, leading towards the development of new and improved drug delivery methods in cancer treatment.
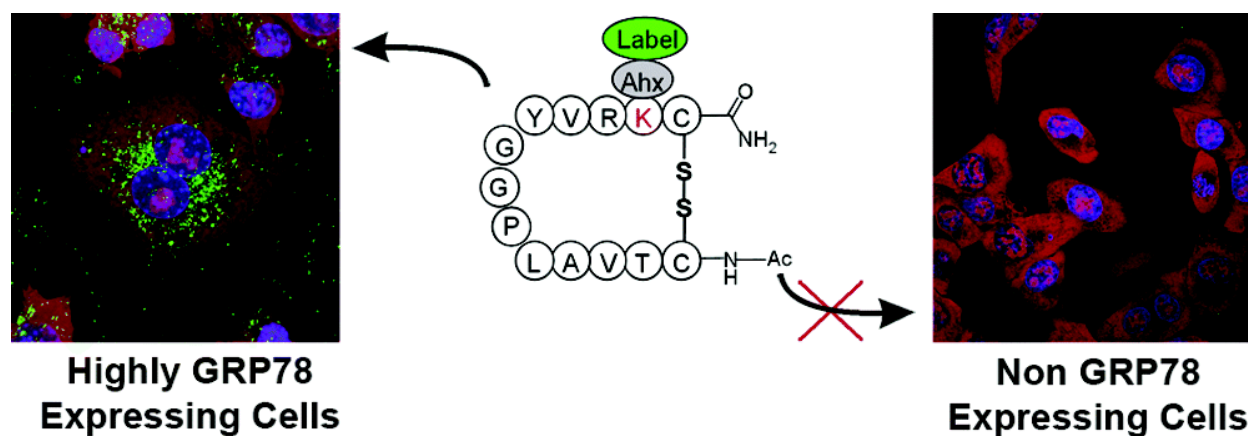
Figure 1.12. Scanning confocal laser fluorescence microscopy images indicating the localization of FITC-labeled Pep42 on the surface of highly GRP78 expressing melanoma cancer cells. [46a] Figure adapted from Kim, Y. et al *Biochemistry* **2006**, *45*, 9434.

1.5 THESIS OBJECTIVES

In hepatoblastoma HepG2 liver cancer cells, GRP78 overexpression was found to play a pivotal role in venous tumor invasion resulting in resistance and metastasis, while underscoring an unmet need to develop more effective treatment methods.[41] Towards this goal, we[43b] along with others[47] have demonstrated that targeting GRP78 overexpression with siRNAs in HepG2 liver cancer cells produce significant GRP78 silencing effects (60-87%), modest cancer cell deaths (~5-10%) and abolished signaling activity for viral entry and infection.[47] Thus, HepG2 cancer cells are clinically relevant tumors for validating our proposed GRP78-targeting strategy.

Towards this ultimate goal, Chapter 2 of this thesis describes the optimized Fmoc-solid phase peptide synthesis of a small library of GRP78-targeting CTPs possessing poly(D/L-Arg)

sequences. The synthetic strategy features an optimization study which compares the influence of the solid-support on peptide synthesis efficiency. Methods for peptide synthesis, LC/MS analyses and purifications are outlined in this chapter.

With pure peptides in hand, structural investigations exploring the potential influence of peptide secondary structures on biological activity was next accomplished. Chapter 3 of this thesis highlights methods in circular dichroism (CD) structural analyses of the CTP sequences. Specifically, the effect of the varying lengths and changes in stereochemistry of the poly(D/L-Arg) sequences on CTP structure and stability were scrutinized.

In order to elucidate the relationship between peptide structure and biologically activity, HepG2 liver cancer cells were cultured as a model and clinically relevant cell line for our GRP78 targeting strategy. Chapter 4 of this thesis highlights peptide biological activity. In collaboration with Dr. Allan D. Blake and students Anthony Maina, Christopher Parronchi, Brittany Blackman Megan Kelly and Mariana Phillips peptides were examined for their biological activity in HepG2 cells and as siRNA delivery agents. These studies are crucial for the development and application of CTPs in our GRP78-targeting approach.

1.6 REFERENCES

1. (a) Thall, P.F.; Cheng, S. *Biometrics*. **1999**, *55*, 746-753., (b) Williams, P.D.; Williams, K.; Lafaver-Roling, S.; Johnson, R.; Williams, A.R. Clin. *J. Oncol. Nurs.* **2011**, *15*, 253-258., (c) Lindley, C.; McCune, J.S.; Thomason, T.E.; Lauder, D.; Sauls, A.; Adkins, S.; Sawyer, W.T. *Cancer Pract.* **1999**, *7*, 59-65.

2. Pirollo, K.F.; Rait, A.; Zhou, Q.; Hwang, S.H.; Dagata, J.A.; Zon, G.; Hogrefe, R.I.; Palchik, G.; Chang, E.H. *Cancer Res.* **2007**, *67*, 2938-2943.

3. Alberici, L.; Roth, L.; Sugahara, K.N.; Agemy, L.; Kotamraju, V.R.; Teesalu, T.; Bordignon, C.; Traversari, C.; Rizzardi, G.P.; Ruoslahti, E. *Cancer Res.* **2013**, *73*, 804-812.

4. Zhao, Y.; Trewyn, B.G.; Slowing, I.I.; Lin, V.S. *J. Am. Chem. Soc.* **2009**, *131*, 8398-8400.

5. McGhee, J.R.; Mestecky, J.; Dertzbaugh, M.T.; Eldridge, J.H.; Hirasawa, M.; Kiyono, H. *Vaccine* **1992**, *10*, 75-88.

6. Weiner, L.M.; Surana, R.; Wang, S. *Nature Rev. Immunol.* **2010**, *10*, 317-327.

7. Goren, D.; Horowitz, A.T.; Zalipsky, S.; Woodle, M.C.; Yarden, Y.; Gabizon, A. *Br. J. Cancer.* **1996**, *74*, 1749-1756.

8. Wulbrand, C.; Seidl, C.; Gaertner, F.C.; Bruchertseifer, F.; Morgenstern, A.; Essler, M.; Senekowitsch-Schmidtke, R. *PLoS One.* **2013**, *8*, e64730.

9. Oraki Kohshour, M.; Mirzaie, S.; Zeinali, M.; Amin, M.; Said Hakhamaneshi, M.; Jalaili, A.; Mosaveri, N.; Jamalan, M. *Chem. Biol. Drug Des.* **2014**, *83*, 259-265.

10. Hall, M.A.; Pinkston, K.L.; Wilganowski, N.; Robinson, H.; Ghosh, P.; Azhdarinia, A.; Vazquez-Arreguin, K.; Kolonin, A.M.; Harvey, B.R.; Sevick-Muraca, E.M. *J. Nucl. Med.* **2012**, *53*, 1427-1437.

11. Chames, P.; Van Regenmortel, M.; Weiss, E.; Baty, D. *Br. J. Pharm.* **2009**, *157*, 220-233.

12. (a) Vives, E.; Schmidt, J.; Pelegrin, A. *Biochim Biophys Acta* **2008**, *1786*, 126-138., (b) Kersemans, V.; Cornelissen, B. *Pharmaceuticals* **2010**, *3*, 600-620., (c) Aina, O.H.; Liu, R.; Sutcliffe, J.L.; Marik, J.; Pan, C.X. Lam KS. *Mol. Pharm.* **2007**, *4*, 631-651.

13. Ye, Y.; Bloch, S.; Xu, B.; Achilefu, S. *J. Med. Chem.* **2006**, *49*, 2268-2275.

14. Janssen, M.L.; Oyen, W.J.; Dijkgraaf, I.; Massuger, L.F.; Freilink, C.; Edwards, D.S.; Rajopadhye, M.; Boonstra, H.; Corstens, F.H.; Boeman, O.C. *Cancer Res.* **2002**, *62*, 6146-6151.

15. Soudy, R.; Gill, A.; Sprules, T.; Lavasanifar, A.; Kaur, K. *J. Med. Chem.* **2011**, *54*, 7523-7534.

16. Peng, L.; Liu, R.; Marik, J.; Wang, X.; Takada, Y.; Lam, K.S. *Nat. Chem. Biol.* **2006**, *7*, 381-391.

17. Dharap, S.S.; Wang, Y.; Chandna, P.; Khandare, J.J.; Qiu, B.; Gunaseelan, S.; Sinko, P.J.; Stein, S.; Farmanfarmaian, A.; Minko, T. *Proc. Natl. Acad. Sci. USA* **2005**, *102*, 12962-12967.

18. (a) Gallop, M.A.; Barrett, R.W.; Dower, W.J.; Fodor, S.P.A.; Gordon, E.M.; *J. Med. Chem.* **1994**, *37*, 1233-1251. (b) Gordon, E.M.; Barrett, R.W.; Dower, W.J.; Fodor, S.P.A.; Gallop, M.A. *J. Med. Chem.* **1994**, *37*, 1385-13401. (c) Balkenhohl, F.; von dem Bussche-Hünnefeld, C.; Lansky, A.; Zechel, C. *Angew. Chem. Int. Ed. Engl.* **1996**, *35*, 2288-2337. (d) Thompson, L.A.; Ellman, J.A.; *Chem. Rev.* **1996**, *96*, 555-600. (e) Antel, J. *Curr. Opin. Drug Discov. Devel.* **1999**, *2*, 224-233. (f) Martin, E.J.; Blaney, J.M.; Siani, M.A.; Spellmeyer, D.C.; Wong, A.K.; Moos, W.H. *J. Med. Chem.* **1995**, *38*, 1431-1436. (g) Smith, G.P.; Scott, J.K. *Methods Enzymol.* **1993**, *217*, 228-257. (h) Fecik, R.A.; Frank, K.E.; Gentry, E.J.; Menon, S.R.; Mitscher, l.A.; Telikepalli, H. *Med. Res. Rev.* **1998**, *18*, 149-185.

19. Aina, O.H.; Liu, R.; Sutcliffe, J.L.; Marik, J.; Pan, C.X.; Lam, K.S. *Mol. Pharm.* **2007**, *4*, 631-651.

20. Geysen, H.M.; Meloen, R.H.; Barteling, S.J. *Proc. Natl. Acad. Sci. USA* **1984**, *81*, 3998-4002.

21. Coin, I.; Beyermann, M.; Bienert, M. *Nat. Protoc.* **2007**, *2*, 3247-3256.

22. Hood, C.A.; Fuentes, G.; Patel, H.; Page, K.; Menakuru, M.; Park, J.H. *J. Pept. Sci.* **2008**, *14*, 97-101.

23. Bacsa, B.; Horváti, K.; Bõsze, S.; Andreae, F.; Kappe, C.O. *J. Org. Chem.* **2008**, *73*, 7532-7542.

24. Kay, B.K.; Kasanov, J.; Yamabhai, M. *Methods* **2001**, *24*, 240-246.

25. El-Mousawi, M.; Tchistiakova, L.; Yurchenko, L.; Pietrzynski, G.; Moreno, M.; Stanimirovic, D.; Ahmad, D.; Alakhov, V. *J. Biol. Chem.* **2003**, *278*, 46681-46691.

26. Ding, H.; Prodinger, W.M.; Kopecek, J. *Bioconj. Chem.* **2006**, *17*, 517-523.

27. Ballinger, M.D.; Shyamala, V.; Forrest, L.D.; Deuter-Reinhard, M.; Doyle, L.V.; Wang, J.X.; Panganiban-Lustan, L.; Stratton, J.R.; Apell, G.; Winter, J.A.; Doyle, M.V.; Rosenberg, S.; Kavanaugh, W.M. *Nat. Biotechnol.* **1999**, *17*, 1199-1204.

28. Wu, H-C.; Chang, D-K.; Huang, C-T. *J. Cancer Mol.* **2006**, *2*, 57-66.

29. Dooley, C.T.; Chung, N.N.; Wilkes, B.C.; Schiller, P.W.; Bidlack, J.M.; Pasternak, G.W.; Houghten, R.A. *Science* **1994**, *266*, 2019.

30. (a) Furka, A.; Sebestyen, F.; Asgedom, M.; Dibo, G. *Int. J. Pept. Protein Res.* **1991**, 37, 487-493. (b) Lam, K.S.; Salmon, S.E.; Hersh, E.M.; Hruby, V.J.; Kazmierski, W.M.; Knapp, R.J. *Nature* **1991**, *354*, 82-84. (c) Zuckermann, R.N.; Kerr, J.M.; Siani, M.A.; Banville, S.C. *Int. J. Pept. Protein Res.* **1992**, *40*, 498.

31. Affleck, R.L. *Curr. Opin. Chem. Biol.* **2001**, *5*, 257-263.

32. DeRoock, I.B.; Pennington, M.E.; Sroka, T.C.; Lam, K.S.; Bowden, G.T.; Bair, E.L.; Cress, A.E. *Cancer Res.* **2001**, *61*, 3308-3313.

33. Aina, O.H.; Marik, J.; Liu, R.; Lau, D.H.; Lam, K.S. *Mol. Cancer Ther.* **2005**, *4*, 806-813.

34. Goodrich, T.T.; Wark, A.W.; Corn, R.M.; Lee, H.J. *Methods Mol. Biol.* **2006**, *328*, 113-130.

35. Winssinger, N.; Damoiseaux, R.; Tully, D.C.; Geierstanger, B.H.; Burdick, K.; Harris, J.L. *Chem. Biol.* **2004**, *11*, 1351-1360.

36. Stetler-Stevenson, W.G.; Gavil, N.V. *Connect Tissue Res.* **2014**, *55*, 13.

37. Haubner, R.; Wester, H.J. *Curr. Pharm. Des.* **2004**, *10*, 1439-1455.

38. Schottelisu, M. Laufer, B.; Kessler, H.; Wester, H.J. *Acc. Chem. Res.* **2009**, 42, 969-980.

39. (a) Lee, A.S. *Methods* **2005**, *35*, 373., (b) Kaufman, R.J. *Genes Dev.* **1999**, *13*, 1211.

40. (a) Pfaffenbach, K.T.; Lee, A.S. *Curr. Opin. Cell Biol.* **2011**, *23*, 150., (b) Rao, R.V.; Peel, A.; Logvinova, A.; del Rio, G.; Hermel, E.; Yokota, T.; Goldsmith, P.C.; Ellerby, L.M.; Ellerby, H.M.; Bredesen, D.E. *FEBS Lett.* **2002**, *514*, 122. (c) Shin, B.Y.; Wang, H;, Yim, A.M.; LaNour, F.; Brichory, F.; Jang, J.H.; Zhao, R.; Puravs, E.; Tra, J.; Michael, C.W.; Misek, D.E.; Hanash, S.M. *J. Biol. Chem.* **2003**, 278, 7607.

41. Zhang, L.H.; Zhang, X. *J. Cell. Biochem.* **2010**, *110*, 1299.

42. Lee A.S. *Cancer Res.* **2007**, *67*, 3496.

43. (a) Patel, P.; Hanawa, E.; Yadav, R.; Samuni, U.; Marzabadi, C.; Sabatino, D. *Bioorg. Med. Chem. Lett.* **2013**, *23*, 5086-5090. (b) Maina, A.; Blackman, B.A.; Parronchi,

C.J.; Morozko, E.; Bender, M.E.; Blake, A.D.; Sabatino, D. *Bioorg. Med. Chem. Lett.* **2013**, *23*, 5270-5274.

44. Misra, U.K.; Pizzo, S.V. *Cancer Biol. Ther.* **2010**, *9*, 142.

45. Arap, M.A. *Genet. Mol. Biol.* **2005**, *28*, 1.

46. (a) Kim, Y.; Lillo, A.M.; Steiniger, S.C.; Liu, Y.; Ballatore, C.; Anichini, A.; Mortarini, R.; Kaufmann, G.F.; Zhou, B.; Felding-Habermann, B.; Janda, K.D. *Biochemistry* **2006**, *45*, 9434. (b) Liu, Y.; Steiniger, S.C.; Kim, Y.; Kaufmann, G.F.; Felding–Habermann, B.; Janda, K.D. *Mol. Pharm.* **2007**, *4*, 435-447. (c) Yoneda, Y.; Steiniger, S.C.; Capková, K.; Mee, J.M.; Liu, Y.; Kaufmann, G.F.; Janda, K.D. *Bioorg. Med. Chem. Lett.* **2008**, *18*, 1632.

47. Alhoot, M.A.; Wang, S.M.; Sekaran, S.D. *PLoS One.* **2012**, *7*, e34060.

CHAPTER 2: SYNTHESIS AND CHARACTERIZATION OF POLY(ARGININE) DERIVED CANCER-TARGETING PEPTIDES

2.1 ABSTRACT

The solid-phase synthesis and characterization of a new library (16) of GRP78 cancer-targeting peptides possessing varying lengths (0-12) of poly(D/L-Arg) sequences have been synthesized, purified and analyzed by LC/MS in this chapter. These peptides are based on the highly specific Pep42 cyclic sequence, H_2N-CTVALPGGYVRVC-$CONH_2$, which has been shown to target the Glucose-Regulated Protein 78 (GRP78) receptors over-expressed on the cell surface of cancer cells. In this study, Pep42 derived poly(arginine) peptides were effectively synthesized by Fmoc-based solid-phase peptide synthesis (SPPS). The use of various Rink amide-linker resins based on the polystyrene-divinylbenzene (PS-DVB), polystyrene-grafted-poly(ethylene glycol) (TentaGel) and poly(ethylene glycol) (NovaPEG) were explored to optimize the SPPS method. Peptide sequences prepared on a hydrophilic (NovaPEG) resin ultimately provided the best results, generating good yields (12-46%) and crude purities >90% following LC/MS analyses. These sequences were further purified by RP-HPLC methods to increase purities (>95%) in preparation for structural, biophysical studies (Chapter 3) and biology (Chapter 4).

2.2 INTRODUCTION
2.2.1 RATIONAL DESIGN OF POLY(ARGININE) DERIVED PEP42 SEQUENCES

As highlighted in Chapter 1, the screening of phage display peptide libraries against tumor cells has isolated a peptide ligand that binds specifically and with high affinity to cell surface GRP78.[1] The GRP78 receptor is localized on the cell surface of cancer cells and not on healthy ones making it a viable biomarker for the development of cancer-targeting approaches.[2] Towards this goal, the Pep42 ligand, corresponding to a cyclic 13-mer sequence, namely H_2N-CTVALPGGYVRVC-$CONH_2$, **7**, was found to bind to GRP78 and internalize anti-cancer drugs

within tumor cells for more potent and selective cancer cell death relative to the administration of anti-cancer drugs without Pep42.[1]

Arginine-rich peptides are a class of cell-permeable peptides that possess the ability to bind to negatively charged bio-molecules, such as the short-interfering RNA (siRNA) and facilitate their cell translocation for RNA interference (RNAi) activity.[3] Moreover, there has been a correlation between cell permeability and the increase in the number of arginine residues (6-12) which elicit optimal translocation activity.[4] Although arginine-rich peptides are highly efficient in mediating *in vitro* cellular uptake of siRNA for bio-activity, their *in vivo* application has been limited by poor specificity, as these peptides are dispersed in almost all cell types.[5]

Thus, combining the tumor-homing capabilities of Pep42, with the poly-arginine sequences known to facilitate siRNA delivery for RNAi activity forms the basis of our new GRP78-targeting gene therapy approach. These two properties produces a drug delivery vehicle that possesses the ability to seek and destroy cancer cells (**Figure 2.1**), with a selectivity that is absent in traditional chemotherapy or radiation treatments. Therefore, our proposed cancer-targeted gene therapy approach aims to produce and new and improved form of cancer therapy.

Targeting Domain   **Complexing Domain**

CTP Sequence: NH_2 - CTVALPGGYVRVC -$(R)_n$- $CONH_2$ n = 0,3,6,9,12

-GRP78 receptor ligand for tumor cell targeting   -poly(Arg) sequence for siRNA binding and cell permeability
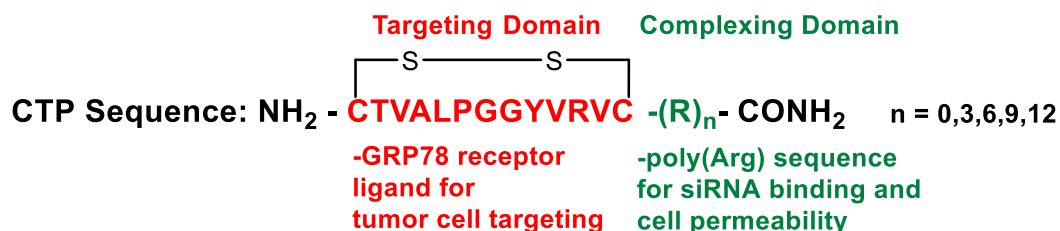
Figure 2.1. Rational design of CTPs synthesized and characterized in this study.

2.2.2 SOLID PHASE PEPTIDE SYNTHESIS (SPPS) METHOD

The solid phase peptide synthesis (SPPS) method has emerged as the method of choice for the rapid production of short (3-5) to medium (20-30) length peptides. The use of an insoluble

polymer support has replaced the solution phase synthesis of peptides. These methods circumvent the need for laborious reaction, work-up and purification steps following each coupling and deprotection procedure.[6] SPPS was pioneered by Bruce Merrifield, who first reported the synthesis of a model tetrapeptide (LAGV) on a polymer bead and was later awarded the Noble prize in Chemistry (1984) for his discovery.[7] SPPS has since then unleashed a wide range of natural and un-natural peptides for applications in biology, chemistry and therapy. In this chapter, methods for SPPS are highlighted and specifically applied to the production of a new class of poly(arginine) cancer-targeting peptides.

Fmoc-SPPS has emerged as the solid phase method of choice for the production of peptides. This strategy features the use of a fluorenylmethyloxycarbonyl (Fmoc) protecting group at the *N*-terminus of the amino acid in order to facilitate its introduction into the SPPS procedure.[8] The first step involves the selection of a suitable polymer support (resin) for the synthesis of the desired peptide sequence. Historically, the Merrifield resin was employed in the synthesis of short sequences that did not require side-chain protecting groups.[7] The Merrifield resin is composed of a polystyrene-divinylbenzene (PS-DVB) cross-linked core (**Figure 2.2A**) and a suitable linker for the production of peptide acids[9] and amides.[10] For the preparation of lengthier and more challenging hydrophobic sequences that are prone to aggregation which diminishes the synthesis efficiency more polar solid-supports have been produced. Resins that have greater swelling tendencies in polar aprotic solvents such as DMF, the solvent of choice in the SPPS procedure have been developed. For example, the amphiphilic polystyrene-graft-poly(ethylene glycol) resin (TentaGel, **Figure 2.2B**),[11] has been used in the solid-phase synthesis of difficult peptide sequences, including peptoids and fluorescently labeled peptides. Recently, a polar poly(ethylene

glycol) (NovaPEG, **Figure 2.2C**)[12] resin has been developed for the efficient preparation of challenging hydrophobic peptides such as the beta-amyloid (1-42).
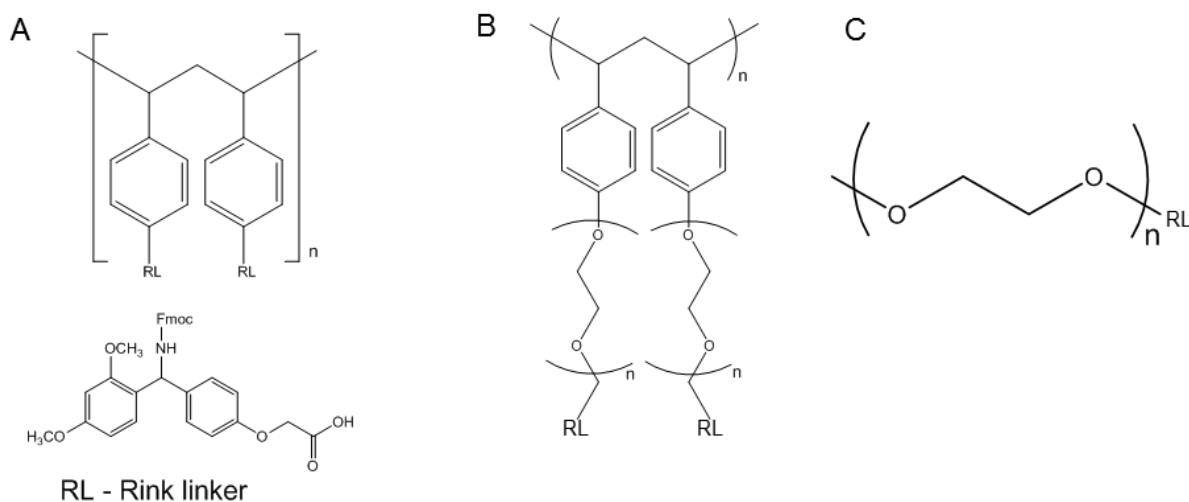
Figure 2.2. Three different resins for Fmoc-SPPS: A) Rink amide-linker polystyrene-divinylbenzene (PS-DVB) B) Rink amide-linker amphiphilic polystyrene-graft-poly(ethylene glycol) resin (TentaGel), and C) poly(ethylene glycol) (NovaPEG).

Following the judicious selection of an insoluble polymer support, the coupling of the *N*-Fmoc amino acid to the solid support is effected by a coupling reagent. The coupling reagent typically functions to convert the *C*-terminal carboxylic acid to a reactive ester which favors coupling to the amino (peptide amides) or hydroxyl (peptide acids) groups on the solid support. Moreover, coupling reagents also facilitate the key peptide bond forming reactions between the *N*-terminal peptide bound support and the *C*-terminal active ester of the coupling *N*-Fmoc amino acid. Many coupling reagents for SPPS have been reported in the literature,[13] among the most useful are the carbodiimide-based couplings. In this case, *N,N'*-diisopropylcarbodiimide (DIC) and 1-hydroxybenzotriazole (HOBt) have been used for the efficient Fmoc-SPPS of a 51-mer peptide bearing the main heparin binding site (60-110) of human pleiotrophin (hPTN).[14] The total synthesis of hPTN was assisted with microwave (MW) radiation, which allowed completion of the MW-

SPPS procedure in 30 hours. This optimized method produced the desired peptide in 51% crude yield and >99% purities following RP-HPLC purification. More reactive coupling reagents have been developed, particularly based on the uronium coupling agents. For instance, *O*-(1H-6-chlorobenzotriazole-1-yl)-1,1,3,3-tetramethyluronium hexafluorophosphate (HCTU) worked particularly well in the solid phase synthesis of challenging peptides with coupling times as short as 1 minute.[15]

The coupling procedure is followed by an Fmoc deprotection step, in which a secondary alkylamine is used to effect the elimination of the Fmoc group without concomitant epimerization of the peptide-bound support. Towards this goal, dilute solutions of alkylamines (*i.e.* 20% piperidine in DMF or 10% piperidine in EtOH/NMP, 10:90 v/v) have been used to generate the fully optimized Fmoc-SPPS (**Figure 2.3**) procedure of a variety of peptide and peptidomimetic sequences. The modern Fmoc-SPPS method is automated and optimized with microwave heating to effect rapid and high yielding coupling and deprotection steps.[16] Following synthesis, peptide cleavage from the solid support and deprotection of side-chain protecting groups are typically accomplished with concentrated trifluoroacetic acid (TFA) with minimal addition (<5%) of reaction scavengers (*i.e.* H_2O, triethylsilane, phenol). These conditions minimize side-product formation and yields the crude peptide in solution for analysis and purification. Thus, the Fmoc-SPPS method is the method of choice for the production of the poly(arginine) derived Pep42 sequences described in this chapter (**Table 2.1**).
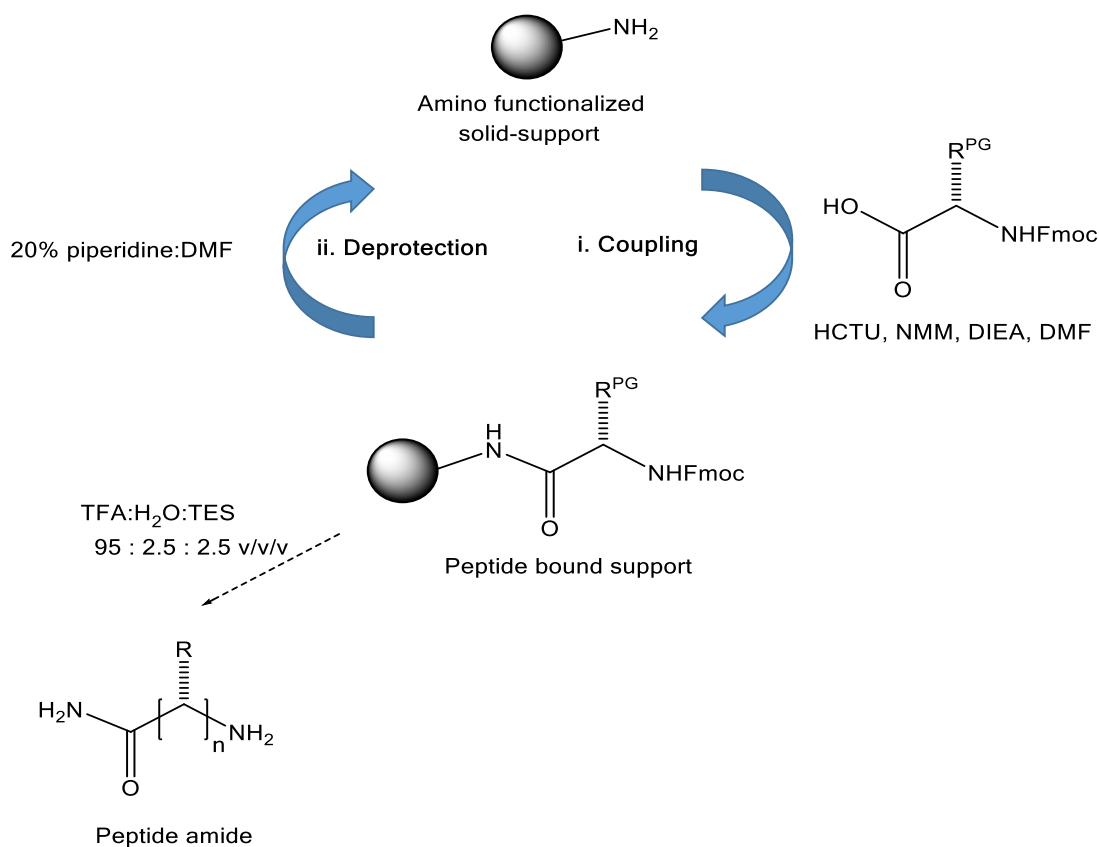
Figure 2.3. Fmoc-Solid Phase Peptide Synthesis (SPPS) method.

2.3 CHAPTER OBJECTIVES

The main objective of this thesis chapter involves the production of an optimal Fmoc-SPPS method for the preparation of the Pep42-poly(arginine) sequences. This optimization procedure studies the influence of the resin on peptide synthesis efficiency. In this study, the non-polar PS-DVB resin was compared to the amphipathic Tentagel and polar NovaPEG resins to determine which solid support fares best in the synthesis procedure. The efficiency of the SPPS method was determined by the peptide % yield recovery and the crude % purity. Following peptide purification by RP-HPLC and characterization by LC/MS, samples were ready for follow-up studies exploring peptide structure, biophysical and biological properties (Chapters 3 and 4).

2.4 RESULTS AND DISCUSSION
2.4.1. FMOC-SPPS OF PEP42-POLY(ARGININE) SEQUENCES

The first aim of this study was to synthesize the peptides in the highest yields and purities.[17] To achieve this goal, Fmoc-SPPS conditions were initially optimized for the hydrophobic Pep42 CTP sequence: H_2N-CTVALPGGYVRVC-$CONH_2$, **2.1**,[1] (**Figure 2.4A**) on a conventional Rink amide-linker Merrifield resin, consisting of a polystyrene-divinylbenzene (PS-DVB) cross-linked core[11] (**Figure 2.3A**). Under these conditions Pep42 crude purities of only 28% was achieved upon analysis by RP-HPLC, (**Figure 2.4B**) indicating that the Fmoc-SPPS conditions with the PS-DVB resin required improvement for the production of Pep42 (**Table 2.1, sequence 2.1**).

In an attempt to improve Pep42 synthesis efficiency, the influence of the solid support on peptide synthesis was next explored. Specifically, the use of more polar resins relative to the PS-DVB support produced encouraging results in related hydrophobic sequences.[11,12,18] The success of solid phase peptide synthesis is strongly related to the solid support chosen and its performance. Using the mole ratio of 1:3:3:6 of resin:Fmoc-amino acid:HCTU:NMM in DMF there should be a balance between the swelling and loading capabilities when choosing a type of resin. Since there is no general rule to decide which type of resin should be used, we considered several properties such as swelling-solvent ratio, length of the desired sequences and the hydrophobicity of the sequence. With lower resin loadings on the more hydrophilic resins such as the NovaPEG, increase swelling properties have been found in DMF leading to enhanced synthesis efficiencies.[12] Conversely, on the higher loading hydrophobic polystyrene resins, less swelling was noticed in DMF which lead to a decrease in synthetic efficiency. Thus, CTP **2.1** was equally prepared on a Rink amide-linker amphiphilic polystyrene-*graft*-poly(ethylene glycol) (TentaGel)[11] and hydrophilic poly(ethylene glycol) (NovaPEG)[12] based solid supports (**Figure 2.3, B and C**) in order to explore the influence of the solid support on peptide synthesis. In these cases, peptide

28

crude purities improved from 28% on a PS-DVB support, to 67% on Tentagel S RAM resin (**Figure 2.4C**) and ultimately to 93% on a poly(ethylene glycol) Rink Amide NovaPEG resin (**Figure 2.4D**). Isolated yields of 14% (15 mg) were recovered for Pep42 on a NovaPEG resin, illustrating sufficient peptide recovery for structure, biophysical and biological studies (Chapters 3 and 4).

With optimized conditions for the synthesis of CTP **2.1**, poly(arginine) derived Pep42, **2.2**, containing a tri(arginine) sequence at the *C*-terminus was made on the Tentagel and NovaPEG resins. The use of more polar solid supports had been reported in the literature to improve synthesis yields and purities of poly(Arg) sequences.[18] In the case of Pep42-R3, **2.2**, an increase in the polarity of the solid support resulted in greater peptide crude purities (69% to 98%) with the Tentagel S RAM and NovaPEG resins, respectively (**Table 2.1**). The unique composition of the NovaPEG polymer matrix affords excellent swelling capabilities in polar aprotic solvents that are commonly used in the SPPS method (*i.e.* DMF or NMP). This feature increases the surface area for reaction on solid phase producing peptides of high quality.[12,18] This is particularly useful in the preparation of amphiphilic sequences such as the Pep42-poly(arginine) series. Similar amphipathic peptides have been shown to aggregate during the course of the SPPS method resulting in diminished yields and purities.[12,16-18] Moreover, poly(arginine) sequences have been particularly difficult to synthesize by conventional Fmoc-SPPS. This is reportedly due to the high steric hindrance and difficulty in deprotection of the arginine side-chain Pbf protecting groups in addition to pre-mature cleavage from the solid support that results from δ-lactam formation (**Figure 2.5**).[18,19] In spite of these hurdles, good synthesis efficiencies (crude purities 93-98%) and recoveries (14-46%) were obtained for the Pep42-poly(arginine) series on a NovaPEG resin (**Table 2.1**), underscoring the importance of the resin in the synthesis of challenging sequences.
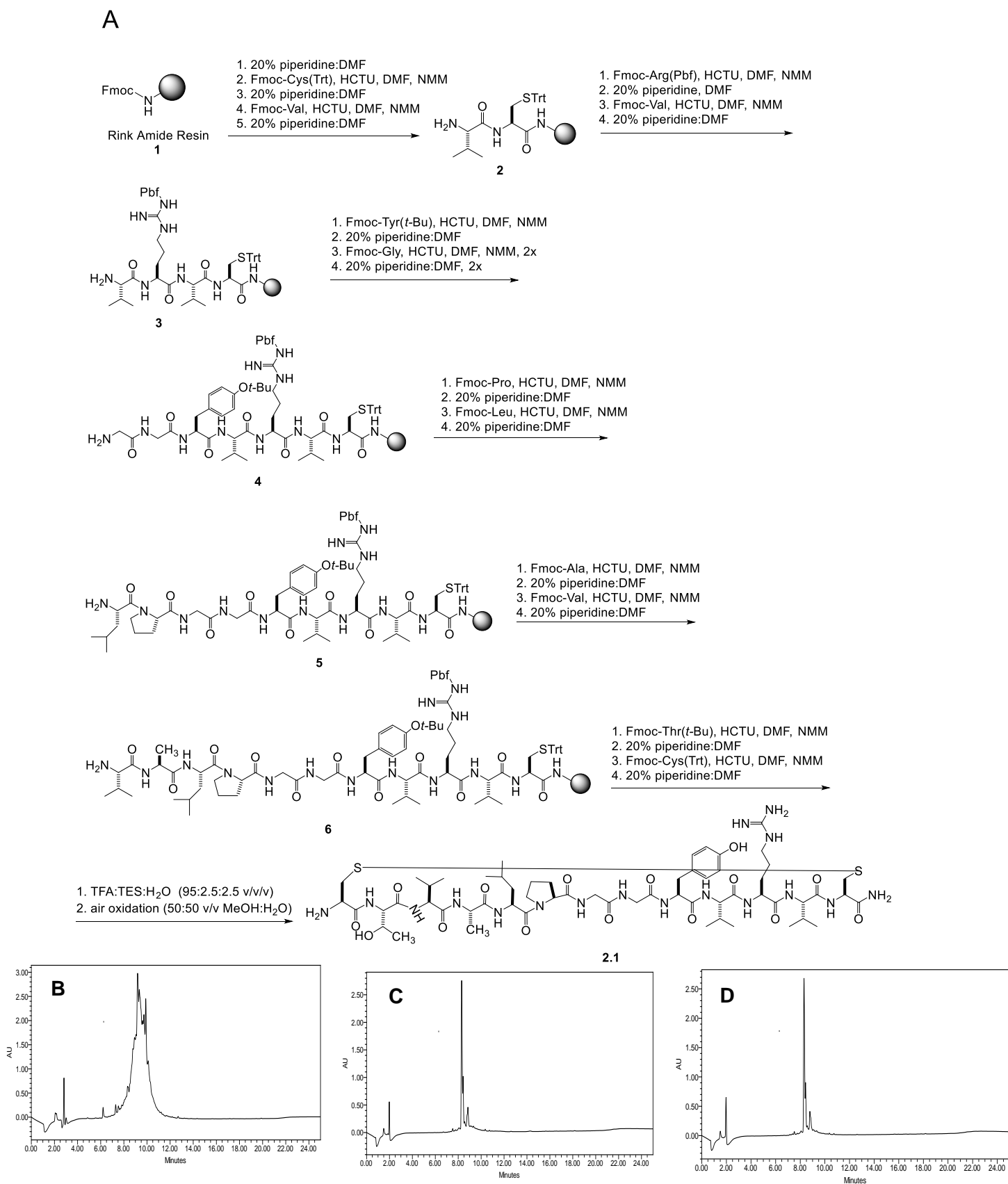
Figure 2.4. Synthesis and characterization of Pep42, **(Table 2.1, sequence 2.1)** A) Fmoc-based Solid Phase Peptide Synthesis and RP-HPLC chromatograms at 214 nm on Rink Amide B) Merrifield C) TentaGel and D) NovaPEG resins.

With the synthesis condition optimized for the Pep42-poly(L-agrinine) series (**Table 2.1, sequences 2.2-2.5**) we synthesized a series of Pep42-poly(D-arginine) sequences (**Table 2.1, sequences 2.6-2.9**) using the same conditions. This Pep42-poly(D-arginine) series was synthesized in order to investigate their stability versus that of the Pep42-poly(L-arginine) series. It is also worthwhile to note that similar synthesis efficiencies (crude purities 86->95%) and recoveries (18-37%) were observed for the Pep42-poly(D-arginine) series (**Table 2.1, sequences 2.6-2.9**). These peptide sequences were synthesized using conventional Fmoc-SPPS on a hydrophilic NovaPEG resin with conditions that were optimized for the Pep42-poly(Arg) series. This highlights the method's ability to incorporate un-natural amino acids that may ultimately improve peptide pharmacokinetic properties.[20]

P = Protecting Group
X = Leaving Group
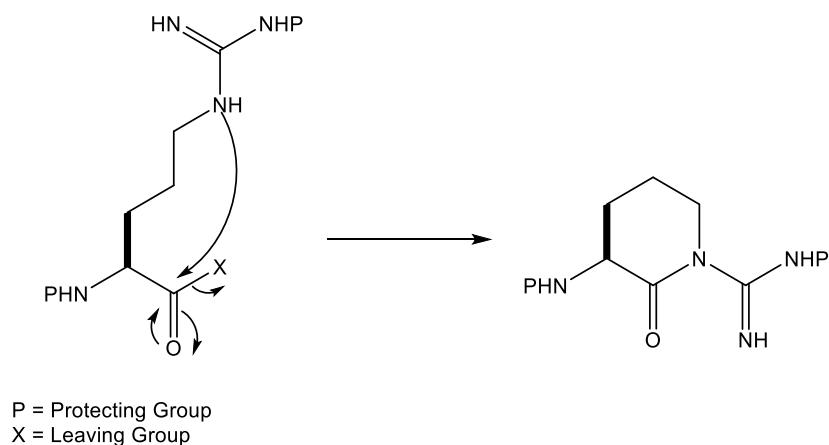
Figure 2.5. Intramolecular cyclization of arginine to the resulting δ-lactam.[18,19] Figure adapted from Garcia-Ramos, Y. et al *J. Pept. Sci.* **2010**, *16*, 675.

In the cleavage and deprotection step we used TFA as the side chain protecting groups of the amino acids are acid labile. This cleavage and deprotection mixture contained TES which acts as a scavenger preventing any side reactions as the protecting groups are being removed ensuring that the desired peptide sequence is intact. The final step following peptide cleavage and

deprotection from the solid support involves the oxidation of the cysteinyl residues to the cyclic disulfide-linked peptides. Recent studies have shown that there is no internalization of the linear reduced form of Pep42 (**Table 2.1 sequence 2.1**) within cancer cells, demonstrating that the cyclic constraint is a crucial structural element for Pep42 cellular binding and internalization.[1] There are various oxidation techniques for the formation of disulfide bonds in peptides and proteins. These include: Ellman's reagent: 5,5′-dithiobis(2-nitrobenzoic acid),[21] potassium ferricyanide,[22] iodine[23] and DMSO,[24] in addition to air oxidation, which involves bubbling a stream of air into the cleavage cocktail.[25] The latter air oxidation method was used in the cyclization step of the Pep42-poly(arginine) sequences synthesized in this study (**Table 2.1**). To evaluate the drug delivery capabilities of CTPs (**Table 2.1, sequences 2.1-2.9)** within cell-based assays, CTPs were fluorescently tagged with fluorescein isothiocyanate (FITC).[26] The FITC fluorophore (λ_{abs}: 494 nm and λ_{em}: 521 nm) was introduced at the *N*-terminus of the CTP sequences to minimize its influence on the biological activity of the peptides. FITC can also react with the sulfhydryl groups of reduced cysteines and the ε-amino of lysines[27] resulting in unwanted side-reactions and with the *N*-terminal residue leading to its deletion from the sequence (**Figure 2.6**).[28] This reaction follows the Edman degradation pathway affording a fluorescent thiohydantoin (FTH) from the last α-amino acid of the peptide sequence. This reaction can be avoided by introduction of a non-α amino acid spacer between thiourea bond and the peptide. Therefore, an aminohexanoic acid (ε-Ahx) spacer was added to inhibit these side-reactions and lead to the formation of stable FITC-labeled sequences (**Table 2.1, sequences 2.10-2.15**).[26]
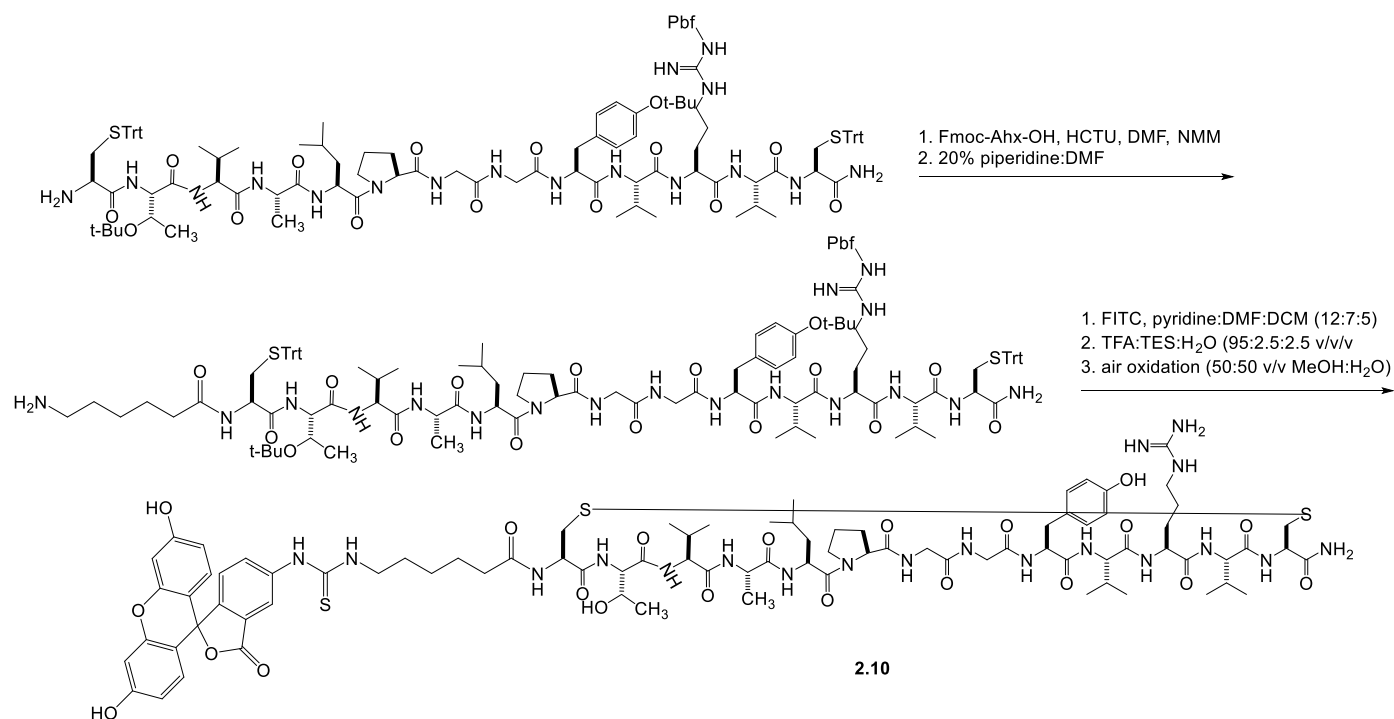
Figure 2.6. FITC-cleavage of the *N*-terminal residue of the peptide bound to the solid support.

2.4.2 ANALYSIS AND PURIFICATION OF PEP42-POLY(ARGININE) SEQUENCES BY LC/MS

Following synthesis of this small library of synthetic peptides (**2.1-2.15**), their purities were determined by RP-HPLC and identities ascertained by molecular weight analyses using LC/MS. The use of an octadecyl (C18) reverse-phase column, packed with 60 Å pore size silica was found to be perfectly suitable for the HPLC analyses of the synthetic peptides.[29] Considering the synthetic peptides vary in length of the poly(Arg) sequences (0-12 residues), the Pep42-poly(arginine) series were found to exhibit a wide range of polarities which influenced solubility, analyses and separation. For example, the Pep42 sequence was found to be rather hydrophobic in comparison to those derived with the poly(Arg) sequences. This is particularly due to the multiple non-polar (Val, Ala, Leu, Ile and Tyr) residues which diminished water solubility. In contrast, peptides with

33

increasing poly(Arg) sequences (3-12) enhanced water solubility while also maintaining solubility in organic solvents such as MeOH and MeCN. In all cases, peptide samples were prepared in a combination of H_2O:MeOH or MeCN (50:50 v/v, 1.0 mL) with minimal addition of an ion-pairing reagent (0.1% TFA or FA) to enhance dissolution for RP-HPLC analyses. RP-HPLC of the peptides (**Table 2.1, sequences 2.1-2.14**) was established with a gradient method of MeCN-H_2O and MeOH-H_2O (2-82%, 1.0 mL/min, 18 min) with TFA (0.1%) as acidic ion pairing reagent that provided the best resolution of the crude peptide samples in combination with H_2O:MeCN (**Figure 2.7**). The peak purities of the peptide sequences were monitored at 214 nm with a photodiode array (PDA) detector. This wavelength is characteristic of the amide bond absorption which provides the most accurate quantitative determination of peptide purities during analyses.[30] This is because all peptides are composed of the same peptide backbone, thereby making the analyses not sequence specific and also not contingent on the eluent system (λ_{MeOH}: 205 nm and λ_{MeCN}: 190 nm). With these conditions, peptides were analyzed with good crude purities (>90%) following SPPS and the post-synthesis work-up procedures (**Table 2.1**).

Considering peptide purity is of paramount importance for structure-activity relationship studies (Chapter 3 and 4), semi-preparative RP-HPLC was next accomplished (YMC-Pack ODS-A C18 column 20 x 250 mm, 5.0 µm particle size). Peptide samples were recovered from the purifications, and analyzed by LC/MS to validate peptide purity (>95%) and identity by molecular weight confirmation. For the latter, ESI-MS was selected as the method of choice for peptide characterization.[31] ESI-MS is a mild ionization method producing minimal fragmentation during the analyses. In the case of the Pep42-poly(arginine) sequences, the desired molecular weights were observed as mass:charge (*m/z*) ratios that were contingent on the number of charged arginine residues found within the sequences (**Table 2.1**).

A

	RT	% Area
1	7.960	1.74
2	8.219	96.60
3	10.193	1.66

B

	RT	% Area
1	8.021	97.32
2	9.547	0.94
3	11.613	1.74
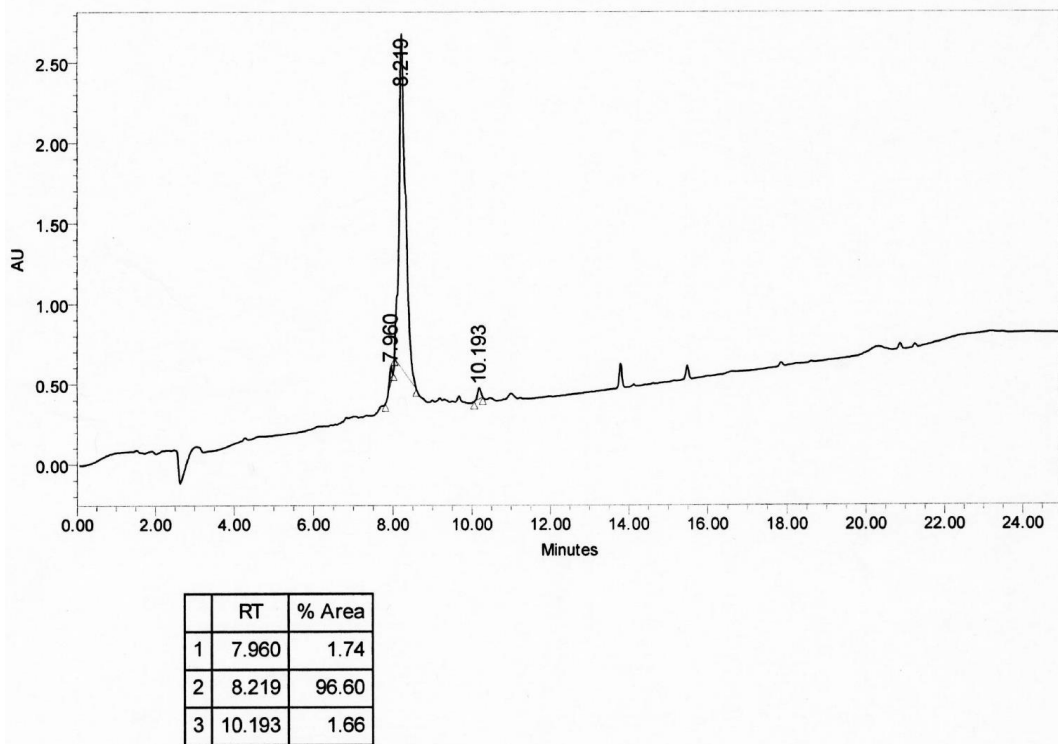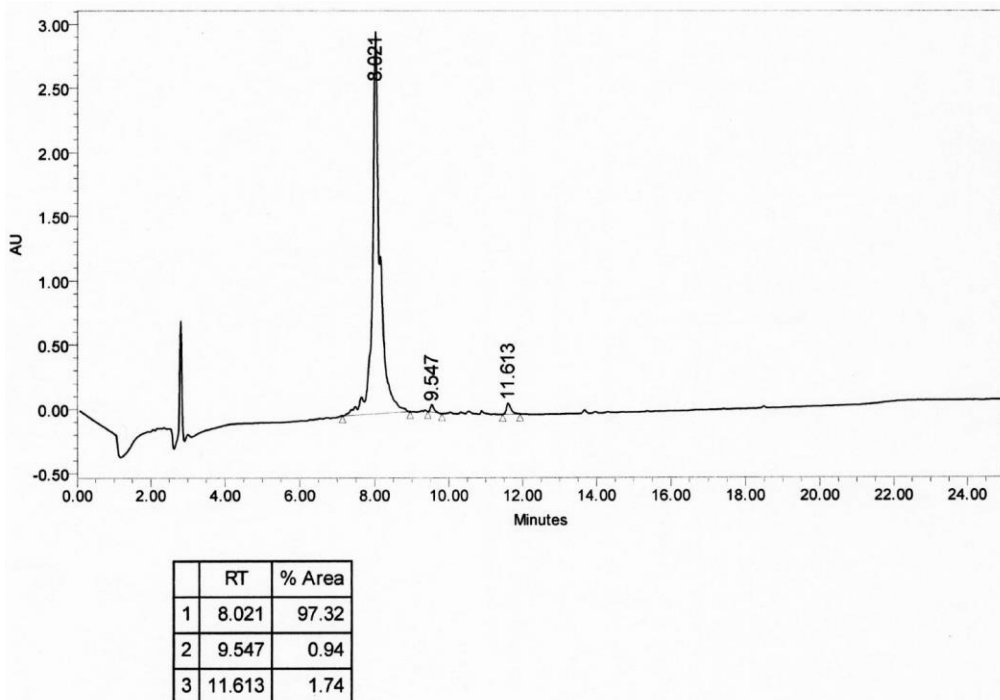
Figure 2.7. Representative RP-HPLC chromatograms of purified Pep42-R9 (**Table 2.1, sequence 2.4**) using A) linear gradient 2-82% MeCN/H_2O (0.1% TFA) over 18 min with a Zorbax RX-C18 column (4.6 x 250 mm, 5.0 μm particle size) at 25 °C and flow rate of 1.0 mL/min with detection at 214 nm and B) linear gradient 2-82% MeOH/H_2O (0.1% FA) over 18 min with a Zorbax RX-C18 column (4.6 x 250 mm, 5.0 μm particle size) at 25 °C and flow rate of 1.0 mL/min with detection at 214 nm.

35

Moreover, peptide purities (>95%) were confirmed in different eluent systems (2-82% MeOH/H$_2$O with 0.1% FA or MeCN/H$_2$O with 0.1% TFA over 18 min) which produced different retention times for the peptide samples while maintaining the desired peptide purity. The samples were then lyophilized to remove the residual acid and stored as dry white powders at -20 °C. It is also worthwhile to note that different retention times, albeit with the same chromatographic conditions, were observed between the Pep42-poly(L- and D-arginine) series. These results were consistent with those observed for diastereomeric mixtures of peptides or samples that analyzed peptide diastereomers by RP-LC/MS.[32] In our case, the Pep42-poly(L- and D-arginine) sequences were separately synthesized in good yields (12-46%) and isolated in purities (>95%) for structure-activity relationship studies. More specifically, D-peptides have been shown to improve peptide pharmacokinetic properties for applications in biology.[33]

Table 2.1. Characterization data for the peptides synthesized in this study.

Entry	Sequence	[a]Crude Purity (%)	[b]Isolated Purity (%)	[c]Isolated Yield (%/mg)	[d]M.W. (g/mol)	[e]Z	[f]RT (min)	[g]RT (min)
2.1	CTVALPGGYVRVC	93	99(98)	14/12.2	667.9 (667.8)	2	11.2	9.4
2.2	CTVALPGGYVRVC-R$_3$	98	99(99)	23/14.9	601.8 (601.6)	3	8.1	8.4
2.3	CTVALPGGYVRVC-R$_6$	97	98(98)	46/24.8	1136.5 (1136.8)	2	8.4	8.6
2.4	CTVALPGGYVRVC-R$_9$	93	98(98)	15/9.2	548.6 (548.7)	5	8.2	8.7
2.5	CTVALPGGYVRVC-R$_{12}$	94	97(96)	29/16.7	803.0 (803.2)	4	7.2	8.0
2.6	CTVALPGGYVRVC-r$_3$	86	98(96)	25/19.4	601.8 (601.6)	3	9.1	8.3
2.7	CTVALPGGYVRVC-r$_6$	>95*	>95(>95)	37/23.6	758.1 (758.2)	3	9.7	8.1
2.8	CTVALPGGYVRVC-r$_9$	86	98(96)	18/12.3	549.1 (548.7)	5	7.7	8.2
2.9	CTVALPGGYVRVC-r$_{12}$	95	96(97)	21/19.3	802.9 (803.2)	4	8.2	5.4
2.10	FITC-Ahx-CTVALPGGYVRVC	95	95(95)	24/15.2	451.9 (452.1)	4	8.7	11.4
2.11	FITC-Ahx-CTVALPGGYVRVC-R$_3$	93	99(95)	15/9.7	603.3(602.9)	3	13.8	12.9
2.12	FITC-Ahx-CTVALPGGYVRVC-R$_6$	98*	98(96)	13/10.2	568.5 (568.9)	4	8.7	9.1
2.13	FITC-Ahx-CTVALPGGYVRVC-R$_9$	93	98(96)	12/9.6	549.5 (549.6)	5	11.7	10.1
2.14	FITC-Ahx-CTVALPGGYVRVC-R$_{12}$	89	96(95)	15/12.0	642.8 (643.0)	5	9.6	9.9
2.15	FITC-Ahx-R$_9$	>95	99 (97)	21/17.4	474.0 (474.3)	4	8.1	8.8
2.16	R$_9$	>95	99(95)	35/23.1	475.0 (475.2)	3	4.9	7.2

[a]Crude purities by RP-HPLC at 214 nm using 2-82% MeCN/H$_2$O with 0.1% TFA over 18 min. [b]Isolated purities by RP-HPLC at 214 nm using 2-82% MeCN(MeOH)/H$_2$O with 0.1% TFA(FA) over 18 min [c]Isolated yields based on the resin loading. [d]Observed mass (expected mass) as [M+H]$^+$/Z as detected by LCMS. [e]Charged state of the peptides as detected by LCMS in positive mode. [f]Retention times using 2-82% MeOH/H$_2$O (0.1% FA) over 18 min. [g]Retention times using 2-82% MeCN/H$_2$O (0.1% TFA) over 18 min.

2.5 CONCLUSIONS

The design, synthesis and characterization of a novel class of poly(arginine) bearing cancer-targeting peptides are described in this chapter. The rational design of the peptides was based on the Pep42 sequence, discovered as a high affinity and selective ligand for the GRP78 cell surface tumor antigen by phage display bio-panning selection.[1] This cancer-targeting domain was extended with varying lengths of poly(D- and L-arginine) sequences to explore the influence of the poly(arginine) on structure, biophysical properties (Chapter 3) and biological activity (Chapter 4). In this study, a small library of cancer-targeting peptides (16) derived from the Pep42-poly(arginine) series were effectively prepared by Fmoc-SPPS. During the optimization studies, the use of a polar, poly(ethylene glycol)-based resin (NovaPEG) provided the best results in the synthesis of the desired peptide sequences. These optimization studies underscored the importance of the solid-support in peptide synthesis efficiency. With an optimized protocol in hand, peptides were obtained in good yields (12-46%) and purities (>95%) following RP-LC/MS analyses and separations. The use of ESI-MS proved instrumental to the characterization of the peptide sequences by molecular weight confirmation. The newly synthesized peptides may function as useful probes for evaluating structure-function relationships with clinically relevant receptor targets (Chapters 3 and 4).

2.6. REFERENCES

1. (a) Kim, Y.; Lillo, A.M.; Steiniger, S.C.; Liu, Y.; Ballatore, C.; Anichini, A.; Mortarini, R.; Kaufmann, G.F.; Zhou, B.; Felding-Habermann, B.; Janda, K.D. *Biochemistry* **2006**, *45*, 9434. (b) Liu, Y.; Steiniger, S.C.; Kim, Y.; Kaufmann, G.F.; Felding–Habermann, B.; Janda, K.D. *Mol. Pharm.* **2007**, *4*, 435-447. (c) Yoneda, Y.; Steiniger, S.C.; Capková, K.; Mee, J.M.; Liu, Y.; Kaufmann, G.F.; Janda, K.D. *Bioorg. Med. Chem. Lett.* **2008**, *18*, 1632.

2. Luo, B.; Lee A.S. *Oncogene* **2013**, *32*, 805.

3. Kim, S.W.; Kim, N.Y.; Choi, Y.B.; Park, S.H.; Yang, J.M.; Shin, S. *J. Control. Release* **2010**, *143*, 335.

4. (a) Futaki, S.; Suzuki, T.; Ohashi, W.; Yagami, T.; Tanaka, S.; Ueda, K.; Sugiura, Y. *J. Biol. Chem.* **2001**, *276*, 5836. (b) Alhakamy, N.A.; Berkland, C.J. *Mol. Pharm.* **2013**, *10*, 1940.

5. Vives, E. *J. Control. Release* **2005**, *109*, 77.

6. (a) Chandrudu, S.; Simerska, P.; Toth, I. *Molecules* **2013**, *18*, 4373. (b) Peterson, Q.P.; Goode, D.R.; West, D.C.; Botham, R.C.; Hergenrother, P.J. *Nat. Prot.* **2010**, *5*, 294.

7. Merrifield, R.B. *J. Am. Chem. Soc.* **1963**, *85*, 2149.

8. (a) Zinieris, N.; Leondiadis, L.; Ferderigos, N. *J. Comb. Chem.* **2005**, *7*, 4. (b) Amblard, M.; Fehrentz, J.A.; Martinez, J.; Subra, G. *Mol. Biotech.* **2006**, *33*, 239.

9. Wang, S.S. *J. Am. Chem. Soc.* **1973**, *95*, 1328.

10. Rink, H. *Tetrahedron Lett.* **1987**, *28*, 3787.

11. (a) Rapp, W.; Zhang, L.; Habish, R.; Bayer, E. *In Peptides: Proceedings of the 20th European Peptide Symposium.* **1988**, 199. (b) Fara, M.A.; Diaz-Mochon, J.; Bradley, M. *Tetrahedron Lett.* **2006**, *47*, 1011.

12. Garcia-Martin, F. Quintanar-Audelo, M.; Garcia-Ramos, Y.; Cruz, L.J.; Gravel, C.; Furic, R.; Cote, S.; Tulla-Puche, J.; Albericio, F. *J. Comb. Chem.* **2006**, *8*, 213.

13. Chantell, C.A.; Onaiyekan, M.A.; Menakuru, M. *J. Pept. Sci.* **2012**, *18*, 88.

14. Friligou, I.; Papadimitriou, E.; Gatos, D.; Matsoukas, J.; Tselios T. *Amino Acids* **2011**, *40*, 1431.

15. Hood, C.A.; Fuentes, G.; Patel, H.; Page, K.; Menakuru, M.; Park, J.H. *J. Pept. Sci.* **2008**, *14*, 97.

16. Collins, J.A.; Porter, K.A.; Singh, S.K.; Vanier, G.C. *Org. Lett.* **2014**, *16*, 940.

17. Coin, I.; Beyermann, M.; Bienert, M. *Nat. Protoc.* **2007**, *2*, 3247.

18. Garcia-Ramos, Y.; Paradis-Bas, M.; Tulla-Puche, J.; Albericio, F. *J. Pept. Sci.* **2010**, *16*, 675.

19. Lloyd-Williams, P.; Albericio, F.; Giralt, E. Chemical Approaches to the Synthesis of Peptides and Proteins, **1997**, CRC: Boca Raton, Florida.

20. Fischer, P.M. *Curr. Prot. Pept. Sci.* **2003**, *4*, 339.

21. Annis, I.; Chen, L.; Barany, G. *J. Am. Chem. Soc.* **1998**, *120*, 7226.

22. Lam-Thanh, H.; Mourier, G.; Menez, A.; Fromageot, P. *Pept. Res.* **1989**, *2*, 229.

23. Pohl, M.; Ambrosius, D.; Groetzinger, J.; Kretzschmar, T.; Saunders, D.; Wollmer, A.; Brandenburg, D.; Bitter-Suermann, D.; Hoecker, H. *Int. J. Pept. Prot. Res.* **1993**, *41*, 362.

24. (a) Otaka, A.; Koide, T.; Shide, A.; Fujii, N. *Tetrahedron Lett.* **1991**, *32*, 1223. (b) Tam, J.P.; Wu, C.R.; Liu, W.; Zhang, J.W. *J. Am. Chem. Soc.* **1991**, *113*, 6657.

25. (a) Stewart, J.M.; Young, J.D. *Solid Phase Peptide Synthesis (Pierce Chemical Company)* **1984**, 2, 53, (b) Albericio, F.; Annis, I.; Royo, M.; Barany, G. *Fmoc Solid Phase Peptide Synthesis (Oxford University Press)* **2000**, 77.

26. Jullian, M.; Hernandez, A.; Maurras, A.; Puget, K.; Amblard, M.; Martinez, J.; Subra, G. *Tetrahedron Lett.* **2009**, *50*, 260.

27. (a) Limal, D.; Briand, J.P.; Dalbon, P.; Jolivet, M. *J. Pept. Res*. **1998**, *52*, 121, (b) Hornik, V.; Afargan, M.M.; Gellerman, G. *PCT. Int. Appl.* **1999**, 11pp.

28. Graham, H.D., Jr.; John, D.M.; Erickson, B.W. *Peptides: Frontiers of Peptide Science, Proceedings of the 15th American Peptide Symposium* **1999**, 140.

29. Mant, C.T.; Cepeniene, D.; Hodges, R.S. *J. Sep. Sci.* **2010**, *33*, 3005.

30. Desportes, C.; Charpentier, M.; Duteurtre, B.; Maujean, A.; Duchiron, F. *J. Chromatogr. A.* **2000**, *893*, 281.

31. Ekström, J.; Murakami, M.; Inzitari, R.; Khosravani, N.; Fanali, C.; Cabras, T.; Fujita-Yoshigaki, J.; Sugiya, H.; Messana, I.; Castagnola, M. *J. Sep. Sci.* **2009**, *32*, 2944.

32. Shi, G.; Lloyd, T.L.; Sy, S.K.; Jiao, Q.; Wernicki, A.; Mutlib, A.; Emm, T.A.; Unger, S.E.; Pieniaszek, H.J. *J. Pharm. Biomed. Anal.* **2003**, *31*, 937.

33. Kim, W.J.; Christensen, L.V.; Jo, S.; Yockman, J.W.; Jeong, J.H.; Kim, Y.H.; Kim, S.W. *Mol. Ther.* **2006**, *14*, 343.

2.7 EXPERIMENTAL SECTION
2.7.1. MATERIALS

Protected amino acids Fmoc-Arg(Pbf), Fmoc-Cys(Trt), Fmoc-Val, Fmoc-Gly, Fmoc-Tyr(*t*-Bu), Fmoc-Pro, Fmoc-Leu, Fmoc-Thr(*t*-Bu), Fmoc-Ala, Fmoc-ε-Ahx constituted the building blocks for making the desired peptide sequences and were purchased from Novabiochem (San Diego, CA). Peptide sequences were fluorescently tagged with FITC from Advanced ChemTech (Louisville, KY). Peptide syntheses were conducted on hydrophilic poly(ethylene glycol) (NovaPEG)[12] Novabiochem (San Diego, CA), Tentagel S RAM, Rapp Polymere[11] (Tuebingen, Germany) and Polystyrene Rink Amide,[10] Advanced ChemTech (Louisville, KY) resins. Trifluoroacetic acid (Biograde) was purchased from VWR (Radnor, PA), *N,N*-dimethylformamide (BioAnalyzed) was obtained from J.T. Baker (St. Loiusville, KY), HCTU was from Advanced ChemTech (Louisville, KY), *N*-methylmorpholine, piperidine and triethylsilane, acetonitrile and dichloromethane were all purchased from Aldrich (Milwaukee, WI) and used without further purification. HPLC grade methanol and acetonitrile were purchased from Aldrich (Milwaukee, WI).

2.7.2. PEPTIDES SYNTHESIS

All peptides were prepared by stepwise solid-phase synthesis protocols using Fmoc chemistry[15] on a PSI 200C peptide synthesizer (Fairfield, NJ), which included coupling of Fmoc-amino acids (300 mol%, 3 eq.), on a hydrophilic poly(ethylene glycol) (NovaPEG)[12] solid support (100 mg, 0.1 mmol) for 20 minutes using [2-(6-chloro-1H-benzotriazole-1-yl)-1,1,3,3-tetramethylaminium hexafluorophosphate] HCTU (72 mg, 300 mol%, 3 eq.), *N*-methylmorpholine, NMM (34 µL, 600 mol%, 6 eq.) in DMF (4.0 mL). The Fmoc deprotections (10 min) were repeated twice, by passing a solution of 20% piperidine in DMF (4.0 mL) into the reaction vessels containing peptide-bound

resin. Peptide coupling and Fmoc-deprotection reactions were repeated until the desired CTP sequences reached completion. The Fmoc-ε-aminohexanoic acid (Ahx) was then coupled to CTPs (**Table 2.1, sequences 2.10-2.15**, followed by Fmoc deprotection and coupling with fluorescein isothiocyanate (FITC). FITC (9.68 µmol, 2 eq.) coupling was performed in pyridine/DMF/DCM (12:7:5, 500 µL) overnight at room temperature (22 ^{o}C). Following synthesis, all peptides were cleaved from the solid support and side-chain protecting groups removed using a mixture of trifluoroacetic acid: triethylsilane: water (TFA:TES:H_2O, 95:2.5:2.5 v/v/v, 3.0 mL) for 4 hours. The peptides were concentrated to a viscous oil, precipitated in cold ether, and isolated as a white pellet upon centrifugation. Following removal of the supernatant, the crude peptides were dissolved in water and analyzed for purity. RP-HPLC was performed on a Waters 2695 Alliance Separations Module equipped with a Waters 2998 Photodiode Array (PDA) detector employing binary gradients of solvents A and B, where A is 0.1% TFA in water and B is 0.1% TFA in spectrophotometric grade acetonitrile. Analytical RP-HPLC was performed using a Zorbax RX-C18 column (4.6 x 250 mm, 5.0 µm particle size) set at a temperature of 25 ^{o}C and at a flow rate of 1.0 mL/min, during a linear gradient 2-82% B over 18 min with detection at 214 nm. In all cases, pure fractions (10.0 µL) were characterized on an Agilent 1100 Series ESI-LCMS with single quadropole mass analyzer for molecular weight confirmation using LC conditions previously described. Samples were purified on Waters 600 Alliance Separations Module equipped with a Waters 2489 Photodiode Array (PDA) detector employing binary gradients of solvents A and B, where A is 2.5% MeOH/0.1% FA in water and B is 0.1% FA in spectrophotometric grade methanol. Crude samples were dissolved in 1.0 mL purified water, filtered using PVDF (0.45 µm) and injected for purification. Preparative RP-HPLC was performed using a YMC-Pack ODS-A C18 column (20 x 250 mm, 5.0 µm particle size) set at a temperature

of 25 °C and at a flow rate of 15 mL/min, during a linear gradient 2-82% B over 18 min with dual detection at 214 nm and 280 nm. Eluants collected after purification were lyophilized to a white solid, re-dissolved in water and analyzed by LCMS to confirm identity and purity.

2.7.3 CHARACTERIZATION DATA

H_2N-CTVALPGGYVRVC-$CONH_2$ (**Table 2.1, sequence 2.1**). ESI-LCMS [2-82% MeOH in H_2O (0.1% FA), 18 min] RT = 11.2 min; [2-82% MeCN in H_2O (0.1% TFA), 18 min] RT = 9.4 min; Calculated for $C_{58}H_{96}N_{16}O_{16}S_2$ [M+2H]$^{2+}$ 667.8 found *m/z* 667.9

H_2N-CTVALPGGYVRVC-R_3-$CONH_2$ (**Table 2.1, sequence 2.2**). ESI-LCMS [2-82% MeOH in H_2O (0.1% FA), 18 min] RT = 8.1 min; [2-82% MeCN in H_2O (0.1% TFA), 18 min] RT = 8.4 min; Calculated for $C_{76}H_{132}N_{28}O_{19}S_2$ [M+3H]$^{3+}$ 601.6 found *m/z* 601.8

H_2N-CTVALPGGYVRVC-R_6-$CONH_2$ (**Table 2.1, sequence 2.3**). ESI-LCMS [2-82% MeOH in H_2O (0.1% FA), 18 min] RT = 8.4 min; [2-82% MeCN in H_2O (0.1% TFA), 18 min] RT = 8.6 min; Calculated for $C_{94}H_{168}N_{40}O_{22}S_2$ [M+2H]$^{2+}$ 601.6 found *m/z* 601.8

H_2N-CTVALPGGYVRVC-R_9-$CONH_2$ (**Table 2.1, sequence 2.4**). ESI-LCMS [2-82% MeOH in H_2O (0.1% FA), 18 min] RT = 8.2 min; [2-82% MeCN in H_2O (0.1% TFA), 18 min] RT = 8.7 min; Calculated for $C_{112}H_{204}N_{52}O_{25}S_2$ [M+5H]$^{5+}$ 548.7 found *m/z* 548.6

H_2N-CTVALPGGYVRVC-R_{12}-$CONH_2$ (**Table 2.1, sequence 2.5**). ESI-LCMS [2-82% MeOH in H_2O (0.1% FA), 18 min] RT = 7.2 min; [2-82% MeCN in H_2O (0.1% TFA), 18 min] RT = 8.0 min; Calculated for $C_{130}H_{240}N_{64}O_{28}S_2$ [M+4H]$^{4+}$ 803.2 found *m/z* 803.0

H_2N-CTVALPGGYVRVC-r_3-$CONH_2$ (**Table 2.1, sequence 2.6**). ESI-LCMS [2-82% MeOH in H_2O (0.1% FA), 18 min] RT = 9.1 min; [2-82% MeCN in H_2O (0.1% TFA), 18 min] RT = 8.3 min; Calculated for $C_{76}H_{132}N_{28}O_{19}S_2$ [M+3H]$^{3+}$ 601.6 found *m/z* 601.8

H$_2$N-CTVALPGGYVRVC-r$_6$-CONH$_2$ (**Table 2.1, sequence 2.7**). ESI-LCMS [2-82% MeOH in H$_2$O (0.1% FA), 18 min] RT = 9.7 min; [2-82% MeCN in H$_2$O (0.1% TFA), 18 min] RT = 8.1 min; Calculated for C$_{94}$H$_{168}$N$_{40}$O$_{22}$S$_2$ [M+3H]$^{3+}$ 758.2 found *m/z* 758.1

H$_2$N-CTVALPGGYVRVC-r$_9$-CONH$_2$ (**Table 2.1, sequence 2.8**. ESI-LCMS [2-82% MeOH in H$_2$O (0.1% FA), 18 min] RT = 7.7 min; [2-82% MeCN in H$_2$O (0.1% TFA), 18 min] RT = 8.2 min; Calculated for C$_{112}$H$_{204}$N$_{52}$O$_{25}$S$_2$ [M+5H]$^{5+}$ 548.7 found *m/z* 549.1

H$_2$N-CTVALPGGYVRVC-R$_{12}$-CONH$_2$ (**Table 2.1, sequence 2.9**). ESI-LCMS [2-82% MeOH in H$_2$O (0.1% FA), 18 min] RT = 8.2 min; [2-82% MeCN in H$_2$O (0.1% TFA), 18 min] RT = 5.4 min; Calculated for C$_{130}$H$_{240}$N$_{64}$O$_{28}$S$_2$ [M+4H]$^{4+}$ 803.2 found *m/z* 802.9

FITC-Ahx-CTVALPGGYVRVC-CONH$_2$ (**Table 2.1, sequence 2.10**). ESI-LCMS [2-82% MeOH in H$_2$O (0.1% FA), 18 min] RT = 8.7 min; [2-82% MeCN in H$_2$O (0.1% TFA), 18 min] RT = 11.4 min; Calculated for C$_{85}$H$_{118}$N$_{18}$O$_{22}$S$_3$ [M+4H]$^{4+}$ 452.1 found *m/z* 451.9

FITC-Ahx-CTVALPGGYVRVC-R$_3$-CONH$_2$ (**Table 2.1, sequence 2.11**). ESI-LCMS [2-82% MeOH in H$_2$O (0.1% FA), 18 min] RT = 13.8 min; [2-82% MeCN in H$_2$O (0.1% TFA), 18 min] RT = 12.9 min; Calculated for C$_{103}$H$_{154}$N$_{30}$O$_{25}$S$_3$ [M+3H]$^{3+}$ 602.9 found *m/z* 603.3

FITC-Ahx-CTVALPGGYVRVC-R$_6$-CONH$_2$ (**Table 2.1, sequence 2.12**). ESI-LCMS [2-82% MeOH in H$_2$O (0.1% FA), 18 min] RT = 8.7 min; [2-82% MeCN in H$_2$O (0.1% TFA), 18 min] RT = 9.1 min; Calculated for C$_{121}$H$_{190}$N$_{42}$O$_{28}$S$_3$ [M+4H]$^{4+}$ 568.9 found *m/z* 568.5

FITC-Ahx-CTVALPGGYVRVC-R$_9$-CONH$_2$ (**Table 2.1, sequence 2.13**). ESI-LCMS [2-82% MeOH in H$_2$O (0.1% FA), 18 min] RT = 11.7 min; [2-82% MeCN in H$_2$O (0.1% TFA), 18 min] RT = 10.1 min; Calculated for C$_{139}$H$_{226}$N$_{54}$O$_{31}$S$_3$ [M+5H]$^{5+}$ 549.6 found *m/z* 549.5

FITC-Ahx-CTVALPGGYVRVC-R$_{12}$-CONH$_2$ (**Table 2.1, sequence 2.14**). ESI-LCMS [2-82% MeOH in H$_2$O (0.1% FA), 18 min] RT = 9.6 min; [2-82% MeCN in H$_2$O (0.1% TFA), 18 min] RT = 9.9 min; Calculated for C$_{157}$H$_{262}$N$_{66}$O$_{34}$S$_3$ [M+5H]$^{5+}$ 643.0 found *m/z* 642.8

FITC-Ahx-R$_9$-CONH$_2$ (**Table 2.1, sequence 2.15**). ESI-LCMS [2-82% MeOH in H$_2$O (0.1% FA), 18 min] RT = 8.1 min; [2-82% MeCN in H$_2$O (0.1% TFA), 18 min] RT = 8.8 min; Calculated for C$_{81}$H$_{132}$N$_{38}$O$_{16}$S [M+4H]$^{4+}$ 474.3 found *m/z* 474.0

H$_2$N-R$_9$-CONH$_2$ (**Table 2.1, sequence 2.16**). ESI-LCMS [2-82% MeOH in H$_2$O (0.1% FA), 18 min] RT = 4.9 min; [2-82% MeCN in H$_2$O (0.1% TFA), 18 min] RT = 7.2 min; Calculated for C$_{54}$H$_{110}$N$_{36}$O$_{10}$ [M+3H]$^{3+}$ 475.2 found *m/z* 475.0

CHAPTER 3: STRUCTURAL STUDIES AND THERMAL STABILITIES OF THE Pep42-(POLY)ARGININE SEQUENCES USING CD SPECTROSCOPY

3.1 ABSTRACT

Circular Dichroism (CD) spectroscopy is an excellent tool for the rapid determination of peptide secondary structures and their stabilities in the far UV region (190 – 260 nm). In this study, the Pep42-poly(L/D-arginine) series were analyzed by CD spectroscopy to determine trends in peptide folds in aqueous media (H$_2$O and phosphate buffered saline, PBS) and organic solvent (2,2,2-trifluoroethanol, TFE). The peptides were found to exhibit secondary structural features which contained both helical and turn conformations that were contingent on sequence and solvent. Moreover, the peptide secondary structures were found to be influenced by the Pep42 disulfide bond. Under reduced conditions (dithiothreitol, DTT), the sequence transitioned to a random coil in water. Interestingly, the Pep42-(D-arginine) sequences exhibited similar trends in their folded structures. However, with noticeable inversion in peptide conformations that were likely due to the change in stereochemistry of the poly(arginine) residues. Thermal denaturation experiments by CD spectroscopy revealed peptide structural stabilities. Notably, increasing temperatures (25–85 °C) produced significant changes in the CD spectra of the Pep42-poly(arginine) sequences. In general, peptides were found to be resistant to thermal denaturation with little random coil observed at elevated temperatures (45–85 °C). However, at these temperatures, the peptides produced transitions from turn-to-helix conformations illustrating the resiliency and flexibility of the Pep42-poly(arginine) secondary structures. This feature is of particular importance to the biology of these peptides, in which structure and stability of the Pep42-poly(arginine) sequences may play an important role in binding to the target GRP78 receptor and internalization within cancer cells for activity (Chapter 4).

3.2 INTRODUCTION
3.2.1 STRUCTURAL STUDIES OF PEPTIDES USING CD SPECTROSCOPY

The CD spectroscopy of peptides refers to their differential absorption of right and left-handed circularly polarized light (**Figure 3.1**).[1] In this technique, unpolarized light typically emanating from a Xenon arc lamp is converted to plane-polarized radiation. Light is then split into right and left-handed circularly polarized components by the passage through a circular polarizer in an alternating electric field. The interaction of the circularly polarized light with chiral chromophores (*e.g.* peptides) in the sample cell produces a CD signal (ellipticity) as a function of wavelength in the UV (190 - 350 nm) region. As such, the CD spectrum provides a unique trace that is contingent on the nature of the chromophore and the asymmetric global conformation of the molecule.
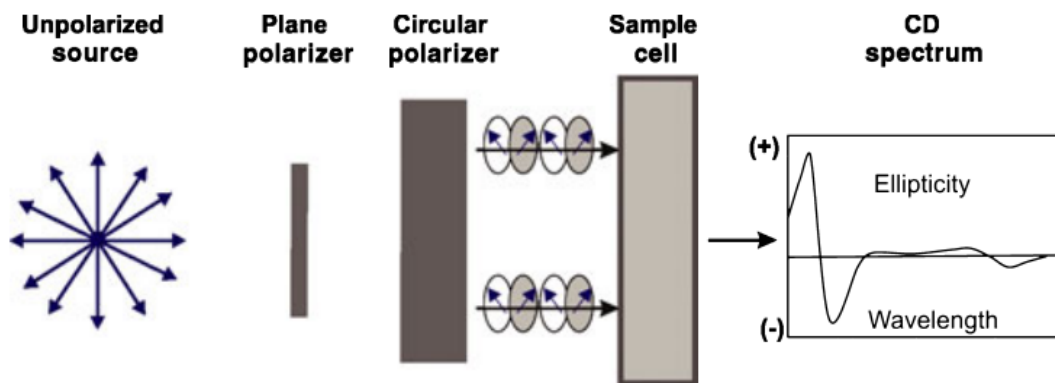
Figure 3.1. CD spectroscopy method and sample analysis.[1] Figure adapted from Ranjbar, B. et al *Chem. Biol. Drug. Des.* **2009,** *74*, 101-120.

More specifically, CD spectroscopy allows for the rapid evaluation of peptide secondary structures, elucidation of their thermodynamic properties and can provide important mechanistic information on their binding properties with other ligands.[2] Therefore, CD spectroscopy is a useful characterization technique for peptides in order to gain a better understanding of their biological

properties. Other methods can be used to elucidate peptide structures such as computational analyses,[3] mass spectrometry,[4] nuclear magnetic resonance (NMR) spectroscopy,[5] and X-ray crystallography.[6] CD spectrophotometry retains two advantages over these other laborious techniques, speed and versatility.[1,2] This is because CD spectroscopy provides a non-destructive method of analyses that can facilitate high-throughput screening of multiple peptide samples in short scanning times (min). This provides opportunity for exploring peptide structure, bio-physical and biological properties.

Peptides are perfectly suitable to the CD study since they are chiral molecules that have the ability to absorb electromagnetic radiation in the far (190 – 260 nm) and near (260 – 350 nm) UV region. The interaction of the peptide backbone with light in the far UV-region produces a CD spectrum that is contingent on the peptide secondary structure. This provides reliable information on the different types of peptide secondary structures in terms of helices, sheets and turn conformations (**Figure 3.2, i**).[1,2] For example, a random coil has a broad positive $n{\rightarrow}\pi^*$ electronic absorption transition centered around 210 nm and an intense negative $\pi{\rightarrow}\pi^*$ transition at about 190 nm. A β-sheet has a negative $\pi{\rightarrow}\pi^*$ transition in between 230 and 210 nm in addition to a strong positive $n{\rightarrow}\pi^*$ transition centered around 196 nm. Peptide turns also have characteristic CD spectra, with a strong positive $n{\rightarrow}\pi^*$ transition in between 220 and 200 nm and a negative band at 190 nm. The CD signature for an α-helix leads to a strong positive $\pi{\rightarrow}\pi^*$ transition at 192 nm, a weaker negative one at 208 nm and a negative $n{\rightarrow}\pi^*$ transition of equal intensity, albeit red shifted at 222 nm. Thus, the CD spectrum in the far UV region (190 – 260 nm) provides a characteristic trace for the peptide backbone geometry shown in **Figure 3.2,i** that is contingent on the φ and ψ peptide dihedral angles shown in **Figure 3.2,ii**,[7] the chirality and absorptivity of the peptide in solution (**Figure 3.2, ii**).[1,2]

i.
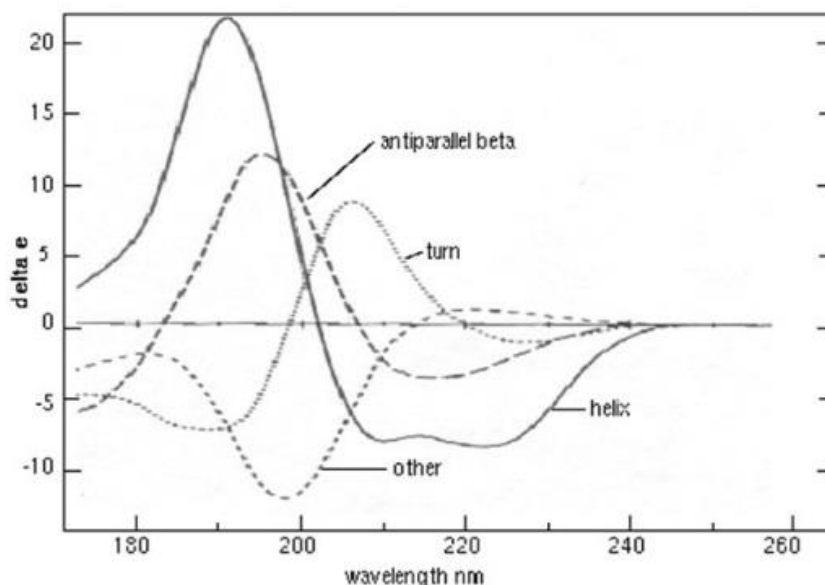
ii.
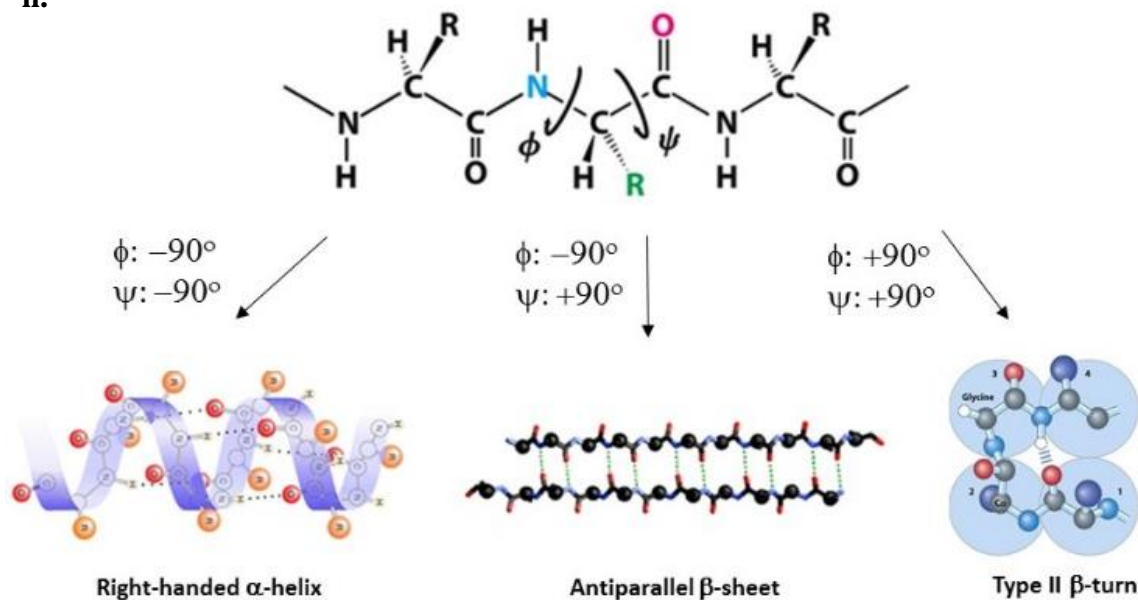
Figure 3.2. Characterization of peptide secondary structures by CD spectroscopy i. Far UV (180 – 260 nm) CD spectra associated with peptide secondary structures: solid curve, α-helix; long dashes, anti-parallel β-sheet; dots, type I β-turn; dots and short dashes, irregular structure. ii. Peptide dihedral angles (φ, ψ) of the α-helix, β-sheet and β-turn secondary structures.[1,2,7] Figure adapted from Ranjbar, B. et al *Chem. Biol. Drug. Des.* **2009**, *74*, 101-120; Greenfield, N.J. et al *Anal. Chem.* **1999**, *18*, 236-244; Ostermeir, K. et al *J. Comput. Chem.* **2014**, *35*, 150-158.

Absorption of the aromatic side-chains in the near UV (260 – 350 nm) region can provide important information on peptide tertiary structures. For example, the absorption of aromatic amino acid side chains such as the indole group in tryptophan (ε_{280nm}: 5560 L·mol^{-1}·cm^{-1}), the phenol group in tyrosine (ε_{280nm}: 1200 L·mol^{-1}·cm^{-1}), the phenyl group in phenylalanine (ε_{260nm}: 195 L·mol^{-1}·cm^{-1}) and the imidazole functional group in histidine (ε_{211nm}: 5700 L·mol^{-1}·cm^{-1}) can all relay important structural information of the peptide (*e.g.* hydrophobic binding sites)[8] or interactions with bound ligands (*e.g.* π-ion interactions).[9] In the near UV absorption region, disulfide bond absorptions in between cysteine residues have been found to occur weakly at around 260 nm. However, the intensity of this signal can be affected by the neighboring amino acid residues.[10] The changes in the CD spectra of natively folded (disulfide linked) or denatured (free thiol) peptides provides important structural and thermodynamic information associated with the fold-to-coil transition.[1,2,10] Therefore, CD spectroscopy has gained widespread use for the determination of peptide structures in addition to the study of other peptide properties such as thermodynamic stability.

3.2.2 THERMAL STABILITY OF PEPTIDES USING CD SPECTROSCOPY

CD spectroscopy can also be used to monitor the thermodynamic stabilities associated with changes in peptide secondary structures in the presence of a denaturation agent. For example, chaotropic salts such as guanidine hydrochloride, GdnHCl, that denature polypeptides by disrupting the non-covalent hydrogen bonds have been used to assess the thermodynamics associated with the unfolding of a colicin E1 channel peptide with increasing [GdnHCl].[11] The anionic detergent, sodium dodecyl sulfate, SDS, has also been commonly used to denature polypeptides and to provide them with a net negative charge for separation on a polyacrylamide gel electrophoresis, PAGE.[12] PAGE is a technique that separates biological molecules such as large polypeptides based on their mass-to-charge ratio as well as conformation. The samples are

loaded into wells at the top of the polyacrylamide gel and an electric field is applied. Since SDS provides the polypeptide with a negative charge these polypeptide fragments migrate to the positive electrode with smaller fragments moving faster and larger polypeptides being retained by the gel.[12] Similarly, changes in pH have drastic effects on peptide structures and activity. For example, the unfolding of hepatic stimulator substance, HSS, a 31 kDa growth promoting factor with an acidic isoelectric point (pI: 4.5) retained biological activity from pH: 4-10.[13] Solvent effects such as buffers with varying ion strengths and solvents have also been shown to influence the stability of the peptide folds.[1,2] For example, 2,2,2-trifluoroethanol, TFE, is most commonly used to stabilize peptide conformations by limiting accessibility of water into the peptide thereby lowering the dielectric constant and reinforcing hydrogen bonds between the carbonyl and amidic NH groups.[19] This has been found in the β-turn geometry observed within the first extracellular loop (residues 92-100) of the angiotensin II AT_{1a} receptor.[14] In contrast, buffers with varying ionic strengths have been used to study the influence of electrostatic interactions on the yeast prion peptide aggregation providing greater mechanistic insight on the thermodynamics associated with the protein mis-folding disorder.[15] Although these methods are highly insightful in studying the energetics, stabilities and mechanisms associated with the changes in peptide conformations, these denaturation conditions are often irreversible, making the reconstitution of the biologically active peptide structure difficult to accomplish. Thermal denaturation is a commonly used and reversible method for denaturing peptide secondary structures. It can provide structural information based on temperature changes and correlate peptide folding patterns with their thermodynamic stabilities.[16] Thus, thermal denaturation experiments of the Pep42-poly(arginine) series using CD spectroscopy is perfectly suitable for determining the stabilities of the biologically active peptide folds.

3.3 CHAPTER OBJECTIVES

The main objective of this thesis chapter involves the structure elucidation and evaluation of the thermal stabilities of the Pep42-poly(L/D-arginine) sequences. CD spectroscopy is the method of choice for providing quick and reliable structural data of the peptides in solution. This study will be conducted in aqueous conditions (H$_2$O, phosphate buffered saline, PBS) to determine the influence of salt on peptide conformation. Moreover, the study of peptide structures will also be determined in TFE, a commonly employed organic solvent that has been shown to stabilize peptide secondary structures in solution.[14,19] The conformational properties of the Pep42-poly(L/D-arginine) sequences will be compared to the native Pep42 and poly(L/D-arginine) controls to determine the influence of each component on peptide geometry. Moreover, the importance of the disulfide bond in the Pep42 sequence will also be determined by the addition of a suitable reducing reagent (*e.g.* DTT). These studies are important for elucidating the biologically active peptide structure. With accurate determination of the peptide fold, thermal denaturation experiments using CD spectroscopy will be used to delineate the stabilities of the peptide structures. This experiment will also correlate the influence of the Pep42 disulfide bond on the stabilities of the peptide geometries. In sum, CD spectroscopy will be used to determine the structural properties of the Pep42-poly(L/D-arginine) sequences. With these data, peptide biological properties will be next investigated (Chapter 4) to complete our structure-activity relationship studies.

3.4 RESULTS AND DISCUSSION
3.4.1 EFFECT OF SOLVENT ON PEPTIDE STRUCTURE

Peptides (**Table 2.1, sequences 2.1-2.9, 2.16**) (50 µM) were dissolved in water, phosphate buffer and TFE to determine the influence of solvent on conformation. Interestingly, all of the peptides exhibited folded secondary structures in the three solvent conditions. In water, Pep42 displayed a

CD signature which was consistent with helical-type structure, with characteristic minimum bands near 210 and 220 nm and a positive one near 190 nm (**Figure 3.3**).[1,2,21-23] In TFE and PBS solvents, Pep42 was found to transition from helix to turn geometry, with characteristic Cotton effects for β-turn structures observed at around 230 nm and near 210 nm.[1,2,23,24] The greater proportion of β-turn structure observed for the Pep42 sequence in PBS and TFE suggests the favorable influence of ionic interactions[13] (PBS) and amphiphilic effects[14,19,24] (TFE) in stabilizing the β-turn (**Figure 3.3**). This geometry is perhaps centered around the Pro-Gly residues and stabilized by the terminal disulfide bond.[25,26] Interestingly, in water the reduced Pep42 (free thiol) exhibits a change in conformation from helical to random coil with increasing temperatures (**Figure 3.15**), highlighting the stabilizing influence of the disulfide bond in Pep42 secondary structure.
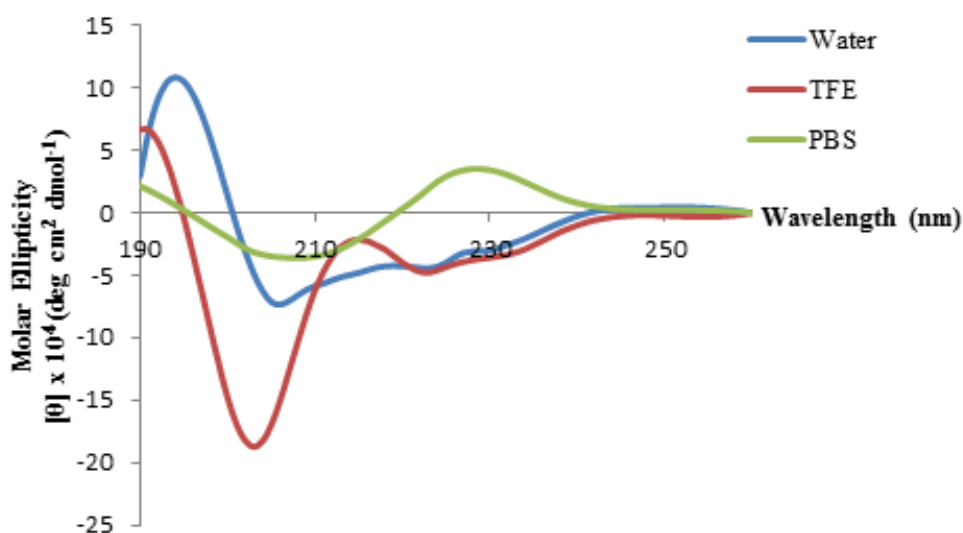
Figure 3.3. CD spectra for Pep42 (**Table 2.1, sequence 2.1**, 50 µM) in water, TFE and PBS at 25 °C.

In comparison, the poly(arginine) sequence, R9 (**Table 2.1, sequence 2.16**, **Figure 3.4**) exhibited a CD spectrum that was found to be typical of a turn geometry in water and PBS solvents,

with a maximum at around 220 nm and a minimum band near 200 nm.[1,2,23,24] The secondary structures of poly(arginine) or arginine rich peptides have been found to be highly variable, with strong dependence on solvent, pH effects and the lengths of the poly(arginine) sequences.[27] In this case, R9 was found to maintain a turn-type geometry in water, PBS and TFE, albeit with noticeable shifts in in the amplitudes of the molar ellipticities at the characteristic wavelengths for turn geometries (**Figures 3.2** and **3.4**).[1,2,23-26]
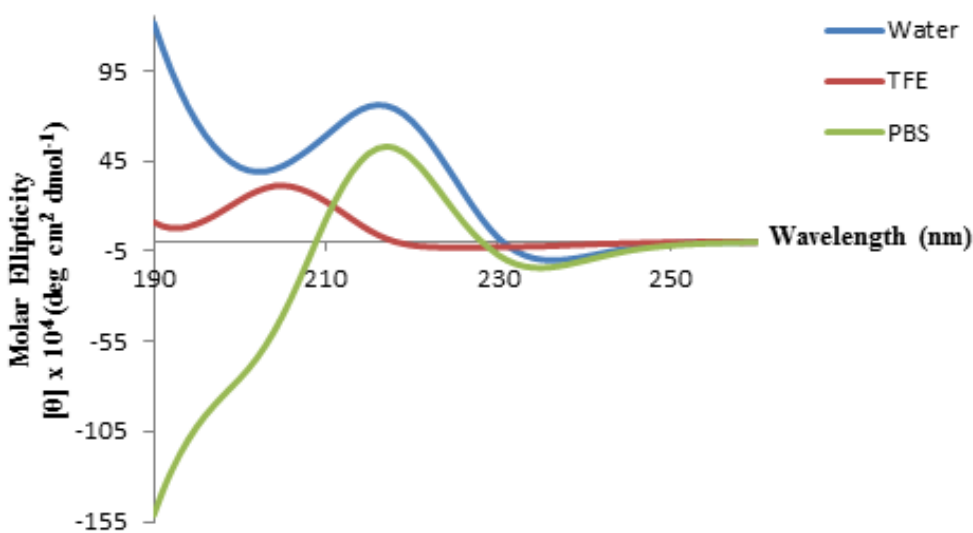
Figure 3.4. CD spectra for R9 (**Table 2.1, sequence 2.16**, 50 µM) in water, TFE and PBS at 25 °C.

Consequently, the Pep42-poly(arginine) sequences (**Table 2.1, sequences 2.2-2.5**) were found to exhibit peptide secondary structures with varying proportions of turn or helical motifs that were dependent on the sequence, length of the poly(arginine) and solvent conditions (**Figures 3.5-3.8**). For example, the Pep42-R$_3$ sequence (**Figure 3.5**) produced a CD spectrum which transitions from helix to turn conformations, as demonstrated by the shift in amplitudes of the molar ellipticities at around 190, 210 and 220 nm. In the case of the lengthier Pep42-R$_{12}$ (**Figure 3.8**) the peptide maintained a *β*-turn geometry with characteristic minimum bands at 230 and 200 nm and a

maximum at 210 nm. [1,2,23-26]   Interestingly, the CD spectra for the polypeptides in TFE buffer (**Figure 3.5-3.8**) shows characteristic minimum bands close to 230 nm and maximum bands near 210 nm which correlates to a type I β-turn conformation.[14] Moreover, the Pep42-poly(D-arginine) series (**Appendix Figures A32-A39**) produced similar trends with the various solvent conditions. The CD spectra also contained noticeable inversions in structures relative the Pep42-poly(L-arginine) sequences due to the change in stereochemistry at the arginine residues. Thus, the Pep42-poly(arginine) sequences (**Table 2.1, sequences 2.1-2.5**) exhibit secondary structures with varying proportions of turn and helical geometries that are contingent on sequence, length of the poly(arginine) and solvent conditions. The structural stabilities of the peptides were next assessed to determine the resiliency of the peptide folds to thermal denaturation.
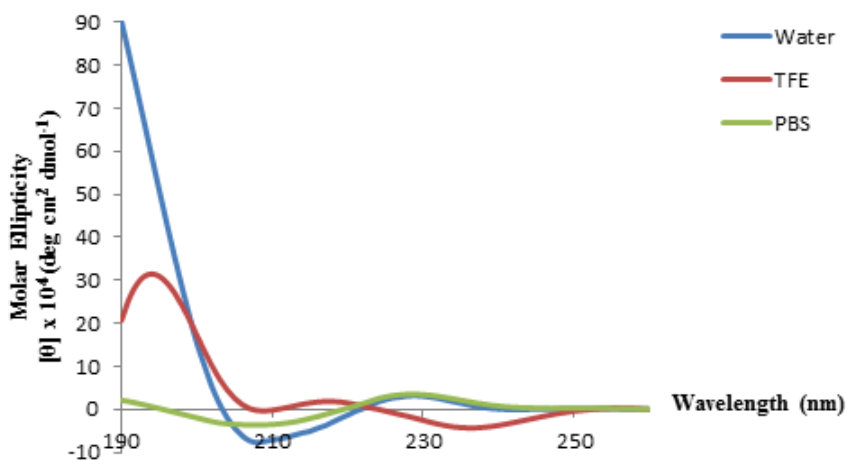
Figure 3.5. CD spectra for Pep42-R3 (**Table 2.1, sequence 2.2**, 50 μM) in water, TFE and PBS at 25 °C.
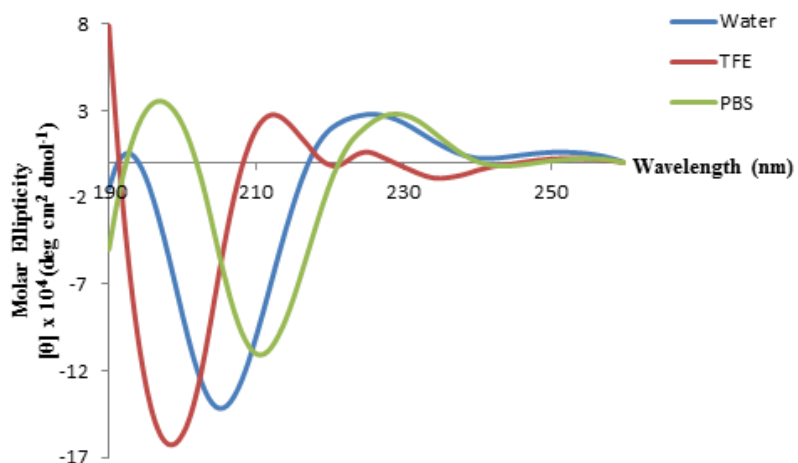
Figure 3.6. CD spectra for Pep42-R6 (**Table 2.1, sequence 2.3**, 50 μM) in water, TFE and PBS at 25 °C.
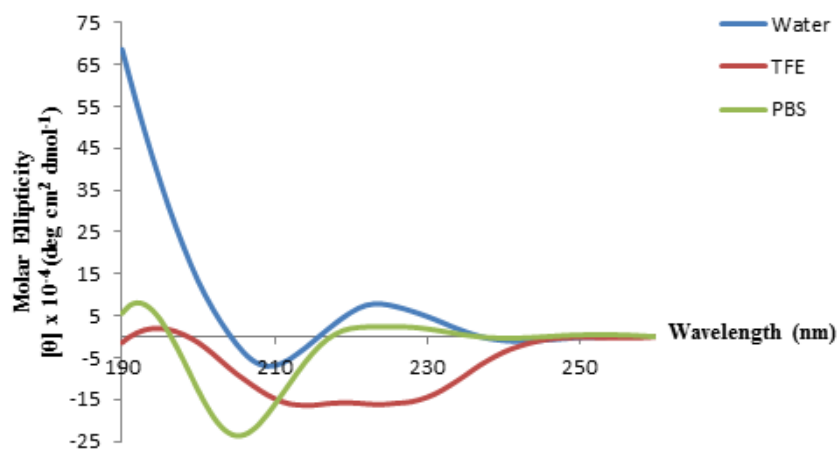
Figure 3.7. CD spectra for Pep42-R9 (**Table 2.1, sequence 2.4**, 50 μM) in water, TFE and PBS at 25 °C.
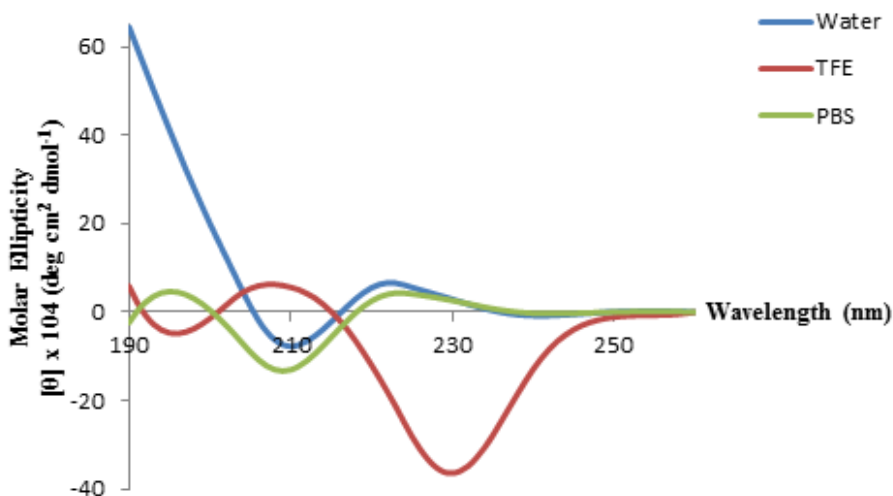
Figure 3.8. CD spectra for Pep42-R12 (**Table 2.1, sequence 2.5**, 50 µM) in water, TFE and PBS at 25 °C.

3.4.2. THERMAL STABILITY OF PEPTIDE STRUCTURES

The thermal stability of the peptide secondary structures observed in water was next studied by acquiring the CD spectrum as a function of temperature (25-85 °C) in the far-UV region (190-260 nm). At room temperature (25 °C), the peptides exhibited the secondary conformations that were observed in **Figures 3.3-3.8**. Elevated temperatures (35-85 °C), produced significant changes in the peptide secondary structures (**Figure 3.9.-3.15**). For example, the Pep42 sequence (**Table 2.1, sequence 2.1**) produced a turn-to-helix transition with increasing temperatures, causing notable changes in the amplitudes of the molar ellipticities at 230, 210 and 190 nm (**Figure 3.9**).
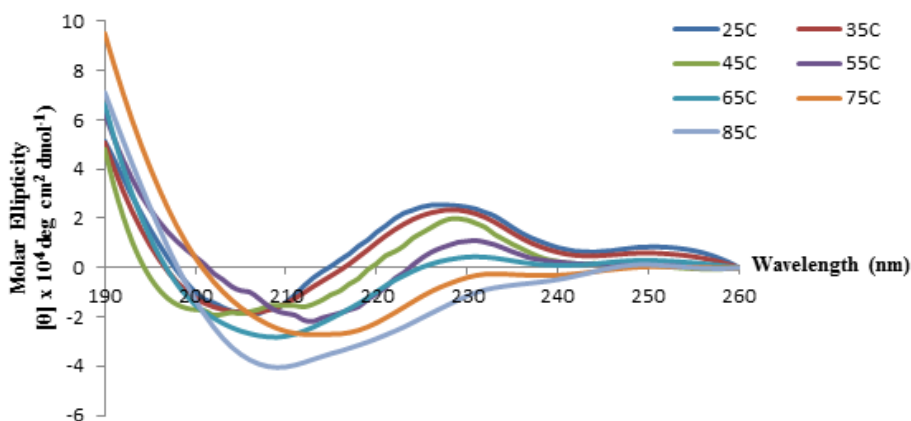
Figure 3.9. Temperature dependent (25 – 85 °C) CD spectra for Pep42 (**Table 2.1, sequence 2.1**, 50 µM).

In comparison, the poly(arginine) sequence (R9, **Table 2.1, sequence 2.16**) produced a turn geometry at room temperature (**Figure 3.4**) which was surprisingly upheld, even at elevated temperatures (35 – 85 °C). In spite of this stability, noticeable decreases in the amplitudes of the molar ellipticies at the characteristic wavelengths (230, 210 and 200 nm) for the β-turn structures were observed (**Figure 3.10**). The β-turn structures in arginine–rich sequences have been observed, although with the concomitant addition of stabilizing agents such as a lipids.[28]
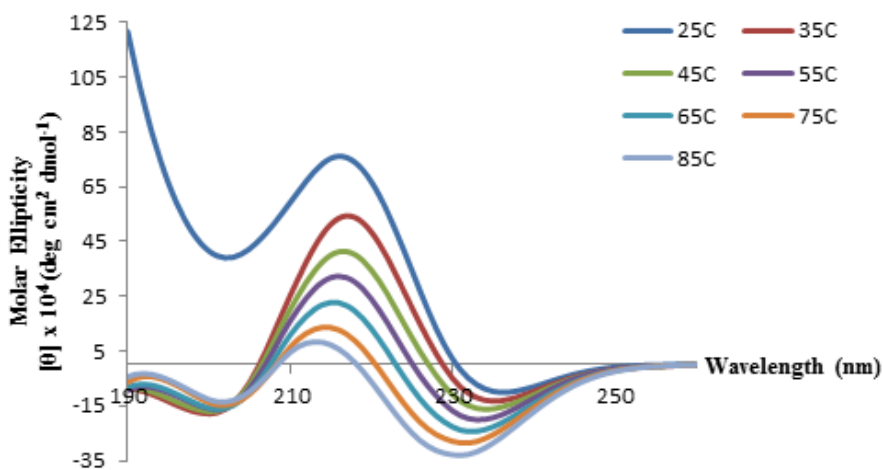
Figure 3.10. Temperature dependent (25 – 85 °C) CD spectra for R9 (**Table 2.1, sequence 2.16**, 50 µM).

Within the Pep42-poly(arginine) series (**Table 2.1, sequences 2.1-2.5**), turn-to-helix transitions with increasing temperatures (25-85 °C) were observed. These were characterized with significant changes in the amplitudes of the molar ellipticities occurring at 230, 210 and 190 nm (**Figure 3.11-3.14**). With exception, the Pep42-R_6 sequence (**Table 2.1, sequence 2.3**, **Figure 3.12**) was found to exhibit a turn-to-coil transition, with the characteristic random coil negative minimum at 190 nm becoming apparent at elevated temperatures (45 – 85 °C). Moreover, the Pep42-poly(D-arginine) series (**Table 2.1, sequences 2.6-2.9**, **Appendix Figures A33-A39**) produced similar trends during the thermal denaturation experiments. The CD spectra also contained noticeable inversions in the structures relative the Pep42-poly(L-arginine) sequences due to the change in stereochemistry at the arginine residues. Thus, increasing temperatures (25 - 85 °C) were found to trigger dynamic changes in peptide conformations without denaturing peptide structure to random coil. This result is not entirely surprising considering under non-reducing conditions disulfide bonds have been shown to maintain stable peptide secondary structures.[26] Moreover, the decrease in the molar ellipticities at the characteristic wavelengths describing peptide structure suggests that the non-covalent interactions, (hydrogen bonding) are disrupted at elevated temperatures compromising the peptide fold. This data also suggests that the observed peptide secondary structures at elevated temperatures (45 – 85 °C) were stabilized by the Pep42 disulfide bond. In order to validate the influence of the disulfide bond on peptide structure and stability, the Pep42 sequence was reduced (DTT) to the free thiol. In this case, reduced Pep42 was found to adopt a helix type structure at ambient temperature and transitioned to a random coil at elevated temperatures (35-85 °C) (**Figure 3.15**). Therefore, peptides were found to readily interconvert between helix and turn geometries while generally resisting peptide secondary structure thermal denaturation in their cyclized forms.
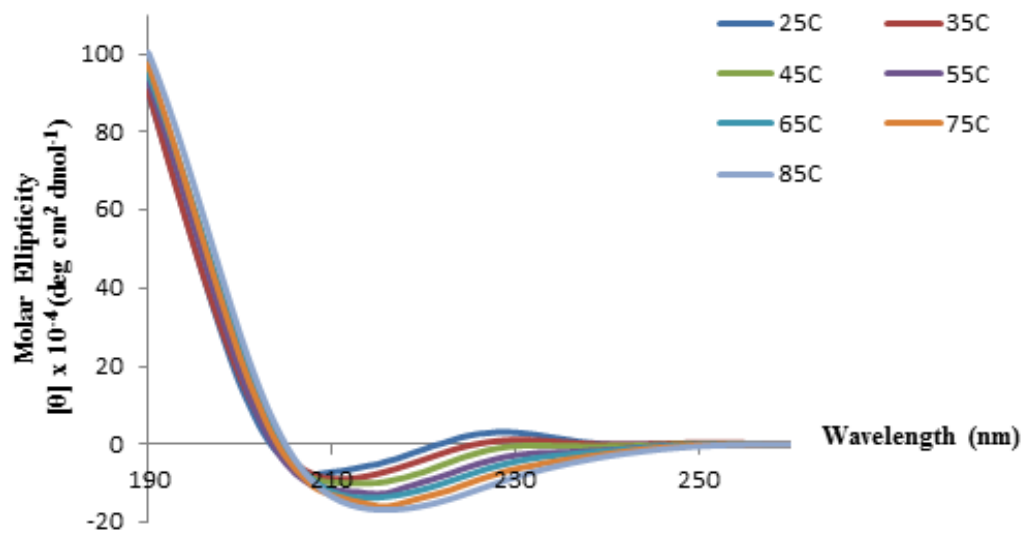
Figure 3.11. Temperature dependent (25 – 85 °C) CD spectra for Pep42-R3 (**Table 2.1, sequence 2.2**, 50 μM).
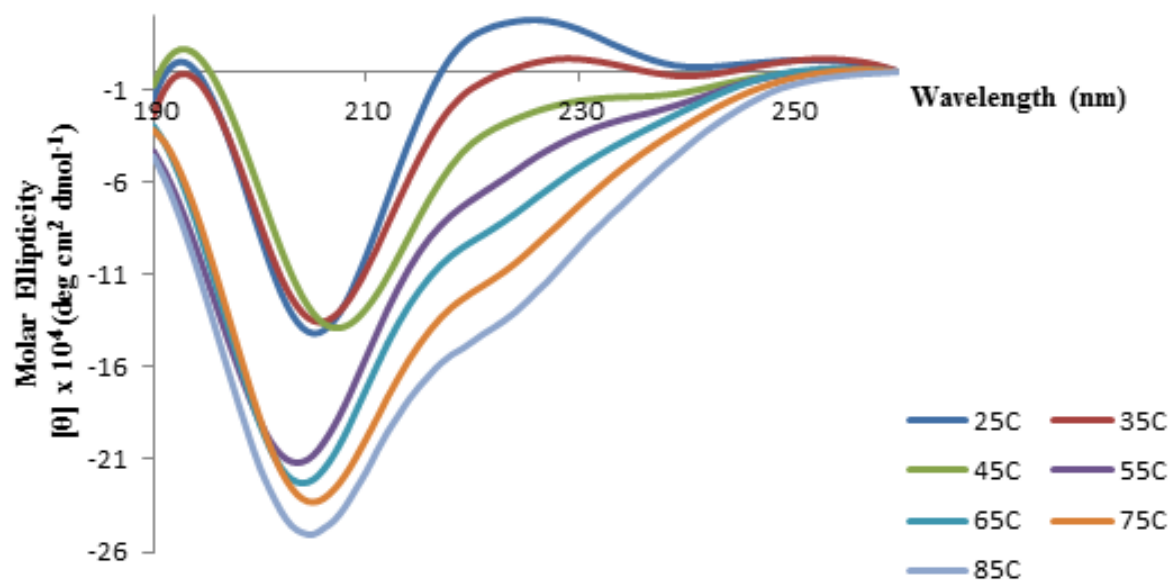
Figure 3.12. Temperature dependent (25 – 85 °C) CD spectra for Pep42-R6 (**Table 2.1, sequence 2.3**, 50 μM).
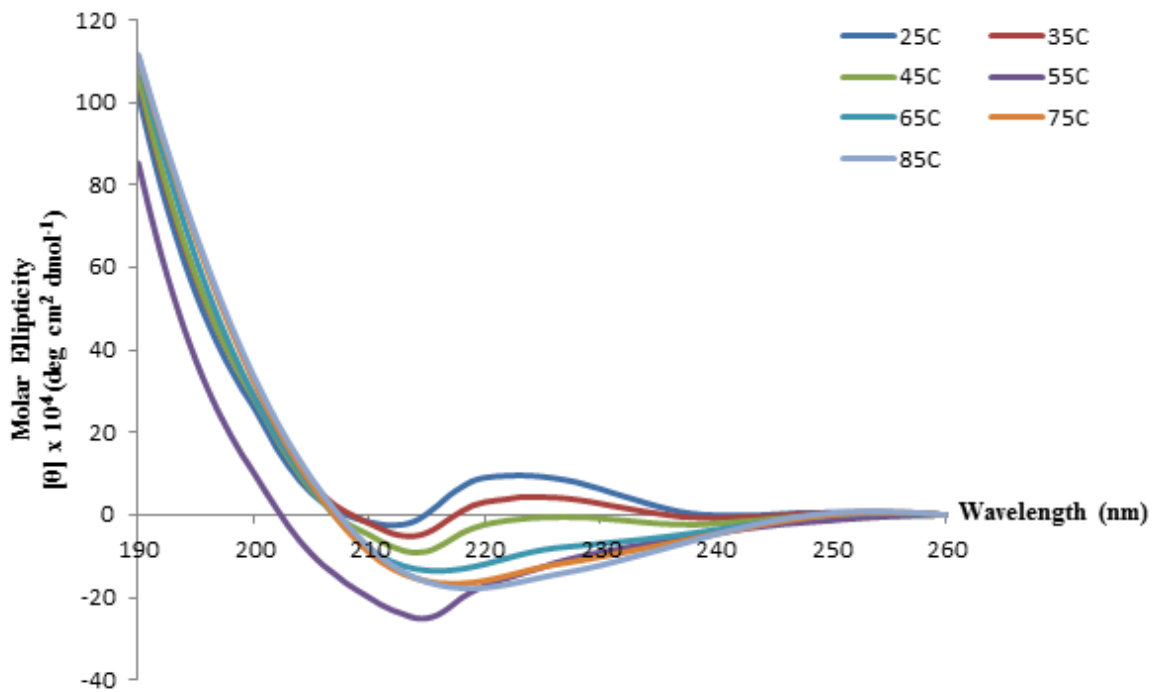
Figure 3.13. Temperature dependent (25 – 85 °C) CD spectra for Pep42-R9 (**Table 2.1, sequence 2.4**, 50 µM).

.
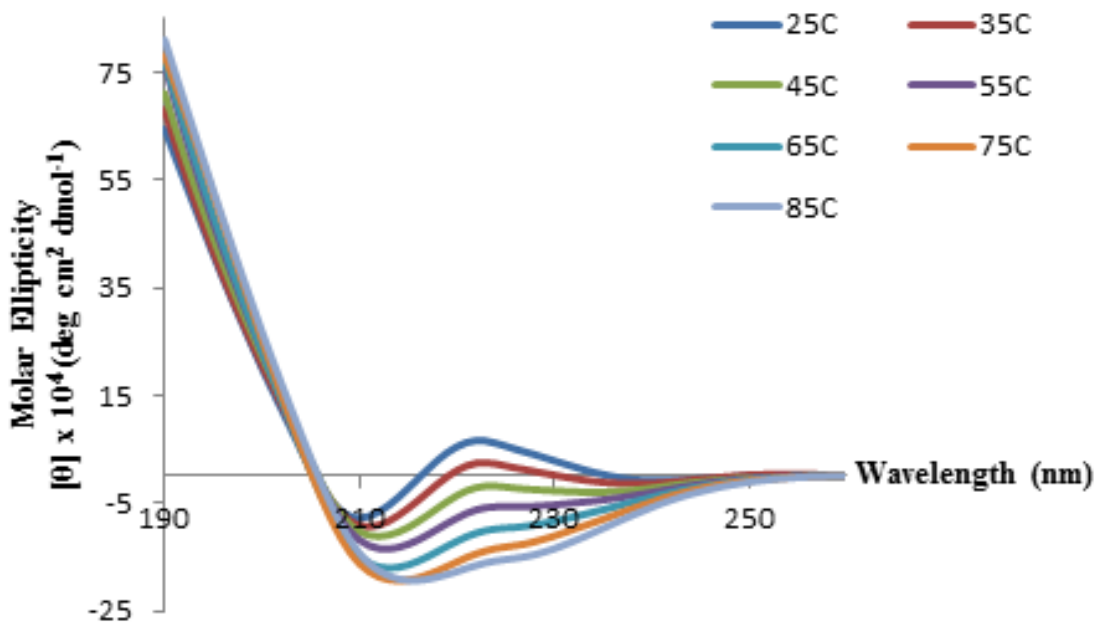
Figure 3.14. Temperature dependent (25 – 85 °C) CD spectra for Pep42-R12 (**Table 2.1, sequence 2.5**, 50 µM).
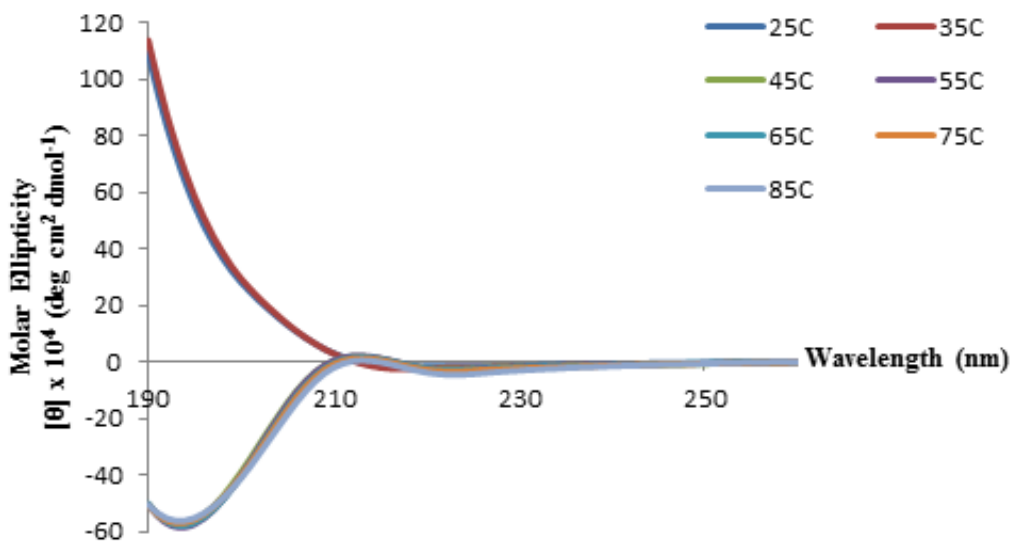
Figure 3.15. Temperature dependent (25 – 85 °C) CD spectra for linear Pep42 (**Table 2.1, sequence 2.1**, 50 μM).

3.5 CONCLUSIONS

The structures and thermal stabilities of the Pep42-poly(arginine) sequences (**Table 2.1, sequences 2.1 – 2.15**) were evaluated in this study. Specifically, the Pep42 sequence was found to display stable folded geometries in aqueous (H_2O, PBS) and organic solvent (TFE) which transitioned from helix and turn conformations (**Figure 3.3**). In comparison, the poly(arginine) sequence, R9, displayed a CD spectrum that was consistent with that of a stable β-turn conformation (**Figure 3.4**). Interestingly, turn-to-helix interconversions were observed for the Pep42 sequence while the poly(arginine) sequence maintained a stable turn geometry at elevated temperatures (45 – 85 °C). Consequently, the Pep42-poly(arginine) sequences demonstrated CD spectra that contained varying proportions of helix and turn conformations in water and PBS solvents that were dependent on the lengths of the poly(arginine) sequences (**Figure 3.5-3.8**). Similar trends on the thermal stabilities of the peptide structures were observed (**Figure 3.11-3.14**), with notable turn-to-helix transitions observed in most cases, while resisting peptide unfolding at the elevated temperatures (45 – 85 °C). The Pep42 disulfide bond was found to play a pivotal role

in maintaining stable peptide secondary structures. Therefore, the Pep42-poly(arginine) peptides (**Table 2.1, sequences 2.1-2.5**) were found to exhibit versatile folds, in which helix and turn-type secondary structures were found to be contingent on solvent, sequence and length of the poly(arginine) residues. These structural properties may translate into important peptide biological activities that are geared towards the development of a targeted gene therapy approach in cancer cells (Chapter 4).

3.6 REFERENCES

1. Ranjbar, B.; Gill, P. *Chem. Biol. Drug. Des.* **2009**, *74*, 101-120.

2. (a) Greenfield, N.J. *Tr. Anal. Chem.* **1999**, *18*, 236-244, (b) Kelly, S.M.; Price, N.C. *Biochim. Biophys. Acta.* **1997**, 1338, 161-185, (c) Kelly, S.M.; Price, N.C. *Curr. Protein Pept. Sci.* **2000**, *1*, 349-384, (d) Kelly, S.M.; Jess, T.J. *Biochim. Biophys. Acta.* **2005**, *1751*, 119-139.

3. Nikiforovich, G.V. *Int. J. Pept. Protein Res.* **1994**, *44*, 513-531.

4. Goodwin, C.R.; Fenn, L.S.; Derewacz, D.K.; Bachmann, B.O.; McLean, J.A. *J. Nat. Prod.* **2012**, *75*, 48-53.

5. Chakraborty, K.; Shivakumar, P.; Raghothama, S.; Varadarajan, R. *Biochem. J.* **2005**, *390*, 573-581.

6. Mirza, Z.; Pillai, V.G.; Zhong, W.Z. *Int. J. Mol. Sci.* **2014**, *15*, 4221-4236.

7. Ostermeir, K.; Zacharias, M. *J. Comput. Chem.* **2014**, *35*, 150-158.

8. Samatova, E.N.; Katina, N.S.; Balobanov, V.A.; Melnik, B.S.; Dolgikh, D.A.; Bychkova, V.E.; Finkelstein, A.V. Protein Sci. **2009**, *18*, 2152-2159.

9. Slutsky, M.M.; Marsh, E.N. *Protein Sci.* **2004**, *13*, 2244-2255.

10. Neubert, L.A.; Carmack, M. *J. Amer. Chem. Soc.* **1974**, *96*, 943-945.

11. Steer, B.A.; Merrill, R.A. *Biochemistry* **1995**, *34*, 7225-7233.

12. Rath, A.; Glibowicka, M.; Nadeau, V.G.; Chen, G.; Deber, C.M. *Proc. Natl. Acad. Sci. USA* **2009**, *106*, 1760-1765.

13. Yang, Z.C.; Yang, L.; Zhang, Y.X.; Yu, H.F.; An, W. *Protein J.* **2007**, *26*, 303-313.

14. Salinas, R.K.; Shida, C.S.; Pertinhez, T.A.; Spisni, A.; Nakai, C.R.; Paiva, C.R.M.; Schreier, S. *Biopolymers* **2002**, *65*, 21-31.

15. Portillo, A.M.; Krasnoslobodtsev, A.V.; Lyubchenko, Y.L. *J. Phys. Condens. Matter.* **2012**, *24*, 164205.

16. Kaushik, J.K.; Bhat, R. *J. Biol. Chem.* **2003**, *278*, 26458-26465.

17. Martin, S.R. Circular dichroism, in Proteins Labfax (Price, N. C, ed.), **1996**, *Bios Scientific Publishers Oxford*, UK, and Academic Press, San Diego, pp 195-204.

18. Price, N.C. Circular dichroism, in Proteins Labfax (Price, N. C, ed.), **1996**, *Bios Scientific Publishers Oxford*, UK, and Academic Press, San Diego, pp 34-41.

19. Guo, H.; Karplus, M. *J. Phys. Chem.* **1994**, *98*, 7104-7105.

20. Farmer, R.S.; Top, A.; Argust, L.M.; Liu, S.; Kiick, K.L. *Pharm. Res*. **2008**, *25*, 700-708.

21. Greenfield, N.J. *Methods Enzymol*. **2004**, *383*, 282-317.

22. Sarver, R.W. Jr.; Krueger, W.C. *Anal. Biochem.* **1991**, *199*, 61-67.

23. Ladokhin, A.S.; Selsted, M.E.; White, S.H. *Biochemistry*, **1999**, *28*, 12313-12319.

24. Sabatino, D.; Proulx, C.; Pohankova, P.; Ong, H.; Lubell, W.D. *J. Am. Chem. Soc.* **2011**, *133*, 12493-12506.

25. Solanas, C.; de la Torre, B.G.; Fernández-Reyes, M.; Santiveri, C.M.; Jiménez, M.A.; Rivas, L.; Jiménez, A.I.; Andreu, D.; Cativiela, C. *J. Med. Chem.* **2010**, *53*, 4119-4129.

26. Khakshoor, O.; Nowick, J.S. *Org. Lett.* **2009**, *11*, 3000-3003.

27. Hayakawa, T.; Kondo, Y.; Yamamoto, H. *Bull. Chem. Soc. (Japan)* **1969**, *42*, 1937-1941.

28. Walrant, A.; Correia, I.; Jiao, C.Y.; Lequin, O.; Bent, E.H.; Goasdoue, N.; Lacombe, C.; Chassaing, G.; Sagan, S.; Alves, I.D. *Biochim. Biophys. Acta.* **2011**, *1808*, 382-393.

3.7 EXPERIMENTAL SECTION
3.7.1 MATERIALS

Purified water, 2,2,2-trifluoroethanol (TFE), Calbiochem (San Diego, CA), ammonium bicarbonate, dithiothreitol (DTT), acetic acid, sodium chloride, potassium chloride, disodium phosphate, monopotassium phosphate were all purchased from Aldrich (Milwaukee, WI) and used without further purification.

3.7.2 DISULFIDE REDUCTION

Reduction was performed by dissolving purified, cyclic Pep42 (1.0 mg, 1.0 µmol) in ammonium bicarbonate pH 8.4 (1.0 mL, 0.1 M). Dithiothreitol (DTT) (1.0 mL, 1.0 M) solution was added and the mixture was reacted under an atmosphere of nitrogen at room temperature (22 °C) for 6 h. The reaction was quenched with acetic acid (5.72 µL, 0.1 M) and lyophilized to dryness overnight prior to LCMS analysis.

3.7.3 INSTRUMENTAL PARAMETERS FOR CD SPECTROSCOPY

The CD spectra of the peptide samples were collected in high-transparency rectangular quartz cuvettes (Fisher Scientific, Pittsburgh, PA) with a path length of 1.0 cm. These were placed in calibrated, temperature regulated cell holders in an Aviv 62A DS CD spectrophotometer (Lakefield, NJ). Baselines for all the cuvettes in the presence of buffer or solvent were collected before each sample scan. Prior to sample analyses, the instrumental parameters relating to bandwidth, time constant, scan rate and the number of scans were optimized.[2] The bandwidth measures the precision at which the monochromator selects light at a specific wavelength for sample analysis. For peptide analyses, the bandwidth was optimized at 1.0 nm. The time constant or the scan rate measures the time in which the CD data is averaged. Typically, increasing the scan

rate provides greater data acquisition which improves the resolution of the CD spectra. The scan

rate for the CD spectra collected in this study was set at 0.5 min. The number of scans is an essential

component for confirming sample reproducibility. An average scan is collected in $5 - 10$ min and

the data acquisition is repeated ($N = 3$) to confirm reproducibility of the results. Moreover,

increasing the number of scans will also improve the signal to noise (S/N) ratio resulting in spectra

with greater resolution and sensitivity.

3.7.4 PREPARATION OF BUFFERS AND SOLVENTS FOR CD SPECTROSCOPY

The buffers and solvents used for sample preparation must not contain any chromophores

within the selected wavelength region for CD analyses. In order to confirm their transparency, the

CD spectrum of the buffer or solvent alone (no sample) was collected and referenced as baseline.

In this study, three solvent conditions were selected and applied to evaluate the effect of solvent

on peptide structure and stability. Distilled water (pH 7.0), phosphate buffered saline (PBS)

consisting of NaCl (8.0 g), KCl (0.2 g), Na_2HPO_4 (1.4 g), KH_2PO_4 (0.2 g) dissolved in distilled

water (1.0 L) and adjusted to pH 7.4, were selected to explore the influence of pH and ionic

strength on peptide structure and stability.[1,2,13] The solvent 2,2,2-trifluoroethanol (TFE) was also

selected to explore the influence of an organic solvent known to stabilize peptide secondary

structures[14,19] on the conformations of the Pep42-poly(arginine) sequences. Prior to sample

preparation, TFE was degassed by passage through a 0.2 µm filter which also removed highly

scattering particles that can interfere with the sample analysis.[17] If the total absorbance exceeds

approximately one unit, the spectral noise will become excessive and approach an automatic cutoff

which may abort the acquistion.[18] It has been shown that overlapping signals arise from absorption

characteristics of buffers and other reagents in the far UV range.[17-19] For example, TFE has a UV

cut-off at 190 nm, while the PBS buffer has a low absorbance above 190 nm and does not interfere

with peptide absorptions in between 214 and 260 nm which makes it a suitable solvent for the CD application of peptides in a desired pH range (6 - 9.5).[20]

3.7.5 PREPARATION OF PEPTIDES FOR CD SPECTROSCOPY

The synthesized peptides in this study (Chapter 2) were isolated in purities >95% by RP-HPLC and characterized by LC/MS making them suitable for CD structural analyses. The concentration of the peptides in water (1.0 mL) was determined by UV-Vis absorption measurements at 280 nm followed by quantitative analyses using the Beer-Lambert equation (**equation 3.1**). The selected wavelength (280 nm) was based on the molar extinction coefficient for tyrosine (ε: 1280 $M^{-1}cm^{-1}$) which allowed for the precise and reproducible determination of the absolute absorption values (A_{280}) for the Pep42-poly(L/D-arginine) sequences. The stoichiometric measurements were then calculated from the Beer-Lambert law (**equation 3.1**) which correlates the absorption of the tyrosine residue in the peptide sample at 280 nm (A_{280nm}) with its concentration (c, mol/L), the molar extinction coefficient of the tyrosine residue in the peptide sequence (ε, $Lmol^{-1}cm^{-1}$) and the path length of the cuvette (l, cm).

$$A_{280nm} = \varepsilon \, c \, l \qquad\qquad (3.1)$$

Peptide samples were prepared at 50 µM in distilled water (pH 7.0), PBS buffer (pH 7.4) and TFE solvent. The samples were then degassed by passage through a 0.2 µm filter which removed highly scattering particles that may interfere with the absorption measurements of the peptide sample in solution. Exactly 1.0 mL of each of the three solvents were dispended into high-transparency rectangular quartz cuvettes (Sigma-Aldrich, Milwaukee, WI) with a path length of 1.0 cm and the baseline at 280 nm was collected and referenced prior to the sample scans.

3.7.6 DATA ACQUISITION

The cuvettes containing the blank or peptides were placed in the sample cell holder and flushed with nitrogen for 20 minutes while the lamp was cooled with a temperature-regulated circulating water bath. At a temperature of 25 °C the CD data was collected in between 190 – 260 nm. The CD spectra collected the signal as a change in sample molar ellipticity (dynode voltage) with changes in wavelengths. Samples were blank corrected, smoothed and the data converted to molar ellipticity values from the equation $[\theta] = \theta/cl$, where θ is the relative ellipticity (mdeg), c is the molar concentration of the peptides (M) and l is the path length of the cell (10 mm). The data was imported into Microsoft Excel and the CD spectra were plotted in terms of molar ellipticity, $[\theta]$, *vs* wavelength (nm). Temperature dependent studies were determined by equilibrating peptide samples (50 µM) in autoclaved distilled water (pH 7.0) at a given temperature (25-85 °C) for 5.0 min under N_2 and collecting the spectrum as previously described.

CHAPTER 4: BIOLOGICAL ACTIVITY OF CANCER-TARGETING PEPTIDES IN HEPG2 HEPATOBLASTOMA CELLS

4.1 ABSTRACT

The specific delivery of GRP78-silencing siRNA into HepG2 cancer cells is described in this study. The use of GRP78-targeting Pep42 in combination with various lengths of poly(arginine) sequences (3-12) were initially evaluated for their ability to bind to GRP78 and internalize within HepG2 cells by flow cytometry. These cancer-targeting peptides retained the ability to bind to GRP78, while demonstrating cell translocation activity that was highly contingent on the lengths of the poly(arginine) sequences. Moreover, peptides were not found to trigger HepG2 cell death. In combination with GRP78-silencing linear, branch and hyperbranch siRNAs, the complexes formed between the cancer-targeting peptides and the siRNAs (CTP:siRNA) were characterized by PAGE, CD spectroscopy, thermal denaturation, TEM and DLS. These experiments confirmed the formation of higher-ordered complexes between the CTP:siRNAs that were found to be stable towards thermal denaturation (25-85 $^{\circ}$C) while resisting degradation in biological media (FBS in DMEM). Transfection of a linear GRP78 silencing siRNA in complex with the CTP-R9 (**Table 2.1, sequence 2.4**) sequence within HepG2 liver cancer cells led to significant GRP78 silencing (50-60%) and modest cell death (5-15%) which paralleled the results obtained from the benchmark Lipofectamine transfections. These results suggests that the CTP-R9 sequence and related CTPs may function as useful GRP78-targeting transfection agents in a wide range of cancer cell types that display the cell surface GRP78 receptor. This discovery is an important contribution towards the development of an effective cancer-targeted gene therapy approach.

4.2 INTRODUCTION

4.2.1. APPLICATION OF PEP42 TO GRP78 TARGETING IN CANCER

Although many biological molecules have emerged as useful cancer therapeutics, three major drawbacks continue to limit their translation to clinical use.[1] Firstly, good cellular uptake typically requires the administration of high sample doses in order to obtain the desired therapeutic effects. Secondly, the efficient passage across the plasma membrane remains a major hurdle for the delivery of highly polar or charged biologicals. And thirdly, their lack of cell or tissue selectivity limits the therapeutic index while causing widespread toxicities. In order to mitigate these issues, cancer-targeting peptides have been explored as specific drug delivery agents. They lead to potent anti-cancer effects and without the concomitant toxicities that are associated with non-selective forms of therapy.[2]

Recent studies have demonstrated that the chaperone protein GRP78[3] is over-expressed and cell surface localized on tumors, contributing to tumor growth, invasion, metastatic spread and resistance to anti-cancer drugs.[4] Therefore, GRP78 has been classified as a valid biological marker for the development of targeted forms of cancer therapy. In the selection of high affinity and specific ligands for GRP78, binding studies have revealed that the substrate binding domain of the GRP78 receptor contains a groove with an affinity for neutral and hydrophobic amino acid residues.[18] This has led to the discovery of a new peptide ligand with an affinity and selectivity for the GRP78 receptor localized on the cell surface of cancer cells but not on healthy tissues.[5]

Phage display bio-panning experiments[6] enabled the selection of a cyclic peptide ligand, namely Pep42, H_2N-CTVALPGGYVRVC-$CONH_2$, **2.1**, which was found to bind to the GRP78 receptor (**Figure 4.1**).[5a] Pep42 possessed the ability to discriminate between the homologous Heat Shock Protein 70 (HSP70) and ubiquitous Bovine Serum Albumin (BSA) underscoring its

selectivity for the GRP78 receptor.[5b] Thus, the Pep42-phage bound specifically to immobilized GRP78 while no binding was observed for the other scrambled peptide control (**Figure 4.1**).[5b]
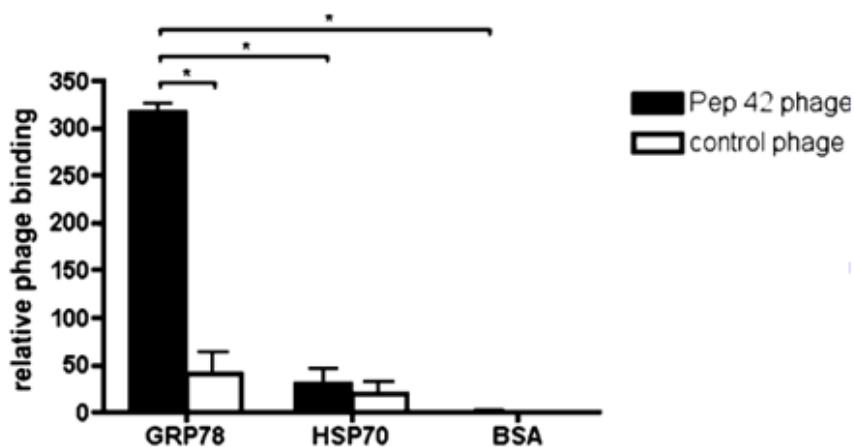
Figure 4.1. Pep42-displaying phages bind specifically to GRP78. GRP78, HSP70, and BSA were coated on microliter wells at 10 μg/mL and incubated with either Pep42-phage or the control phage that possessed a scrambled peptide sequence. Phage input was 109 cfu per well. Results were expressed as mean ± standard error of the mean (SEM) of triplicate wells.[5b] Figure adapted from Liu, Y. et al *Mol. Pharm.* **2007**, *4*, 435-447.

The selection of Pep42 as a GRP78 binding ligand prompted a series of binding experiments with a broad range of human cell types, ranging from tumors such as melanoma (Me6652/4), osteosarcoma (SJSA-1), hepatoblastoma (HepG2), lung adenocarcinoma (A549) and normal human lung or dermal fibroblast (CCD-11Lu or HDFa, respectively) cell lines.[5b] Flow cytometry revealed that the FITC-labeled Pep42 (red curve) bound to the cell surface of tumor cells but not the normal controls (**Figure 4.2, A**). Conversely, the scrambled FITC-labeled peptide control (green curve) did not demonstrate any significant binding affinity to the cell types (**Figure 4.2, A**). An anti-GRP78 polyclonal antibody was then used to determine binding specificity by blocking cell surface GRP78 on the HepG2 cells prior to FITC-labeled Pep42 treatment. In this case, a drastic decrease in the fluorescence signal was observed relative to the unblocked control (**Figure 4.2, C**). To further validate the Pep42:GRP78 binding interaction, a photoaffinity labeling

experiment was conducted to covalently bind Pep42 to the GRP78 receptor prior to western blotting (**Figure 4.2, B**). These results confirmed the Pep42:GRP78 binding interaction on the tumor cells (HepG2 and Me6652/4) but not on the normal human cells (HdFa). Furthermore, knockdown of GRP78 with siRNA treatment (**Figure 4.2, D**) abolished Pep42 binding to the GRP78 receptor, lending additional support for the GRP78 binding specificity of the Pep42 ligand on the surface of solid tumors.[5b]
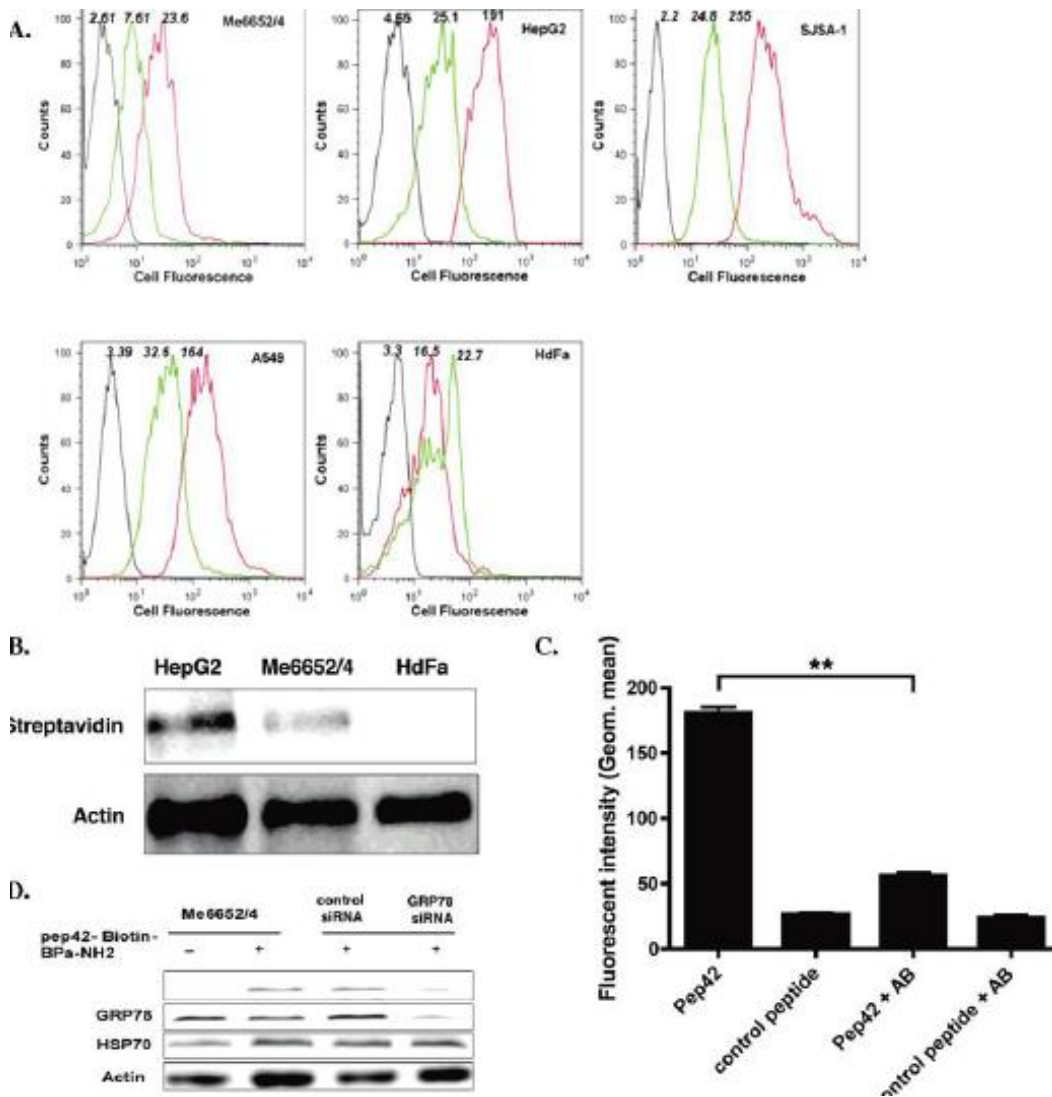

Figure 4.2. Pep42:GRP78 binding on the surface of tumor cells. A) Cells incubated with either 50 nM FITC- Pep42 (red curve) or FITC- scrambled peptide (green curve) for 25 min at 4 °C. The black curves correspond to cells incubated in the absence of any peptide. B) Pep42 binding to tumor cells using photoaffinity labeling. C) Inhibition of Pep42 binding to HepG2 cells by blocking with anti-GRP78

antibody followed by Pep42 or scrambled peptide treatment. **Difference of cells treated with Pep42 only, Student's t test, $p < 0.01$. D) Effect of GRP78 silencing on Pep42 binding to Me6652/4 cells.[5b] Figure adapted from Liu, Y. et al *Mol. Pharm.* **2007**, *4,* 435-447.

Confocal laser scanning fluorescence microscopy was used to provide additional evidence for the Pep42:GRP78 cell surface binding and to explore translocation activity.[5] Pep42-quantum dots (Pep42-QD) were applied for tracking cellular localization in A549 osteocarcinoma cells.[5b] In combination with transferrin and cholera toxin subunit B, Pep42 was found to bind to GRP78 harboring A549 cells and to accumulate in the endoplasmic reticulum with these known markers of endocytosis.[7,8] In order to elucidate the mechanism of Pep42 intracellular transport, several inhibitors of endocytosis were examined, including a known inhibitor of clathrin mediated endocytosis, chlorpromazine.[9] In its presence, Pep42 and transferrin did not internalize within A549 osteocarcinoma cells (**Figure 4.3**). Considering transferrin has been shown to internalize within cells by clathrin mediated endocytosis[7], Pep42 was speculated to internalize within cells in a similar mechanism.[5b]

Considering the GRP78 targeting and specific internalization within cancer cells but not in normal cell types, Pep42 was next evaluated as a targeting vector for the selective delivery of anti-cancer drugs in tumors.[5] Pep42 has been effectively conjugated with potent chemotherapeutics (Taxol and Doxorubicin), photosensitizers (hematoporphyrin) and the apoptotic D-(KLAKLAK)$_2$ sequence for eradicating tumors *in-vitro* and in mouse bearing tumor models.[5] Therefore, the specific Pep42:GRP78 binding interaction may form the basis for the development of new and improved drug delivery methods in cancer treatment.
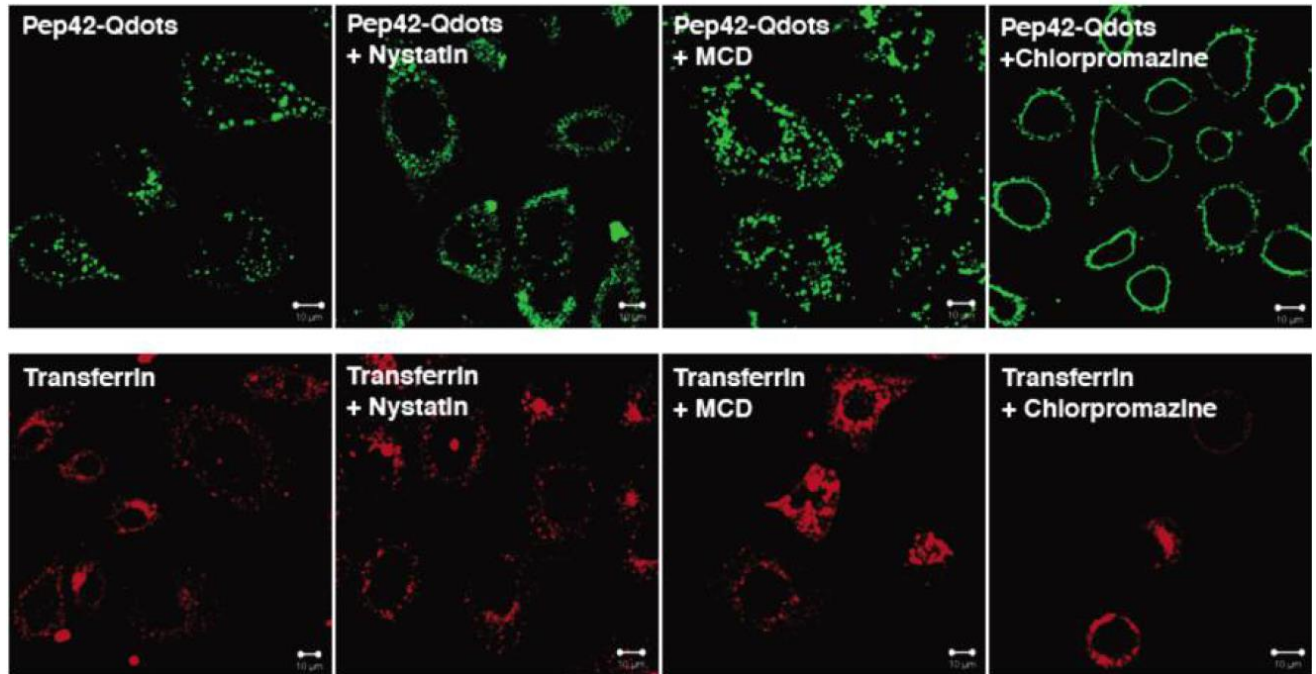
Figure 4.3. Pep42-QD internalization within A549 osteocarcinoma cells. Comparison of labeled Pep42-QD-525 *vs*. AF-594 transferrin with and without incubation of known inhibitors of endocytosis (25 μM nystatin, 30 μM chlorpromazine and 5 mM methyl β-cyclodextrin). Figure adapted from Liu, Y. et al *Mol. Pharm.* **2007**, *4,* 435-447

4.2.2. POLY(ARGININE) CELL PENETRATING PEPTIDES AS siRNA DELIVERY AGENTS

Small interfering RNA (siRNA) has shown great potential in the RNA interference (RNAi) method for gene therapy by silencing malignant mRNA expression that is associated with a wide range of genetic disorders, especially in cancer.[10] In spite of their potential utility, siRNAs are plagued by poor pharmacokinetic properties which includes, poor cell permeability and stability, which limits their therapeutic efficacy.[11] Therefore, a suitable carrier (*i.e.* transfection reagent) is necessary to facilitate the intracellular delivery of siRNA for the RNAi application. The siRNA carriers are based on viral[12], synthetic polymers[13] and biomacromolecule[14] vectors that have the ability to condense and deliver siRNA across the amphiphilic plasma membrane. Albeit these transfection methods have shown promising preliminary results *in-vitro* and *in-vivo*, they do suffer

from inherent limitations which restricts their widespread utility. For example, viral vectors and synthetic polymers are afflicted by aberrant toxicities and poor specificities. Meanwhile biomacromolecules tend to degrade rapidly in biological media providing short therapeutic indices.[11] In an effort to address these limitations, poly(arginine) peptides have been employed as efficient siRNA condensing and transfection reagents in cancer cells and in subcutaneous tumor bearing mice models. For example, the arginine peptide-mediated delivery of HER-2 siRNA induced inhibition of tumor growth *in vivo* (**Figure 4.4**).[15] Moreover, poly(D-arginine) peptides have been shown to confer greater metabolic stability due to the un-natural D-Arg residues, thereby improving pharmacokinetic properties. However, their lack of tissue specificity results in widespread dispersion of siRNAs in almost all cell types, resulting in detrimental 'off-target' gene silencing which compromises the treatment method.[19] In order to mitigate these side-effects, cancer-targeting peptides have been coupled to poly(arginine) sequences to facilitate the selective internalization of siRNA into tumors for RNAi activity. This strategy has been applied for the transvascular delivery of siRNA into the central nervous system with the use of an acetylcholine receptor (AchR) targeting peptide (RVG) that was coupled to a nona-arginine (R9) sequence.[16] Thus, the combination a cancer-targeting peptide with a poly(arginine) sequence forms the basis of a cancer-targeting gene therapy approach.
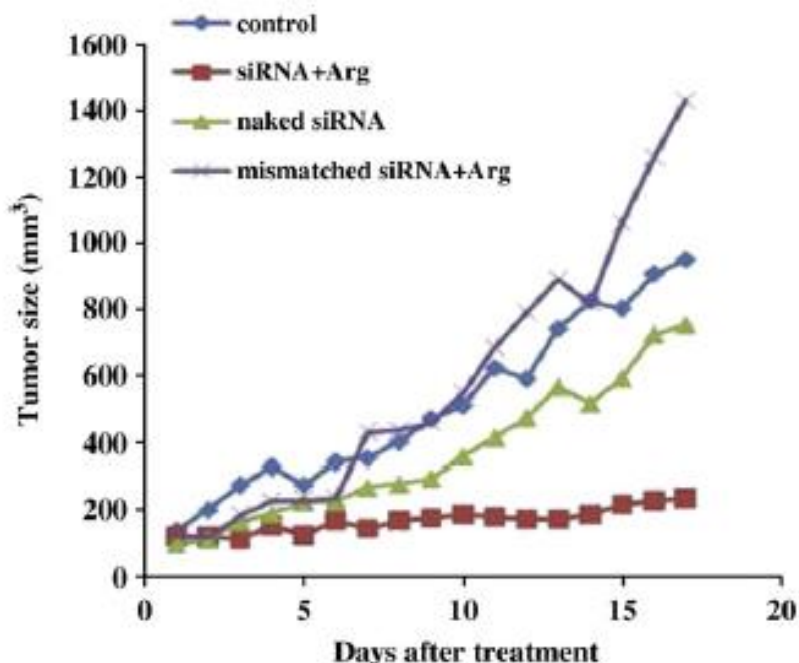
Figure 4.4. Arginine+siRNA inhibition of tumor growth in nude mice. SKOV-3 cancer cells (5×10^6 cells/mouse) were transplanted in the mice. Once the tumors reached approximately 100 mm^3, the mice were treated with arginine/HER-2-specific siRNA, arginine/HER-2-mismatched siRNA, or naked siRNA. As control, 5% glucose solution (placebo) was injected. Data=mean, n=6. S.D. of the data points is not shown for clarity.[16] Figure adapted from Kim, S.W. et al *J. Control. Rel.* **2010**, *143*, 335-343.

4.3 CHAPTER OBJECTIVES

The main objective of this thesis chapter involves the biological study of the Pep42-poly(arginine) series (**Table 2.1, sequences 2.1-2.5**). In collaboration with Drs. Allan D. Blake, Constantine Bitsaktsis (Department of Biological Sciences, Seton Hall University) and students, Brittany Blackman MSc, Christopher Parronchi (BSc student), Megan Kelly (PhD student) and Mariana Phillips (PhD student) peptide biology in HepG2 cells will be studied. The peptide-GRP78 binding interaction will be evaluated by flow cytometry. FITC-labeled peptides will be added to the GRP78 harboring HepG2 cells in order to determine binding affinity by fluorescence measurements. GRP78 binding selectivity will also be determined by flow cytometry. In this case, an unlabeled anti-GRP78 polyclonal antibody will be used to block GRP78 prior to the

administration of FITC-labeled peptides. A decrease in fluorescence signaling relative to the control experiment (FITC-peptide+HepG2 cells) will indicate peptide binding specificity. Furthermore, a Trypan blue cell death assay will be used to assess the cytotoxicities of the peptides prior to siRNA complex and transfection studies. The combination of Pep42-poly(arginine) sequences, CTP (**Table 2.1, sequences 2.2-2.5**) with linear, branch and hyperbranch GRP78-silencing siRNAs[17] is expected to produce stable higher-ordered complexes that will be characterized by PAGE, thermal denaturation, TEM and DLS. Dr. Uri Samuni (Department of Chemistry, Queen's College CUNY) and Reeta Yadav (PhD student) will assist with the TEM images and DLS measurements. With completed characterization of the CTP:siRNA complexes, transfection experiments will be conducted in HepG2 cells to determine the extent of GRP78 silencing and cancer cell death. These experiments will provide the necessary foundation for the development of our cancer-targeting gene therapy approach (**Figure 4.5**).

GRP78 targeting ligand:

$$\overbrace{S-S}$$

CTVALPGGYVRVC-R_n n = 0, 3, 6, 9, 12

GRP78 targeting domain   siRNA binding domain

Pep42   -   poly(L/D-arginine)

Linear
siRNA

Branch
siRNA

HyperBranch
siRNA

**CTP:siRNA
Complex Formation**

-cancer cells with GRP78 receptor
-healthy cells without GRP78 receptor

**Downregulation of GRP78
protein followed by
cancer cell apoptosis**
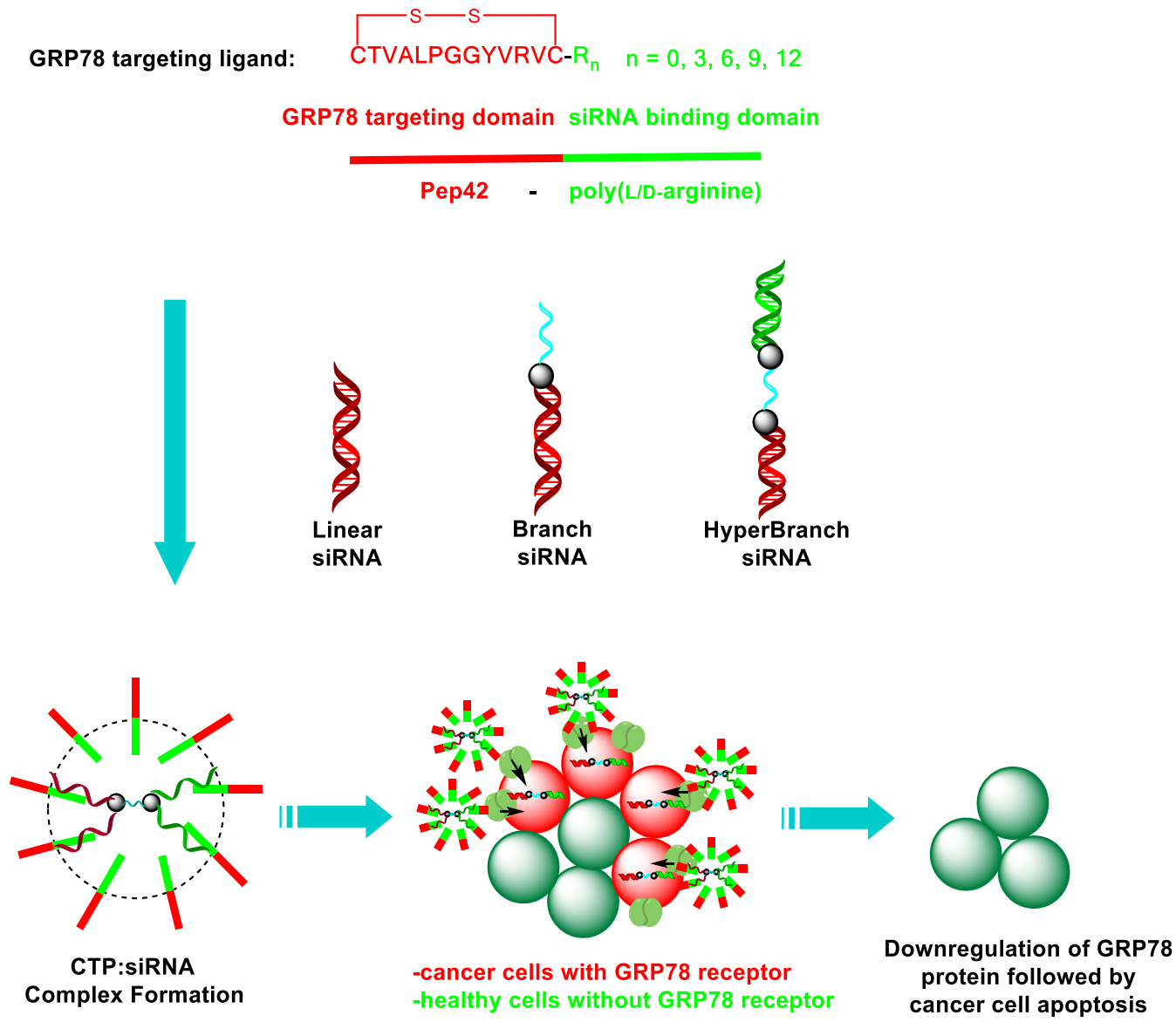
Figure 4.5. Proposed cancer-targeting gene therapy approach.

4.4 RESULTS AND DISCUSSION
4.4.1. SELECTION OF HEPG2 HEPATOBLASTOMA CELLS

Hepatoblastoma (HB) is an embryonal form of liver cancer that is found in childhood and in the early stages of adolescence.[19] HepG2 hepatoblastomas have been isolated and cultured for the pre-clinical study of pediatric liver diseases.[20] The HepG2 cell line originated in 1979 by Barbara Knowles and colleagues, 'derived from the liver tissue of a 15 year old white male with a well differentiated hepatocellular carcinoma'.[20,21] It has also been shown that cell surface GRP78 is associated with tumor invasion in HepG2 cells making it a clinically relevant model for validating our GRP78-targeting strategy.[22]

4.4.2. GRP78 BINDING AND SELECTIVITY OF FITC-PEP42-POLY(ARGININE) SEQUENCES IN HEPG2 HEPATOBLASTOMA CELLS

The ability for the peptides to bind to HepG2 cells' GRP78 and potentially exhibit cell permeability was initially assessed by flow cytometry in collaboration with the Drs. Blake and Bitsaktsis groups (**Figure 4.6.**). The internal fluorescence of the HepG2 cells was recorded and normalized according to the FITC signals observed for the peptides and corresponding GRP78 antibody (**Figure 4.6.A**). The results showed that the peptide blocker partially (~50%) inhibited the binding of the FITC-Ab on the cell surface of the HepG2 cells. Comparatively, FITC-labeled Pep42 (100 nM) exhibited similar signaling activity with and without the peptide blocker, supporting the Pep42-GRP78 binding and specificity on HepG2 cells (**Figure 4.6.D and E**).[5a,b] In contrast, FITC-labeled poly(arginine), (FITC-R9, 100 nM), displayed similar fluorescent signaling with and without the peptide blocker (10 mg/mL), illustrating non-specific HepG2 cell binding (**Figure 4.6.F and G**). Moreover, the FITC-signaling activity for this peptide was found to be 5-fold greater than the FITC-Ab and the FITC-Pep42, suggesting internalization may contribute to the enhanced fluorescent signaling activity. Interestingly, the results obtained from the FITC-

labeled poly(arginine) derived Pep42 sequences (**Appendix 22A-29A**) were found to support this

assumption, with significant increases in fluorescent signaling on the HepG2 cells $(12 - 46\%)$ with

increasing lengths on the poly(arginine) sequences $(3 - 12)$.
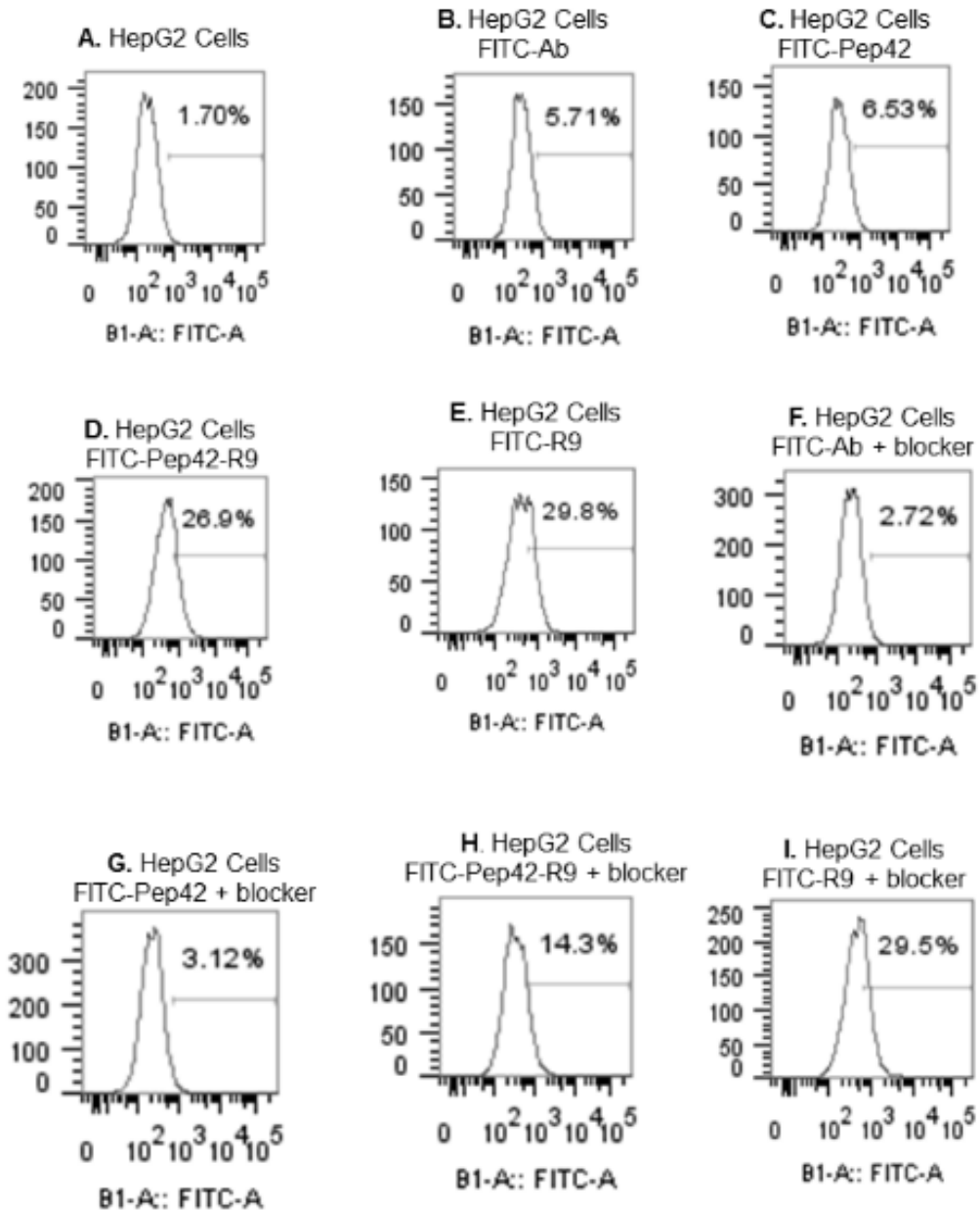
Figure 4.6. Flow cytometry data on HepG2 cells. FITC signaling collected at 521 nm on HepG2 cells (50, 000 cells/mL) alone, HepG2 cells in the presence of Alexa Fluor 488-labeled N20-anti-GRP78 primary antibody (100 nM), FITC-labeled Pep42 (100 nM), FITC-labeled Pep42-R9 (100 nM), FITC labeled R9 without (a-e) and with (f-i) N-20 GRP78 peptide blocker (10 mg/mL). Data acquired in collaboration with Drs. Blake and Bitsaktsis research groups.

To support these results, laser scanning confocal microscopy was used to capture images of the HepG2 cells incubated with the FITC-labeled peptides (**Figure 4.7**).
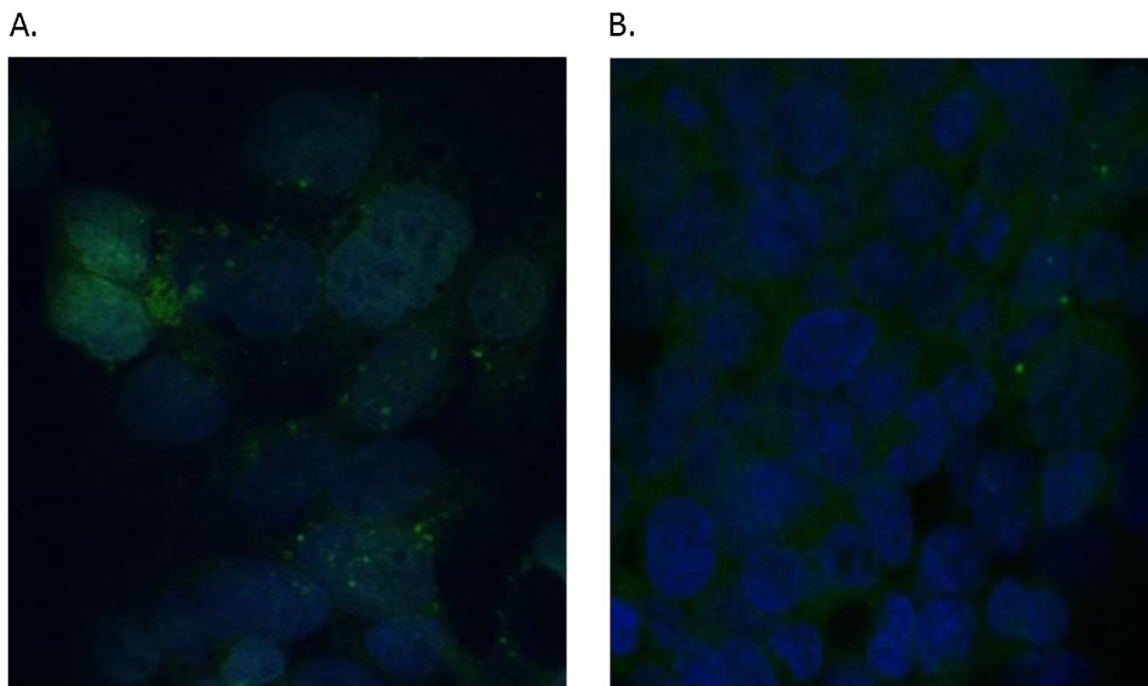
Figure 4.7. Laser scanning confocal microscopy of HepG2 cells without (a) and with (b) N-20 GRP78 blocking peptide (2.0 µg/mL). HepG2 cells (50, 000 cells/mL) were incubated with FITC-Pep42-R9 (2.0 µg/mL) and counterstained with DAPI (0.5 µg/mL in PBS). The FITC signal from the peptides is visualized as green whereas DAPI stains the cells' nuclei blue. Data acquired in collaboration with the Drs. Blake and Bitsaktsis research groups.

The FITC signaling in green was detected with the labeled Pep42-R9 sequence (2.0 µg/mL) and found to be closely associated with the blue DAPI (Ex/Em 345/455) (0.5 µg/mL in PBS) stained HepG2 cells' nuclei, suggesting cell internalization (**Appendix Figure 22A**). There was a reduction in the FITC signal observed when the FITC-labeled Pep42-R9 sequence was co-administered with the N-20 GRP78 blocking peptide, providing additional evidence for the CTP-GRP78 binding selectivity and its correlation to cell translocation activity.[5a,b] In comparison, reduced FITC signaling was observed on the HepG2 cells with the Pep42 sequence in the absence of poly(arginine) (**Appendix Figures 22A-29A**). Comparable FITC signaling was observed with and without peptide blocker for the control R9 sequence (**Appendix Figures 22A-22A**). These

results correlated to the data obtained from the flow cytometry (**Figures 4.6.D-G**) and support the ability for the Pep42-poly(arginine) sequences to bind to GRP78 and internalize within the HepG2 cells.

4.4.3. CELL VIABILITY OF POLY(ARGININE) DERIVED CANCER-TARGETING PEPTIDES IN HEPG2 CANCER CELLS

The cytotoxicities of the Pep42-poly(arginine) derived cancer-targeting peptides was assessed by comparing the number of viable HepG2 cells following incubation with peptides (**Table 2.1, sequences 2.1-2.5**) over a 48 h period. Using a Trypan blue cell exclusion assay which stains dead cells blue,[23] low levels (5-10%) of cell death were observed for the peptides (**Table 2.1, sequences 2.1-2.5**) at 0.15 mM (**Figure 4.8.A**). In a dose response assay, the Pep42-R$_9$ (**Table 2.1, sequence 2.4**) sequence was found to exhibit 5-10% cancer cell death at 0-1.5 mM indicating that the peptide is an ideal candidate for drug delivery with low cytotoxicity levels (**Figure 4.8.B**).
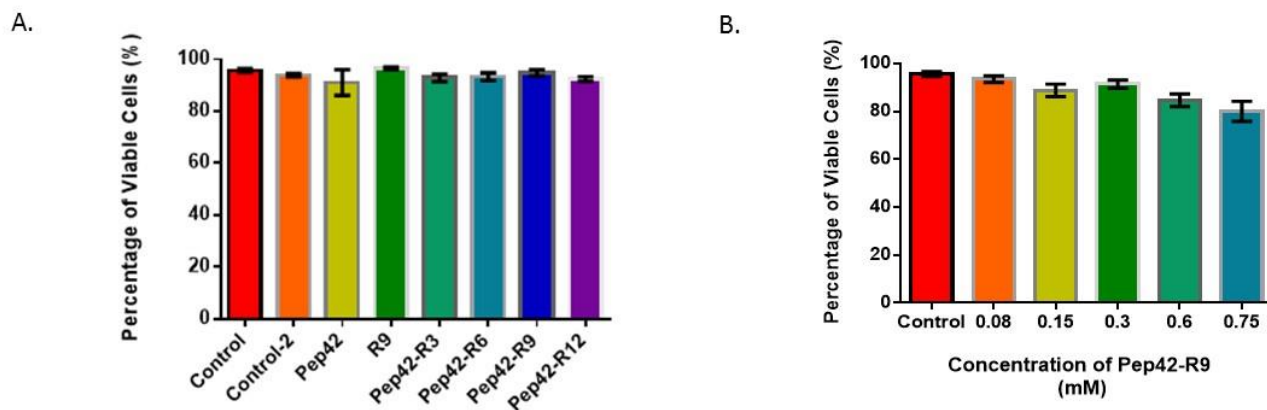
Figure 4.8. HepG2 cancer cell viability following 48 h transfection with A) Pep42 (**2.1**), Pep42-R$_3$ (**2.2**), Pep42-R$_6$ (**2.3**), Pep42-R$_9$ (**2.4**) and Pep42-R$_{12}$ (**2.5**) with a concentration of 0.15 mM and B) Pep42-R$_9$ (**2.4**) with varying concentrations (0-1.5 mM). The resulting data was collected in replicate (n $\geq$ 3) and analyzed with GraphPad Prism 5.9. Statistical significance was determined by ANOVA (p < 0.05). Data acquired in collaboration with Dr. Blake's research group.

4.4.4. FORMATION OF CTP:siRNA COMPLEXES

To evaluate the formation of CTP-R9:siRNA complex, a gel shift assay was employed to determine the optimal stoichiometric ratios of CTP and siRNA for complex formation. In this

experiment, complex formation is stimulated by the electrostatic interactions in between the polycationic CTP-R9 sequence (**Table 2.1, sequence 2.4**) and negatively charged siRNA. The CTP:siRNA complex will have a slower electrophoretic mobility on a native (no urea) PAGE relative to the unbound siRNA. This is partially related to the masking of the negatively charged oligonucleotide, which tends to freely migrate towards the cathode of the PAGE (located at the bottom of the gel). Specifically, a single-stranded siRNA (1.0 µmol) was mixed with the CTP-R9 (0.5-2.5 µmol) in various N:P ratios (1-50) in an annealing 30% sucrose (Tris-Acetate-EDTA) TAE buffer (pH 8.3), incubated for 30 min at 37 °C and loaded on a native PAGE. Following electrophoresis, the resolved samples were detected with Stains All™ dye (Aldrich) which forms a dark blue complex with the siRNA.[24] Expectedly, a decrease in the electrophoretic migration of the siRNA with increasing quantities (0.5-2.5 µmol) of the CTP-R9 was detected (**Figure 4.9**). Moreover, a decrease in the intensity of the siRNA band with increasing CTP-R9 quantities (0.5-2.5 µmol) was also observed, further supporting the complex formed in between the CTP:siRNA.
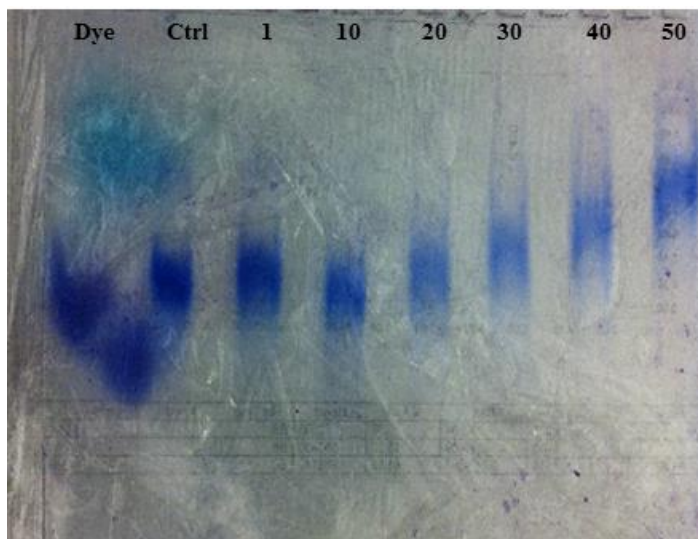
Figure 4.9. Native PAGE gel shift assay. Linear single strand siRNA (1.0 µmol) and increasing (1-50:1) stoichiometric ratios of CTP-R9 (1.0 – 50 µmol).

4.4.5. CHARACTERIZATION OF THE CTP-R9:siRNA COMPLEXES

The sizes, shapes and stabilities of the CTP:siRNA complexes were next evaluated. Dynamic Light Scattering (DLS) measurements were initially performed on a 90 plus particle size analyzer (Brookhaven Instruments Corporation) employing a 90° scattering angle and a 35 mW incident laser (658 nm). CTP-R9:siRNA (13 μM, 50:1 CTP:siRNA) samples were prepared in phosphate buffer (140 mM KCl, 1.0 mM $MgCl_2$, 5.0 mM $NaHPO_4$ adjusted to pH 7) and sonicated for 30 minutes before taking measurements. The reported effective diameters (nm) were calculated as the average of 5 runs with the corresponding standard deviation for each sample (**Table 4.1.**). The effective diameters of the complexes formed between CTP:siRNA indicated a bimodal distribution of particles (two particle size populations). The larger particle sizes observed (1400 nm) held a >2-fold increase relative to the unbound siRNA (600 nm) or CTP-R9 (40 nm). This data unequivocally supports the formation of the Pep42-R9:siRNA complex. DLS measurements for the remaining CTP:siRNA complexes can be found in the **Appendix Figure A65**.

Sample	Effective Diameter (nm)
CTP-R9	40 ± 4
siRNA	4 ± 1 110 ± 18 600 ± 95
CTP-R9:siRNA	210 ± 14 1400 ± 78

Table 4.1. Samples (0.05-0.15 μM) were prepared in pre-filtered (0.2 μm filter) pH 7.0 phosphate buffer (140 mM KCl, 1.0 mM $MgCl_2$, 5.0 mM $NaHPO_4$) and sonicated for 30 minutes before taking measurements. The reported diameter is the average of 5 runs for each sample reported with the standard deviations about the mean. Data acquired in collaboration with Dr. Uri Samuni (Queen's College CUNY).

Transmission electron microscopy (TEM) was next employed to obtain images of the CTP:siRNA complexes. The collected TEM images demonstrate a variety of sizes and shapes for the CTPs, siRNAs and their complexes (**Figure 4.10**). For example, the CTP-R9 (**Figure 4.10, A**) displays uniformly shaped spherical structures that were well dispersed throughout the optical grids. The peptide was much smaller (30 nm) in size compared to the siRNA alone (1500 nm) and the siRNA:CTP complex (400 nm) (**Figure 4.10, B** and **C**). The siRNA sample displayed aggregates of various sizes and shapes (**Figure 4.10 B**). Whereas, the CTP-R9:siRNA complex induced the formation of larger sized (1000 nm) spherically shaped aggregates that were in agreement with the effective diameters observed from the DLS measurements (**Table 4.1**). Moreover, similar trends were also observed for the remaining CTP:siRNA complexes (**Appendix Figures A23-A29**), underscoring the efficiency of the Pep42-R9 sequence in condensing siRNAs of varying lengths, sequences and morphologies.
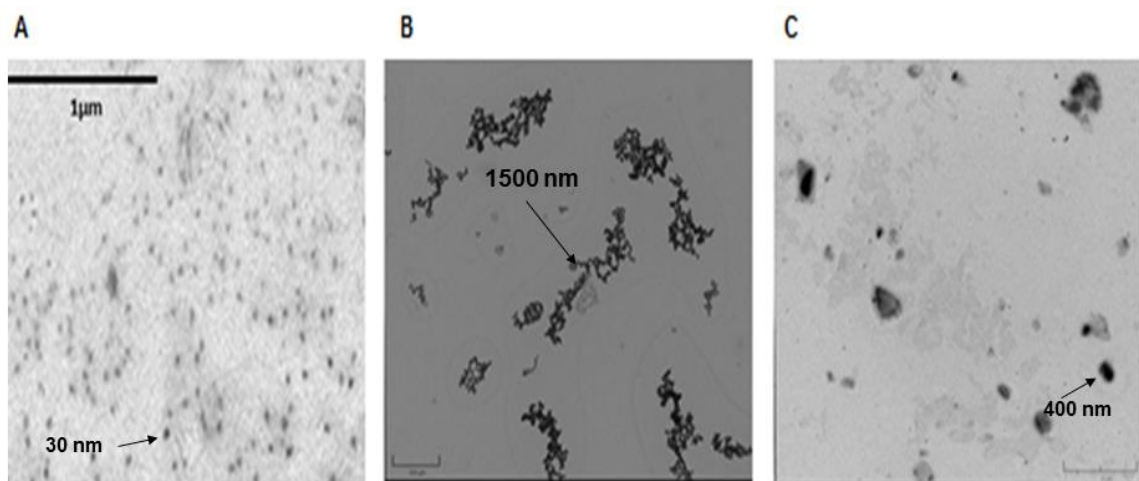
Figure 4.10. TEM images of A) CTP-R9, B) siRNA and C) CTP-R9:siRNA complex. Samples (0.13 µM) were mixed with 1.0% uranyl acetate in ethanol (1:1 v/v), sonicated for 10 minutes, and added to a carbon film coated copper grid, 300 mesh (electron microscopy sciences, Hatfield, PA) and dried overnight prior to viewing under the transmission electron microscope (JEOL, model JEM-1200 EX). Images were taken with a SIA–L3C CCD camera (Scientific Instruments and Applications, Inc.) using the software Maxim DL5 (Diffraction Limited, Ottawa, Canada). Data acquired in collaboration with Dr. Samuni (Queen's College CUNY).

The influence of the CTP-R9:siRNA complex on peptide and siRNA secondary structure was next evaluated by CD spectroscopy (**Figure 4.11**). In its free state, siRNA adopts the canonical A-type RNA helix, which has a characteristic CD signature, with a minimum peak at around 240 nm and a broad maximum in between 255-290 nm.[25] The CTP-R9 displayed a secondary structure in PBS that was contingent on a turn conformation (**Figure 3.7**) characterized by a minimum band at around 210 nm and maximum molar ellipticities centered around 220 and 190 nm.[26] In comparison, the CTP:siRNA complexes produced profound shifts in the CD spectra, with noticeable changes in the molar ellipticities occurring at the characteristic wavelengths of their respective secondary structures (**Figure 4.11**). These results also suggest the formation of higher–ordered structures between the CTP:siRNA complexes. Similar trends were observed for the remaining CTP:siRNA complexes (**Appendix Figures A43-52**).
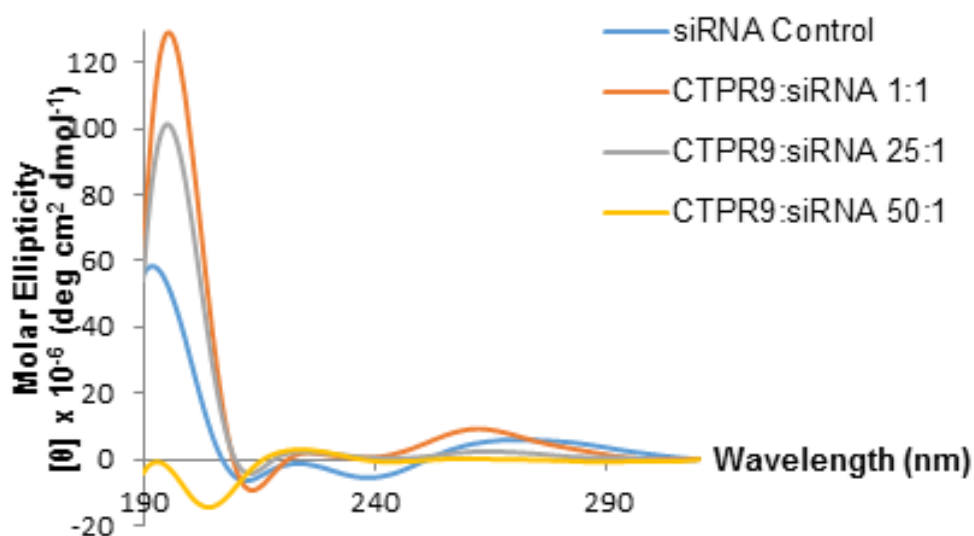
Figure 4.11. CD spectra of CTP-R9:siRNA complexes (13 μM, 1-50:1 mol/mol) in PBS (137 mM NaCl, 2.7 mM KCl, 10 mM Na$_2$HPO$_4$, 2.0 mM KH$_2$PO$_4$ adjusted to pH 7.4) at 25 ºC.

The thermal stabilities of the CTP-R9:siRNA complexes were next assessed by thermal denaturation experiments at 260 nm using temperature-regulated UV-Vis spectroscopy. The

double-stranded siRNA was found to exhibit a helix-to-coil transition[25] with increasing temperatures (5-90 °C) that produced a thermal denaturation temperature (T_m: 72 °C). Titration of CTP-R9 (0.26 – 13 µmol) to the siRNA (0.26 µmol) produced significant changes in the thermal denaturation curves (**Figure 4.12**). These changes were associated with a sharp decrease in hyperchromicities (30% to ≤10%) which abolished the helix-to-coil transition[25] in the siRNA thermal denaturation. Presumably, at optimal CTP:siRNA (15 µM, 50:1 mol/mol) concentrations the siRNA no longer forms a double-stranded RNA hybrid. Similar trends were observed in the thermal denaturation curves of the remaining CTP:siRNA complexes (**Appendix Figure A23**).
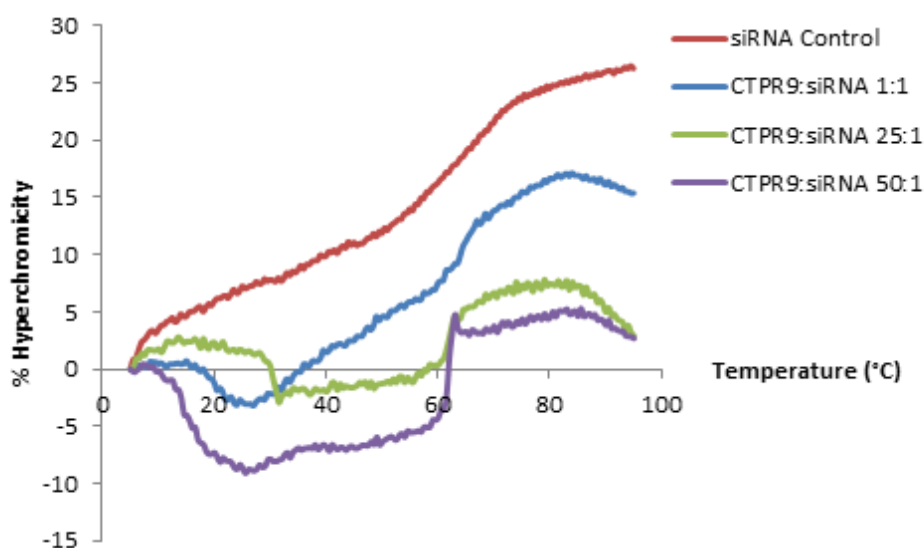
Figure 4.12. Thermal denaturation studies of the CTP:siRNA complex. Samples were prepared by mixing CTP:siRNA (15 µM, 1-50:1 mol/mol) in phosphate buffer (140 mM KCl, 1.0 mM MgCl$_2$, 5.0 mM NaHPO$_4$) and placing on a heat block incubator set at 37 °C for 1 hour. Samples were cooled to room temperature and placed in the fridge overnight prior to thermal denaturation studies. Samples were then placed in a temperature regulated (5 °C) cell holder and heated (5 – 95 °C) for sample absorption measurements at 260 nm.

4.4.6. BIOLOGICAL ACTIVITY OF CTP:siRNA COMPLEXES IN HEPG2 CELLS

The native siRNA sequences are typically prone to nuclease digestion in biological media, limiting their therapeutic potential.[27] Thus, the ability for the CTP:siRNA complexes to maintain metabolic stability is an important pre-requisite for effective and long-lasting RNAi activity. To determine the serum stability of these samples, the CTP-R9:siRNA complex and siRNA alone were subjected to a 10% fetal bovine serum (FBS) in Dulbecco's Modified Eagle Medium (DMEM) treatment. Aliquots were quenched at timed intervals and run on a denaturing (urea) PAGE to resolve the samples. Stains-All™ (Aldrich) staining generated the desired siRNA bands with and without the CTP-R9 (**Figure 4.13**). In this assay, the CTP:siRNA complexes retained their integrity for up to 8 hours, (**Figure 4.13, B**) while the siRNA control produced degradation products that were visible as lower migrating bands even after a 5 minute FBS treatment (**Figure 4.13, A**). Thus, the CTP-R9 was found to confer significant nuclease resistance to the siRNA, while the free-form siRNA was degraded within 4 hours in 10% FBS/DMEM.
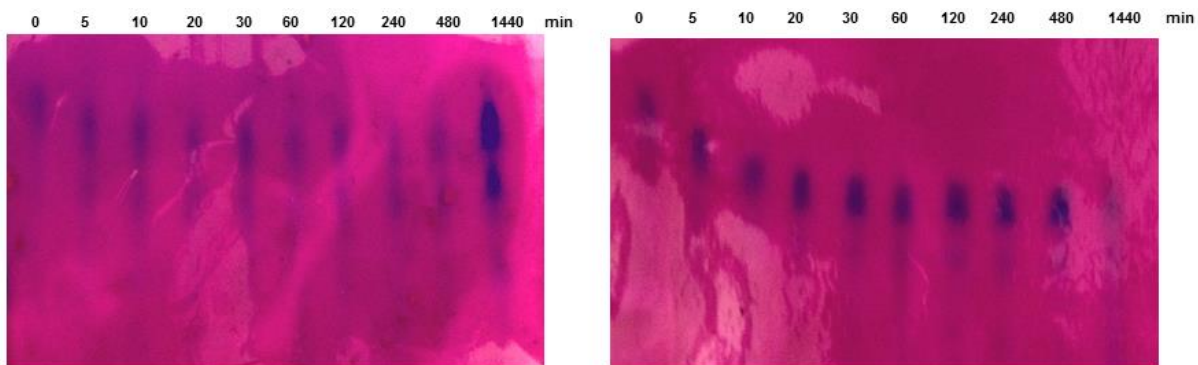
Figure 4.13. 18% denaturing (urea) PAGE of A) siRNA (20 μM) and B) CTP:siRNA (20 μM) in 10% FBS in DMEM. Samples were incubated (0.15 mL, 10% FBS/DMEM) at 37 ºC and at measured time points, aliquots (10 μL) were treated with gel loading buffer (10 μL of 80 % formamide in TBE), heated at 95 ºC and resolved on denaturing PAGE. The gels were stained with Stains-All™ (Aldrich) to view the siRNA decomposition patterns.

With metabolically stable constructs in hand, the RNAi activity of the CTP:siRNA complexes was next evaluated in HepG2 hepatoblastoma cells (**Figure 4.14**). A CTP:siRNA

complex (50:1 mole ratio, 20 µM) was prepared in binding buffer (50 mM Tris-HCl, pH 8.0, 100 mM NaCl, 5.0 mM EDTA) for transfection within the HepG2 cells. The transfected cells were incubated (48 h, 37 °C, 5% CO_2), lysed (RIPA lysis buffer, Invitrogen), and proteins were resolved by SDS PAGE and transferred to a PVDF membrane for western blotting. Immunoblotting with an anti-GRP78 primary antibody and a secondary antibody coupled to horseradish peroxidase (HRP) detected the GRP78 expression levels. Analysis of the chemiluminescence produced by the 3,3',5,5'-tetramethylbenzidine (TMB) substrate of HRP produced reduced GRP78 (~50%) at quantities that were comparable to the benchmark Lipofectamine:siRNA transfections (**Figure 4.14, A** and **B**).[17] When HepG2 cells were transfected with siRNA using lipofectamine as a transfecting agent there was a 40-50% downregulation of GRP78 with 40-80 pmol siRNA respectively,[17] which is comparative with the results obtained with CTP:siRNA transfections of HepG2 cells (**Figure 4.14, A and B**) This shows that the CTP provides a similar degree of transfection thereby proving that these CTPs can be utilized as delivery vehicles for marcomolecules into cells. Finally, a Trypan blue cell viability assay was used to track the number of dead HepG2 cells (~15%) following GRP78 silencing (**Figure 4.14, C**), which validates the RNAi activity for the CTP:siRNA constructs within HepG2 liver cancer cells.
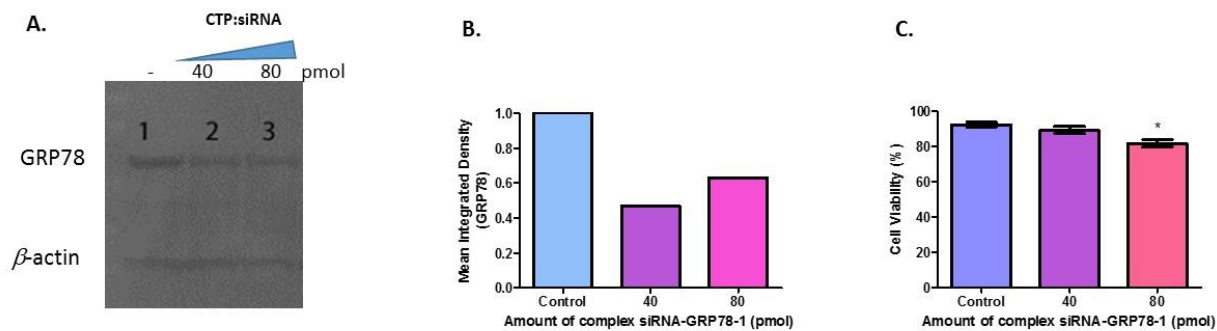
Figure 4.14. RNAi activity of the CTP:siRNA complex in HepG2 cells. A) Western blot and B) data analysis by autoradiography of GRP78 expression (n=1) following CTP:siRNA transfection (0, 40 and 80 pmol siRNA, 50:1 mole ratio CTP:siRNA, in Tris buffer pH 8). C) Cell viability data (0, 40 and 80 pmol

siRNA, 50:1 mole ratio CTP:siRNA, 20 μM in 50 μL of OPTIMEM) determined by Trypan blue viability assay (mean ± S.E.M.; n=3, *P< 0.05). Data acquired in collaboration with Dr. Blake's research group.

4.5 CONCLUSIONS

In this study, the biological activity of poly(arginine) derived Pep42 cancer-targeting peptides, CTPs, has been evaluated. These peptides demonstrated the inherent ability to bind to the GRP78 receptor, cell surface localized on HepG2 liver cancer cells. High affinity and selective GRP78 binding was validated by flow cytometry and confocal microscopy underscoring their potential utility as tumor-homing gene delivery agents. Towards this goal, CTPs were combined with GRP78-silencing siRNAs to generate the putative CTP:siRNA complex. Characterization studies of the CTP:siRNA complexes were performed by gel shift binding assays, which ascertained the optimal CTP:siRNA stoichiometric ratios for complex formation. Additionally, TEM, DLS and CD spectroscopy validated the sizes, shapes and higher-ordered nanostructures formed between the CTP:siRNA. Thermal denaturation experiments were then performed to study the changes in secondary structures of the CTPs and siRNAs during complex formation. A 10% FBS in DMEM treatment was used to confirm their metabolic stability for cell-based assays. In HepG2 hepatoblastoma cells, CTP-R9 demonstrated efficient siRNA transfection according to the potent suppression of GRP78 expression (~50% at 40 pmol siRNA) and comparable cell deaths (~15%) relative to the benchmark Lipofectamine:siRNA transfections that were previously established.[17] Thus, the CTPs developed in this study are not only applicable for efficient siRNA transfections, but also formulate the basis of our cancer-targeting gene therapy approach.

4.6 REFERENCES

1. Abad-Zapatero, C.; Champness, E.J.; Segall, M.D. *Future Med. Chem.* **2014**, *6*, 577-593.

2. (a) Aina, O.H.; Liu, R.; Sutcliffe, J.L.; Marik, J.; Pan, C.X.; Lam, K.S. *Mol. Pharm.* **2007**, *4*, 631-651, (b) Vives, E.; Schmidt, J.; Pelegrin, A. *Biochim. Biophys. Acta.* **2008**, *1786*, 126-138, (c) Wang, J.; Lei, Y.; Xie, C.; Lu, W.; Wagner, E.; Xie, Z.; Gao, J.; Zhang, X.; Yan, Z.; Liu, M. *Bioconj. Chem.* **2014**, *25*, 414-423, (d) Liu, J.; Liu, J.; Chu. L.; Wang, Y.; Duan, Y.; Feng, L.; Yang, C.; Wang, L.; Kong, D. *Int. J. Nanomed.* **2011**, *6*, 59-69, (e) Pela, M.; Saxena, P.; Luciani, R.; Santucci, M.; Ferrari, S.; Marverti, G.; Marraccini, C.; Martello, A.; Pirondi, S.; Genovese, F.; Salvadori, S.; D'Arca, D.; Ponterini, G.; Costi, M.P.; Guerrini, R. *J. Med. Chem.* **2014**, *57*, 1355-1367.

3. (a) Pfaffenbach, K.T.; Lee, A.S. *Curr. Opin. Cell Biol.* **2011**, *23*, 150-156, (b) Lee, A.S. Methods **2005**, *35*, 373-381.

4. (a) Kaufmann, R.J. *Genes Dev.* **1999**, 13, 1211-1233., (b) Lee, A.S. *Trends Biochem. Sci.* **2001**, 26, 504-510. (c) Arap, M.A.; Lahdenranta, J.; Mintz, P.J.; Hajitou, A.; Sarkis, A.S.; Arap, W.; Pasqualini, R. *Cancer Cell* **2004**, 6, 275-284, (d) Sato, M.; Yao, V.J.; Arap, W.; Pasqualini, R. *Adv. Genet.* **2010**, *69*, 97-115, (e) Virrey, J.J.; Dong, D.; Stiles, C.; Patterson, J.B.; Pen, L.; Ni, M.; Schonthal, A.H.; Chen, T.C.; Hofman, F.M.; Lee, A.S. *Mol. Cancer Res.* **2008**, *6*, 1268-1275.

5. (a) Kim, Y.; Lillo, A.M.; Steiniger, S.C.; Liu, Y.; Ballatore, C.; Anichini, A.; Mortarini, R.; Kaufmann, G.F.; Zhou, B.; Felding-Habermann, B.; Janda, K.D. *Biochemistry* **2006**, 45, 9434-9444. (b) Liu, Y.; Steiniger, S.C.; Kim, Y.; Kaufmann, G.F.; Felding-Habermann, B.; Janda, K.D. *Mol. Pharm.* **2007**, 4, 435-447. (c) Yoneda, Y.; Steiniger, S.C.; Čapková, k.; Mee, J.M.; Liu, Y.; Kaufmann, G.F.; Janda, K.D. *Bioorg. Med. Chem. Lett.* **2008**, 18, 1632-1636.

6. Arap, M.A. *Gen. Mol. Biol.* **2005**, *28*, 1-9.

7. Le Roy, C.; Wrana, J.L. *Nature Rev.* **2005**, *6*, 112-126.

8. Fittipaldi, A.; Ferrari, A.; Zoppe, M.; Arcangeli, C.; Pellegrini, V.; Beltram, F.; Giacca, M. *J. Biol. Chem.* **2003**, *278*, 34141-34149.

9. Vercauteren, D.; Vandenbroucke, R.E.; Jones, A.T.; Rejman, J.; Demeester, J.; De Smedt, S.C.; Sanders, N.N.; Braeckmans, K. *Mol. Ther.* **2010**, *18*, 561-569.

10. Masiero, M.; Nardo, G.; Indracollo, S.; Favaro, E. *Mol. Aspects Med.* **2007**, *28*, 143-166.

11. Jones, C.H.; Chen, C.K.; Ravikrishnan, A.; Rane, S.; Pfeifer, B.A. *Mol. Pharm.* **2013**, *10*, 4082-4098.

12. Robbins, P.D.; Tahara, H.; Ghivizzanni, S.C. *Trends Biotechnol.* **1998**, *16*, 35-40.

13. Wu, J.; Huang, W.; He, Z. *Scientific World Journal* **2013**, 630654.

14. McNaughton, B.R.; Cronican, J.J.; Thompson, D.B.; Liu, D.R. *Proc. Natl. Acad. Sci. USA* **2009**, *106*, 6111-6116.

15. Kim, S.W.; Kim, N.Y.; Choi, Y.B.; Park, S.H.; Yang, J.M.; Shin, S. *J. Control. Rel.* **2010**, *143*, 335-343.

16. Kumar, P.; Wu, H.; McBride, J.L.; Jung, K.E.; Kim, M.H.; Davidson, B.L.; Lee, S.K.; Shankar, P.; Manjunath, N. *Nature* **2007**, *448*, 39-43.

17. Maina, A.; Blackman, B.A.; Parronchi, C.J.; Morozko, E.; Bender, M.E.; Blake, A.D.; Sabatino, D. *Bioorg. Med. Chem. Lett.* **2013**, *23*, 5270-5274.

18. Arap, M.A.; Lahdenranta, J.; Mintz, P.J.; Hajitou, A.; Sarkis, A.S.; Arap, W.; Pasqualini, R. *Cancer Cell* **2004**, *6*, 275-284.

19. Finegold, M.J. Hepatic tumors in childhood. *Pathology of pediatric gastrointestinal and liver disease*, Springer-Verlag, New York (2004), p. 300.

20. Lopez-Terrada, D.; Cheung, S.W.; Finegold, M.J.; Knowles, B.B. *Human Pathol*. **2009**, *40*, 1512-1515.

21. Aden, D.P.; Fogel, A.; Plotkin, S. Damjanov, I.; Knowles, B.B. *Nature* **1979**, *282*, 615-616.

22. Wu, L.F.; Guo, Y.T.; Zhang, Q.H.; Xiang, M.Q.; Deng, W.; Ye, Y.Q.; Pu, Z.J.; Feng, J.L.; Huang, G.Y. *Int J. Mol. Sci.* **2014**, *15*, 525-544.

23. Altman, S.A.; Randers, L.; Rao, G. *Biotechnol. Prog.* **1993**, *9*, 671-674.

24. Wade, M.F.; O'Conner, J.L. *BioTechniques* **1992**, *12*, 794-796.

25. Gray, D.M.; Hung, S.H.; Johnson, K.H. *Methods Enzymol*. **1995**, *246*, 19-34.

26. (a) Ladokhin, A.S.; Selsted, M.E.; White, S.H. *Biochemistry* **1999**, *38*, 12313-12319, (b) Sabatino, D.; Proulx, C.; Pohankova, P.; Ong, H.; Lubell, W.D. *J. Am. Chem. Soc.* **2011**, *133*, 12493-12506.

27. Bumcrot, D.; Manoharan, M.; Koteliansky, V.; Sah, D.W.Y. *Nat. Chem. Biol.* **2006**, 2, 711-719.

28. Brown, J.C.; Pusey, P.N.; Goodwin, J.W.; Ottewill, R.H. *J. Phys.* **1975**, *5*, 664-682.

29. Adav, S.S.; Lin, J.C.T.; Whiteley, C.G.; Lee, D.L.; Peng, X.F.; Zhang, Z.P. *Biotech. Adv.* **2010**, *28*, 255-280.

30. Mason, T. *Fluorescent and Luminescent Probes for Biological Activity*, New York: Academic Press, **1999**

31. Wilson, T. (ed.) *Confocal Microscopy*, New York: Academic Press, **1990**

4.7 EXPERIMENTAL SECTION
4.7.1. FORMATION OF CTP:siRNA COMPLEXES

Poly(arginine)-Pep42 CTPs (**Table 2.1, sequences 2.2-2.5**) were added in increasing concentrations (0.5-2.5 μmol) relative to the siRNA (0.5 μmol) in annealing buffer (50 mM Tris-HCl, pH 8.0, 100 mM NaCl, 5.0 mM EDTA). The samples were incubated at 37 ℃ for 1 hour, cooled to room temperature and incubated at 4 ℃ overnight.

4.7.2. POLYACRYLAMIDE GEL ELECTROPHORESIS (PAGE) GEL SHIFT ASSAY OF CTP:siRNA COMPLEXES

The CTP:siRNA samples were analyzed by adding stoichiometric ratios (13 μM, 1-50:1, mol/mol) of CTP:siRNA in a 30% sucrose buffer (1X TAE, 10 μL). These complexes were then analyzed by electrophoresis on a native 18% polyacrylamide gel (22.5 mL acrylamide and *N,N'*-methylene bisacrylamide, 22.5 mL autoclaved water) in 10X TBE buffer, 22.5 mL (acrylamide and *N,N*-methylene bisacrylamide) and 22.5 mL of autoclaved water (pH 8). The gel was run at 500 V for 2.5 hours, which was followed by detection with Stains-All™ for 2 hours in order to visualize the CTP:siRNA bands.

4.7.3. STRUCTURAL AND THERMAL ANALYSIS OF CTP:siRNA COMPLEXES

The CTP-R9:siRNA complexes (1-50:1, 13 μM) were dissolved in phosphate buffer (140 mM KCl, 1.0 mM $MgCl_2$, 5.0 mM $NaHPO_4$) and transferred to 1.0 mL silica quartz cuvette (1.0 cm path length) for CD spectroscopy on an Aviv 62A DS CD spectrophotometer (Lakefield, NJ). The baselines for all the cuvettes in the presence of phosphate buffer were collected before each sample scan was collected. Prior to sample analyses, the instrumental parameters relating to bandwidth, time constant, scan rate and the number of scans were optimized. For sample (CTP:siRNA) analyses, the bandwidth was optimized at 1 nm. The time constant or the scan rate measures the time in which the CD data is averaged. The scan rate for the CD spectra collected in this study was set at 0.5 min. The number of scans (N = 3) was performed on each sample to

confirm reproducibility. The data was imported into Microsoft Excel and the CD spectra were plotted in terms of molar ellipticity *vs* wavelength. The thermal stability of CTP-R9:siRNA (1-50:1, 13 μM) was determined using the same samples on a UV-Vis spectrophotometer at 260 nm with increasing temperatures (5 - 95 °C).

4.7.4. DYNAMIC LIGHT SCATTERING (DLS)

DLS is a useful method for measuring the size of the peptide molecule. By shining the monochromatic light of the laser on the samples in Brownian motion causes a Doppler Shift when the light hits the moving particles changing the wavelength of the incoming light. By measuring the diffusion coefficient the size distribution can be commuted as this change in wavelength is related to the size of the particle.[28] These DLS measurements were performed on a 90 plus particle size analyzer (Brookhaven Instruments Corporation) employing a 90° scattering angle and a 35 mW incident laser (658 nm). Samples (13 μM) were diluted in a pH 7.0 buffer consisting of 140 mM KCl, 1.0 mM $MgCl_2$, 5.0 mM $NaHPO_4$ and sonicated for 30 minutes before taking measurements. The reported diameters are the average of 5 runs for each sample with the corresponding standard deviations.

4.7.5. TRANSMISSION ELECTRON MICROSCOPY (TEM)

Transmission electron microscopy is a technique in which a beam of electrons is passed through a thin specimen. Some of the electrons will interact with the specimen, however the electrons that are transmitted through the specimen are magnified and focused on an image detector that allows for an image of the specimen to be formed. This image provides the size of the particle to be measured as well as the determination of aggregation which is very common with biological molecules. The diluted samples from the DLS measurements were mixed in a 1:1 (v/v) ratio with 1% uranyl acetate in ethanol and sonicated for 10 minutes. An aliquot (5.0 μL) was transferred to

a carbon film coated copper grid, 300 mesh (electron microscopy sciences, Hatfield, PA) and the excess solution was removed immediately using an absorbent paper. The grids were dried overnight and viewed under the transmission electron microscope (JEOL, model JEM-1200 EX). Images were taken with a SIA–L3C CCD camera (Scientific Instruments and Applications, Inc.) using the software Maxim DL5 (Diffraction Limited, Ottawa, Canada).

4.7.6. HEPG2 CELL CULTURE

The human hepatoblastoma, HepG2 cells (American Type Culture Collection, Manhasset, VA) were cultured in T25 cm^2 and T75 cm^2 flasks (Grenior Bio-one Cell star, FL) in Dulbecco's Modified Eagle Medium (DMEM) with GlutaMAX and heat-inactivated 10% Fetal Bovine Serum (Gibco, CA), containing 1.0% penicillin/streptomycin (Gibco, CA), in an incubator set at 37 ℃ with a humidified atmosphere of 5.0% CO_2. Cells were routinely passaged at 75% confluence using Dulbecco's PBS (Gibco, CA) and 0.05% Trypsin-EDTA (1X), Phenol Red (Gibco, CA) and then split into a 1:10 dish ratio. Cells used in the transfection experiments were cultured in 6 - 96-well culture plates and allowed to recover for 24 hours before treatment.

4.7.7. FLOW CYTOMETRY

In flow cytometry, cells flow through a flow chamber rapidly one at a time, approximately 500 cells per second. A small laser beam of very bright light hits each cell and the fluorophore present on the surface or within the cell absorbs the light of a particular wavelength and emits a different wavelength of light that is detected as a specific color depending on the fluorophore.[29] In this manner cell population counts can be tracked by fluorescent signaling. HepG2 cell were plated in DMEM at a concentration of 50,000 cells/mL in 12-well plates and incubated for 48 hours at 37°C. Cell monolayers were then washed with PBS (pH 7.4) and dissociated using cell dissociation buffer (Life Technologies Corporation, Grand Island, NY). Cells were then labelled with either

anti-GRP78 (N-20) mAb-AlexaFluor 488 (100 nM), or one of the following peptides (100 nM): FITC-Pep42, FITC-Pep42-R3, FITC-Pep42-R6, FITC-Pep42-R9, FITC-Pep42-R12, or FITC-R9. For the inhibition assays, cells were initially blocked with GRP78 N-20 blocking peptide (10 mg/mL), followed by incubation with either N20 mAb (100 nM) or with one of the FITC-Pep42 peptides. Expression of GRP78 on HepG2 cells and binding of the Pep42 peptides was assessed by flow cytometry.

4.7.8. LASER SCANNING CONFOCAL MICROSCOPY

The application of laser scanning confocal microscopy allows for the identification of cells and sub-microscopic components with a high degree of specificity through the use of multi-labeled specimens.[30] In this technique, a laser beam is focused through an aperture onto the surface of a specimen. The beam of light is then scattered and recollected excluding the original excitation wavelength which is used to form an image of the specimen.[31]

HepG2 cells were cultured at a cell density of 50,000 cells/mL in DMEM and plated on sterile glass coverslips (22x22mm) in 6-well plates for 72 hours. After 72 hours, the media was removed and replaced with fresh DMEM for 24 hours. Following incubation, the cells were washed with PBS and fixed with a 2.0% paraformaldehyde solution in PBS for 7 minutes. Coverslips were treated in the presence or absence of GRP78 N-20 blocking peptide (417 µg/mL, 1:100 dilution in PBS) or in the presence of 1.0% BSA for 30 minutes at room temperature. Following treatment, the coverslips were incubated with either anti-GRP78 (N-20) AlexaFluor 488 antibody (2.0 µg/mL), FITC-Pep42, FITC-Pep42 R9, or FITC-R9 (1.0 µg/mL, 1:1000 dilution in PBS) and incubated for 2 hours at room temperature. Coverslips were washed with PBS, counterstained with DAPI (0.5 µg/mL in PBS) for 3 minutes, washed a final time with PBS and

viewed on a Confocal Laser Scanning Microscope with the 60X oil objective lens in combination with the Olympusview software program.

4.7.9. CTP:siRNA TRANSFECTION IN HepG2 CELLS

HepG2 cells were transfected with the siRNAs, (40-80 pmol) and CTPs (4.0 nmol) in binding buffer (50 mM Tris-HCl, pH 8.0, 100 mM NaCl, 5.0 mM EDTA). The HepG2 cell monolayers were plated and incubated at 37 °C with 5.0% CO_2. After 24 h, the serum free basal medium was removed and replaced with growth medium. Transfected cells were cultured (48 h) and lysed (RIPA lysis buffer, Invitrogen) after transfection for analysis.

4.7.10. SDS-PAGE AND WESTERN BLOTTING

Cell lysates were resolved on NuPAGE 10% Bis-Tris gels and electroblotted onto polyvinyldifluoride (PVDF) membranes. Membranes were treated for 90 min in a blocking buffer containing 5% (w/v) of non-fat dehydrated milk to minimize non-specific binding. Total HepG2 cells' GRP78 expression was immunodetected with a 1:200 dilution of anti-GRP78 N-20 antibodies. The membrane associated immunoreactivity was then detected using a 1:5000 dilution of a horseradish peroxidase-conjugated anti-goat secondary antibody and detected using ECL Plus chemiluminescence. The resulting autoradiograph was scanned, quantified with NIH ImageJ and expressed as integrated pixel density.

4.7.11. CELL VIABILITY

Cell viability was determined in 24-well plates with HepG2 cells cultured in serum-free basal medium for 24 h and then incubated in the presence or absence of varying concentrations of CTP:siRNA (20 µM) for 48 h at 37 °C. The samples were removed with Enzyme Free Dissociation Buffer for 3 minutes at 37 °C. Samples were pelleted and re-suspended in Dulbucco's PBS (1.0 mL) and Trypan blue 0.4% stain (100 µL) was added, a stain for only dead cells.[17] Samples were

quantified using a Countess automated cell counter. The resulting data was analyzed with GraphPad Prism 4.0 and statistical significance was determined by ANOVA ($p < 0.05$).

CHAPTER 5: CONCLUSIONS AND CONTRIBUTIONS TO KNOWLEDGE

5.1 CONCLUSIONS AND CONTRIBUTIONS TO KNOWLEDGE MADE IN THIS THESIS

5.1.1 SYNTHESIS AND CHARACTERIZATION OF POLY(ARGININE) DERIVED CANCER-TARGETING PEPTIDES

The rational design, solid phase synthesis and characterization of a small library (16) of poly(arginine) cancer-targeting peptides has been realized in Chapter 2 of this thesis. These peptides (**Table 2.1**) are based on the cyclic peptide Pep42 sequence, H_2N-CTVALPGGYVRVC-$CONH_2$ known to selectively bind to cell surface GRP78 found on a number of different tumors and not on normal cells. Arginine rich sequences have been shown to condense oligonucleotides (*eg*. siRNA) and facilitate their cell translocation activity for applications in gene therapy. Towards the development of a cancer-targeting gene therapy approach, a new series of Pep42-poly(L/D-arginine) peptides with varying lengths of poly(L/D-arginine) sequences have been furnished in this study. The synthesis strategy necessitated optimization of the conventional Fmoc-Solid Phase Peptide Synthesis (Fmoc-SPPS) method. The use of a polar, highly swelling NovaPEG resin, based on a polyethylene glycol matrix, was found to yield the best synthesis efficiencies for the non-polar Pep42 and the amphipathic Pep42-poly(L/D-arginine) peptides. This is because the polar NovaPEG resin reduces peptide aggregation and facilitates high yielding coupling reactions of challenging Fmoc-amino acids, such as Fmoc-L/D-Arg(Pbf). Following Fmoc-SPPS, analysis and purification by RP-LC/MS provided the desired peptides in good yield (10 - 46%) and purities >95%. Confirmation of the identities of the peptide sequences was established by ESI-MS, which indicated mass:ratios (*m/z*) that were consistent with the varying charged states of the poly(arginine) sequences.

With pure peptides in hand, their structural properties and thermal stabilities were next assessed (Chapter 3). CD spectroscopy was used to determine peptide structures in various solvents (water, phosphate buffer and 2,2,2-trifluoroethanol) followed by their thermal stabilities in a physiologically relevant phosphate buffer. These experiments form the basis of our structure-activity relationship study, in an attempt to elucidate the influence of peptide structure on its biological activity (Chapter 4). The peptides were found to exhibit folded structures in varying solvents, readily transitioning between helical and turn conformations with little observation of random coil or disordered structures at room temperature, 22 °C, (**Figure 3.3-3.8**). Interestingly, the cyclic Pep42 sequence was found to display a helical-type structure in water and trifluoroethanol, while in phosphate buffer, the peptide backbone torsion angles were found to bend in a turn-type geometry. In comparison, the R9 sequence portrayed a distorted type turn conformation in various solvent conditions. Meanwhile, the Pep42-poly(L/D-arginine) series expectedly exhibited a combination of turn and helical geometries. The peptide folded structures were also found to be generally resistant towards thermal denaturation at elevated temperatures (45 – 85 °C). Turn-to-helix transitions were observed for the Pep42-poly(L/D-arginine) sequences with increasing temperatures (25 – 85 °C) in water. It was rationalized that the disulfide bond played a critical role in maintaining stable peptide folded structures, even at elevated temperatures (45 – 85 °C). This hypothesis was confirmed by the reduction (DTT) of the Pep42 disulfide bond, which revealed a helix-to-coil peptide transition at elevated temperatures (45 – 85 °C). With a better understanding of peptide structure and bio-physical properties, peptide biology was next examined towards the development of a targeted gene therapy approach in cancer cells (Chapter 4).

5.1.2 BIOLOGICAL ACTIVITY OF POLY(ARGININE) DERIVED CANCER-TARGETING PEPTIDES IN HepG2 CANCER CELLS

In Chapter 4 of this thesis, the discovery of a new siRNA delivery vector for potential applications in cancer-targeting gene therapy is described. In collaboration with the Blake and Bitsaktsis research groups (Department of Biological Sciences, Seton Hall University) peptide biology was realized. Initially, FACS analyses of FITC-labeled cancer-targeting peptides revealed GRP78 binding on HepG2 liver cancer cells that mirrored the GRP78 binding affinity and specificity of the FITC-labeled anti-GRP78 primary antibody. Thus, the poly-arginine derived Pep42 sequences were found to behave as GRP78-targeting ligands on HepG2 liver cancer cells. Moreover, the Pep42-poly(arginine) cancer-targeting peptides were not found to be toxic in HepG2 cells (<10% cell death) following a Trypan blue cell death staining assay. This result is important for the safe administration of cancer-targeting peptides in cancer treatment regimens. This revelation may be also applicable to other GRP78 overexpressing tumors, such as those belonging but not limited to hepatocarcinoma, neuroblastoma, lymphoma and glioblastoma. Towards this ultimate goal, the poly(arginine) derived cancer-targeting peptides were condensed with siRNA targeting the GRP78 mRNA oncogene. PAGE, DLS, TEM, CD spectroscopy and thermal denaturation experiments using UV-Vis spectroscopy demonstrated the formation of stable cancer-targeting peptides:siRNA, CTP:siRNA, complexes. In HepG2 liver cancer cells, a representative CTP:siRNA complex was transfected into the cells, cultured and assayed for GRP78 knockdown and cell death activity. In this assay, GRP78 silencing (50-60%) and cell death (5-15%) were found to be consistent with those observed from the benchmark Lipofectamine:siRNA transfections. This result underscores the potential utility of the CTPs in the targeted delivery of siRNA in cancer cells for potent and selective RNAi effects.

5.2 PUBLICATIONS AND CONFERENCE PRESENTATIONS

- *Manuscripts submitted for publication*

1. <u>Stesha C. Joseph</u>, Ivonne Martinez, Brittany A. Blackman, Christopher J. Parronchi, Megan Kelly, Mariana Phillips, Michael Beaury, Constantine Bitsaktsis, Allan D. Blake and David Sabatino **Synthesis, Characterization and Cytotoxicity of Poly(arginine) derived cancer-targeting peptides in HepG2 Liver Cancer Cells.** *Journal of Peptide Science* **2014**, doi: 10.1002/psc.2665.

2. <u>Stesha C. Joseph</u>, Ivonne Martinez and David Sabatino **Synthesis and Characterization of a Cancer Targeting Peptide** *NJAS Bulletin* **2014**, *manuscript in revision*.

- *Manuscripts in preparation*

1. <u>Stesha C. Joseph</u>, Anthony Maina, Brittany A. Blackman, Christopher J. Parronchi, Reeta Yadav, Megan Kelly, Mariana Phillips, Uri Samuni, Constantine Bitsaktsis ,Allan D. Blake and David Sabatino. **GRP78 targeting and silencing in HepG2 liver cancer cells with cancer-targeting peptide:siRNA complexes**. *manuscript in preparation*

- *Poster Presentations*

1. <u>Stesha C. Joseph</u>, Anthony Maina, Brittany A. Blackman, Allan Blake, and David Sabatino. Cancer-targeted delivery of siRNA in HepG2 hepatocellular carcinoma. IBC 16th Annual TIDES Conference, Providence, RI, May 12, 2014.

2. <u>Stesha C. Joseph</u>, Brittany A. Blackman, Christopher J. Parronchi, Allan D. Blake, and David Sabatino, **Synthesis Characterization and Biological Activity of Glucose Regulated Protein 78 (GRP78) Cancer-Targeting Peptides.** NYAS, Chemical Biology Discussion Year-End Symposium, New York, NY, June 5, 2013.

3. <u>Stesha C. Joseph</u>, Anthony Maina, Mariana Phillips, Lathamol Kurian, Emily Borland, Ivonne Martinez, and David Sabatino, **Cancer-targeting Peptides in Cancer Therapy**. 17th Annual Petersheim Academic Symposium, Seton Hall University, South Orange, NJ, April 23, 2013.

4. <u>Stesha C. Joseph</u>, William Penny, Ivonne Martinez, and David Sabatino, **Cancer-targeting Peptides as Cancer Specific Drug Delivery Systems.** NJAS, 57th Annual Meeting, Seton Hall University, South Orange, NJ, April 21, 2012.

5. <u>Stesha C. Joseph</u>, Lathamol Kurian, Leah R. Poland, Tammy A. Silva, and David Sabatino, **How do we make peptides in the lab?** 16th Annual Petersheim Academic Symposium, Seton Hall University, South Orange, NJ, April 12, 2011.

APPENDIX

TABLE OF CONTENTS

A.   **Supplemental RP HPLC chromatograms and MS spectra**

B.   **CTP Analysis by CD Spectroscopy**

|	RT	Area	% Area	Height
1	11.385	17264091	95.32	1295598
2	12.026	543759	3.00	88547
3	12.349	304602	1.68	40883

Figure A1. RP-HPLC analysis of purified Pep42 (**Table 2.1, sequence 2.1**) using a linear gradient 2-82% MeOH/H$_2$O (0.1% FA) over 18 min using a Zorbax RX-C18 column (4.6 x 250 mm, 5.0 μm particle size) set at a temperature of 25 °C at a flow rate of 1.0 mL/min with detection at 214 nm.
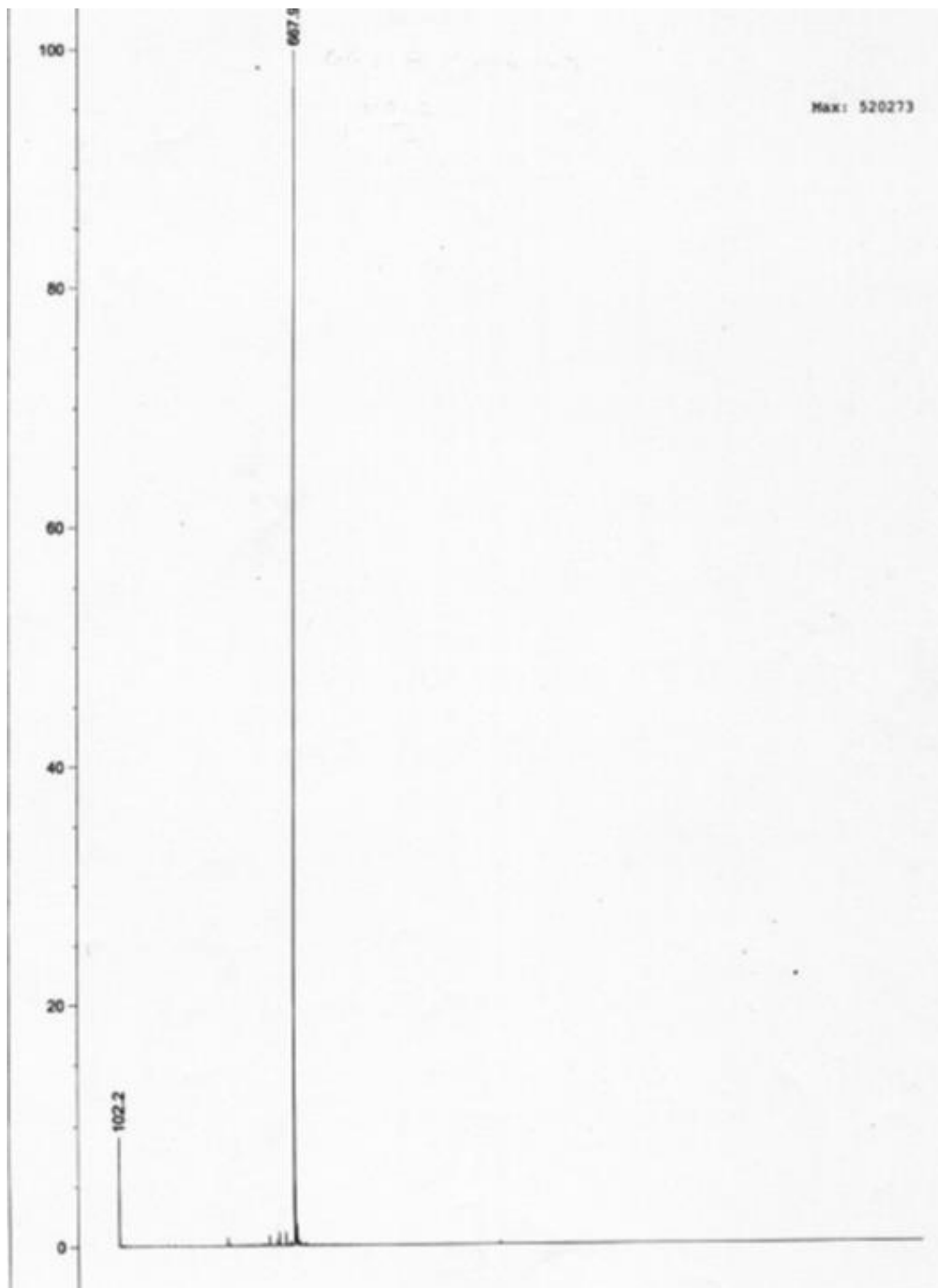
Figure A2. ESI-LCMS analysis of purified Pep42 (**Table 2.1, sequence 2.1**) using a linear gradient 2-82% MeOH/H$_2$O (0.1% FA) over 18 min using a Zorbax RX-C18 column (4.6 x 250 mm, 5.0 μm particle size) set at a temperature of 25 °C at a flow rate of 1.0 mL/min with detection at 214 nm.
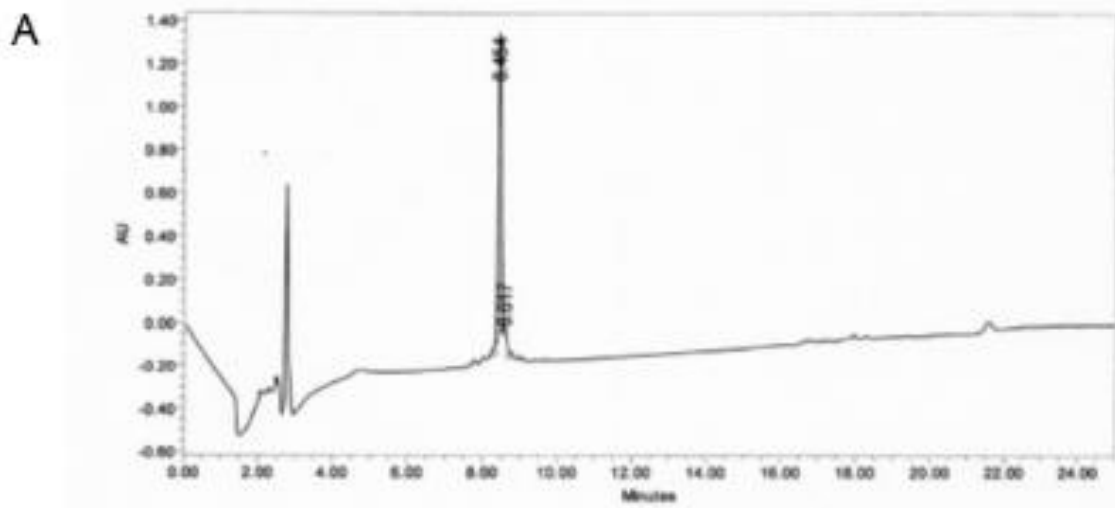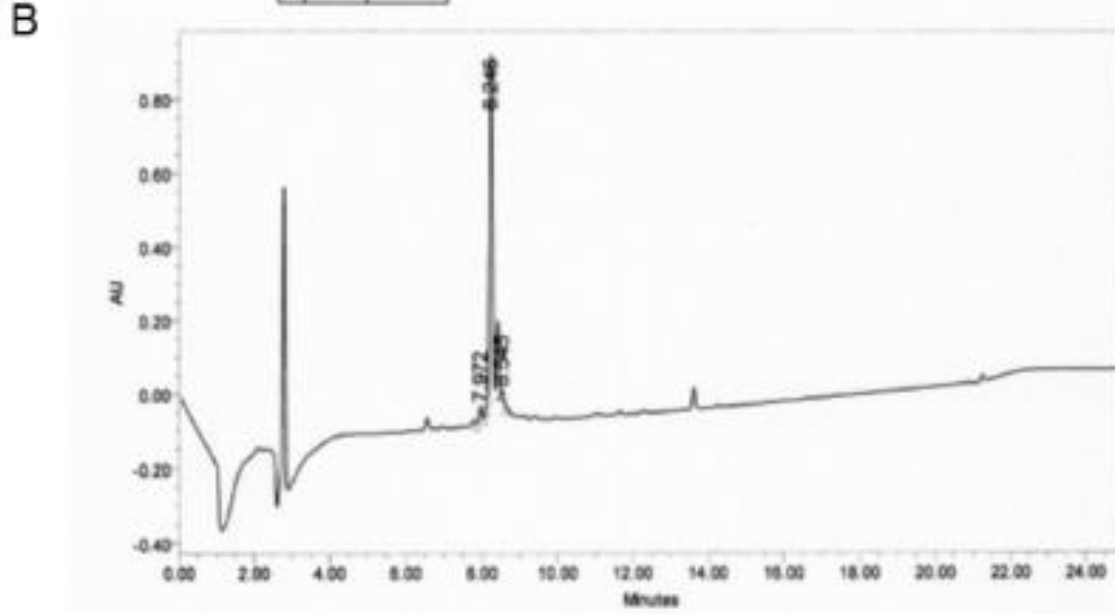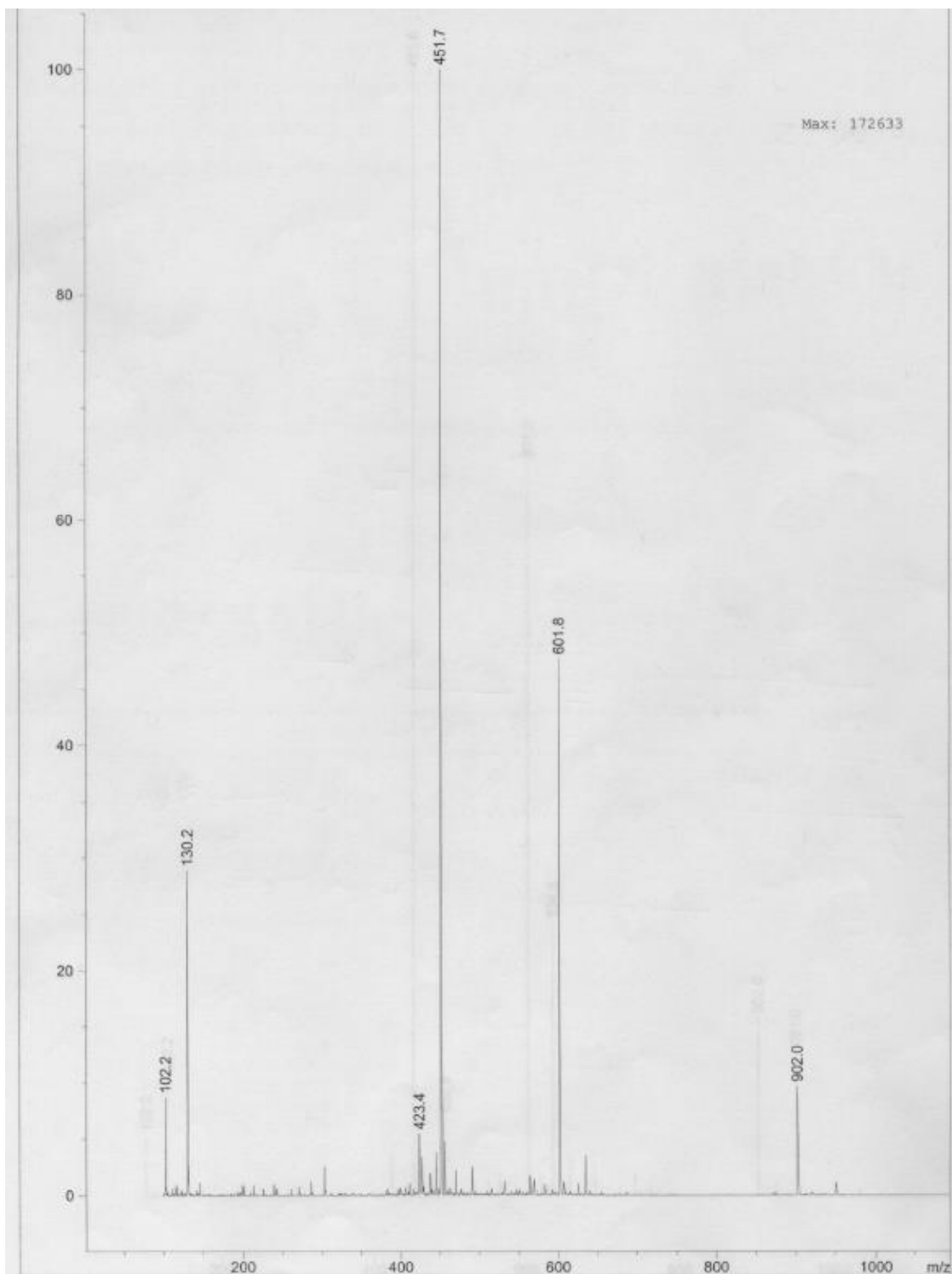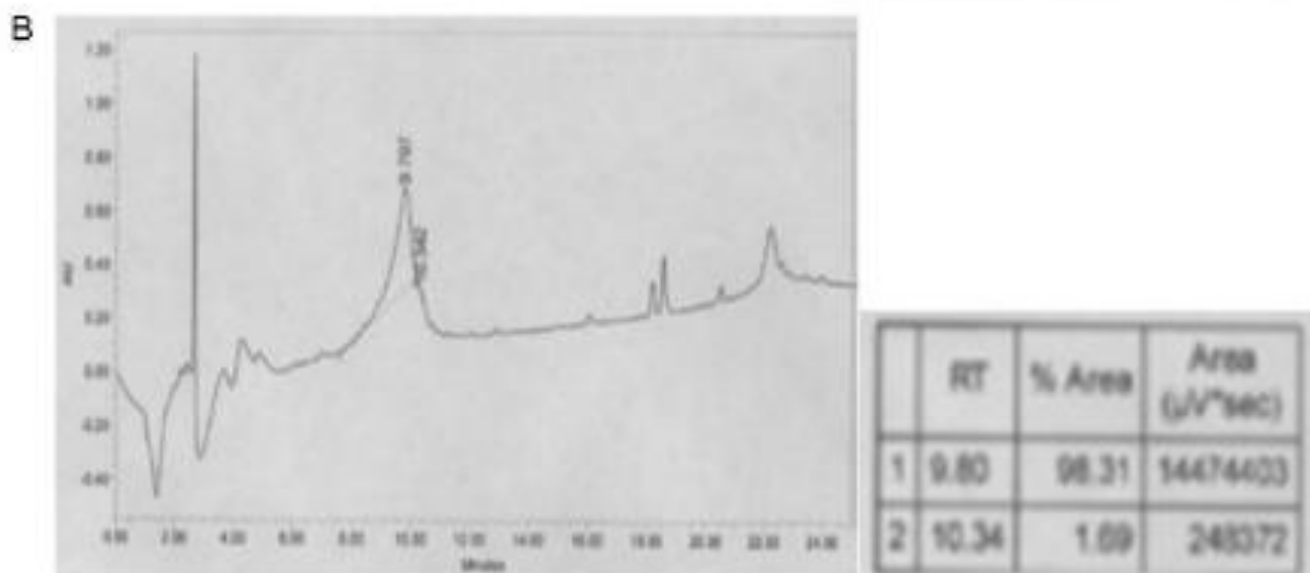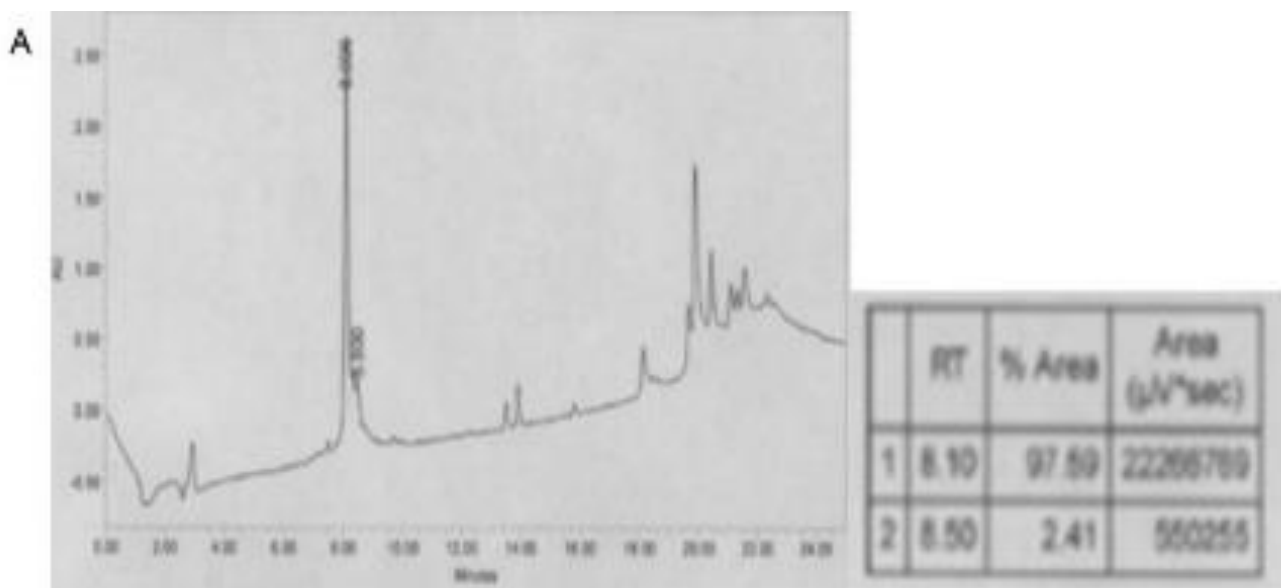
Figure A3. Representative RP-HPLC chromatograms of purified Pep42-R3 (**Table 2.1, sequence 2.2**) using A) linear gradient 2-82% MeCN/H$_2$O (0.1% TFA) over 18 min with a Zorbax RX-C18 column (4.6 x 250 mm, 5.0 μm particle size) at 25 °C and flow rate of 1.0 mL/min with detection at 214 nm and B) linear gradient 2-82% MeOH/H$_2$O (0.1% FA) over 18 min with a Zorbax RX-C18 column (4.6 x 250 mm, 5.0 μm particle size) at 25 °C and flow rate of 1.0 mL/min with detection at 214 nm.
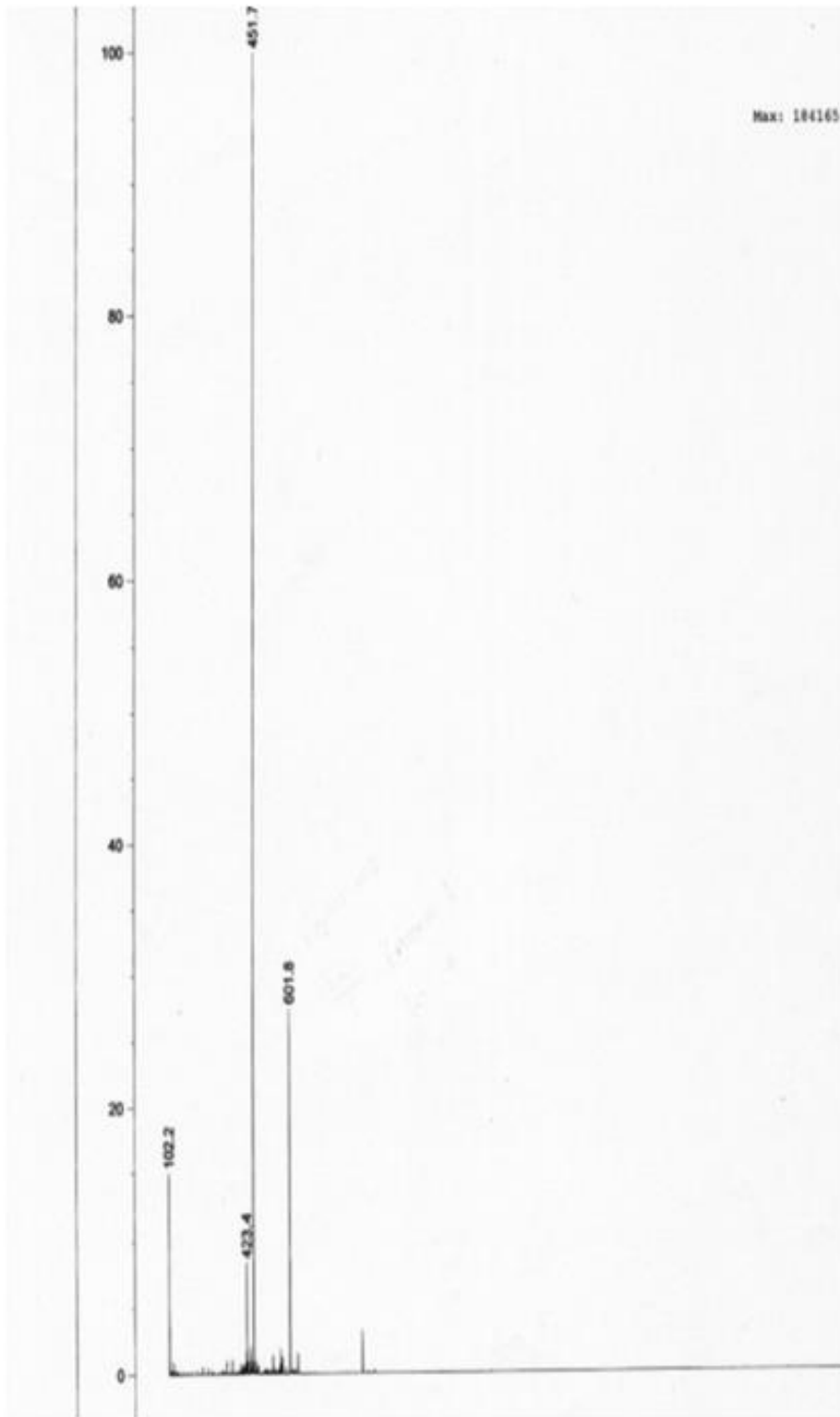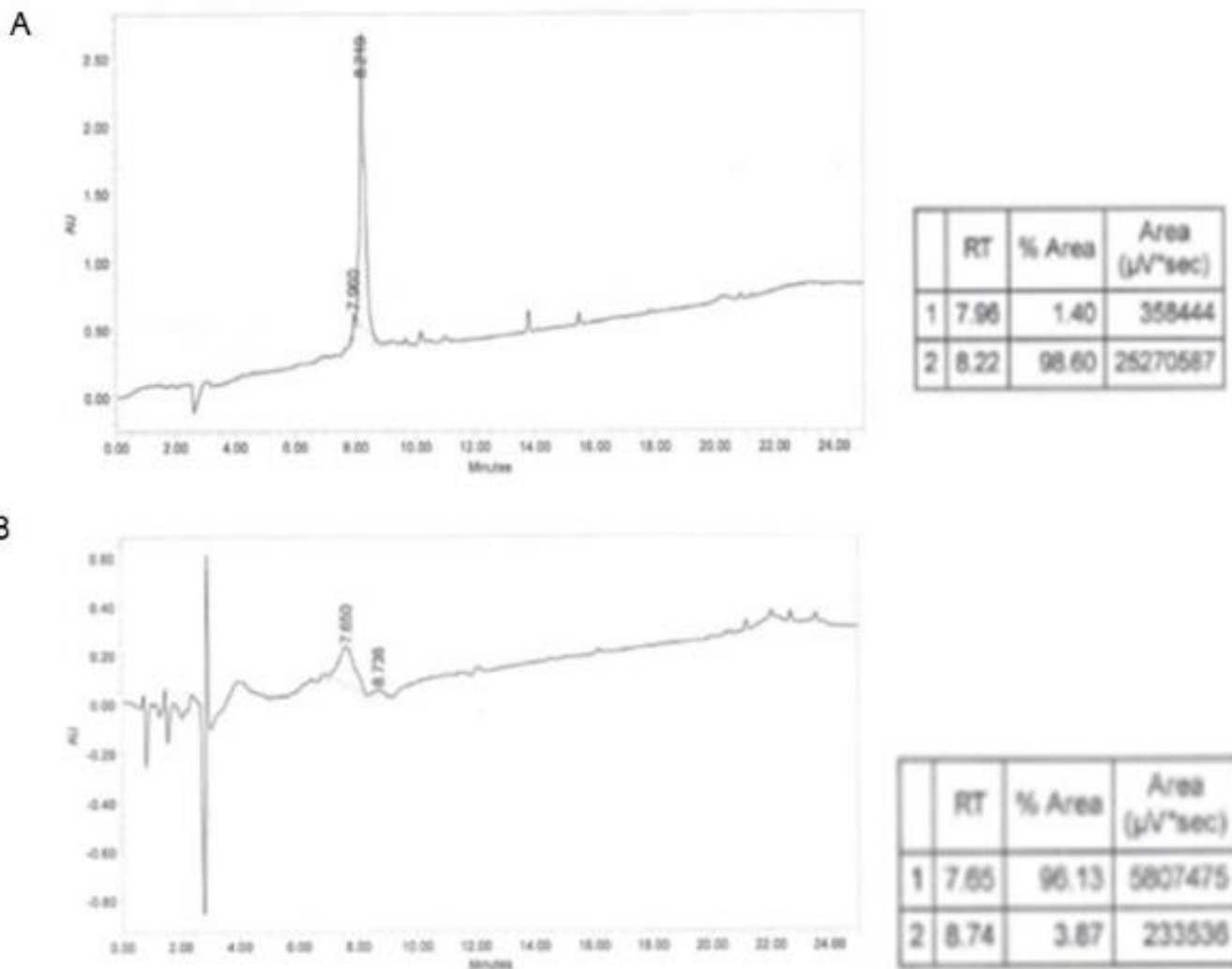
Figure A4. ESI-LCMS analysis of purified Pep42-R3 (**Table 2.1, sequence 2.2**) using a linear gradient 2-82% MeOH/H$_2$O (0.1% FA) over 18 min using a Zorbax RX-C18 column (4.6 x 250 mm, 5.0 µm particle size) set at a temperature of 25 °C at a flow rate of 1.0 mL/min with detection at 214 nm.

A
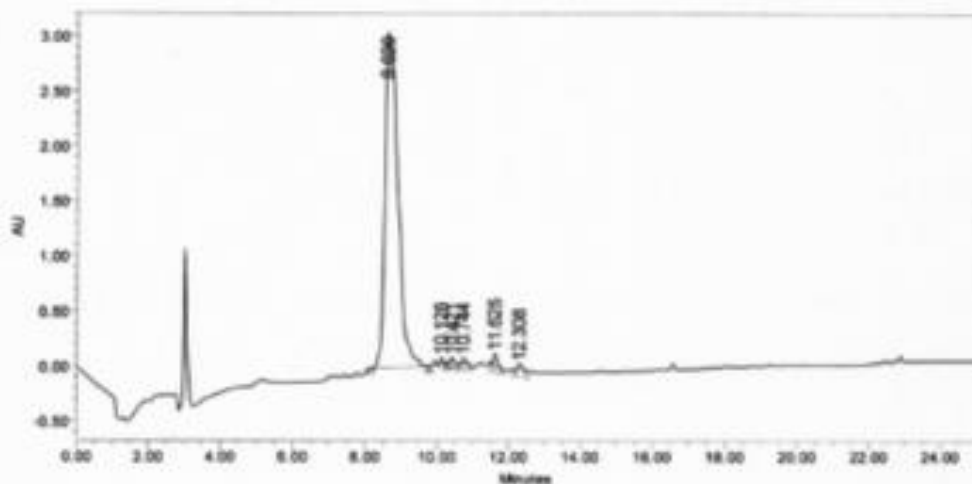
	RT	% Area
1	8.620	95.99
2	10.128	0.69
3	10.421	0.26
4	10.744	0.43
5	11.625	0.97
6	12.308	0.66

B
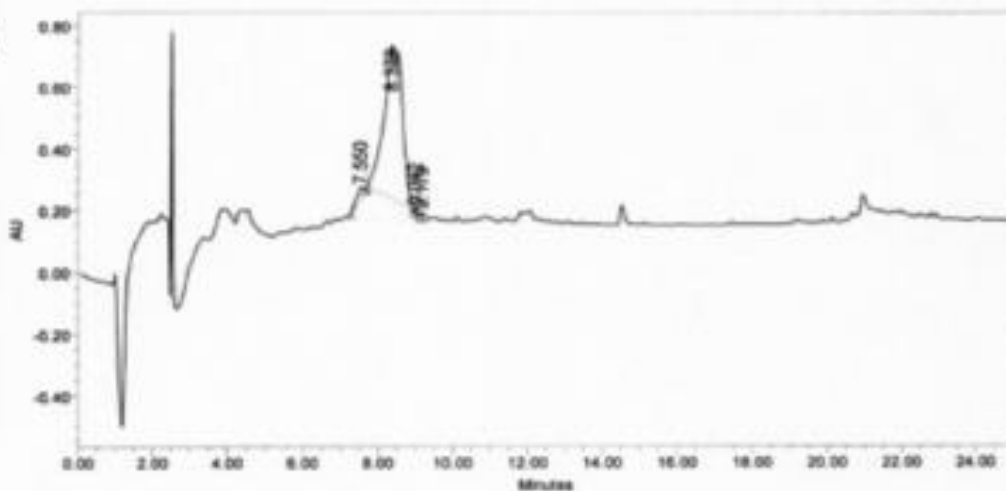
	RT	% Area
1	7.550	2.47
2	8.378	96.90
3	9.012	0.30
4	9.179	0.32

Figure A5. Representative RP-HPLC chromatograms of purified Pep42-R6 (**Table 2.1, sequence 2.3)** using A) linear gradient 2-82% MeCN/H_2O (0.1% TFA) over 18 min with a Zorbax RX-C18 column (4.6 x 250 mm, 5.0 μm particle size) at 25 °C and flow rate of 1.0 mL/min with detection at 214 nm and B) linear gradient 2-82% MeOH/H_2O (0.1% FA) over 18 min with a Zorbax RX-C18 column (4.6 x 250 mm, 5.0 μm particle size) at 25 °C and flow rate of 1.0 mL/min with detection at 214 nm.
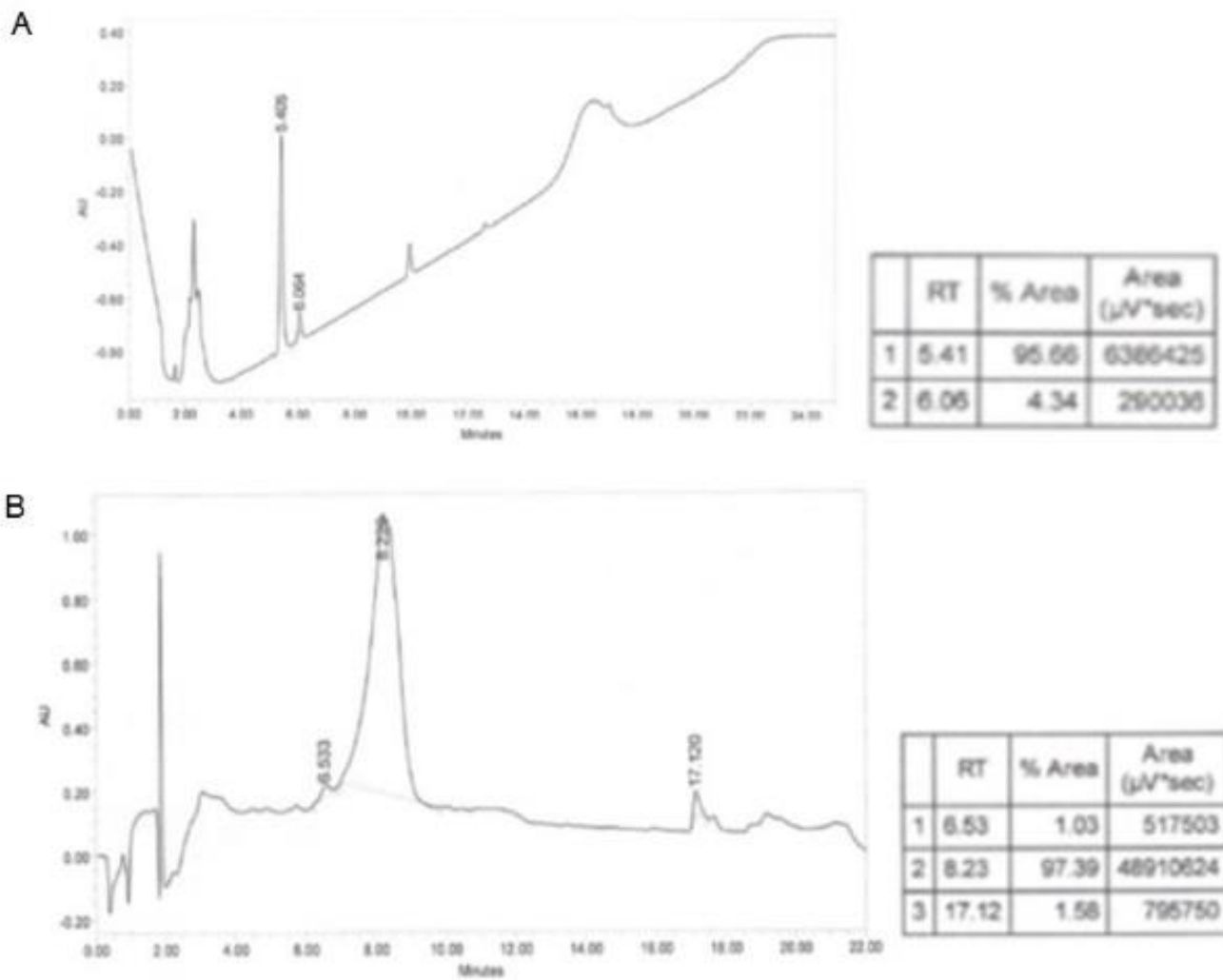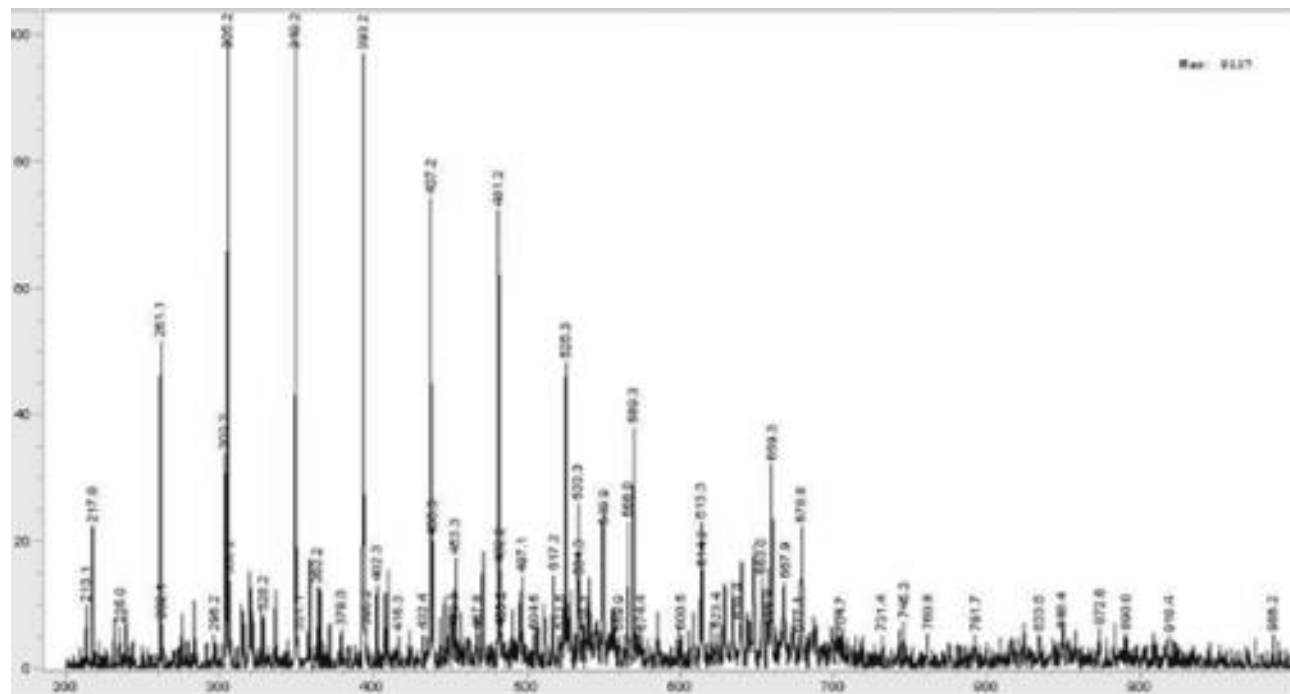
114
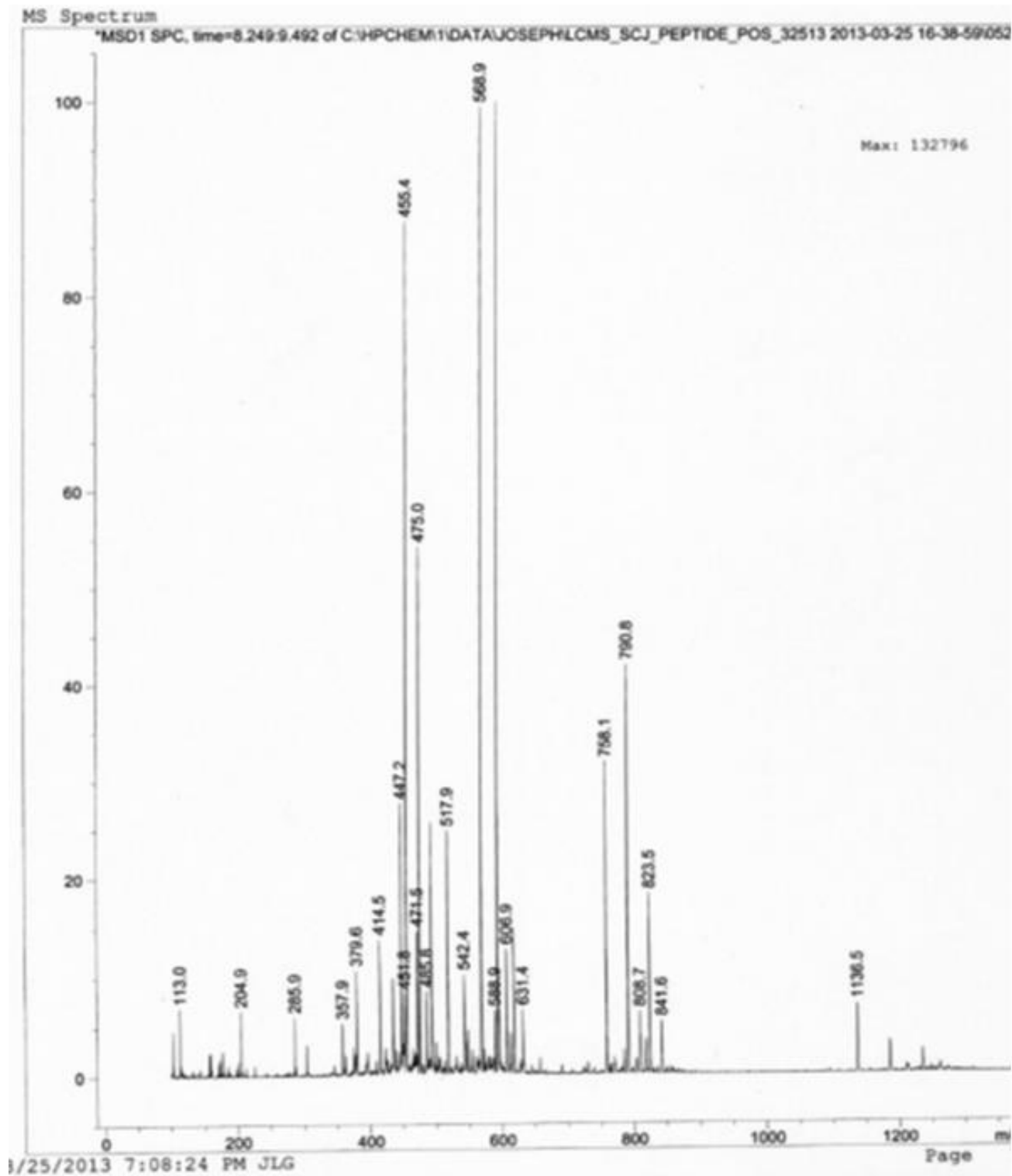
Figure A6. ESI-LCMS analysis of purified Pep42-R6 (**Table 2.1, sequence 2.3)** using a linear gradient 2-82% MeOH/H$_2$O (0.1% FA) over 18 min using a Zorbax RX-C18 column (4.6 x 250 mm, 5.0 µm particle size) set at a temperature of 25 °C at a flow rate of 1.0 mL/min with detection at 214 nm.

115
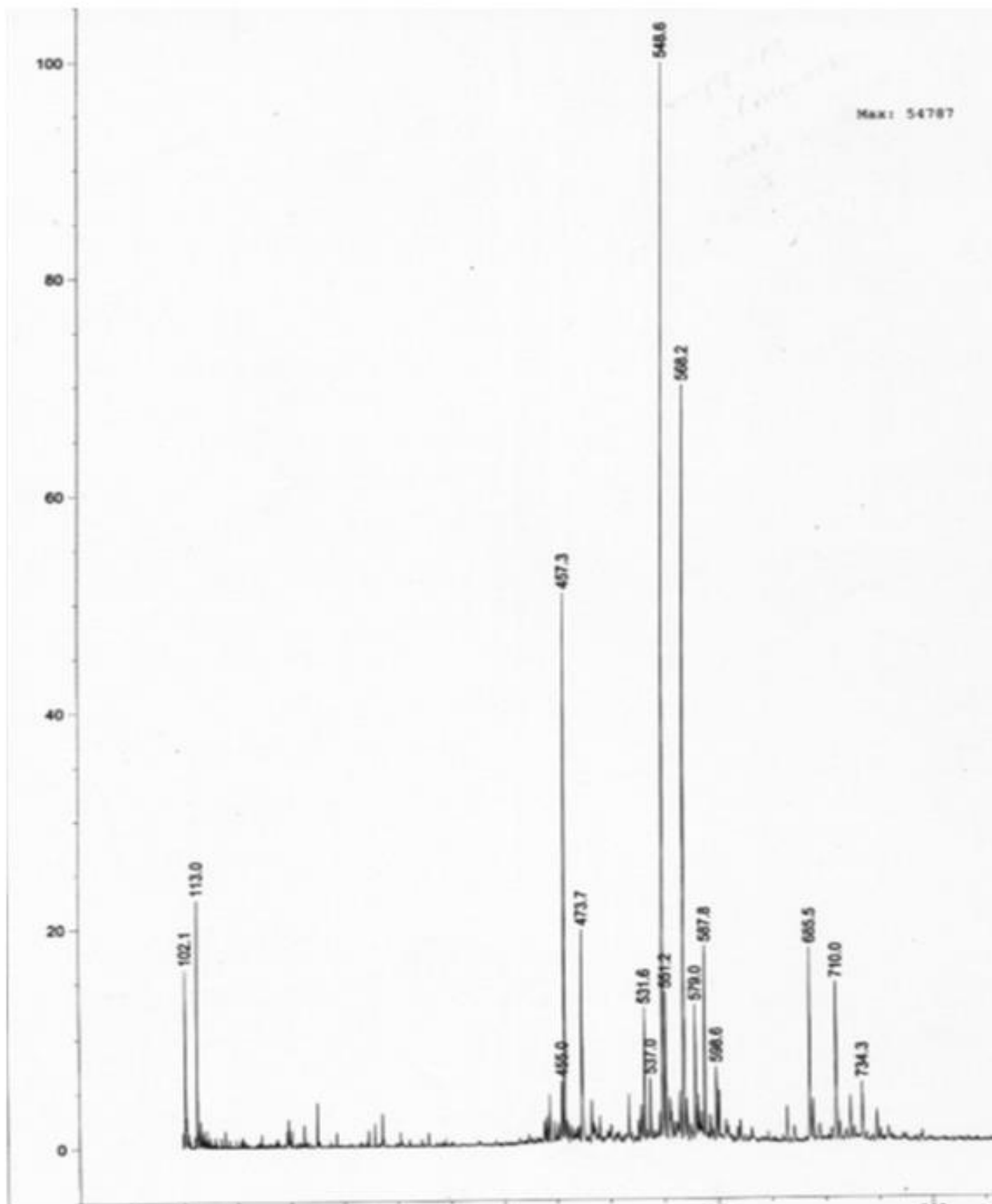
Figure A7. ESI-LCMS analysis of purified Pep42-R9 (**Table 2.1, sequence 2.4**) using a linear gradient 2-82% MeOH/H$_2$O (0.1% FA) over 18 min using a Zorbax RX-C18 column (4.6 x 250 mm, 5.0 μm particle size) set at a temperature of 25 °C at a flow rate of 1.0 mL/min with detection at 214 nm.

A
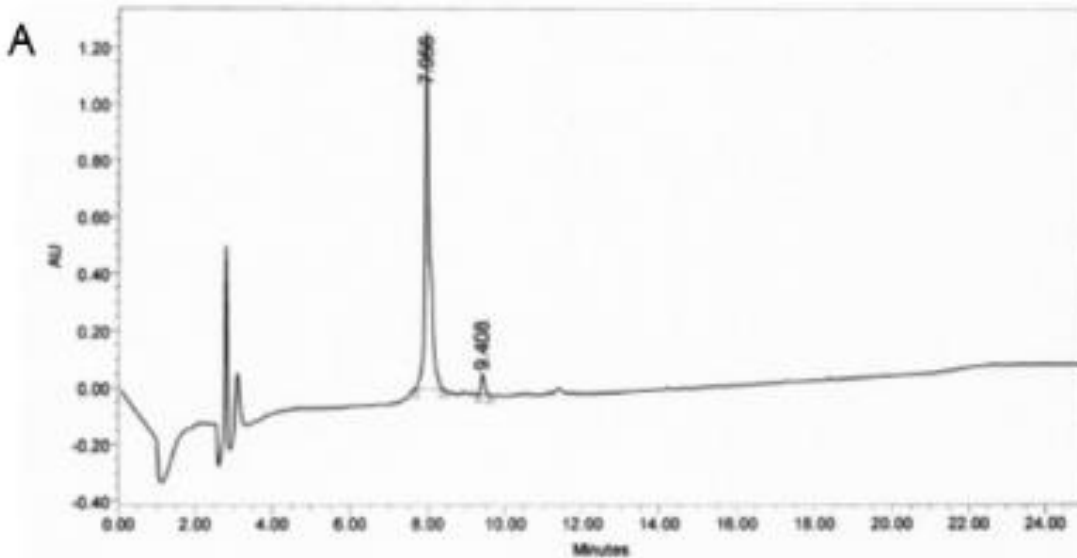
	RT	% Area
1	7.956	95.89
2	9.408	4.11

B
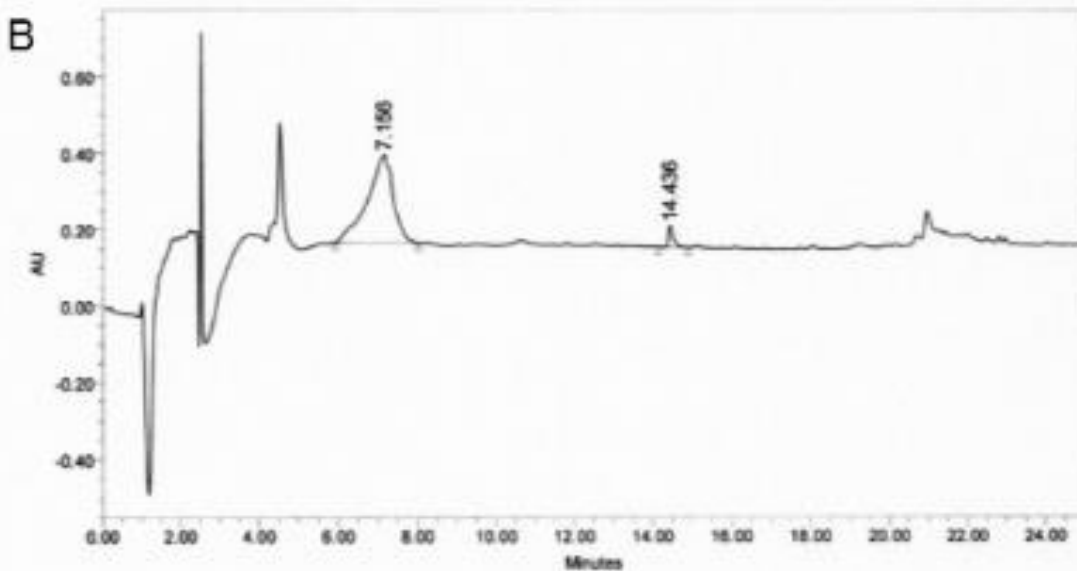
	RT	% Area
1	7.156	95.49
2	14.436	4.51

Figure A8. Representative RP-HPLC chromatograms of purified Pep42-R12 (**Table 2.1, sequence 2.5**) using A) linear gradient 2-82% MeCN/H$_2$O (0.1% TFA) over 18 min with a Zorbax RX-C18 column (4.6 x 250 mm, 5.0 μm particle size) a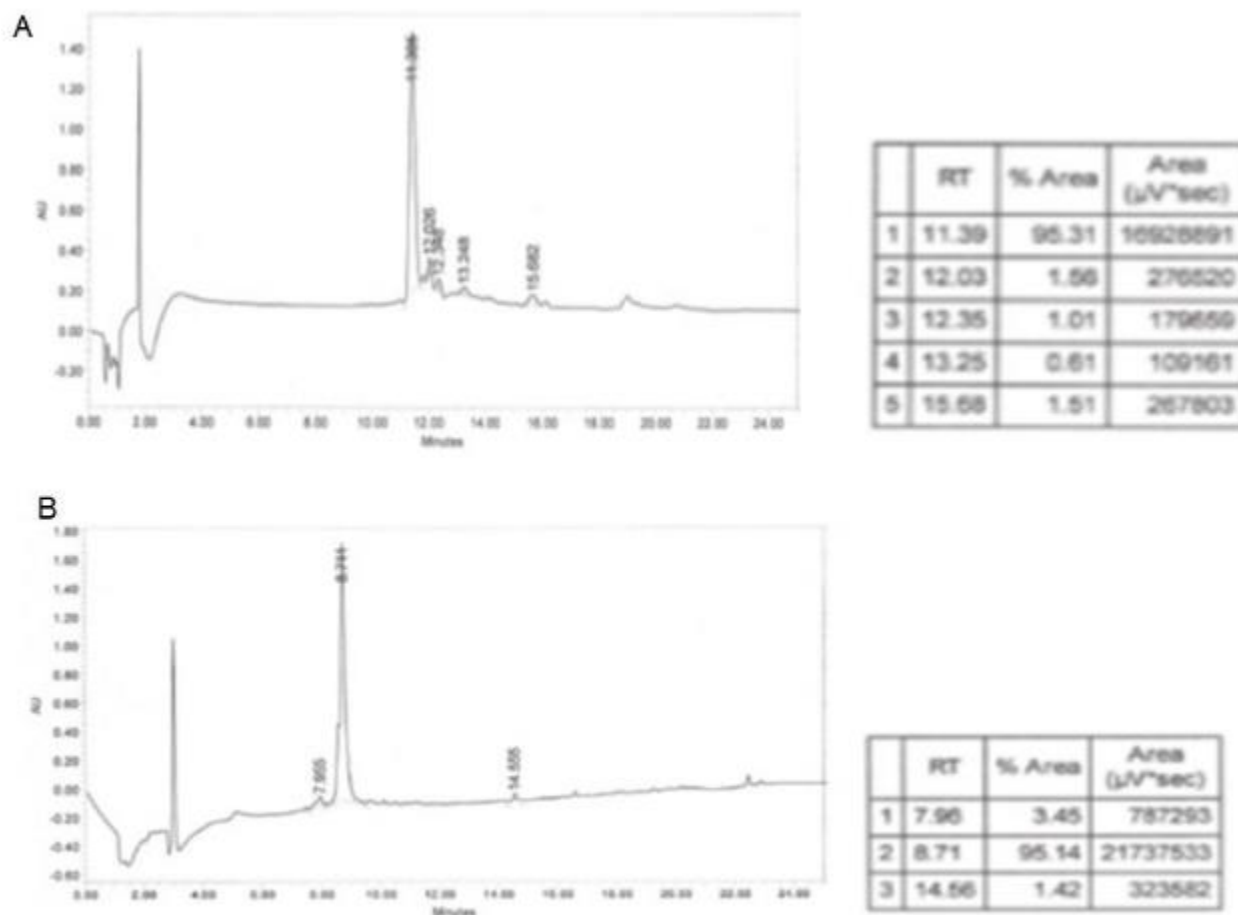t 25 °C and flow rate of 1.0 mL/min with detection at 214 nm and B) linear gradient 2-82% MeOH/H$_2$O (0.1% FA) over 18 min with a Zorbax RX-C18 column (4.6 x 250 mm, 5.0 μm particle size) at 25 °C and flow rate of 1.0 mL/min with detection at 214 nm.
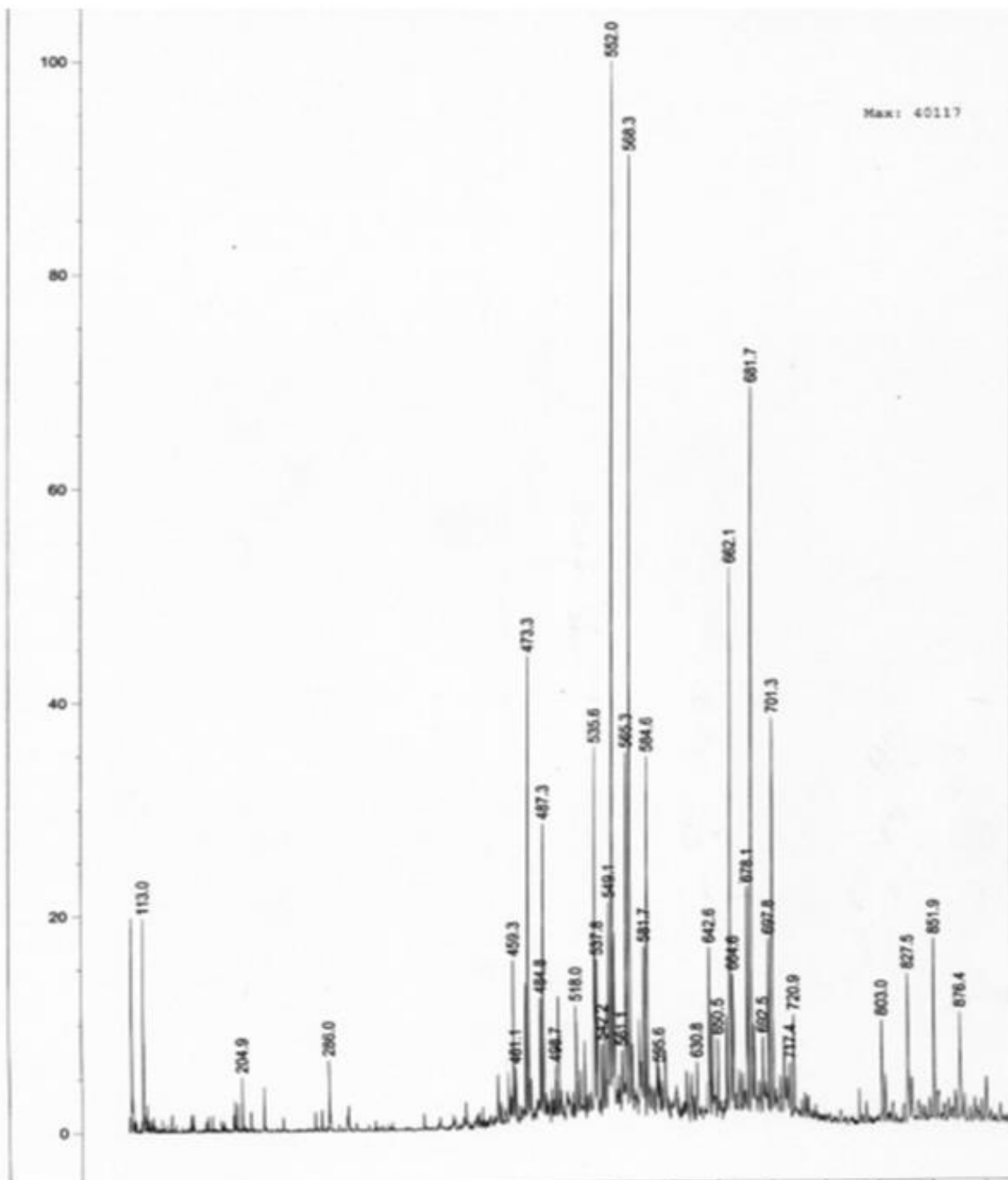
Figure A9. ESI-LCMS analysis of purified Pep42-R12 (**Table 2.1, sequence 2.5**) using a linear gradient 2-82% MeOH/H₂O (0.1% FA) over 18 min using a Zorbax RX-C18 column (4.6 x 250 mm, 5.0 µm particle size) set at a temperature of 25 °C at a flow rate of 1.0 mL/min with detection at 214 nm.
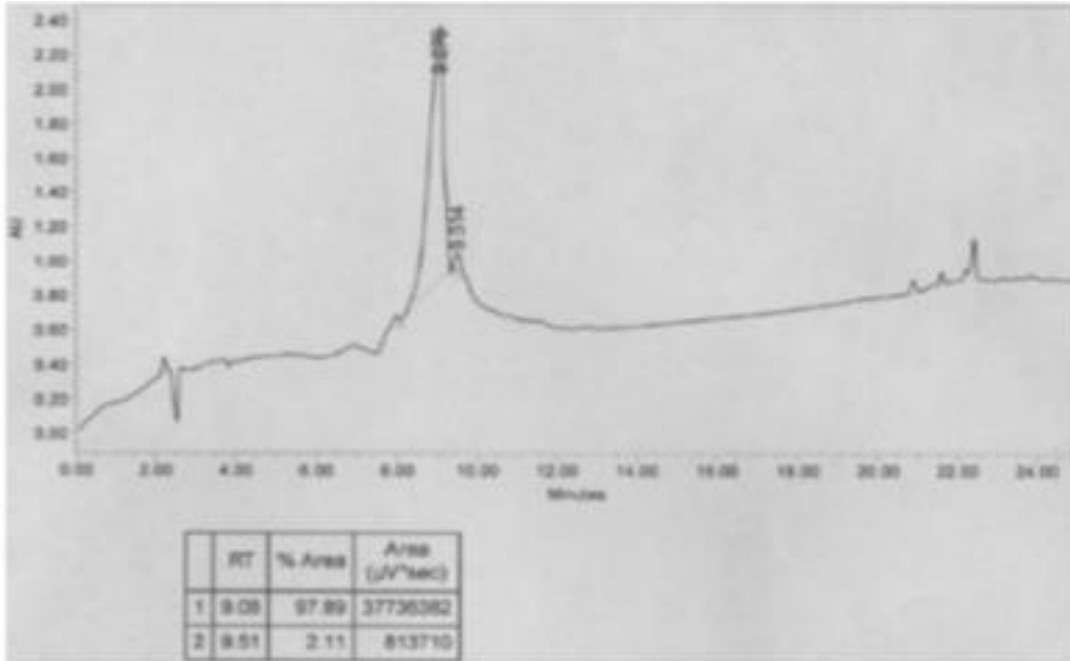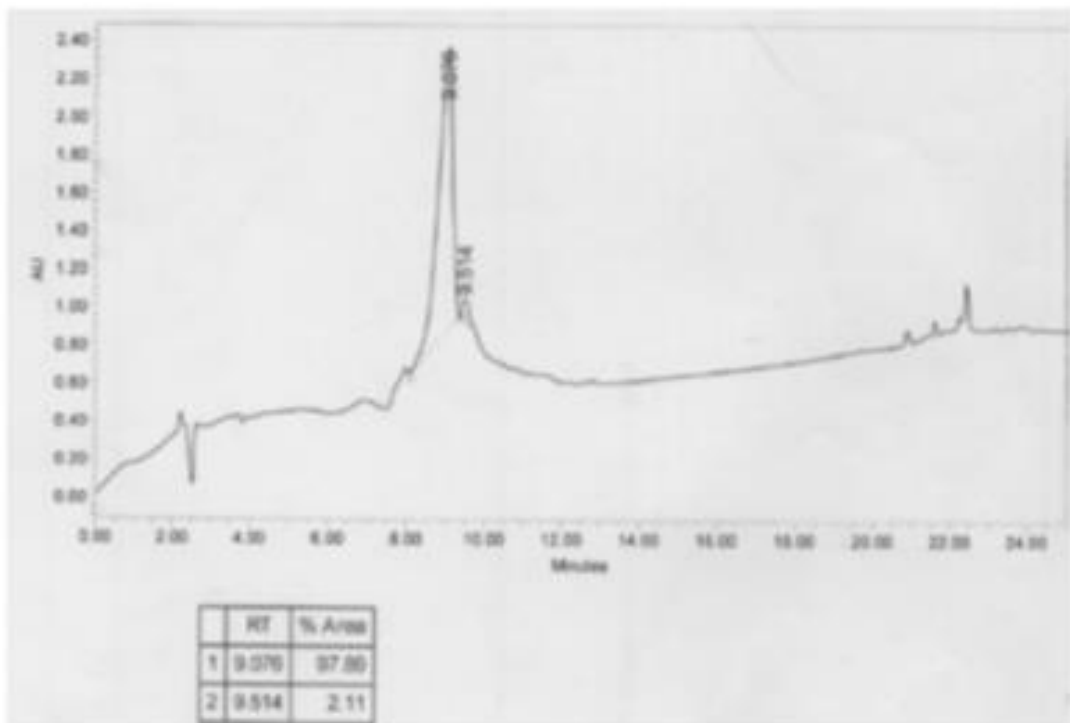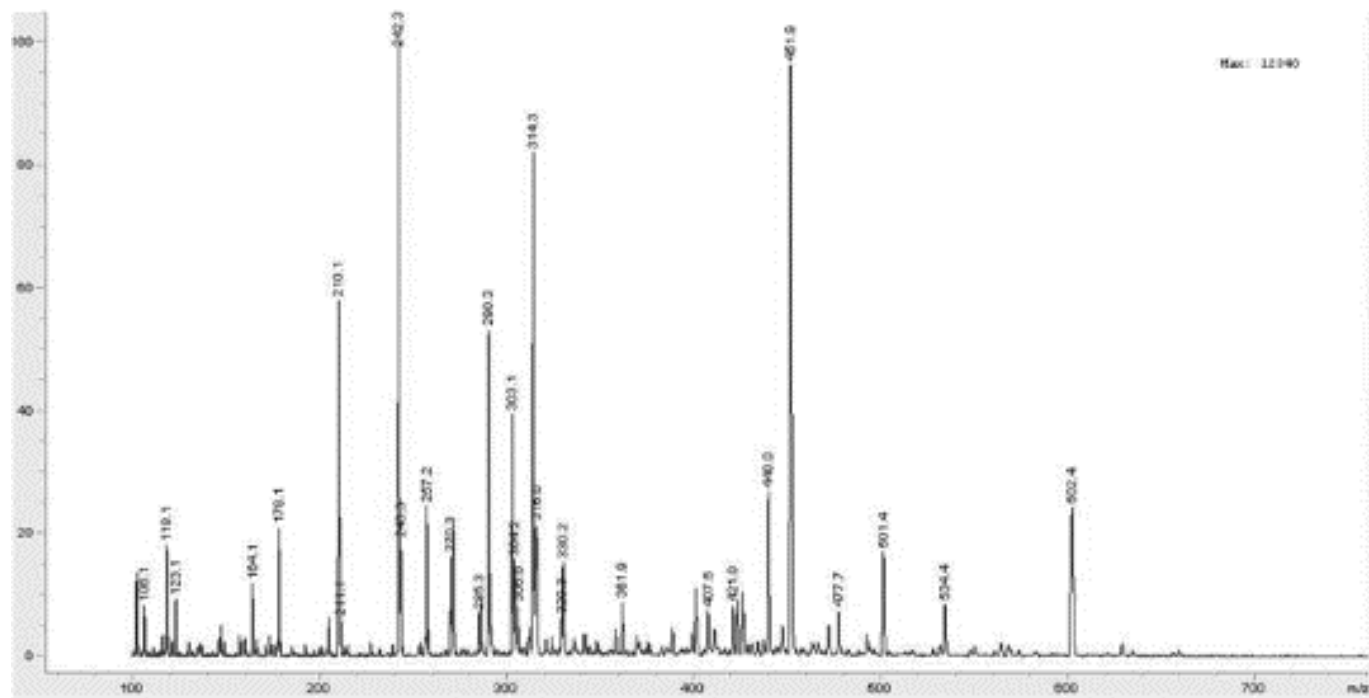
Figure A10. Representative RP-HPLC chromatograms of purified Pep42-r3 (**Table 2.1, sequence 2.6**) using A) linear gradient 2-82% MeCN/H$_2$O (0.1% TFA) over 18 min with a Zorbax RX-C18 column (4.6 x 250 mm, 5.0 μm particle size) at 25 °C and flow rate of 1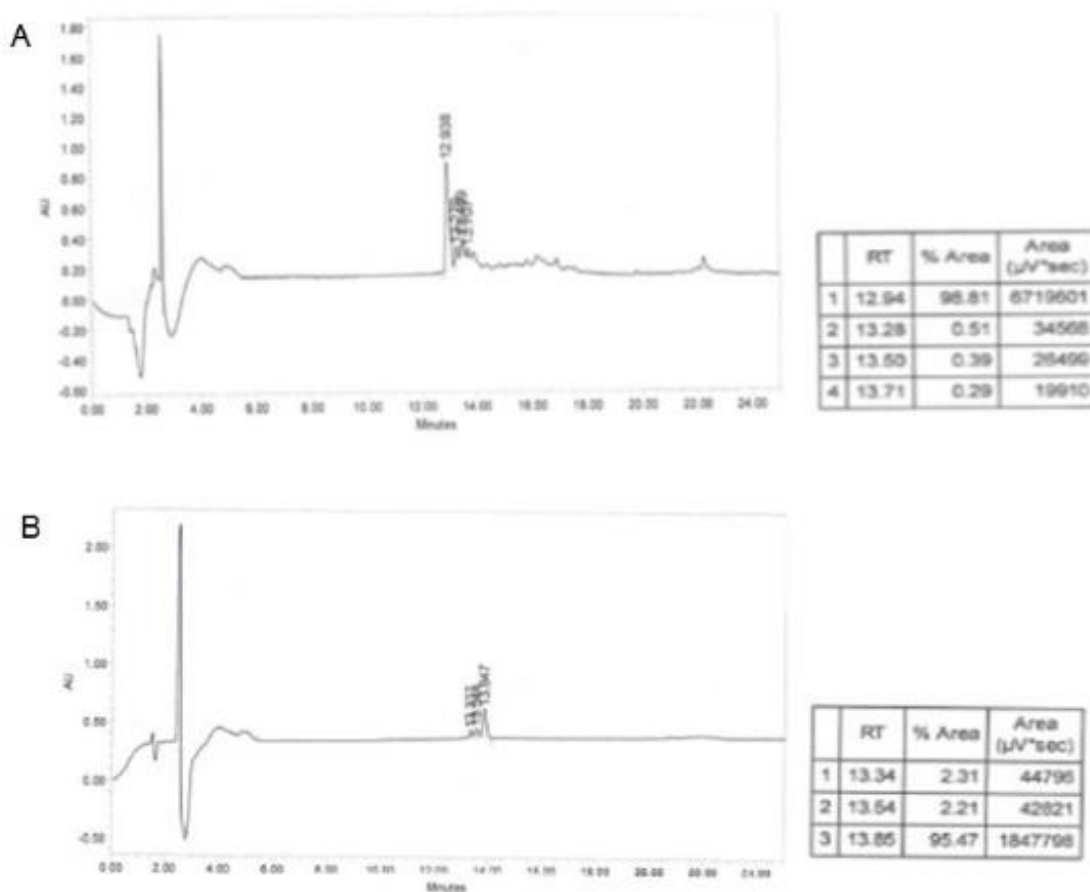.0 mL/min with detection at 214 nm and B) linear gradient 2-82% MeOH/H$_2$O (0.1% FA) over 18 min with a Zorbax RX-C18 column (4.6 x 250 mm, 5.0 μm particle size) at 25 °C and flow rate of 1.0 mL/min with detection at 214 nm.

Figure A11. ESI-LCMS analysis of purified Pep42-r3 (**Table 2.1, sequence 2.6**) using a linear gradient 2-82% MeOH/H$_2$O (0.1% FA) over 18 min using a Zorbax RX-C18 column (4.6 x 250 mm, 5.0 μm particle size) set at a temperature of 25 °C at a flow rate of 1.0 mL/min with detection at 214 nm.

Figure A12. Representative RP-HPLC chromatograms of purified Pep42-r6 (**Table 2.1, sequence 2.7**) using A) linear gradient 2-82% MeCN/H$_2$O (0.1% TFA) over 18 min with a Zorbax RX-C18 column (4.6 x 250 mm, 5.0 μm particle size) at 25 °C and flow rate o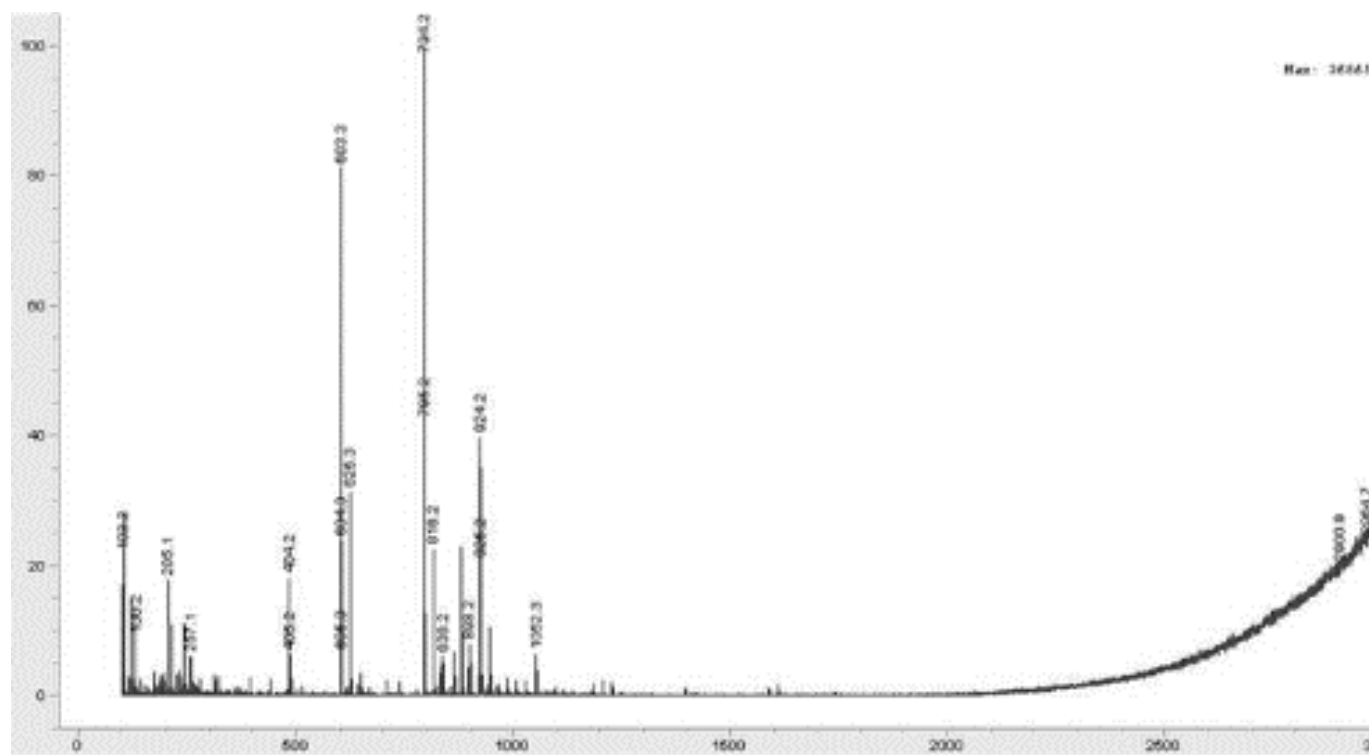f 1.0 mL/min with detection at 214 nm and B) linear gradient 2-82% MeOH/H$_2$O (0.1% FA) over 18 min with a Zorbax RX-C18 column (4.6 x 250 mm, 5.0 μm particle size) at 25 °C and flow rate of 1.0 mL/min with detection at 214 nm.

Figure A13. ESI-LCMS analysis of purified Pep42-r6 (**Table 2.1, sequence 2.7**) using a linear gradient 2-82% MeOH/H₂O (0.1% FA) over 18 min using a Zorbax RX-C18 column (4.6 x 250 mm, 5.0 µm particle size) set at a temperature of 25 °C at a flow rate of 1.0 mL/min with detection at 214 nm.
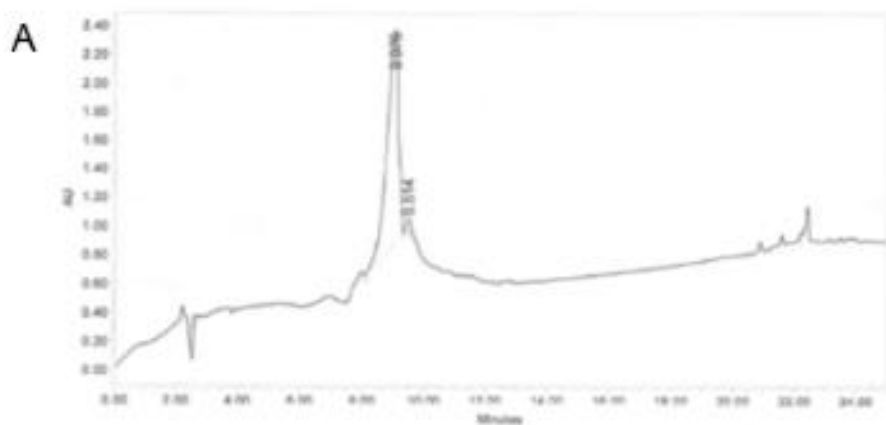
Figure A14. Representative RP-HPLC chromatograms of purified Pep42-r9 (**Table 2.1, sequence 2.8**) using A) linear gradient 2-82% MeCN/H_2O (0.1% TFA) over 18 min with a Zorbax RX-C18 column (4.6 x 250 mm, 5.0 μm particle size) at 25 °C and flow rate of 1.0 mL/min with detection at 214 nm and B) linear gradient 2-82% MeOH/H_2O (0.1% FA) over 18 min with a Zorbax RX-C18 column (4.6 x 250 mm, 5.0 μm particle size) at 25 °C and flow rate of 1.0 mL/min with detection at 214 nm.
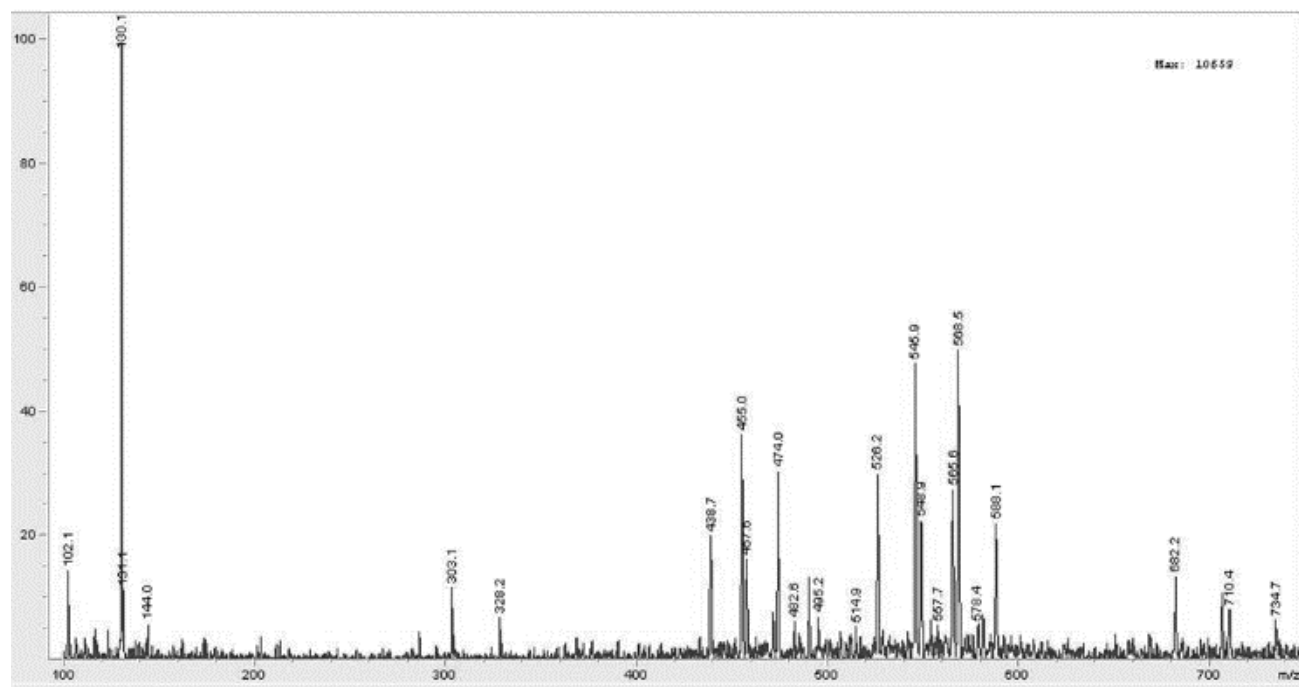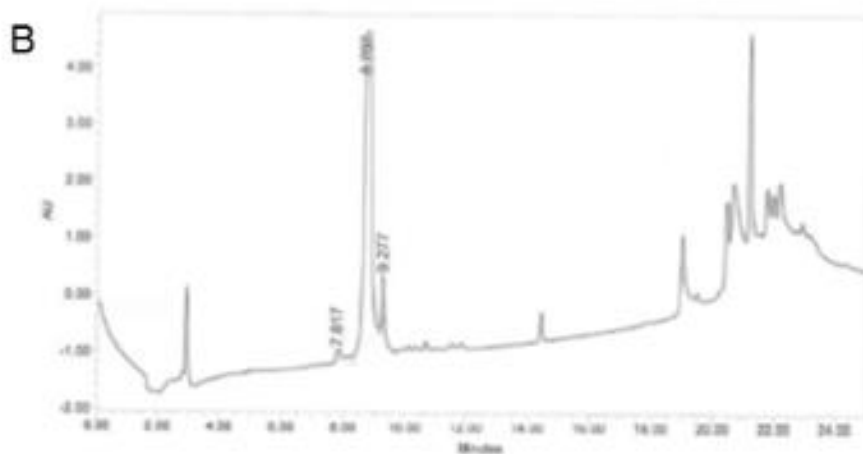
Figure A15. ESI-LCMS analysis of purified Pep42-r9 (**Table 2.1, sequence 2.8**) using a linear gradient 2-82% MeOH/H$_2$O (0.1% FA) over 18 min using a Zorbax RX-C18 column (4.6 x 250 mm, 5.0 µm particle size) set at a temperature of 25 °C at a flow rate of 1.0 mL/min with detection at 214 nm.

A

	RT	% Area	Area (µV*sec)
1	5.41	95.66	6366425
2	6.06	4.34	290036

B

|	RT	% Area	Area (µV*sec)
1	6.53	1.03	517503
2	8.23	97.39	48910624
3	17.12	1.58	795750

Figure A16. Representative RP-HPLC chromatograms of purified Pep42-r12 (**Table 2.1, sequence 2.9**) using A) linear gradient 2-82% MeCN/H_2O (0.1% TFA) over 18 min with a Zorbax RX-C18 column (4.6 x 250 mm, 5.0 µm particle size) at 25 °C and flow rate of 1.0 mL/min with detection at 214 nm and B) linear gradient 2-82% MeOH/H_2O (0.1% FA) over 18 min with a Zorbax RX-C18 column (4.6 x 250 mm, 5.0 µm particle size) at 25 °C and flow rate of 1.0 mL/min with detection at 214 nm.

125

Figure A17. ESI-LCMS analysis of purified Pep42-r12 (**Table 2.1, sequence 2.9)** using a linear gradient 2-82% MeOH/H₂O (0.1% FA) over 18 min using a Zorbax RX-C18 column (4.6 x 250 mm, 5.0 μm particle size) set at a temperature of 25 °C at a flow rate of 1.0 mL/min with detection at 214 nm.

A

	RT	% Area	Area (μV*sec)
1	11.39	95.31	16926891
2	12.03	1.56	276520
3	12.35	1.01	179659
4	13.25	0.61	109161
5	15.68	1.51	267803

B

	RT	% Area	Area (μV*sec)
1	7.96	3.45	787293
2	8.71	95.14	21737533
3	14.56	1.42	323582

Figure A18. Representative RP-HPLC chromatograms of purified FITC-Ahx-Pep42 (**Table 2.1, sequence 2.10)** using A) linear gradient 2-82% MeCN/H$_2$O (0.1% TFA) over 18 min with a Zorbax RX-C18 column (4.6 x 250 mm, 5.0 μm particle size) at 25 °C and flow rate of 1.0 mL/min with detection at 214 nm and B) linear gradient 2-82% MeOH/H$_2$O (0.1% FA) over 18 min with a Zorbax RX-C18 column (4.6 x 250 mm, 5.0 μm particle size) at 25 °C and flow rate of 1.0 mL/min with detection at 214 nm.

127

Figure A19. ESI-LCMS analysis of purified FITC-Ahx-Pep42 (**Table 2.1, sequence 2.10**) using a linear gradient 2-82% MeOH/H₂O (0.1% FA) over 18 min using a Zorbax RX-C18 column (4.6 x 250 mm, 5.0 µm particle size) set at a temperature of 25 °C at a flow rate of 1.0 mL/min with detection at 214 nm.

	RT	% Area	Area (μV*sec)
1	12.94	98.81	6719601
2	13.28	0.51	34568
3	13.50	0.39	26499
4	13.71	0.29	19910

	RT	% Area	Area (μV*sec)
1	13.34	2.31	44795
2	13.54	2.21	42821
3	13.85	95.47	1847798

Figure A20. Representative RP-HPLC chromatograms of purified FITC-Ahx-Pep42-R3 (**Table 2.1, sequence 2.11**) using A) linear gradient 2-82% MeCN/H$_2$O (0.1% TFA) over 18 min with a Zorbax RX-C18 column (4.6 x 250 mm, 5.0 μm particle size) at 25 °C and flow rate of 1.0 mL/min with detection at 214 nm and B) linear gradient 2-82% MeOH/H$_2$O (0.1% FA) over 18 min with a Zorbax RX-C18 column (4.6 x 250 mm, 5.0 μm particle size) at 25 °C and flow rate of 1.0 mL/min with detection at 214 nm.
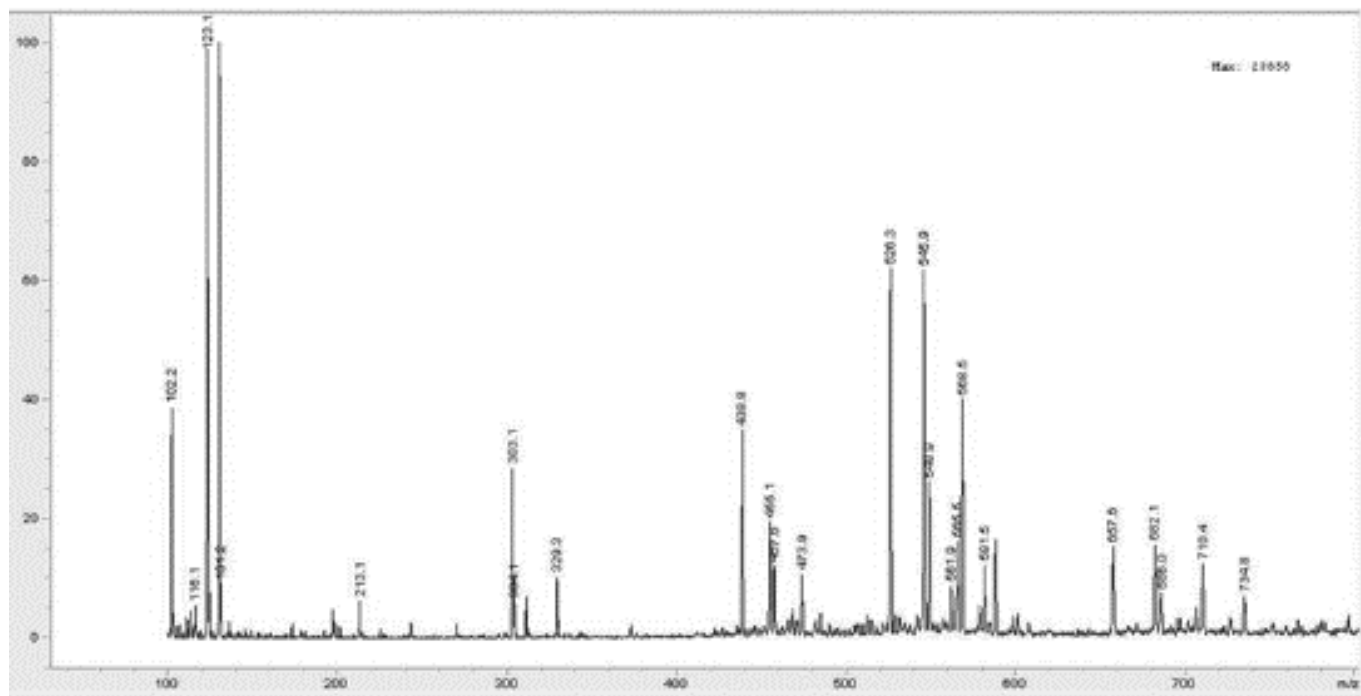
Figure A21. ESI-LCMS analysis of purified FITC-Ahx-Pep42-R3 (**Table 2.1, sequence 2.11**) using a linear gradient 2-82% MeOH/H₂O (0.1% FA) over 18 min using a Zorbax RX-C18 column (4.6 x 250 mm, 5.0 µm particle size) set at a temperature of 25 °C at a flow rate of 1.0 mL/min with detection at 214 nm.
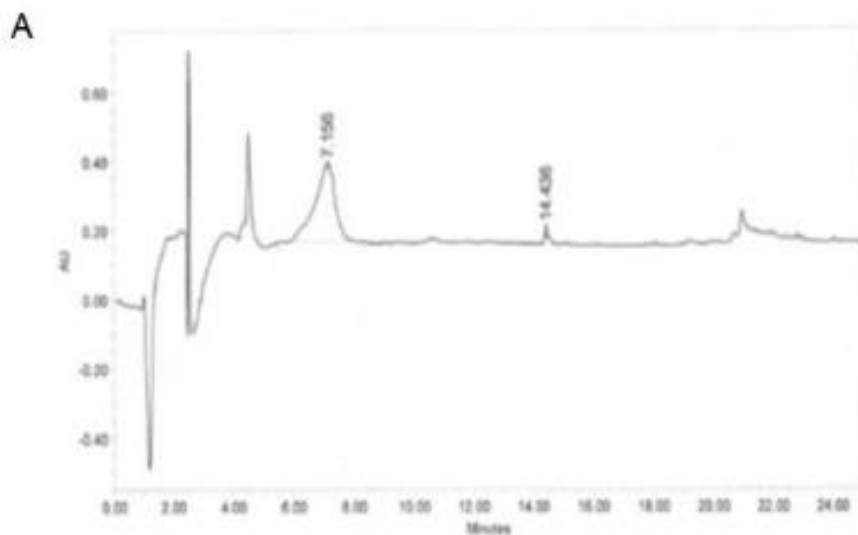
Figure A22. Representative RP-HPLC chromatograms of purified FITC-Ahx-Pep42-R6 (**Table 2.1, sequence 2.12**) using A) linear gradient 2-82% MeCN/H$_2$O (0.1% TFA) over 18 min with a Zorbax RX-C18 column (4.6 x 250 mm, 5.0 μm particle size) at 25 °C and flow rate of 1.0 mL/min with detection at 214 nm and B) linear gradient 2-82% MeOH/H$_2$O (0.1% FA) over 18 min with a Zorbax RX-C18 column (4.6 x 250 mm, 5.0 μm particle size) at 25 °C and flow rate of 1.0 mL/min with detection at 214 nm.
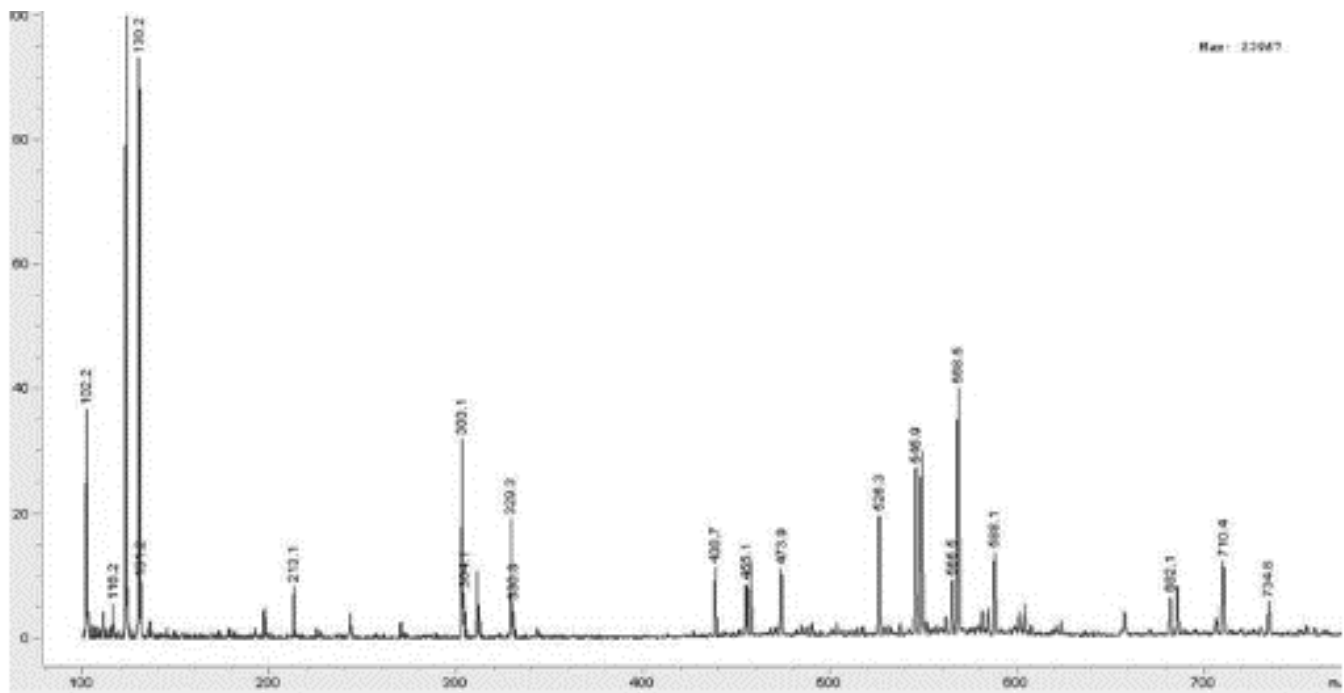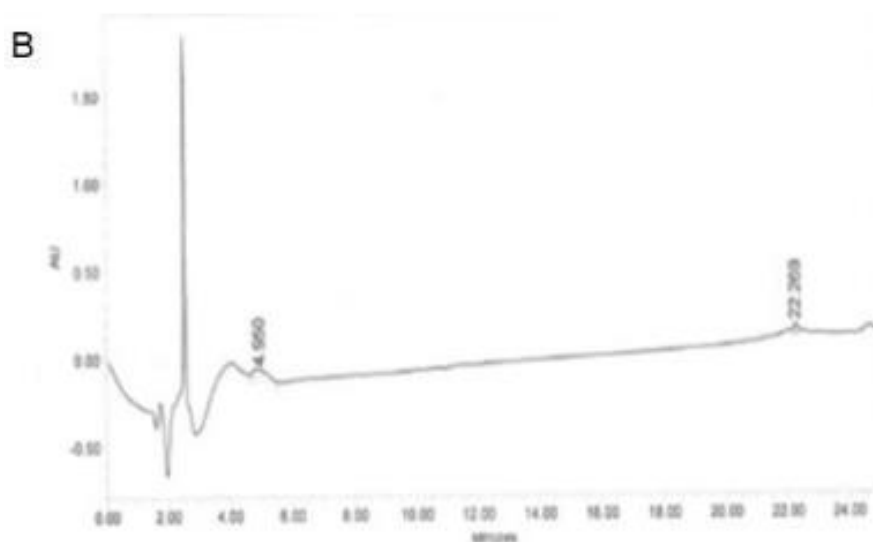
Figure A23. ESI-LCMS analysis of purified FITC-Ahx-Pep42-R6 (**Table 2.1, sequence 2.12**) using a linear gradient 2-82% MeOH/H$_2$O (0.1% FA) over 18 min using a Zorbax RX-C18 column (4.6 x 250 mm, 5.0 µm particle size) set at a temperature of 25 °C at a flow rate of 1.0 mL/min with detection at 214 nm.
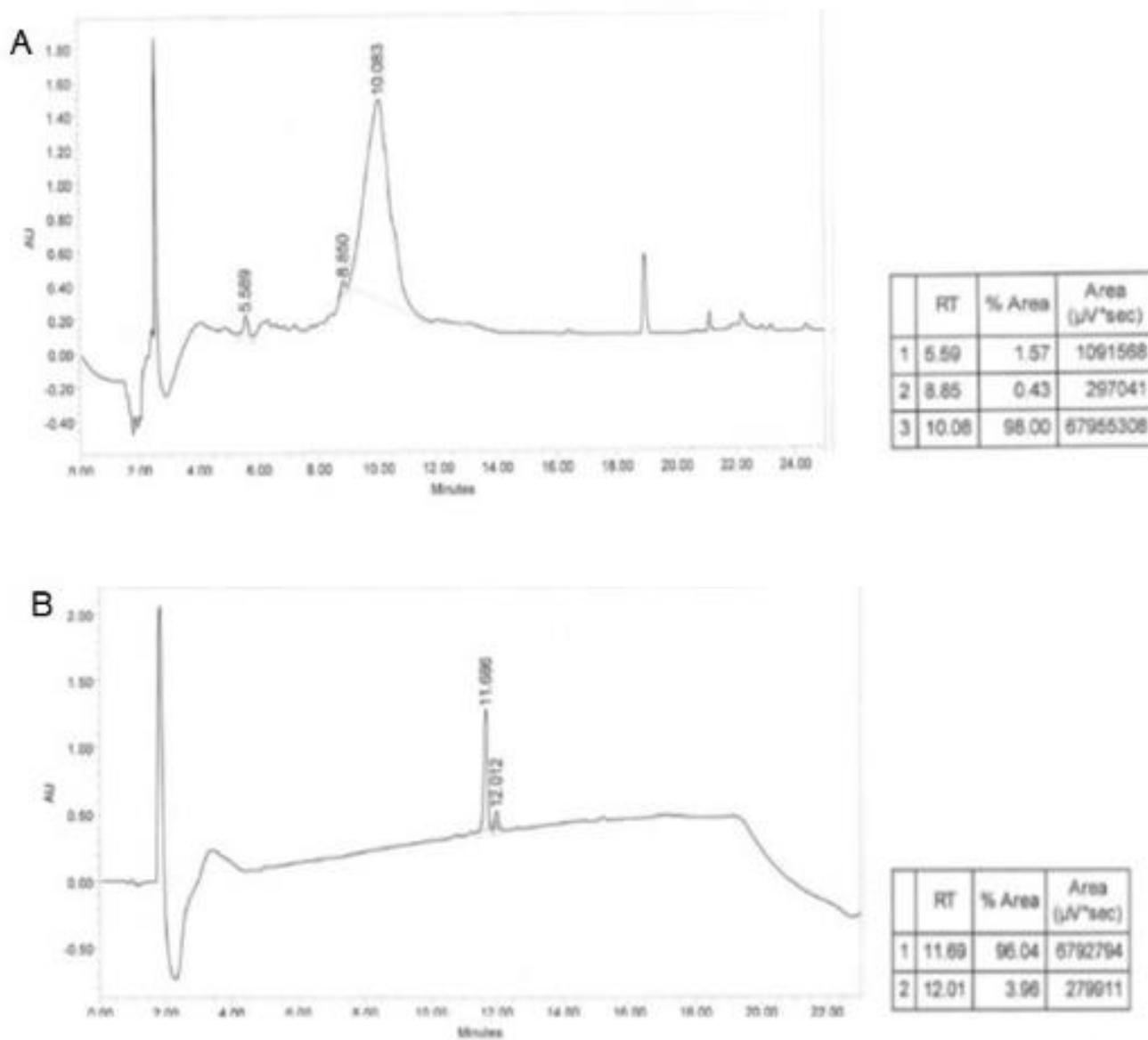
Figure A24. Representative RP-HPLC chromatograms of purified FITC-Ahx-Pep42-R9 (**Table 2.1, sequence 2.13**) using A) linear gradient 2-82% MeCN/H$_2$O (0.1% TFA) over 18 min with a Zorbax RX-C18 column (4.6 x 250 mm, 5.0 µm particle size) at 25 °C and flow rate of 1.0 mL/min with detection at 214 nm and B) linear gradient 2-82% MeOH/H$_2$O (0.1% FA) over 18 min with a Zorbax RX-C18 column (4.6 x 250 mm, 5.0 µm particle size) at 25 °C and flow rate of 1.0 mL/min with detection at 214 nm.
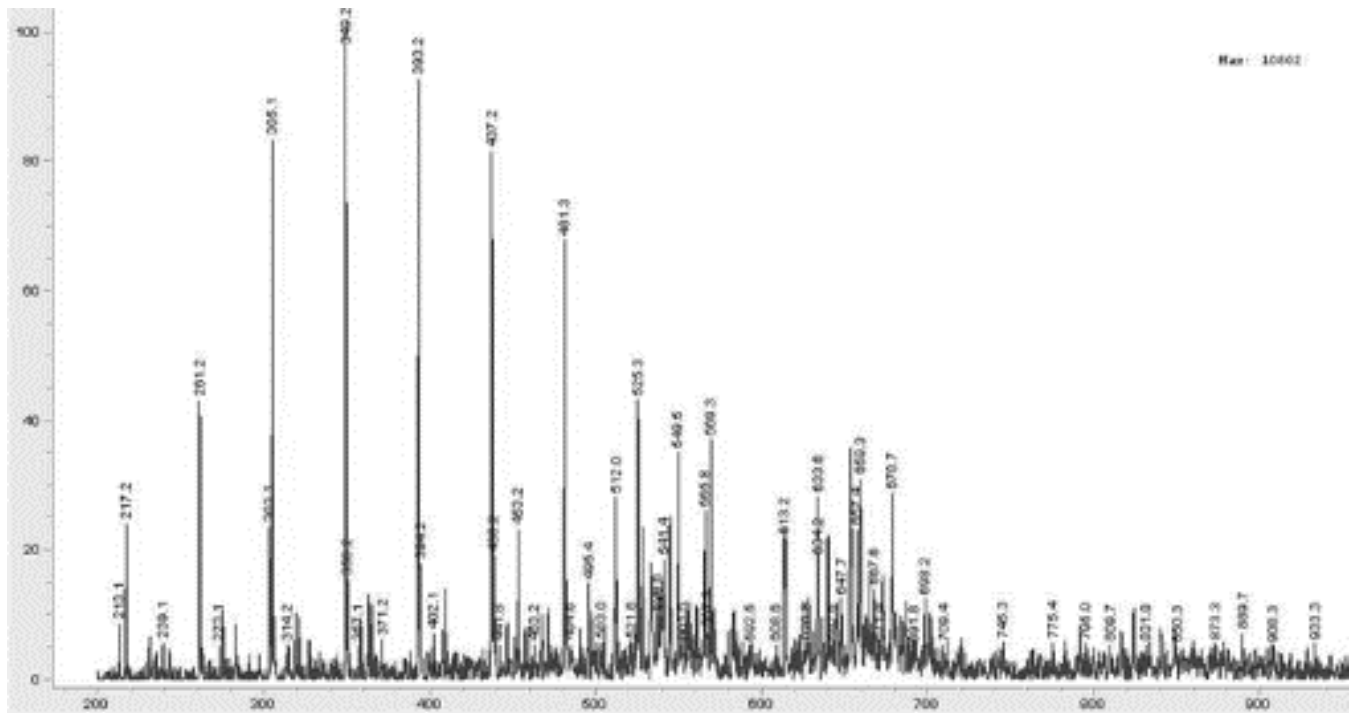
Figure A25. ESI-LCMS analysis of purified FITC-Ahx-Pep42-R9 (**Table 2.1, sequence 2.13)** using a linear gradient 2-82% MeOH/H$_2$O (0.1% FA) over 18 min using a Zorbax RX-C18 column (4.6 x 250 mm, 5.0 μm particle size) set at a temperature of 25 °C at a flow rate of 1.0 mL/min with detection at 214 nm.

A
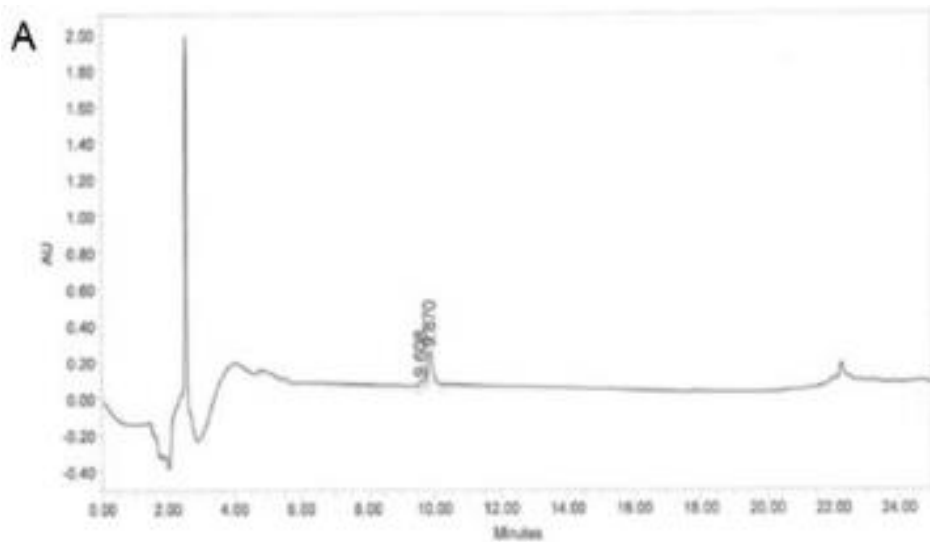
|	RT	% Area	Area (µV*sec)
1	9.61	4.72	69913
2	9.87	95.28	1410272

B
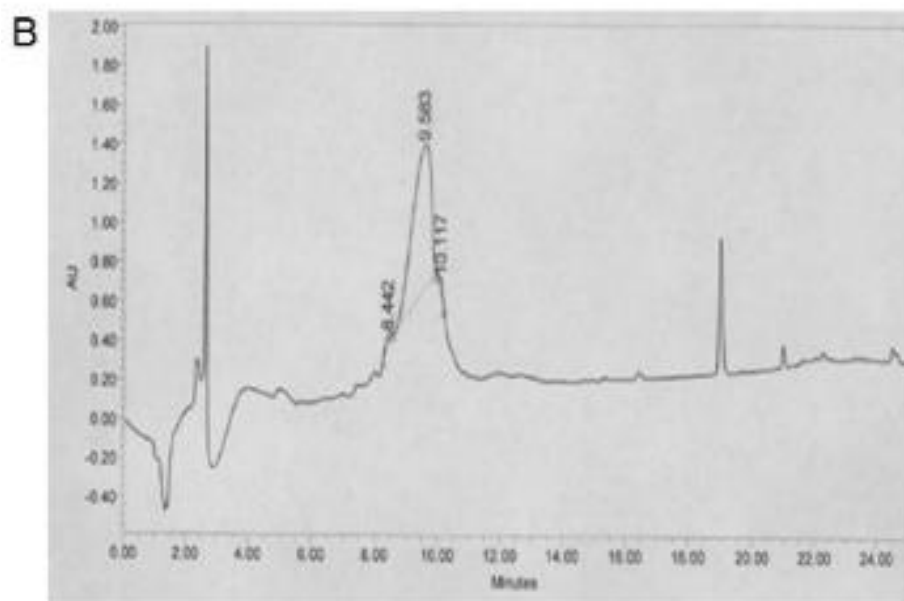
	RT	% Area	Area (µV*sec)
1	8.44	1.78	559109
2	9.58	96.61	30295228
3	10.12	1.61	505027

Figure A26. Representative RP-HPLC chromatograms of purified FITC-Ahx-Pep42-R12 (**Table 2.1, sequence 2.14**) using A) linear gradient 2-82% MeCN/H_2O (0.1% TFA) over 18 min with a Zorbax RX-C18 column (4.6 x 250 mm, 5.0 µm particle size) at 25 °C and flow rate of 1.0 mL/min with detection at 214 nm and B) linear gradient 2-82% MeOH/H_2O (0.1% FA) over 18 min with a Zorbax RX-C18 column (4.6 x 250 mm, 5.0 µm particle size) at 25 °C and flow rate of 1.0 mL/min with detection at 214 nm.
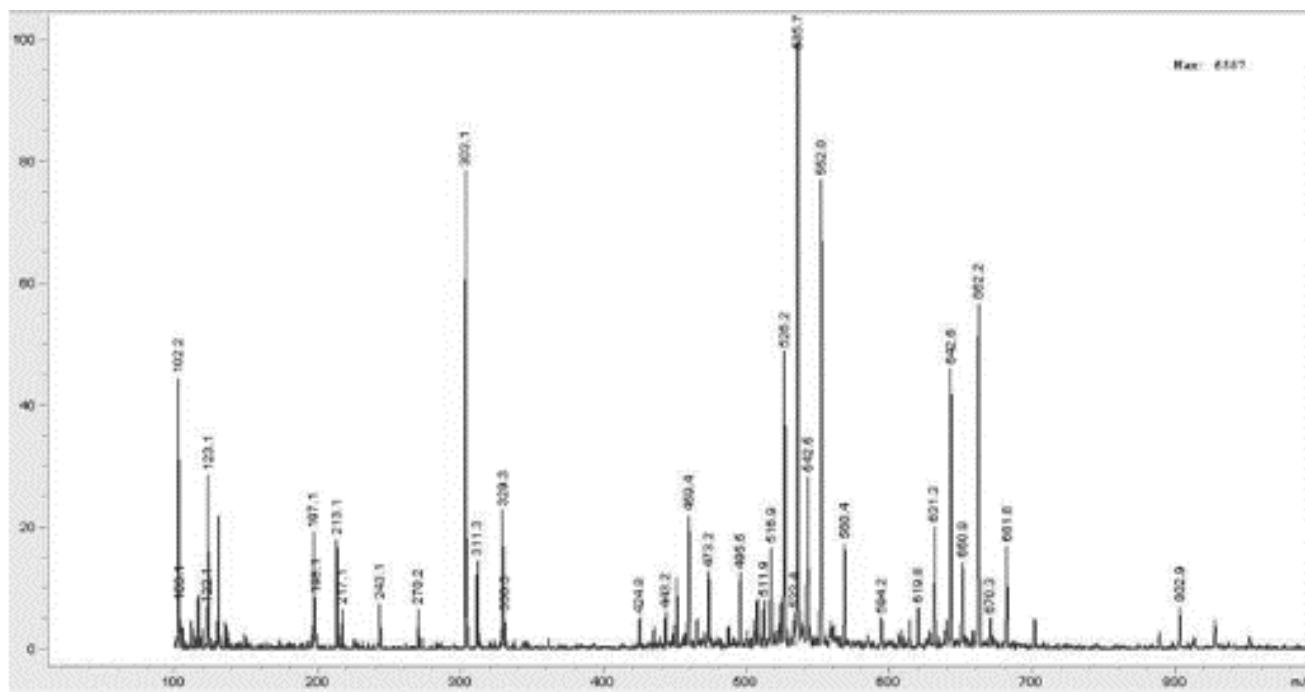
Figure A27. ESI-LCMS analysis of purified FITC-Ahx-Pep42-R12 (**Table 2.1, sequence 2.14)** using a linear gradient 2-82% MeOH/H$_2$O (0.1% FA) over 18 min using a Zorbax RX-C18 column (4.6 x 250 mm, 5.0 µm particle size) set at a temperature of 25 °C at a flow rate of 1.0 mL/min with detection at 214 nm.

A

	RT	% Area	Area (µV*sec)
1	7.28	1.12	91010
2	8.82	98.88	8039426

B

	RT	% Area	Area (µV*sec)
1	6.12	1.08	155729
2	7.19	2.09	300562
3	8.14	96.82	13913546
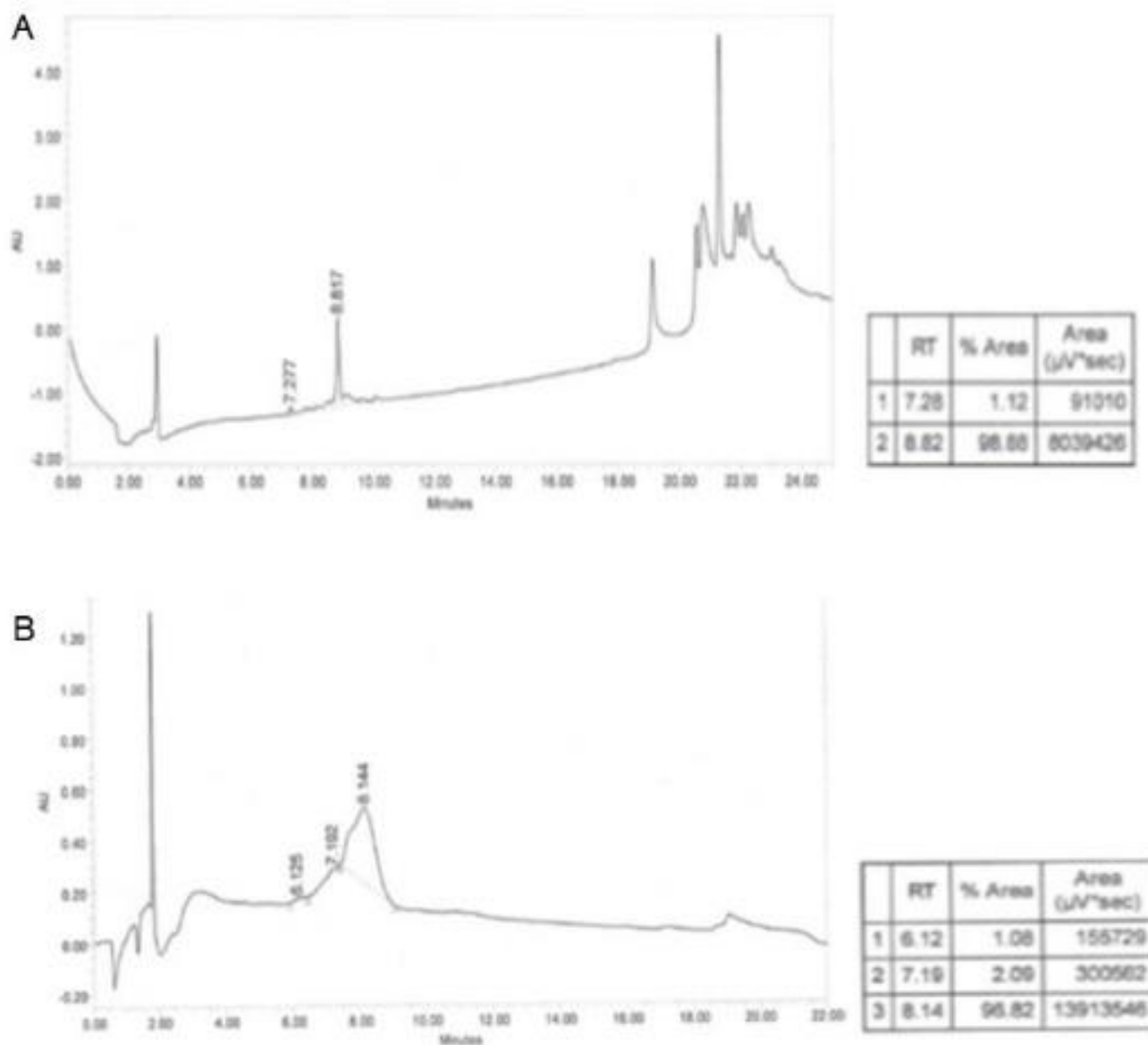
Figure A28. Representative RP-HPLC chromatograms of purified FITC-Ahx-R9 (**Table 2.1, sequence 2.15**) using A) linear gradient 2-82% MeCN/H_2O (0.1% TFA) over 18 min with a Zorbax RX-C18 column (4.6 x 250 mm, 5.0 µm particle size) at 25 °C and flow rate of 1.0 mL/min with detection at 214 nm and B) linear gradient 2-82% MeOH/H_2O (0.1% FA) over 18 min with a Zorbax RX-C18 column (4.6 x 250 mm, 5.0 µm particle size) at 25 °C and flow rate of 1.0 mL/min with detection at 214 nm.

Figure A29. ESI-LCMS analysis of purified FITC-Ahx-R9 (**Table 2.1 sequence 2.15**) using a linear gradient 2-82% MeOH/H$_2$O (0.1% FA) over 18 min using a Zorbax RX-C18 column (4.6 x 250 mm, 5.0 µm particle size) set at a temperature of 25 °C at a flow rate of 1.0 mL/min with detection at 214 nm.

Figure A30. Representative RP-HPLC chromatograms of purified Poly-R9 (**Table 2.1, sequence 2.16**) using A) linear gradient 2-82% MeCN/H₂O (0.1% TFA) over 18 min with a Zorbax RX-C18 column (4.6 x 250 mm, 5.0 μm particle size) at 25 °C and flow rate of 1.0 mL/min with detection at 214 nm and B) linear gradient 2-82% MeOH/H₂O (0.1% FA) over 18 min with a Zorbax RX-C18 column (4.6 x 250 mm, 5.0 μm particle size) at 25 °C and flow rate of 1.0 mL/min with detection at 214 nm.
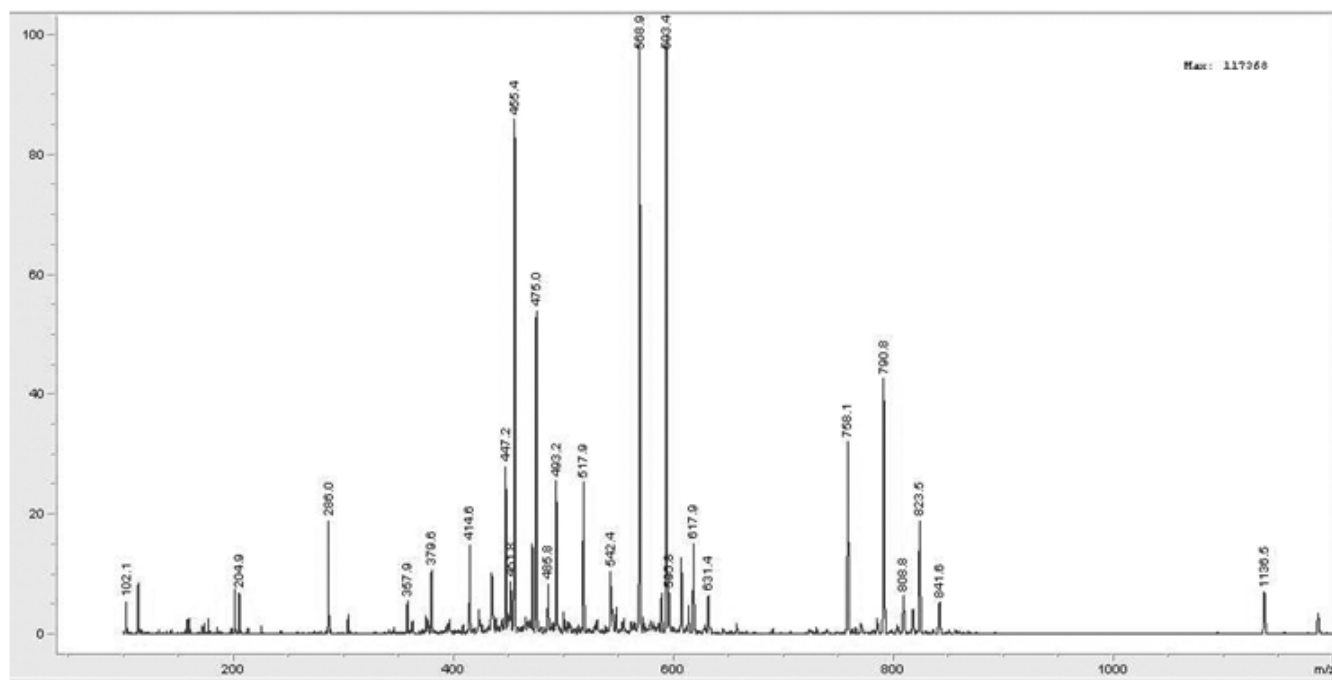
Figure A31. ESI-LCMS analysis of purified Poly-R9 (**Table 2.1, sequence 2.16**) using a linear gradient 2-82% MeOH/H₂O (0.1% FA) over 18 min using a Zorbax RX-C18 column (4.6 x 250 mm, 5.0 μm particle size) set at a temperature of 25 °C at a flow rate of 1.0 mL/min with detection at 214 nm.
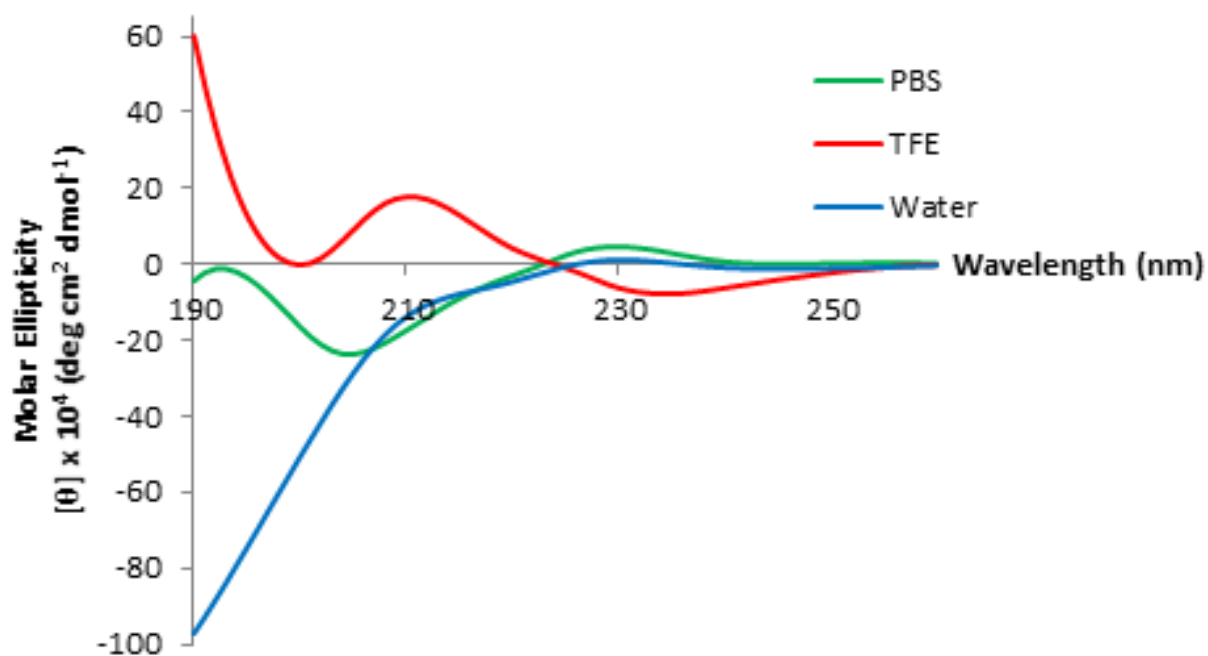
Figure A32. CD spectra for Pep42-r3 (**Table 2.1, sequence 2.6**, 50 μM) in water, TFE and PBS at 25 °C.
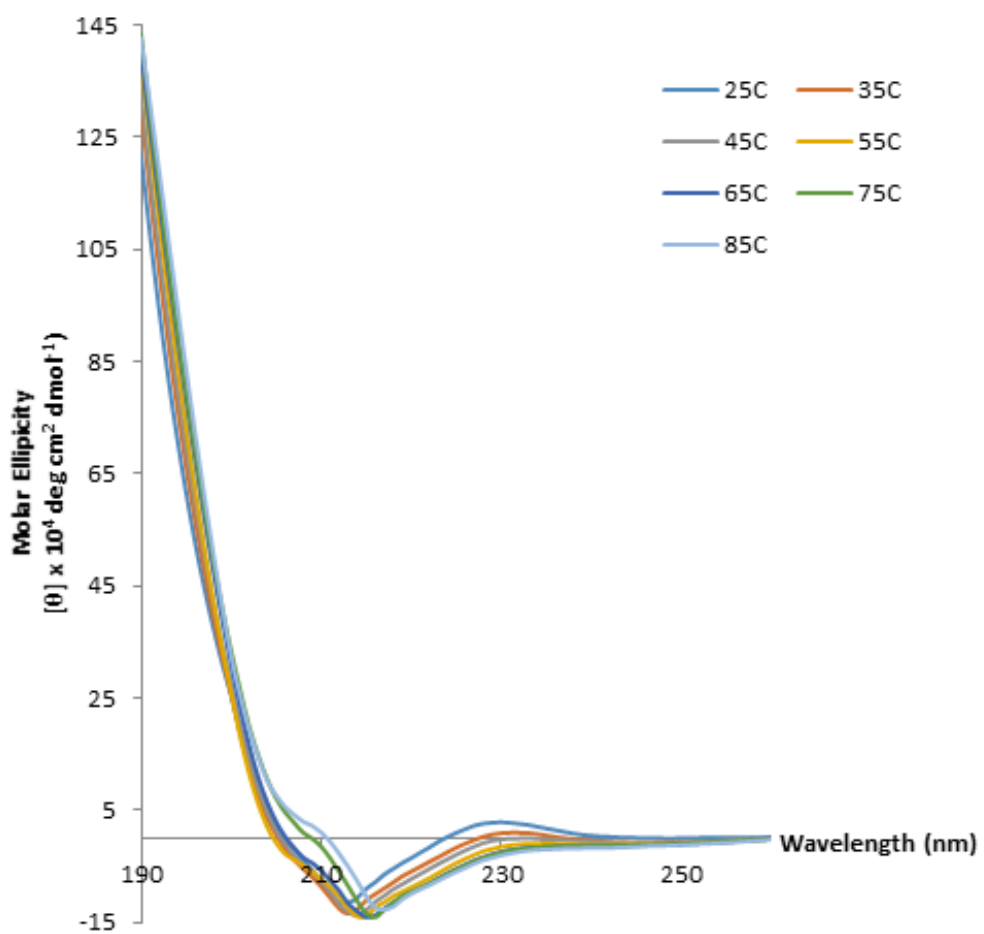
Figure A33. Temperature dependent (25 – 85 ºC) CD spectra for Pep42-r3 (**Table 2.1, sequence 2.6**, 50 μM).
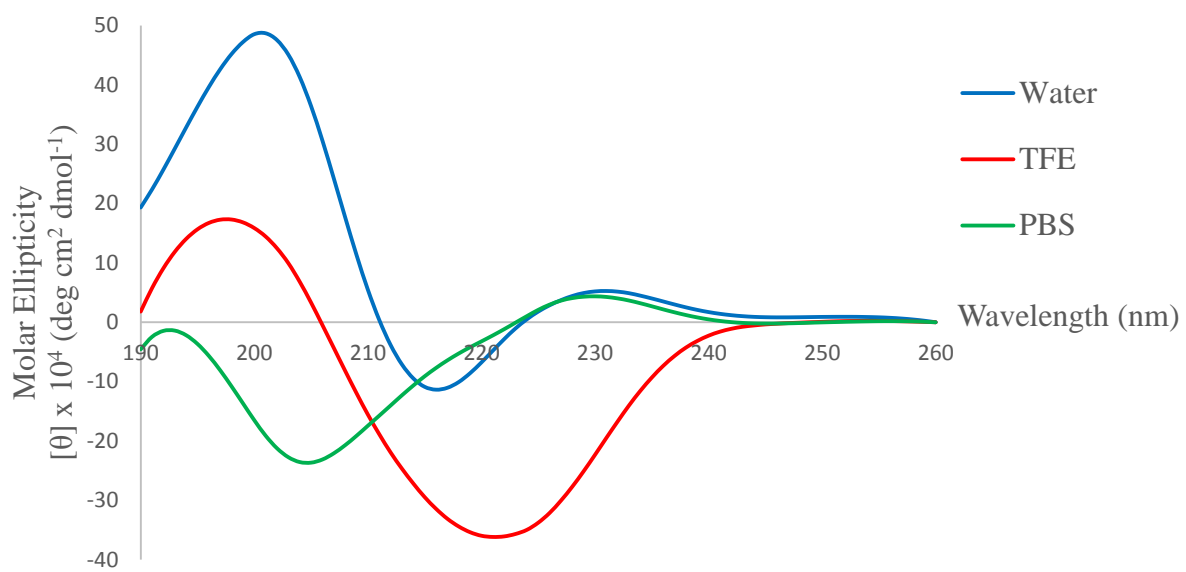
Figure A34. CD spectra for Pep42-r6 (**Table 2.1, sequence 2.7**, 50 μM) in water, TFE and PBS at 25 °C.
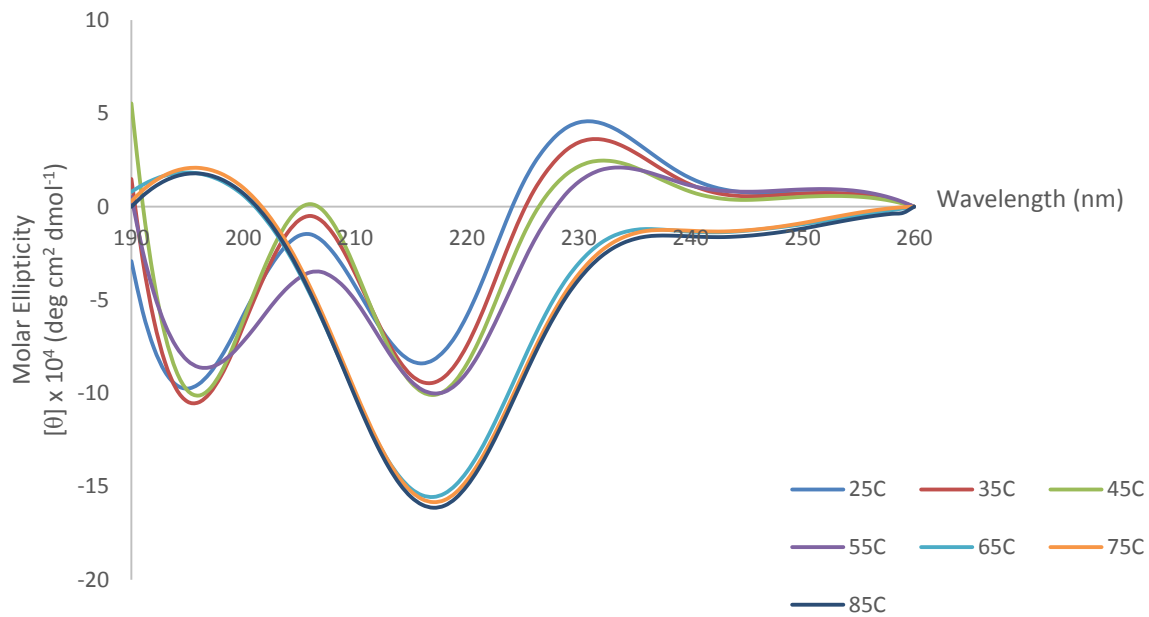
Figure A35. Temperature dependent (25 – 85 °C) CD spectra for Pep42-r6 (**Table 2.1, sequence 2.7**, 50 μM).
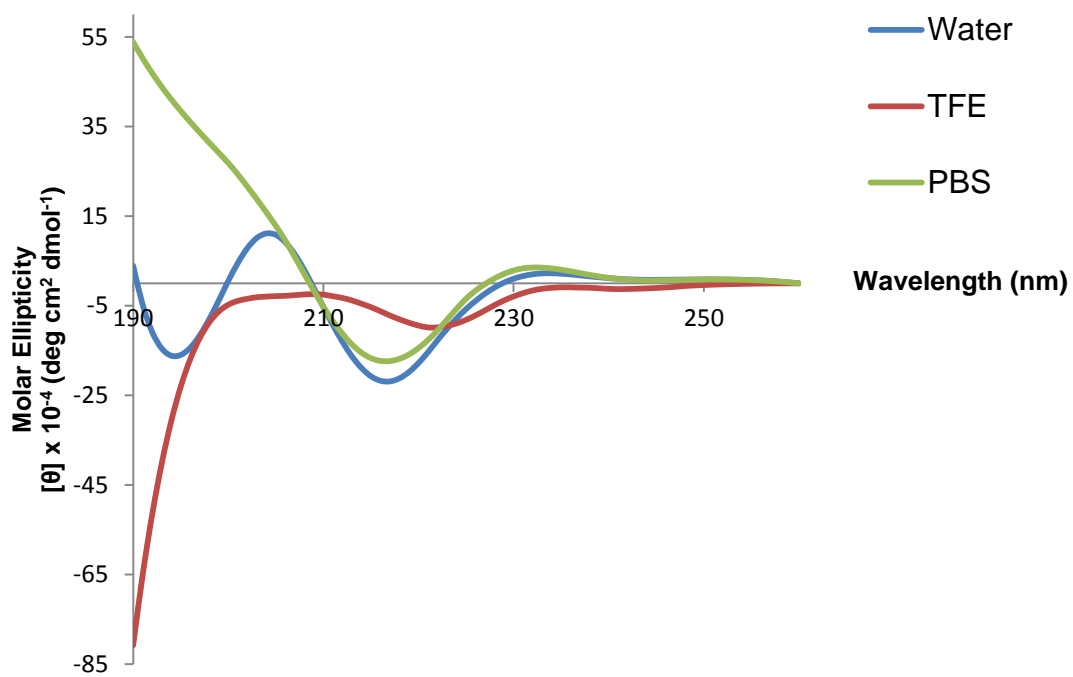
Figure A36. CD spectra for Pep42-r9 (**Table 2.1, sequence 2.8**, 50 μM) in water, TFE and PBS at 25 °C.
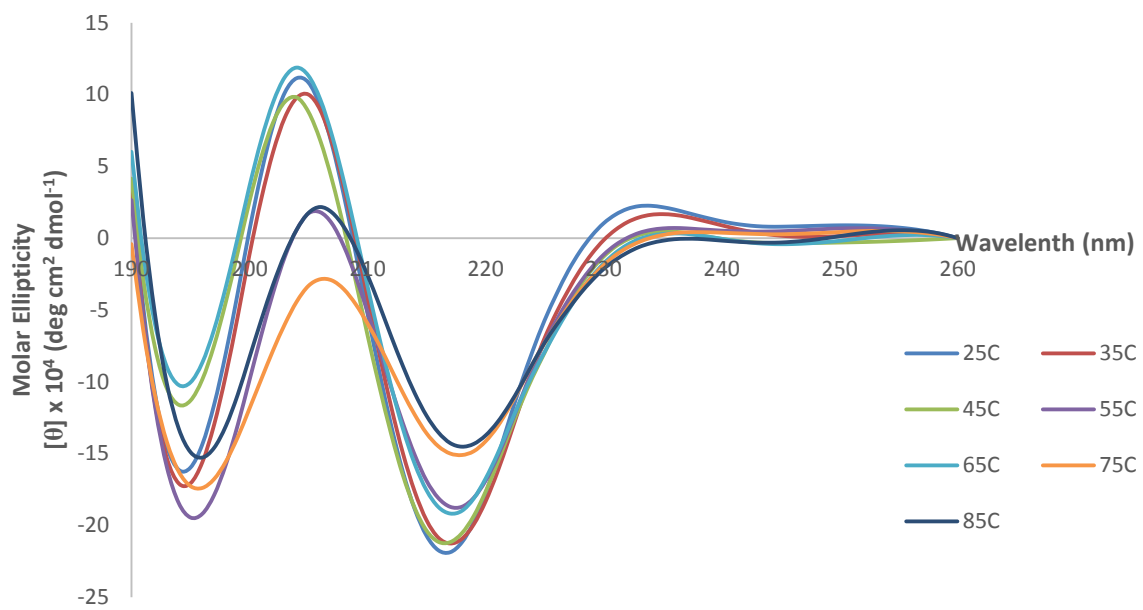
Figure A37. Temperature dependent (25 – 85 °C) CD spectra for Pep42-r9 (**Table 2.1, sequence 2.8**, 50 µM).
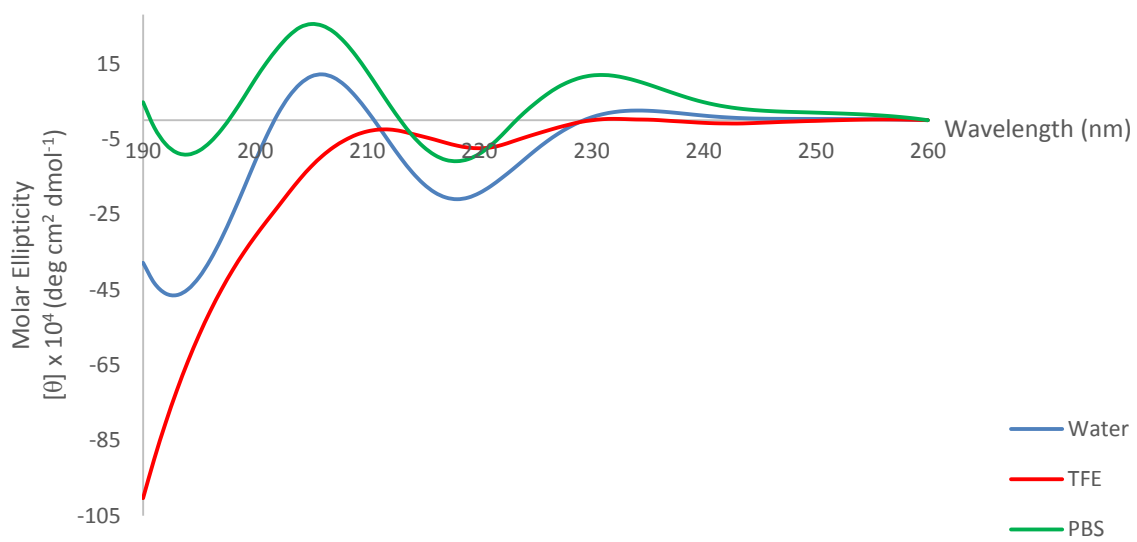
Figure A38. CD spectra for Pep42-r12 (**Table 2.1, sequence 2.9**, 50 µM) in water, TFE and PBS at 25 °C.
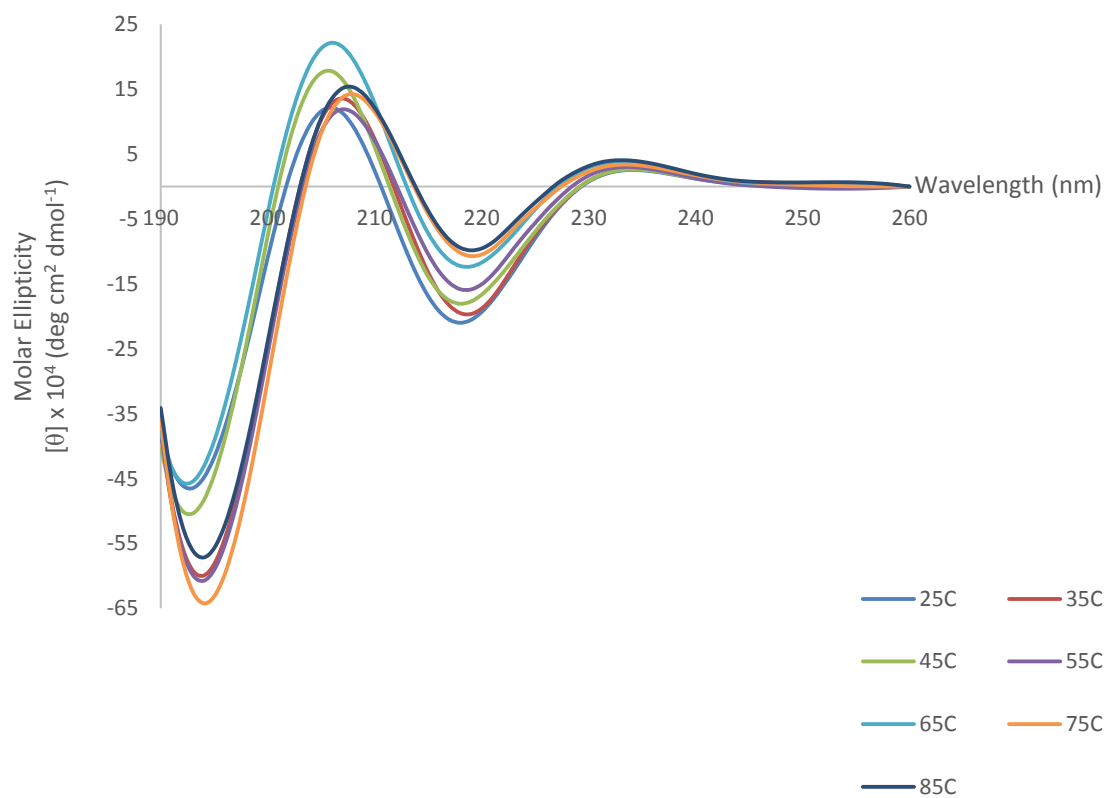
Figure A39. Temperature dependent (25 – 85 °C) CD spectra for Pep42-r12 (**Table 2.1, sequence 2.9**, 50 μM).
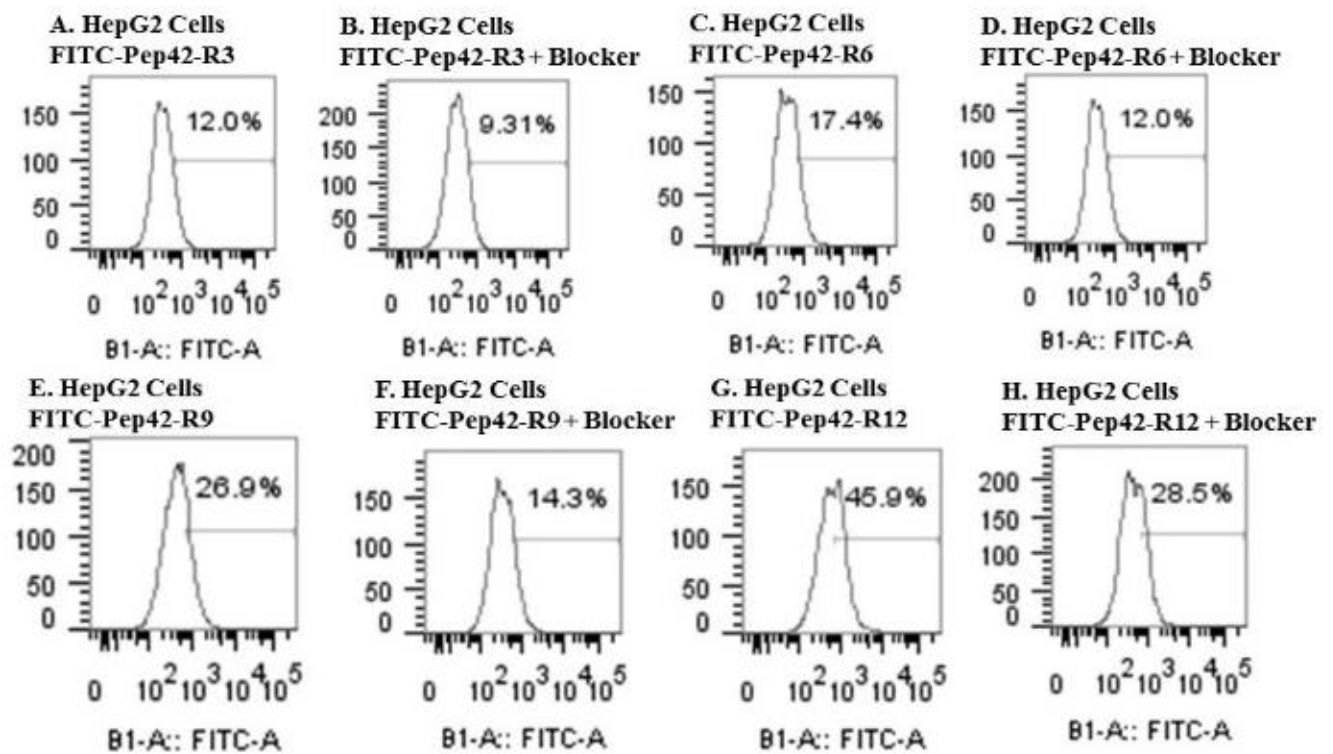
Figure A40. Flow cytometry data on HepG2 cells. FITC signaling collected at 521 nm HepG2 cells (50, 000 cells/mL) in the presence of Alexa Fluor 488-labeled N20-anti-GRP78 primary antibody (100 nM) and FITC-labeled poly(arginine) peptides (100 nM) without (a, c, e, g) and with (b, d, f, h) peptide blocker (10 mg/mL). Data acquired in collaboration with Drs. Blake and Bitsaktsis research groups.
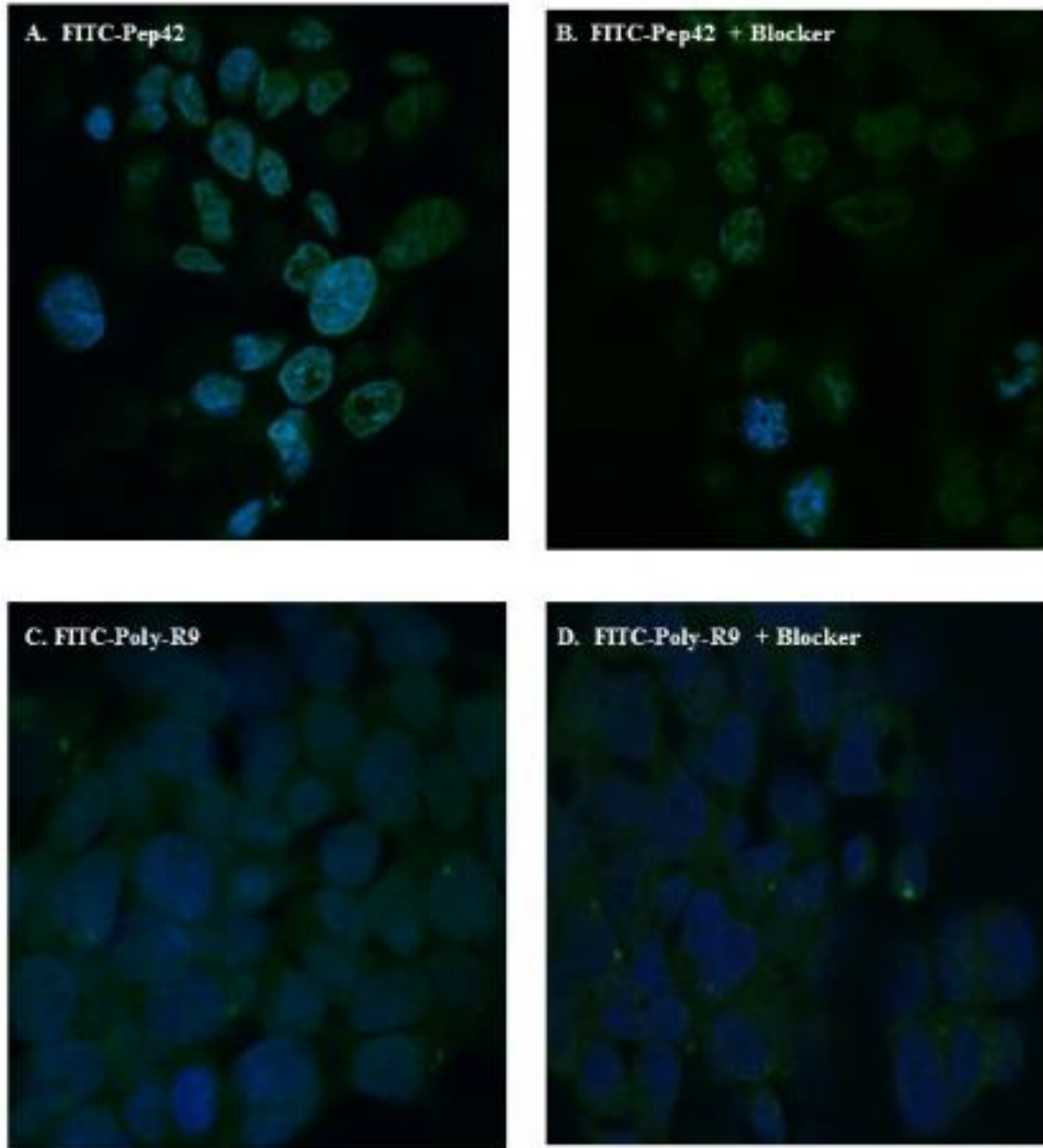
Figure A41. Laser scanning confocal microscopy of HepG2 cells. (a) FITC-Pep42 (b) FITC-Pep42 with N-20 GRP78 blocking peptide (2.0 µg/mL) (c) FITC-Poly-R9 and (d) FITC-Poly-R9 with N-20 GRP78 blocking peptide (2.0 µg/mL). HepG2 cells (50, 000 cells/mL) were incubated with FITC-Pep42 and FITC-Poly-R9 (2.0 µg/mL) and counterstained with DAPI (0.5 µg/mL in PBS). The FITC signal from the peptides is visualized as green whereas DAPI stains the cells' nuclei blue. Data acquired in collaboration with Drs. Blake and Bitsaktsis research groups.
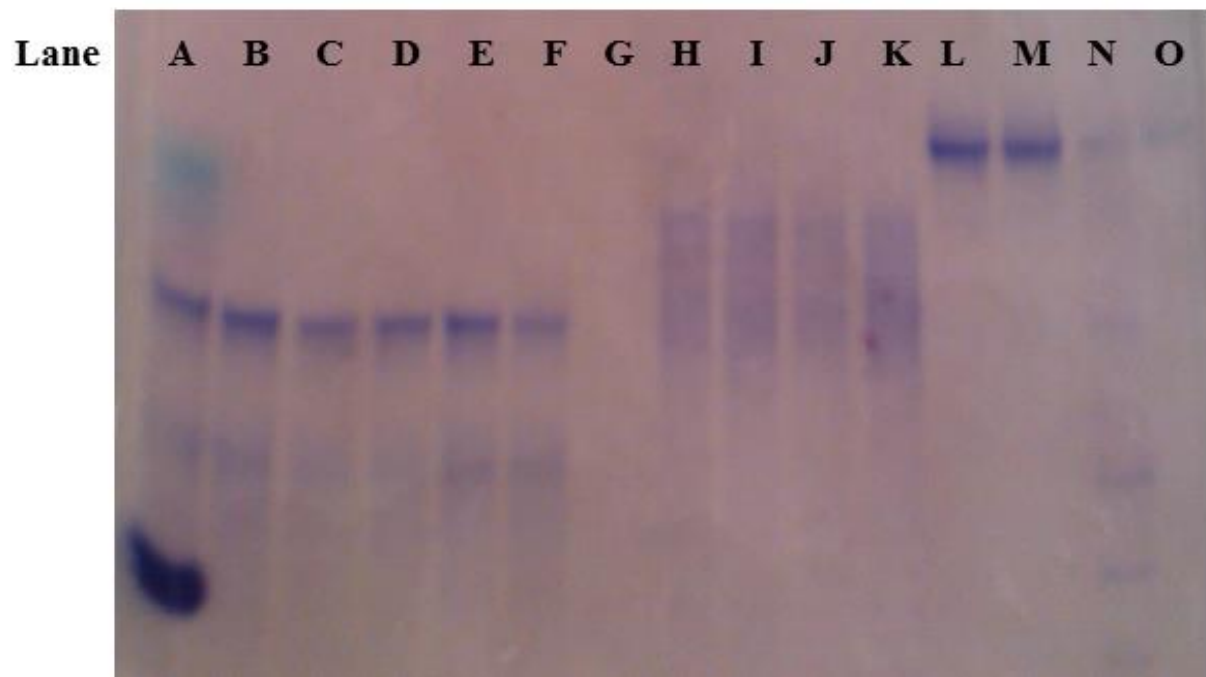
Figure A42. Native PAGE gel shift assay of siRNA:CTP (1:1-50 mol:mol, 1 μmol). siRNA with Dye (Lane A); siRNA:Pep42-R9 Lane B, 1:1; Lane C, 1:25; Lane D, 1:50; siRNA:Pep42-R12 Lane E, 1:1; Lane F, 1:25; Lane G, 1:50; branch siRNA (Lane H); branch siRNA:Pep42-R12 Lane I, 1:1; Lane J, 1:25; Lane K,1:50; hyperbranch siRNA (Lane L); hyperbranch siRNA:Pep42-R12 Lane M, 1:1; Lane N, 1:25, Lane O, 1:50.
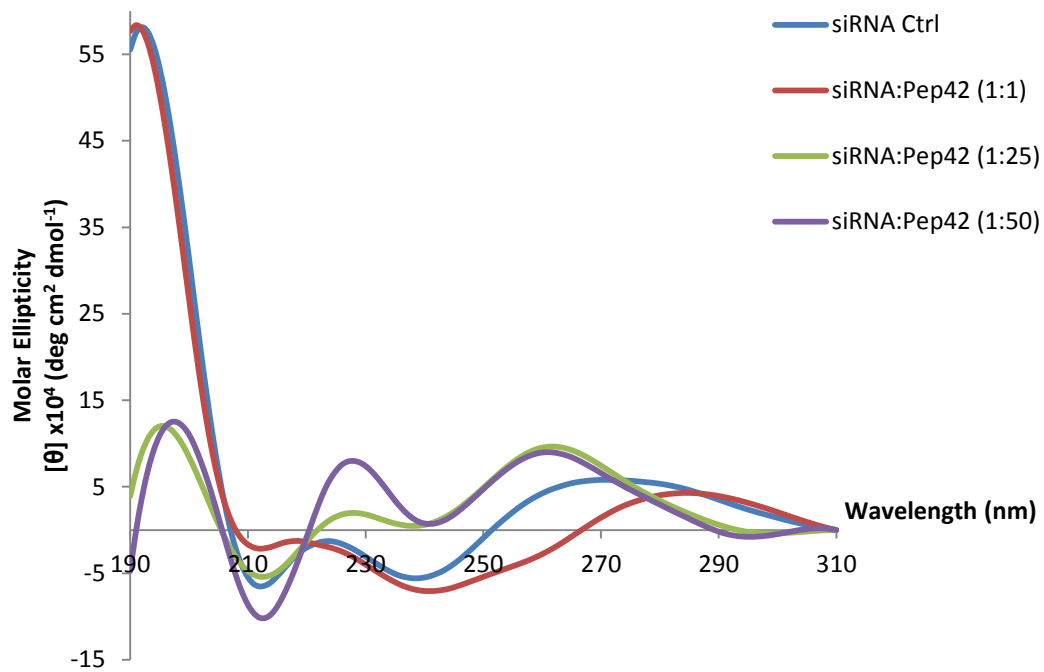
Figure A43. CD spectra of siRNA:Pep42 complexes (13 μM, 1-50:1 mol/mol) in PBS (137 mM NaCl, 2.7 mM KCl, 10 mM Na₂HPO₄, 2.0 mM KH₂PO₄ adjusted to pH 7.4) at 25 ºC.
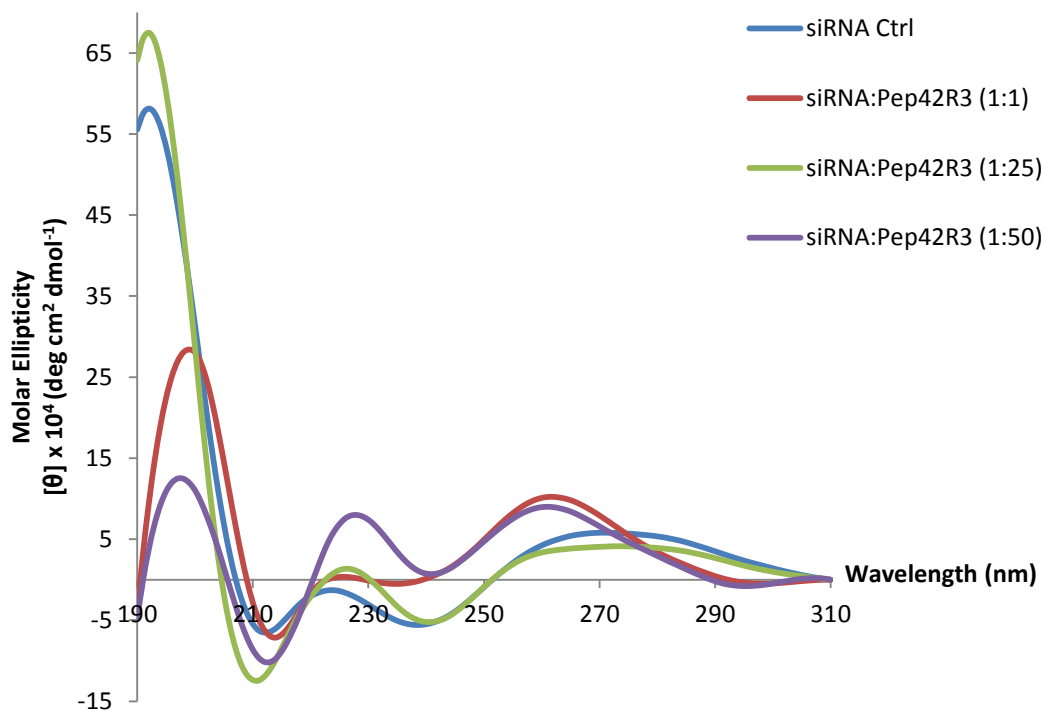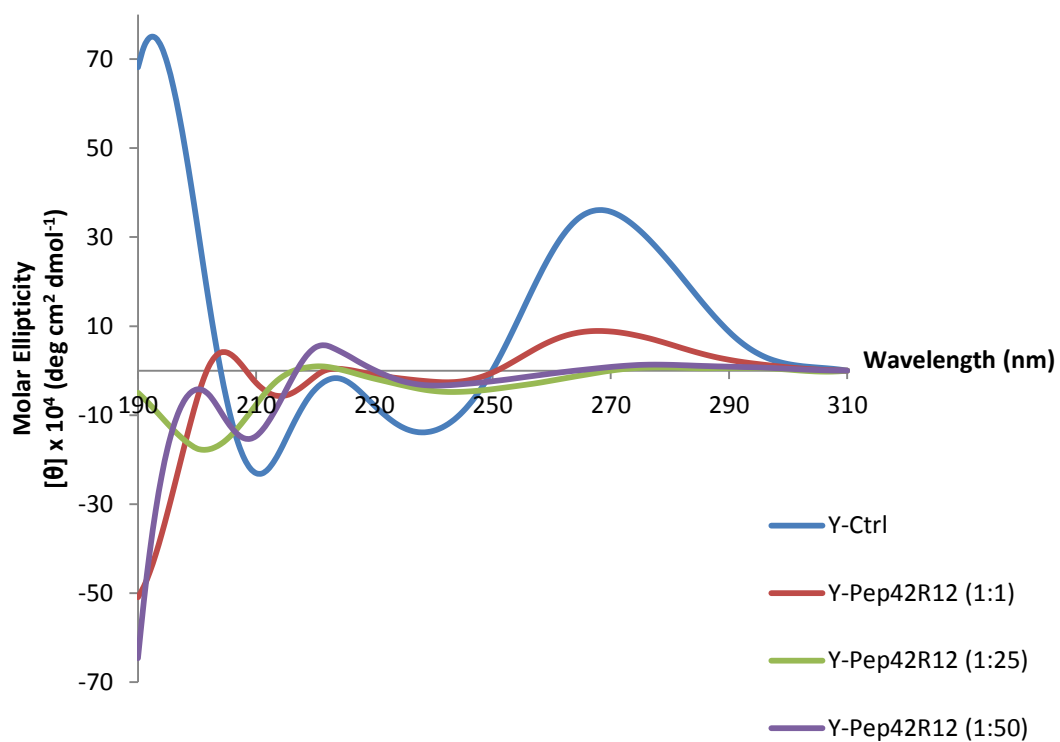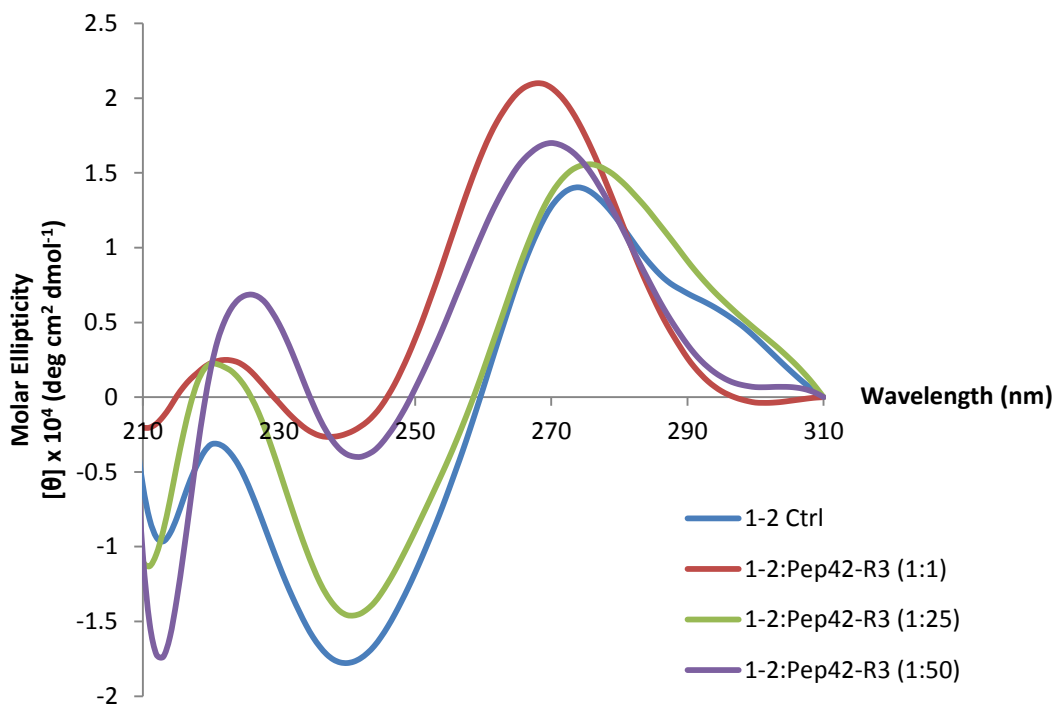
Figure A44. CD spectra of siRNA:Pep42-R3 complexes (13 μM, 1-50:1 mol/mol) in PBS (137 mM NaCl, 2.7 mM KCl, 10 mM Na$_2$HPO$_4$, 2.0 mM KH$_2$PO$_4$ adjusted to pH 7.4) at 25 $^{\circ}$C.
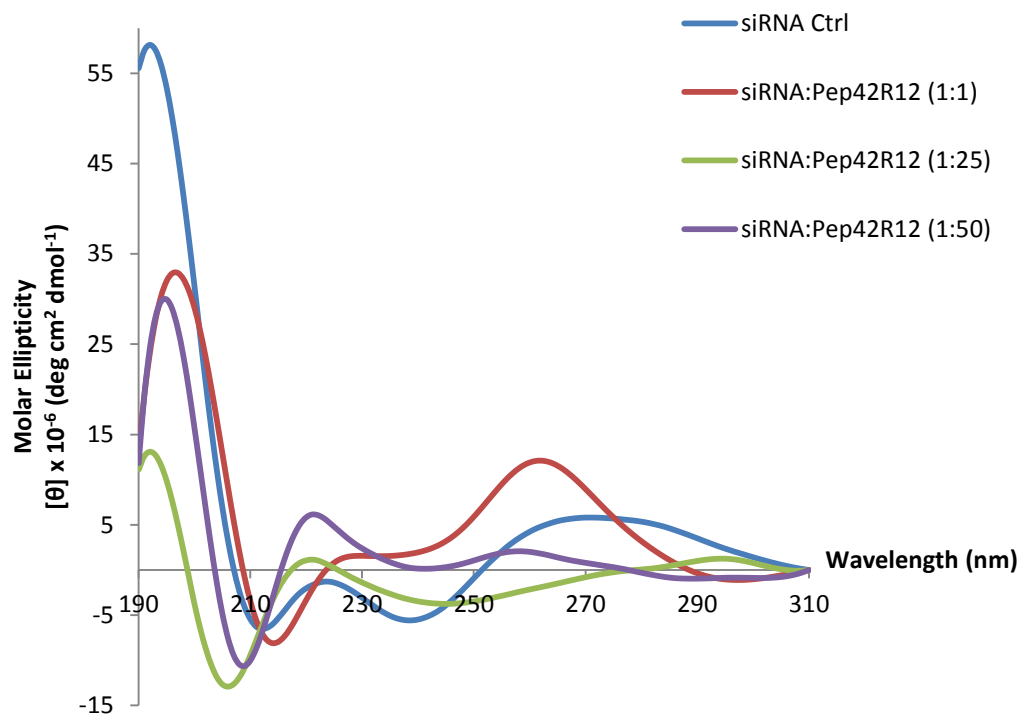
Figure A45. CD spectra of siRNA:Pep42-R12 complexes (13 μM, 1-50:1 mol/mol) in PBS (137 mM NaCl, 2.7 mM KCl, 10 mM Na_2HPO_4, 2.0 mM KH_2PO_4 adjusted to pH 7.4) at 25 ºC.
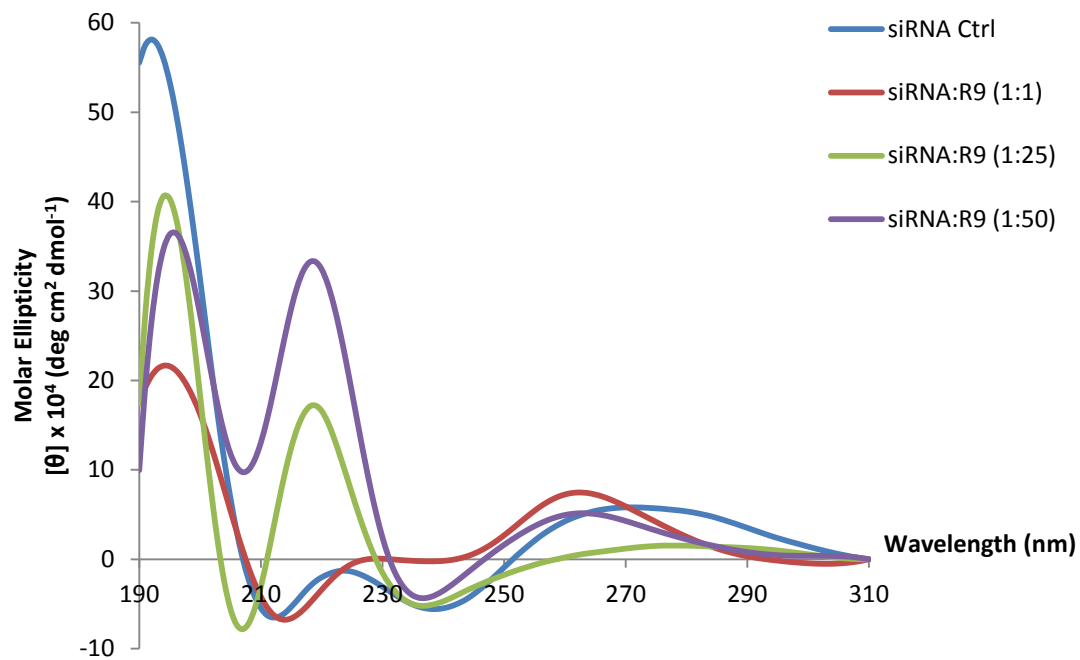
Figure A46. CD spectra of siRNA:R9 complexes (13 μM, 1-50:1 mol/mol) in PBS (137 mM NaCl, 2.7 mM KCl, 10 mM Na$_2$HPO$_4$, 2.0 mM KH$_2$PO$_4$ adjusted to pH 7.4) at 25 °C.
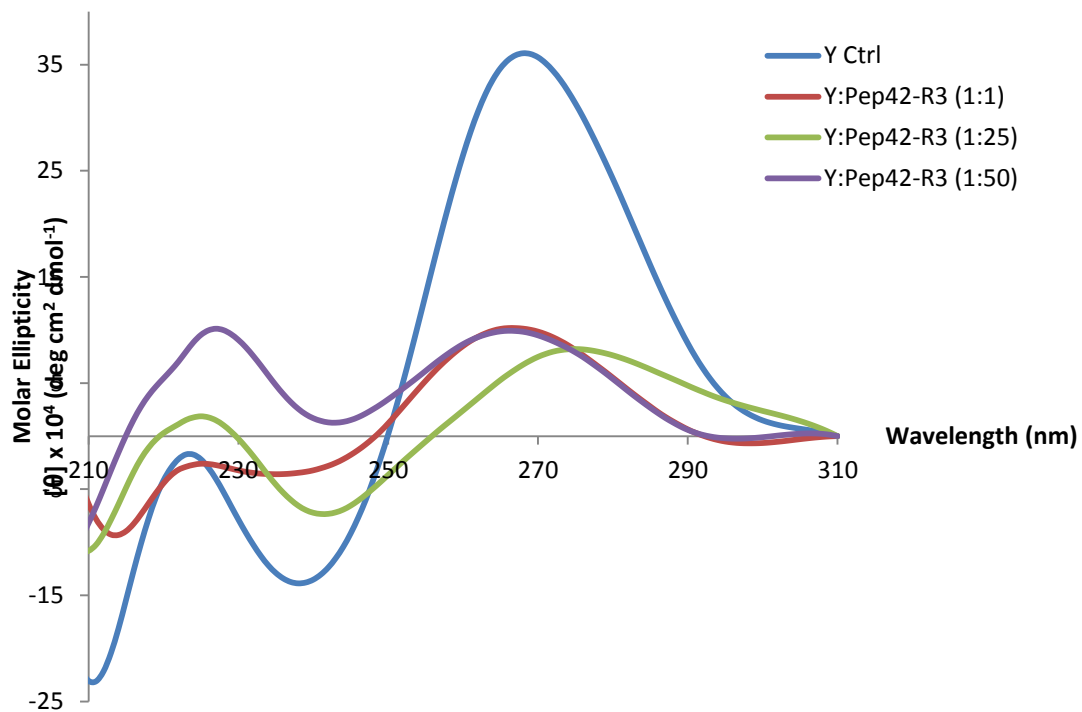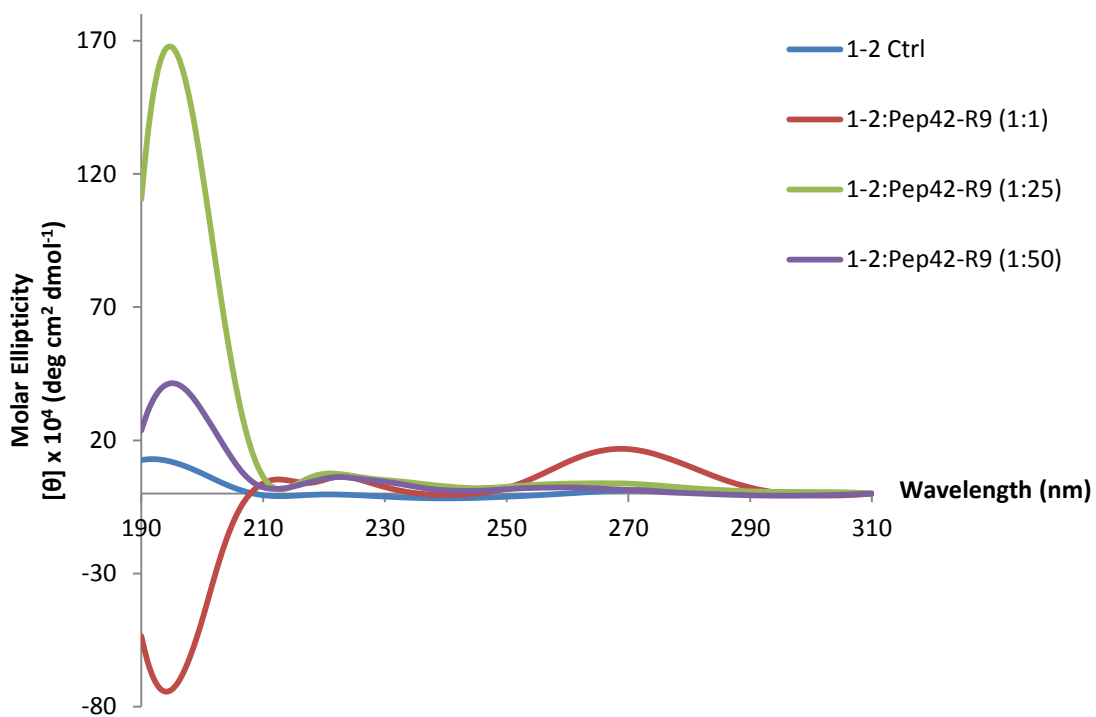
Figure A47. CD spectra of branch siRNA(Y):Pep42-R3 complexes (13 μM, 1-50:1 mol/mol) in PBS (137 mM NaCl, 2.7 mM KCl, 10 mM Na_2HPO_4, 2.0 mM KH_2PO_4 adjusted to pH 7.4) at 25 ºC.
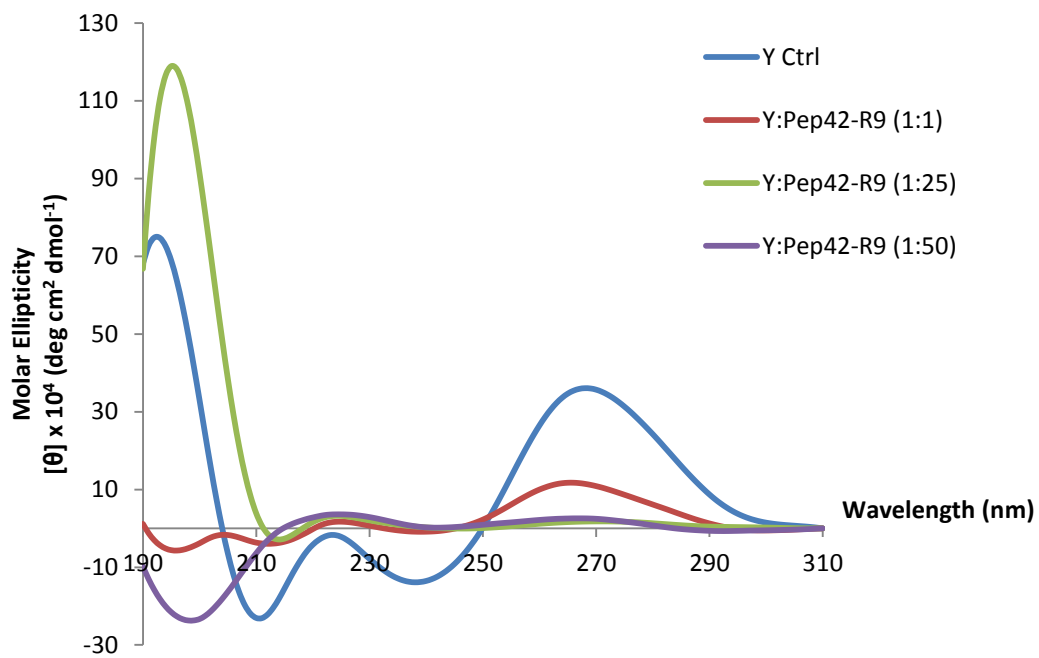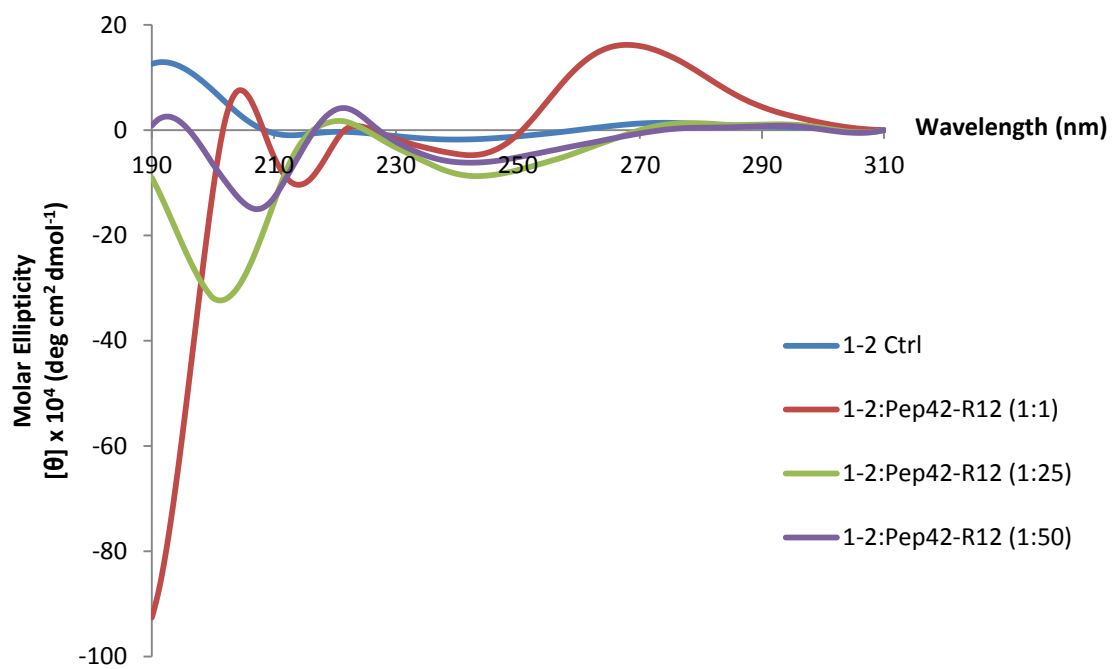
Figure A48. CD spectra of branch siRNA(Y):Pep42-R9 complexes (13 μM, 1-50:1 mol/mol) in PBS (137 mM NaCl, 2.7 mM KCl, 10 mM Na_2HPO_4, 2.0 mM KH_2PO_4 adjusted to pH 7.4) at 25 ℃.

Figure A49. CD spectra of branch siRNA (Y):Pep42-R12 complexes (13 μM, 1-50:1 mol/mol) in PBS (137 mM NaCl, 2.7 mM KCl, 10 mM Na_2HPO_4, 2.0 mM KH_2PO_4 adjusted to pH 7.4) at 25 °C.

Figure A50. CD spectra of hyperbranch siRNA (1-2):Pep42-R3 complexes (13 μM, 1-50:1 mol/mol) in PBS (137 mM NaCl, 2.7 mM KCl, 10 mM Na$_2$HPO$_4$, 2.0 mM KH$_2$PO$_4$ adjusted to pH 7.4) at 25 ℃.

Figure A51. CD spectra of hyperbranch siRNA (1-2):Pep42-R9 complexes (13 µM, 1-50:1 mol/mol) in PBS (137 mM NaCl, 2.7 mM KCl, 10 mM Na_2HPO_4, 2.0 mM KH_2PO_4 adjusted to pH 7.4) at 25 °C.

Figure A52. CD spectra of hyperbranch siRNA (1-2):Pep42-R12 complexes (13 μM, 1-50:1 mol/mol) in PBS (137 mM NaCl, 2.7 mM KCl, 10 mM Na_2HPO_4, 2.0 mM KH_2PO_4 adjusted to pH 7.4) at 25 ºC.
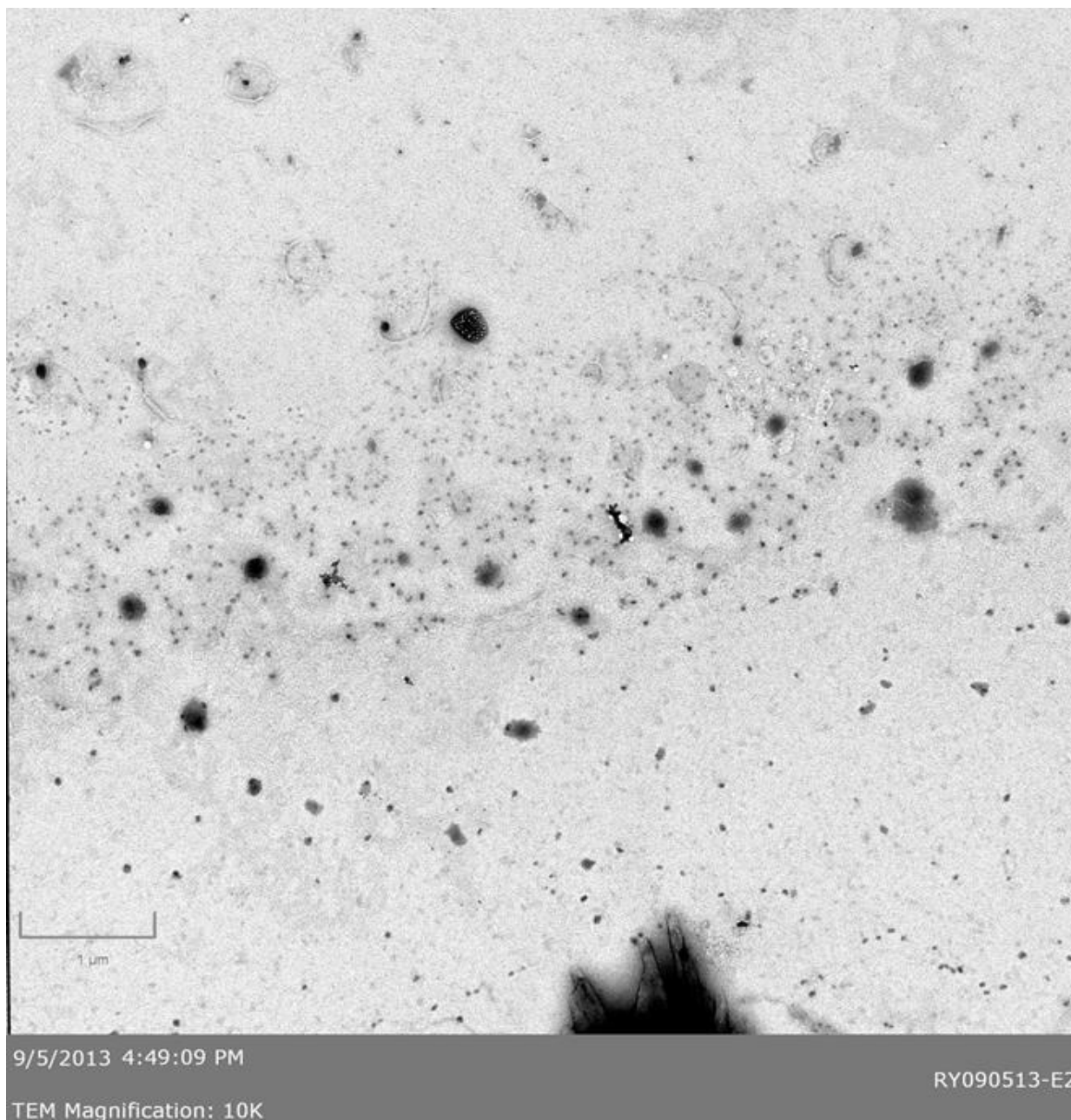
Figure A53. TEM image of Pep42-R9 (**Table 2.1, sequence 2.4**) showing different populations. Mostly prevalent are populations ranging from 30 -100 nm which are probably the monomeric forms of the peptide. There are some larger sizes present (approx. 200nm) which look like aggregates of the smaller ones. Data acquired in collaboration with Dr. Samuni (Queen's College CUNY).
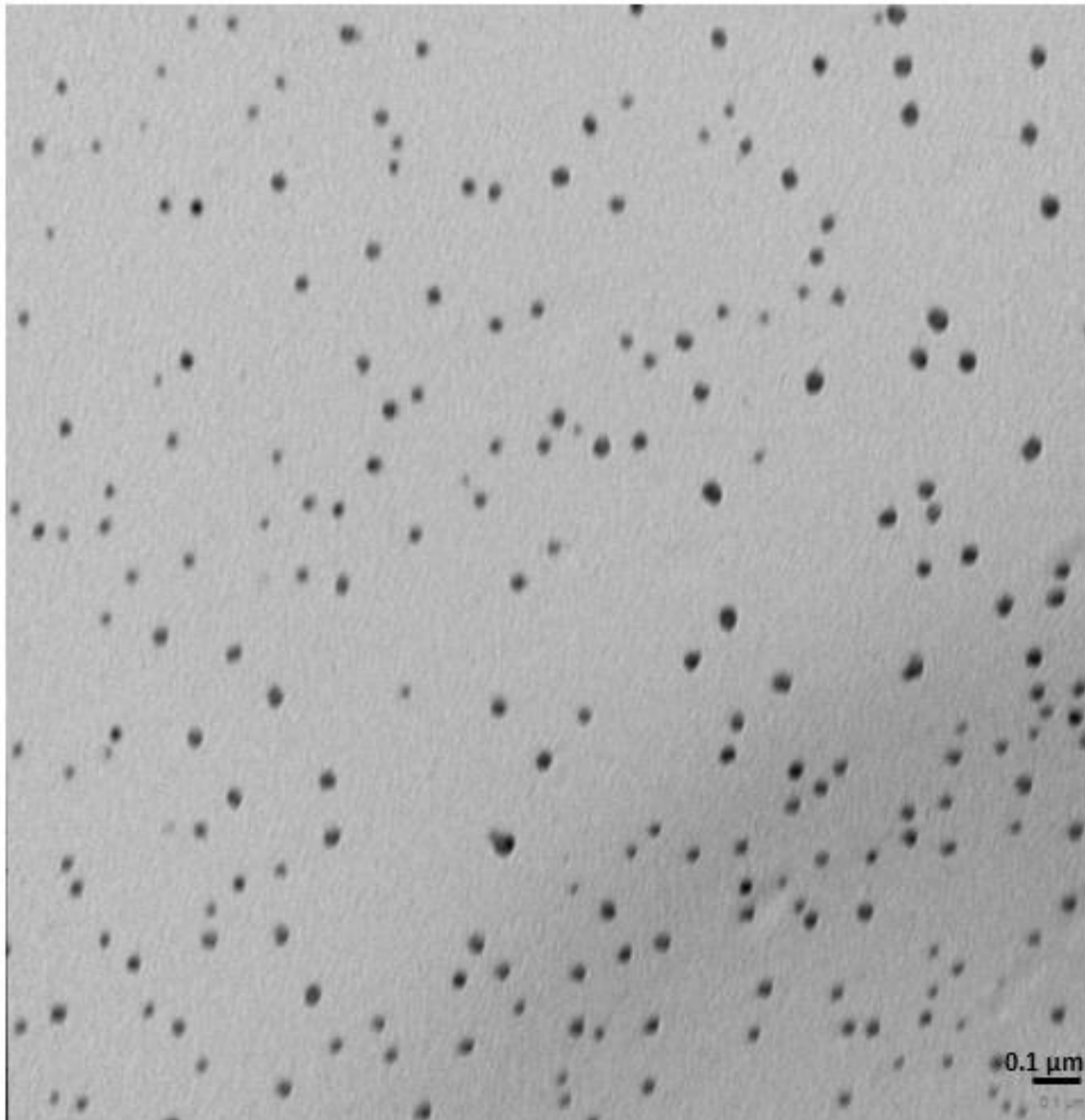
Figure A54. TEM images of branch siRNA generating well distributed uniform particles, average size 20-25 nm. Sample (0.13 μM) were mixed with 1.0% uranyl acetate in ethanol (1:1 v/v), sonicated for 10 minutes, and added to a carbon film coated copper grid, 300 mesh (electron microscopy sciences, Hatfield, PA) and dried overnight prior to viewing under the transmission electron microscope (JEOL, model JEM-1200 EX). Images were taken with a SIA–L3C CCD camera (Scientific Instruments and Applications, Inc.) using the software Maxim DL5 (Diffraction Limited, Ottawa, Canada). Data acquired in collaboration with Dr. Samuni (Queen's College CUNY).
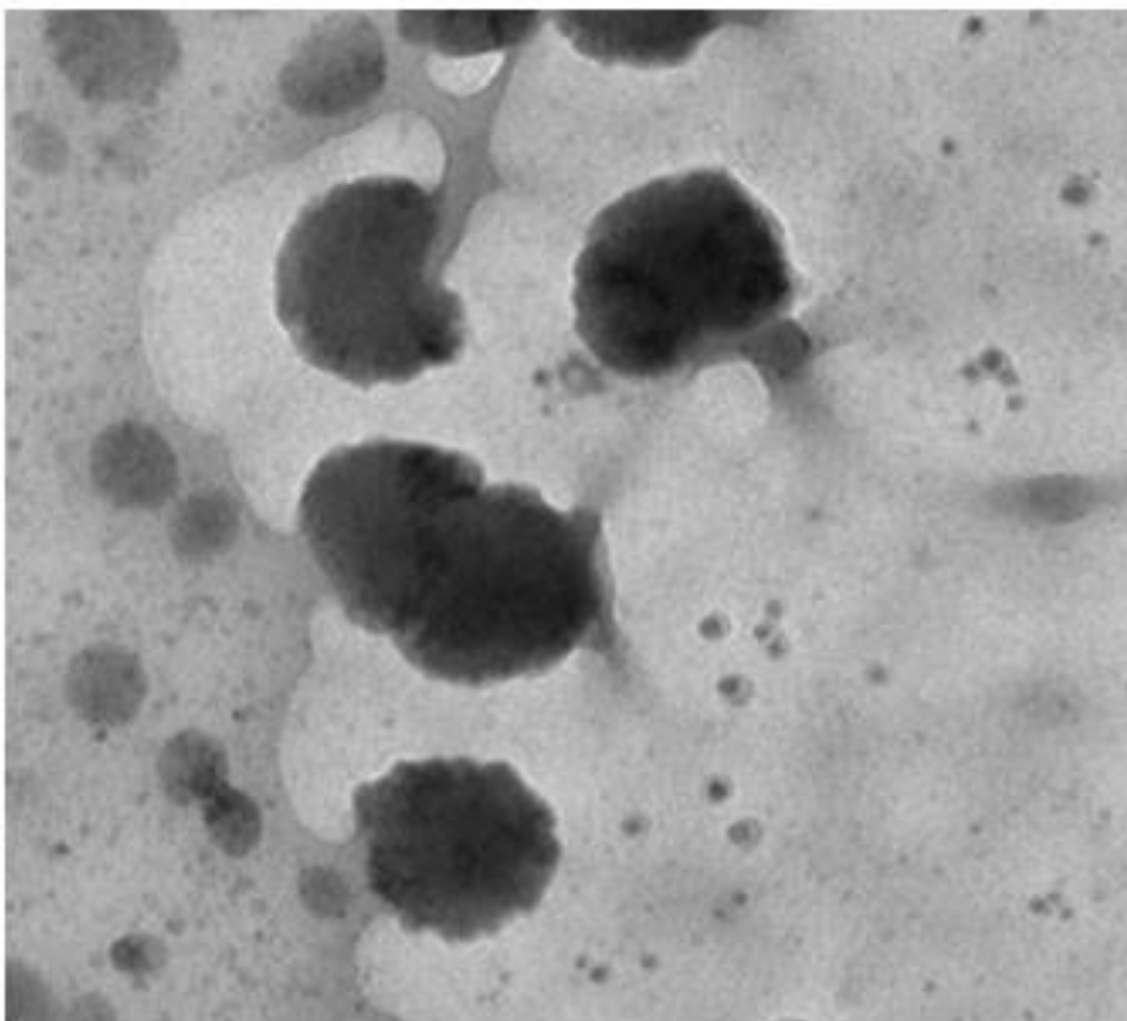
Figure A55. TEM images of branch siRNA:CTP-R9 complex. The TEM image of complex branch siRNA:CTP-R9 shows a population with a size range of 50 – 100 nm (circular shaped complexes). A population of smaller particles of about 10 nm is also seen which is likely to be the control siRNA. The complex (0.13 μM) was mixed with 1.0% uranyl acetate in ethanol (1:1 v/v), sonicated for 10 minutes, and added to a carbon film coated copper grid, 300 mesh (electron microscopy sciences, Hatfield, PA) and dried overnight prior to viewing under the transmission electron microscope (JEOL, model JEM-1200 EX). Images were taken with a SIA–L3C CCD camera (Scientific Instruments and Applications, Inc.) using the software Maxim DL5 (Diffraction Limited, Ottawa, Canada). Data acquired in collaboration with Dr. Samuni (Queen's College CUNY).
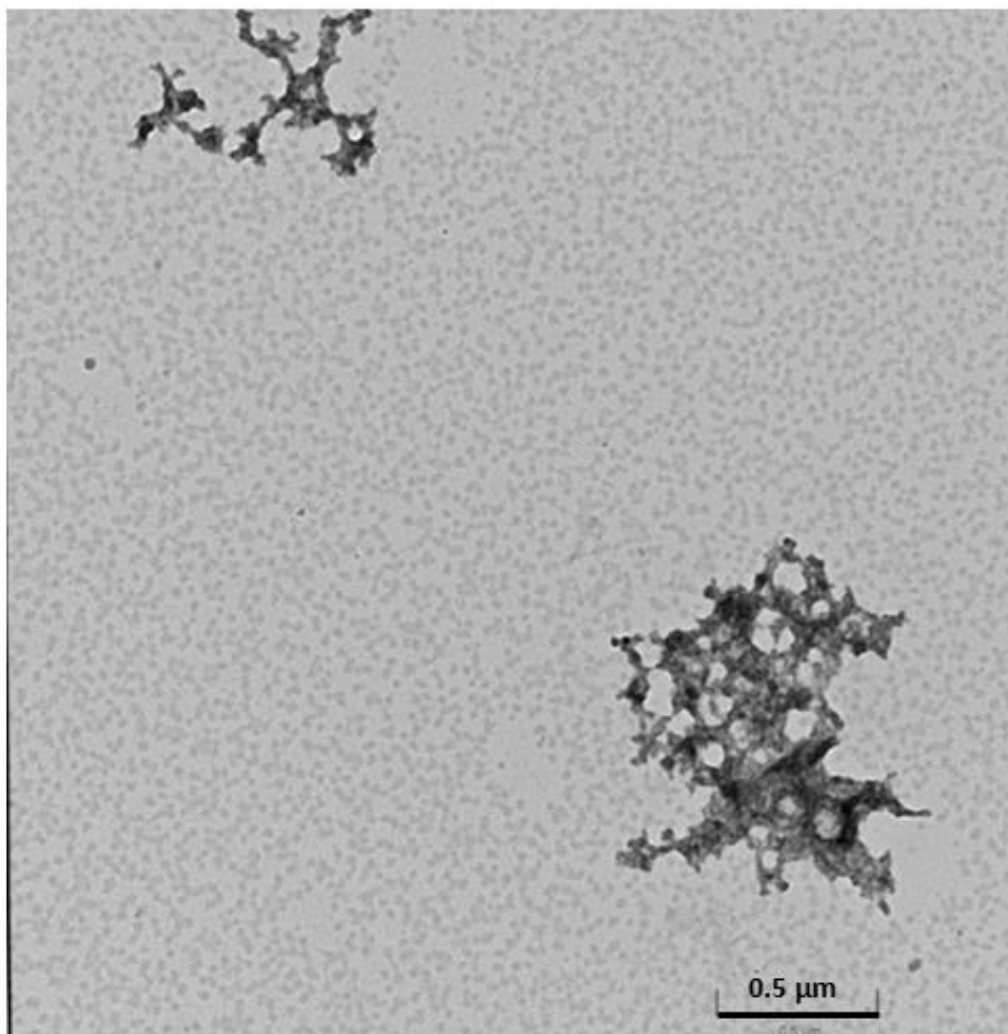
Figure A56. TEM image of hyperbranch siRNA. There is a range of sizes of the hyperbranch siRNA. The prevalent population is the spherical monomer particles with an approximate size of 25 nm. There is a minor fraction of medium size particles in the range of 100 nm (not seen in this picture) and a few large aggregates (700-2000 nm). Sample (0.13 μM) was mixed with 1.0% uranyl acetate in ethanol (1:1 v/v), sonicated for 10 minutes, and added to a carbon film coated copper grid, 300 mesh (electron microscopy sciences, Hatfield, PA) and dried overnight prior to viewing under the transmission electron microscope (JEOL, model JEM-1200 EX). Images were taken with a SIA–L3C CCD camera (Scientific Instruments and Applications, Inc.) using the software Maxim DL5 (Diffraction Limited, Ottawa, Canada). Data acquired in collaboration with Dr. Samuni (Queen's College CUNY).
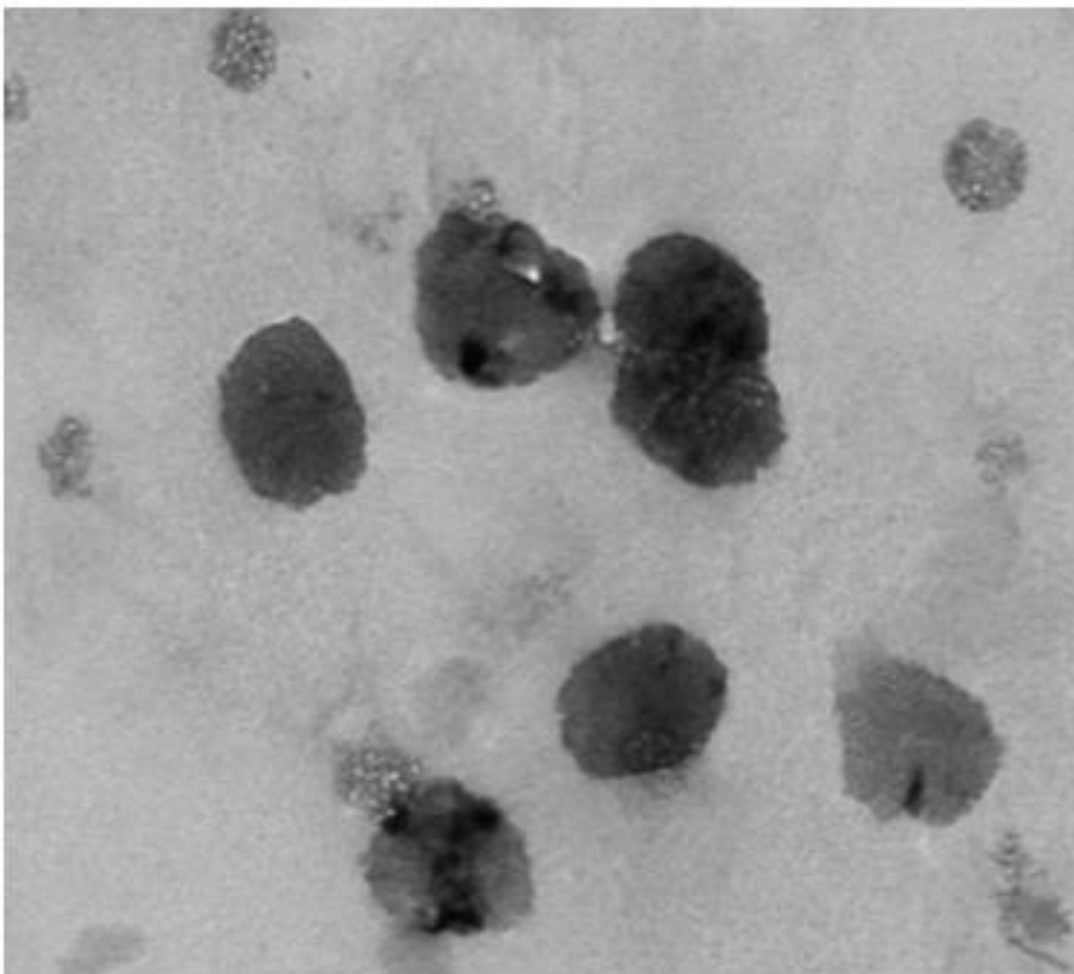
Figure A57. TEM image of hyperbranch siRNA:Pep42-R9. Uniformly distributed circular shaped complexes sizes 300-500 nm. This population correlates with the one seen in DLS (340 nm). Also seen are smaller sized particles (approx. 100-300 nm). These may be smaller complexes. Complex (0.13 µM) was mixed with 1.0% uranyl acetate in ethanol (1:1 v/v), sonicated for 10 minutes, and added to a carbon film coated copper grid, 300 mesh (electron microscopy sciences, Hatfield, PA) and dried overnight prior to viewing under the transmission electron microscope (JEOL, model JEM-1200 EX). Images were taken with a SIA–L3C CCD camera (Scientific Instruments and Applications, Inc.) using the software Maxim DL5 (Diffraction Limited, Ottawa, Canada). Data acquired in collaboration with Dr. Samuni (Queen's College CUNY).
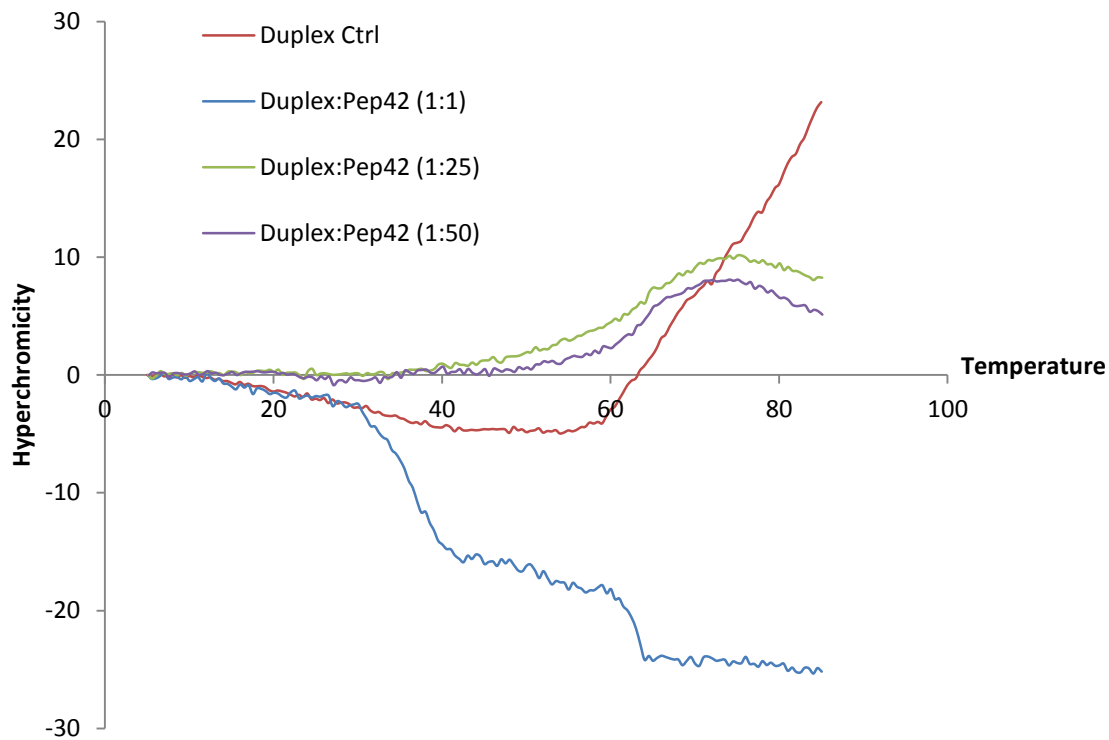
Figure A58. Thermal denaturation studies of the siRNA (duplex):Pep42 complex. Samples were prepared by mixing siRNA:Pep42 (15 µM, 1-50:1 mol/mol) in phosphate buffer (140 mM KCl, 1.0 mM MgCl$_2$, 5.0 mM NaHPO$_4$) and placing on a heat block incubator set at 37 ºC for 1 hour. Samples were cooled to room temperature and placed in the fridge overnight prior to thermal denaturation studies. Samples were then placed in a temperature regulated (5 ºC) cell holder and heated (5 – 95 ºC) for sample absorption measurements at 260 nm.
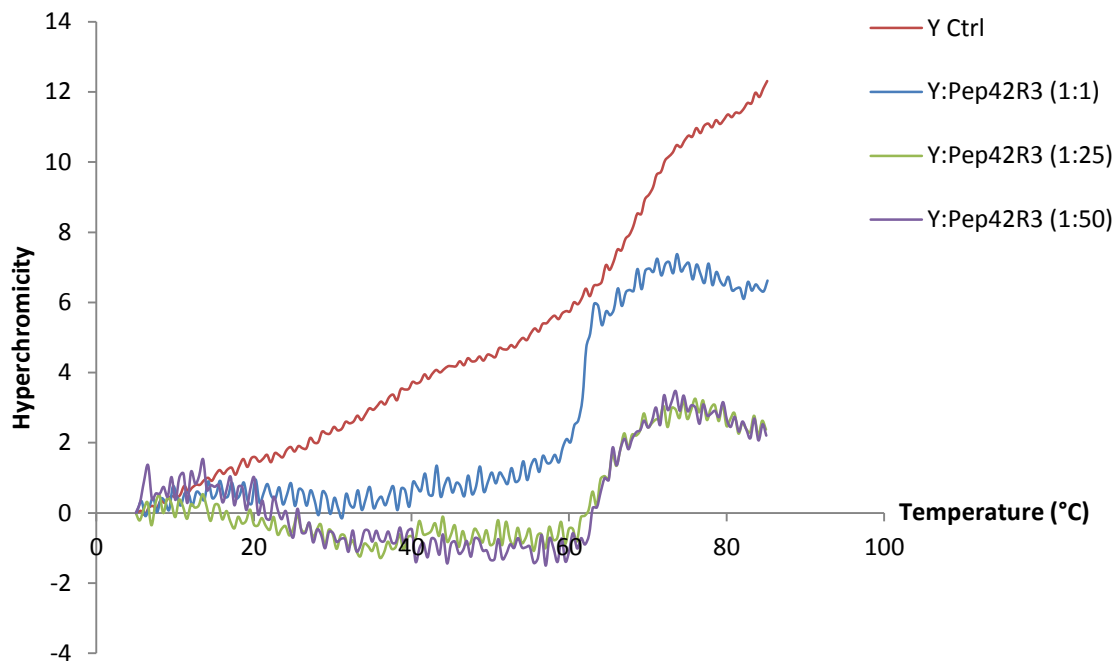
Figure A59. Thermal denaturation studies of the branch siRNA(Y):Pep42-R3 complex. Samples were prepared by mixing branch siRNA(Y):Pep42-R3 (15 μM, 1-50:1 mol/mol) in phosphate buffer (140 mM KCl, 1.0 mM MgCl$_2$, 5.0 mM NaHPO$_4$) and placing on a heat block incubator set at 37 °C for 1 hour. Samples were cooled to room temperature and placed in the fridge overnight prior to thermal denaturation studies. Samples were then placed in a temperature regulated (5 °C) cell holder and heated (5 – 95 °C) for sample absorption measurements at 260 nm.
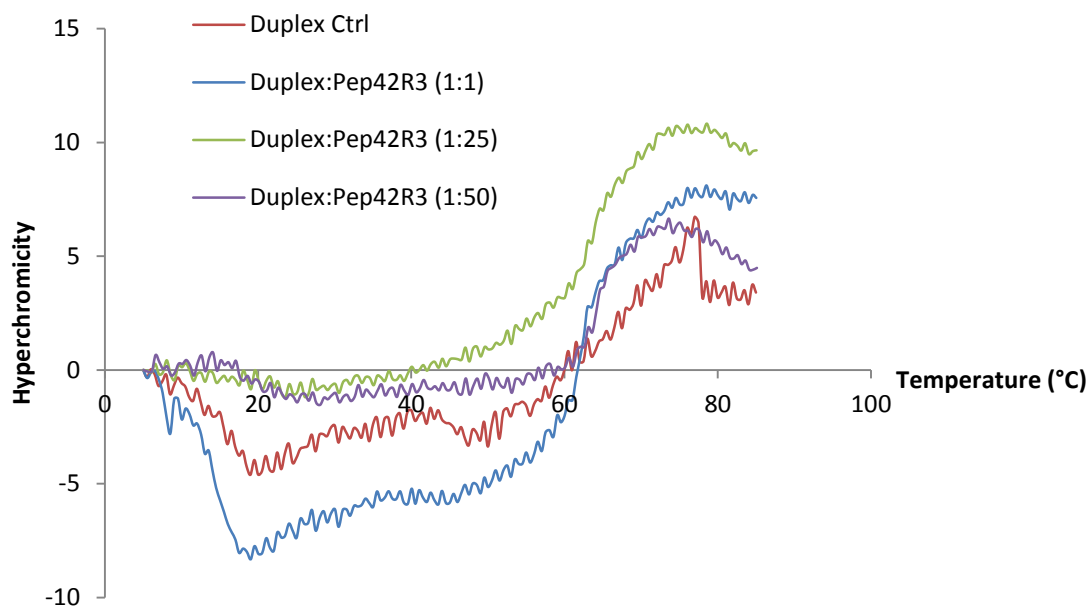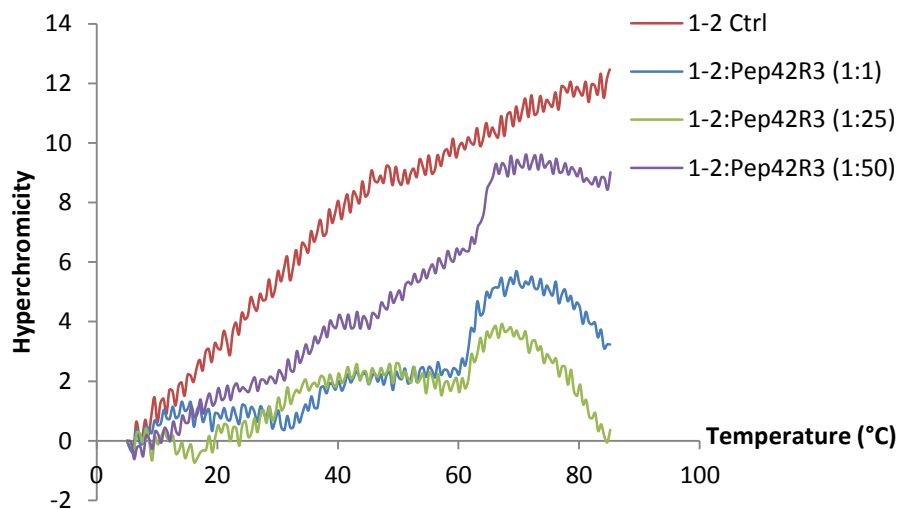
Figure A60. Thermal denaturation studies of the siRNA (duplex):Pep42-R3 complex. Samples were prepared by mixing siRNA (duplex):Pep42-R3 (15 μM, 1-50:1 mol/mol) in phosphate buffer (140 mM KCl, 1.0 mM MgCl$_2$, 5.0 mM NaHPO$_4$) and placing on a heat block incubator set at 37 ºC for 1 hour. Samples were cooled to room temperature and placed in the fridge overnight prior to thermal denaturation studies. Samples were then placed in a temperature regulated (5 ºC) cell holder and heated (5 – 95 ºC) for sample absorption measurements at 260 nm.

Figure A61. Thermal denaturation studies of the hyperbranch siRNA (1-2):Pep42-R3 complex. Samples were prepared by mixing hyperbranch siRNA (1-2):Pep42-R3 (15 μM, 1-50:1 mol/mol) in phosphate buffer (140 mM KCl, 1.0 mM $MgCl_2$, 5.0 mM $NaHPO_4$) and placing on a heat block incubator set at 37 °C for 1 hour. Samples were cooled to room temperature and placed in the fridge overnight prior to thermal denaturation studies. Samples were then placed in a temperature regulated (5 °C) cell holder and heated (5 – 95 °C) for sample absorption measurements at 260 nm.

Sample	Effective Diameter from DLS (nm)
Pep42-R9	40 ± 4
Branch (Y) siRNA	170 ± 9
Pep42-R9: branch siRNA (Y)	900 ± 50 170 ± 9
Hyperbranch (1-2) siRNA	20-2000
Pep42R9:hyperbranch siRNA (1-2)	340 ± 2

Table A62. Samples (0.05-0.15 μM) were prepared in pre-filtered (0.2 μm filter) pH 7.0 phosphate buffer (140 mM KCl, 1.0 mM MgCl$_2$, 5.0 mM NaHPO$_4$) and sonicated for 30 minutes before taking measurements. The reported diameter is the average of 5 runs for each sample reported with the standard deviations about the mean. Data acquired in collaboration with Dr. Samuni (Queen's College CUNY).